Diss ETH Nr. 19620

# Methyl-Coenzyme M Reductase: Mechanistic Studies with $^{2}H$ and $^{13}C$ Labels

A dissertation submitted to the
ETH ZÜRICH
for the degree of

Doctor of Sciences

presented by

Silvan Scheller

dipl. Chem. ETH
born 27. May, 1981
Citizen of Thalwil (ZH)

Accepted on the recommendation of
Prof. Dr. B. Jaun, examiner
Prof. Dr. D. Hilvert, co-examiner

Zürich 2011

Für meine Familie

This work has been supported by a research grant from the
Swiss National Foundation.

**Danksagung**

Allen Personen, welche zum Gelingen dieser Arbeit beigetragen haben, möchte ich herzlich danken.

An erster Stelle danke ich meinem Doktorvater Professor Dr. Bernhard Jaun für seine Unterstützung und sein Vertrauen während der Doktoratszeit. Ich danke ihm für die lehrreichen und spannenden wissenschaftlichen Diskussionen sowie für das Gewähren der nötigen Freiheiten, welche wichtig sind für eine selbstständige wissenschaftliche Entwicklung.
Zudem danke ich ihm für die zahlreichen Wochenenden, die er investierte um den Isotopenaustausch in Ethyl-Coenzym M vollständig zu simulieren, was die Bestimmung der involvierten Isotopeneffekte erlaubte.

Professor Dr. Donald Hilvert danke ich für die Übernahme des Koreferates und für die gründliche Korrektur dieser Arbeit.

Professor Dr. Rudolf Thauer danke ich für die fruchtbare Zusammenarbeit und für wichtige Beiträge zu biologischen Fragestellungen. Herzlichen Dank auch für seine Gastfreundschaft am Max Planck Institut Marburg während den zahlreichen Forschungs-aufenthalten.
Ein spezieller Dank gebührt Dr. Meike Brefort (Goenrich) für die sehr angenehme und effiziente Zusammenarbeit, sowie für das Lehren der nötigen Techniken um MCR rein und hochaktiv zu isolieren. Alle Enzymassays wurden mit ihr gemeinsam durchgeführt.
Reinhard Böcher danke ich für das gemeinsame Züchten und Ernten von Archäen, für technische Unterstützung bei Assays unter $^{13}C$-markiertem Methan und für den Bau der modifizierten French Press Apparatur um hohe Drücke von $^{13}CH_4$ zu erzeugen.

Dr. Marc-Olivier Ebert danke ich für das Einrichten spezieller NMR-Aufnahmetechniken und für technische Unterstützung bei den Messungen.
Guido Grassi danke ich für die Synthese von $^{12}CH_3I$, welches zur Herstellung von $^{13}C$-abgereichertem Methyl-Coenzym M verwendet wurde.

Den Mitgliedern der Forschungsgruppe (Prof. Jaun, Stefan, Siegi und David) sowie des NMR-Teams (Oli, Philipp, Reiner und René) danke ich herzlich für das angenehme Arbeitsklima.
Speziell möchte ich mich bei Stefan bedanken für die Einführung in die NMR-Messungen von Methan-Isotopologen und für das Beibringen von Arbeitstechniken zur Reinigung und Analyse von freiem Cofaktor F430.
Siegi, mit welcher ich das Labor die längste Zeit teilte, danke ich für ihre aufmunternde Art und unsere interessanten Diskussionen.
Ich danke David für die gemeinsame Zeit im Labor während des letzten Abschnittes meiner Doktorarbeit und für die gemeinsamen Bergwanderungen in der Hirschegg.
Meinem Bachelor-Studenten Andreas danke ich für seine Mitarbeit zur Reinigung von freiem Cofaktor F430 und anschliessenden Protonen-Inventar Versuchen mit dem freien Cofaktor F430.

Allen Kollegen an und ausserhalb der ETH danke ich für Unterstützung jeglicher Art.

Ich danke meiner Familie und meinem Freund Bob, dass sie immer hinter mir standen.

**Parts of this thesis have been published:**

S. Scheller, M. Goenrich, R. Boecher, R. K. Thauer, B. Jaun:
"The key nickel enzyme of methanogenesis catalyses the anaerobic oxidation of methane" *Nature* **2010**, *465*, 606.

S. Scheller, M. Goenrich, S. Mayr, R. K. Thauer, B. Jaun:
"Intermediates in the Catalytic Cycle of Methyl Coenzyme M Reductase: Isotope Exchange is Consistent with Formation of a σ-Alkane-Nickel complex" *Angew. Chem. Int. Ed.* **2010**, *49*, 8112.

## Table of Contents

## Summary

Methyl-coenzyme M reductase (MCR) is the enzyme catalyzing the last step of methane formation in all methanogenic archaea.
The initial substrates of these organisms (usually $CO_2$ or acetate) are reduced with hydrogen as the electron donor in a cascade of steps catalyzed by different metalloenzymes to eventually give an *S*-methyl group bound to coenzyme M:

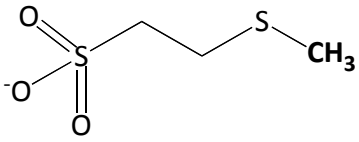


**Methyl-coenzyme M**

The nickel enzyme MCR catalyzes the reduction of the sulfur-bound methyl group of methyl-coenzyme M with the thiol coenzyme B to methane and the corresponding disulfide according to the following scheme:

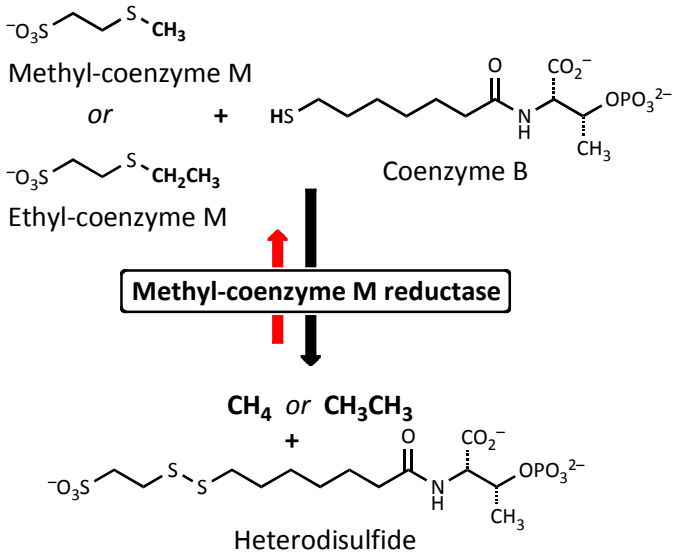


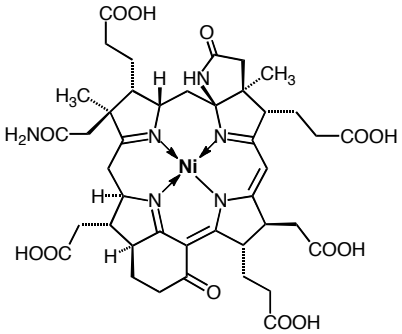


Coenzyme F430

Coenzyme F430, with its central nickel ion in the +1 oxidation state (shown above, right side), is the prosthetic group of the enzyme.

We investigated the reverse reaction (red arrow) under equilibrium conditions with substrates and products present. With $^{13}CH_4$ in the gas phase, activation of methane could be detected by the amount of $^{13}C$-labeled methyl-coenzyme M formed. A methane activation rate of 11.4 nmol per min per mg enzyme was measured with 1 bar $^{13}CH_4$ at 60 °C. At lower temperatures, the rate of methane activation was lower, but could be measured accurately even at 4 °C. Experiments varying the methane pressure from 0.05 bar to 16 bar demonstrated a linear correlation between the reaction rate and the pressure up to about 8 bar methane.

The measured rate of methane activation by MCR is similar to the rate of methane activation carried out by consortia of sulfate reducing bacteria living together with close homologues of methanogens[1]. According to the "hypothesis of reverse methanogenesis"[2, 3], these ANME archaea carry out anaerobic oxidation of methane with enzymes very similar to those used by the methanogens but in the reverse direction. The rate of methane activation catalyzed by MCR measured in this work is sufficiently high to fully support the hypothesis of reverse methanogenesis.

Isotope effects of methane activation were investigated with $CH_2D_2$ and with a mixture of $CH_4$ and $CD_4$. A primary isotope effect of 2.44 ± 0.22 and a secondary isotope effect of 1.17 ± 0.05 per D was deduced from combining both sets of experiments.

Studying the reaction to methane and to ethane in deuterated medium revealed the occurrence of intermediates. Measuring the rate of deuterium incorporation into the substrate methyl-coenzyme M in deuterated medium, combined with methane activation studies in deuterated medium, allowed discrimination between the potential reaction pathways shown below (red arrows).

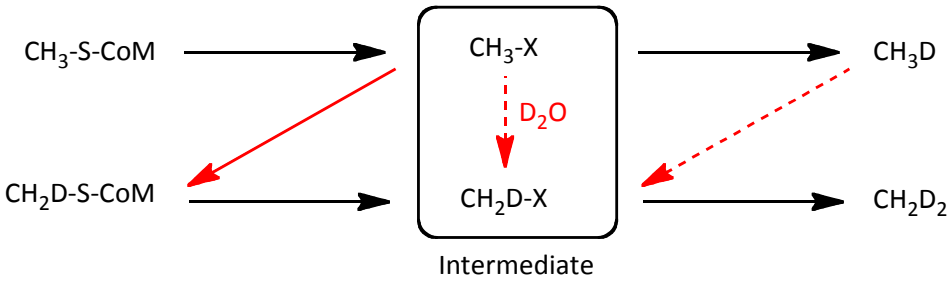


Only the additional pathway indicated by the solid, red arrow contributed to the observed isotope exchange. The intermediate is partitioned in a ratio of 20:1 between methane formation and substrate "re-formation." At lower temperatures, more deuterium is introduced into the remaining substrate relative to the amount of methane formed.

With the non-natural substrate ethyl-coenzyme M, the ratio of ethane formation versus substrate re-formation from the intermediate was determined to be about 1:100. In this case, formation of ethane from the intermediate is rate limiting, which allowed multiple turnovers of substrate "re-formation" to be observed before a substantial amount of ethane was produced.

We found that deuterium from the medium was introduced at *both* carbon atoms of the *S*-ethyl group of ethyl coenzyme M. With a $^{13}C$ label in the ethyl group (highlighted in red), the following isotope exchange pattern was observed:

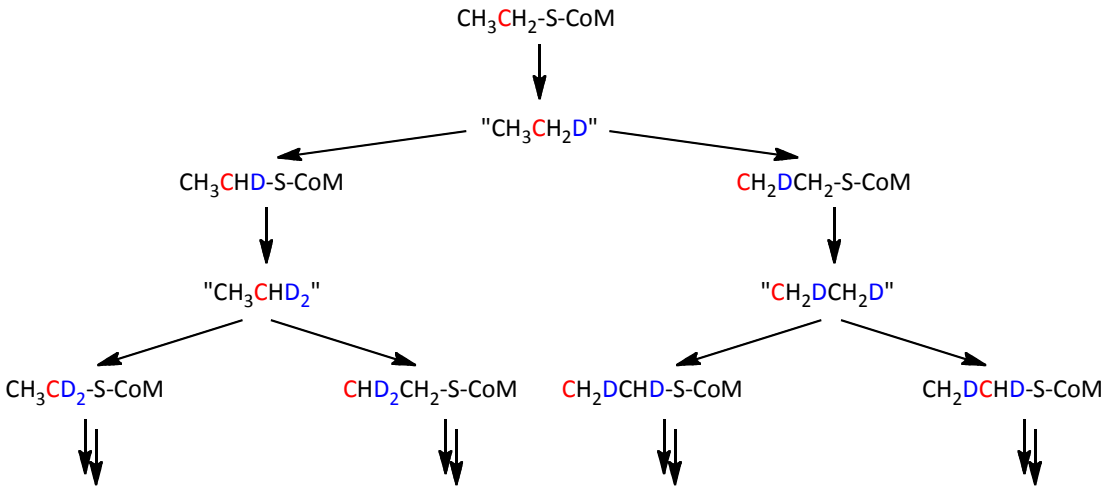

It appears that all C-H and C-D bonds of the prospective alkane are already set up in the intermediate (in quotation marks), through a formal replacement of sulfur by deuterium.

Using $^{13}$C-NMR spectroscopy (inverse gated, with simultaneous broadband proton and deuterium decoupling), all isotopologues that were formed to a molar fraction of more than 0.1%, including the two isotopologues with a fully deuterated ethyl group, could be quantified.

Through a comprehensive kinetic simulation (up to and including the rate limiting step) of the observed time course of all possible isotopologues of $^{13}$C-labeled ethyl-coenzyme M, the primary and the two secondary isotope effects ($\alpha$ and $\beta$) could be deduced for intermediate formation as well as for the C-H bond activation of the intermediate:

| Isotope effect (IE) | Intermediate formation | C-H / C-D activation from intermediate |
|---|---|---|
| primary IE | 1.1 ± 0.1 | 2.5 ± 0.1 |
| $\alpha$ secondary IE (per D) | 1.25 ± 0.10 | 1.25 ± 0.10 |
| $\beta$ secondary IE (per D) | 1.00 ± 0.05 | 1.00 ± 0.05 |

The isotope effects measured for methane formation arise mainly from intermediate formation, because for the native substrate methyl-coenzyme M, formation of the intermediate is rate limiting. A secondary isotope effect of 1.191 ± 0.005 per D was measured. The primary solvent isotope effect ($H_2O/D_2O$) was estimated to be about 1.1 to 1.2. For methane formation, a large $^{12}$C/$^{13}$C kinetic isotope effect of $k_{12}/k_{13}$ = 1.050 ± 0.005, consistent with C-S bond breaking in the rate determining step, could be determined by analyzing the remaining substrate at high conversion.

The experimentally determined pattern of isotope exchange, the isotope effects, and the partitioning of the newly discovered intermediate are

discussed in the context of earlier results on the stereochemical course and mechanistic proposals reported in the literature. A new mechanism, judged to be consistent with all experimental data, is presented that proceeds through Ni(III)-hydride, hydrido-alkyl-Ni(III) species and σ-alkane-Ni(I) complexes.

## Zusammenfassung

Methyl-Coenzym M Reduktase (MCR) katalysiert den letzten Schritt der Methanbildung in allen methanogenen Archäen. In deren Stoffwechsel werden kleine organische Moleküle (überwiegend $CO_2$ oder Acetat) durch Wasserstoff schrittweise zu Methan als Endprodukt reduziert. Nach Umwandlungen durch diverse Metallenzyme entsteht als letzte Zwischenstufe Methyl-Coenzym M:

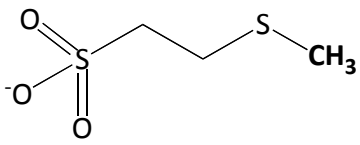


**Methyl-Coenzym M**

Das Nickelenzym MCR katalysiert nun die Reduktion von Methyl-Coenzym M mit dem Thiol Coenzym B zu den Produkten Methan und dem gemischten Disulfid der beiden Substrate gemäss folgendem Schema:

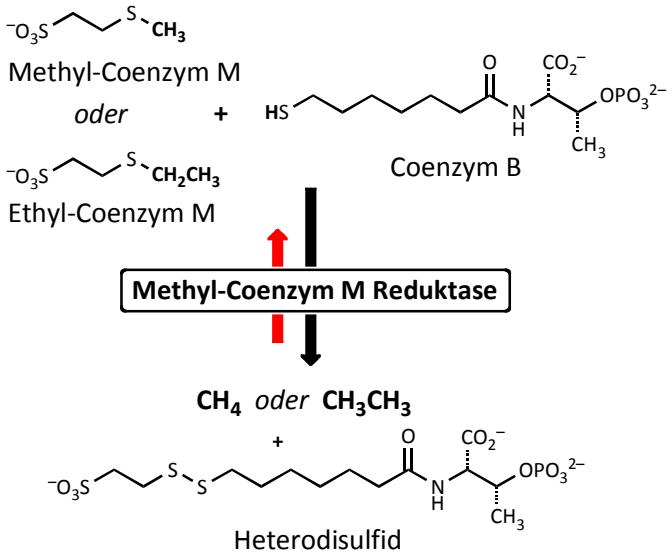


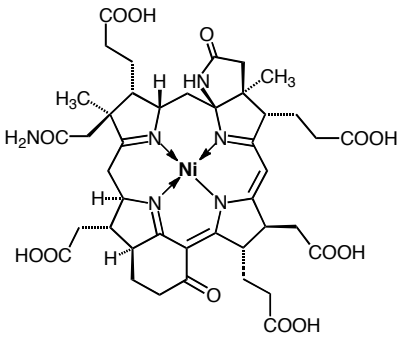


Coenzym F430

Tief in der aktiven Tasche des Enzyms ist Coenzym F430 (obige Abbildung, rechte Seite) verankert, dessen Nickel Zentralion im aktiven Enzymzustand in der Oxidationsstufe 1 vorliegt.

In der vorliegenden Arbeit wurde die endergone Rückreaktion (roter Pfeil) unter Gleichgewichtsbedingungen untersucht. Der Einsatz von $^{13}CH_4$ in der Gasphase ermöglichte es, das neu gebildete Methyl-Coenzym M als $^{13}CH_3$-S-Coenyzm M nachzuweisen.
Bei 60 °C und einem Methandruck von 1 bar wurde eine Methanaktivierungsrate von 11.4 nmol pro min pro mg reinem Enzym gemessen. Bei tieferen Temperaturen sank die Enzymaktivität; die Geschwindigkeit der Methanaktivierung konnte aber auch bei 4 °C noch genau bestimmt werden. Experimente bei unterschiedlichem Methandruck zeigten eine lineare Abhängigkeit der Reaktionsgeschwindigkeit vom Druck zwischen 0.05 und 8 bar.
Der gemessene Wert der Methanaktivierungsgeschwindigkeit durch das reine Enzym ist vergleichbar mit jenem Wert, der *in vivo* für die anaerobe Methanoxidation mit Sulfat bestimmt wurde[1]. Dieser Prozess findet in Konsortien von sulfatreduzierenden Bakterien und ANME-Arachäen, die verwandt sind mit methanogenen Archäen, statt. Gemäss der „Hypothese der umgekehrten Methanogenese“[2, 3] übernehmen die ANME-Archäen die anaerobe Oxidation von Methan mit Hilfe sehr ähnlicher Enzyme wie sie in der Methanogenese verwendet werden, aber in umgekehrter Richtung. Die Übereinstimmung der Methanaktivierungsrate durch die reine MCR mit derjenigen *in vivo* bestätigt den ersten Schritt der Hypothese der umgekehrten Methanogense.
Der Nachweis der *in vitro* Methanaktivierung durch MCR erlaubte es nun Isotopeneffekte der Methanaktivierung zu untersuchen. Die Isotopeneffekte wurden mit $CH_2D_2$ als Substrat und mit einem Gemisch von $CH_4$ und $CD_4$ gemessen.

Die Kombination beider Serien von Experimenten ermöglichte es den primären und sekundären Isotopeneffekt zu bestimmen. Der primäre Isotopeneffekt entspricht 2.44 ± 0.22, der sekundäre Isotopeneffekt 1.17 ± 0.05 pro D.

Aus Experimenten der Methanbildung in deuteriertem Medium konnte auf Zwischenprodukte innerhalb des katalytischen Zyklus geschlossen werden. Deuterium wird in das Substrat Methyl-Coenzym M bedeutend schneller eingebaut als Methan zu Methyl-Coenzym M umgewandelt wird (gesamte Rückreaktion). In Kombination mit Experimenten zur Methanaktivierung in deuteriertem Medium konnte darauf geschlossen werden, dass nur ein zusätzlicher Reaktionsweg vom Zwischenprodukt zum Substrat existiert, dargestellt als durchgezogener, roter Pfeil in der untenstehenden Skizze.

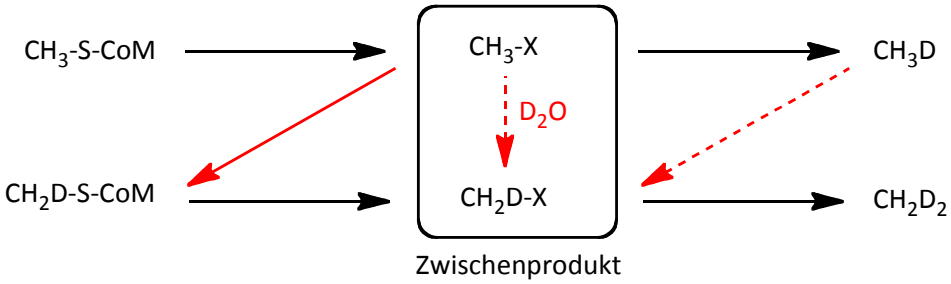


Das Verhältnis von Vorwärtsreaktion zu Rückreaktion (Methanbildung zu Substratbildung) ausgehend vom Zwischenprodukt beträgt 20:1. Bei Temperaturen unter 60 °C wird verhältnismässig mehr Substrat wiederhergestellt als Methan gebildet.
Untersuchungen mit dem nicht natürlichen Substrat Ethyl-Coenzym M zeigten, dass der Deuteriumeinbau ins Substrat ungefähr gleich schnell vor sich geht wie mit Methyl-Coenzym M, obwohl die Geschwindigkeit der Ethanbildung viel langsamer ist als bei der Methanbildung. Ein Verhältnis Vorwärtsreaktion zu Rückreaktion von 1:100 wurde bestimmt und erlaubte es, mehrere Zyklen von Deuteriumeinbau zu studieren, bevor ein nennenswerter Umsatz zu Ethan stattgefunden

hatte. Der Deuteriumeinbau fand überraschenderweise an beiden Kohlenstoffatomen innerhalb der *S*-Ethylgruppe statt. Durch $^{13}$C-markiertes Ethyl-Coenzym M konnten die Reaktionswege des Isotopenaustausches eindeutig verfolgt werden, wie in der untenstehenden Skizze dargestellt ($^{13}$C-Markierung rot).

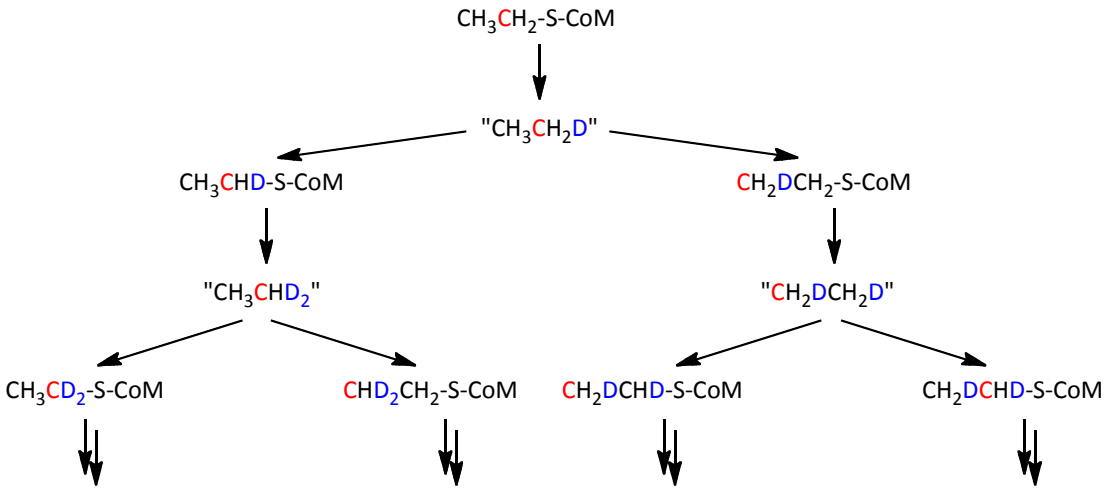


Im Zwischenprodukt (in "Anführungszeichen") ist die isotopologische Zusammensetzung des entstehenden Ethans offensichtlich bereits definiert. Anscheinend werden alle C-H und C-D Bindungen bereits ausgebildet und der Thioether Schwefel ist formal durch Deuterium ersetzt.

Mittels $^{13}$C-NMR-Spektroskopie („inverse-gated", bei gleichzeitiger Protonen- und Deuteriumbreitbandentkopplung) konnten alle Isotopologe, deren Anteil 0.1% überstieg, quantifiziert werden. Um die involvierten Isotopeneffekte zu bestimmen, wurde das kinetische System bis und mit dem geschwindigkeitsbestimmenden Schritt simuliert. Sowohl die verschiedenen Isotopeneffekte auf die Zwischenproduktbildung als auch auf die C-H/C-D-Bindungsspaltung im Zwischenprodukt wurden variiert bis eine gute Übereinstimmung mit der gemessenen Zeitabhängigkeit der verschiedenen Isotopologen erreicht wurde:

| Isotopeneffekt (IE) | Ausbildung des Zwischenproduktes | C-H / C-D Aktivierung vom Zwischenprodukt |
|---|---|---|
| Primärer IE | 1.1 ± 0.1 | 2.5 ± 0.1 |
| Sekundärer $\alpha$ IE (pro D) | 1.25 ± 0.10 | 1.25 ± 0.10 |
| Sekundärer $\beta$ IE (pro D) | 1.00 ± 0.05 | 1.00 ± 0.05 |

Für das natürliche Substrat Methyl-Coenzym M ist die Bildung des Zwischenproduktes geschwindigkeitsbestimmend. Die Isotopeneffekte der Methanbildung entsprechen deshalb denjenigen der Ausbildung des Zwischenproduktes. In einem Konkurrenzexperiment wurde ein sekundärer Isotopeneffekt von 1.191 ± 0.005 pro D auf die Methanbildung gemessen. Der Lösungsmittelisotopeneffekt ($H_2O/D_2O$) betrug ungefähr 1.1 bis 1.2. Der kinetische $^{12}C/^{13}C$ Isotopeneffekt auf die Methanbildung wurde mittels Analyse des verbliebenen Substrates bei hohem Umsatz gemessen und betrug 1.050 ± 0.005. Dieser ausgeprägte Isotopeneffekt bestätigt dass die C-S Bindung im geschwindigkeitsbestimmenden Schritt gespalten wird.

Die Bedeutung der Entdeckung eines Zwischenproduktes, des Musters des Isotopenaustausches und der gemessenen Isotopeneffekte wird im Lichte früherer mechanistischer Vorschläge sowie in Bezug auf den früher berichteten sterochemischen Verlauf der Reaktion diskutiert.
Um alle gemessenen Isotopeneffekte und das gefundene Isotopenaustauschmuster zu erklären, wird ein neuer Mechanismus diskutiert, der über ein Ni(III)-hydrid, eine hydrido-alkyl-Ni(III) Spezies und über einen σ-koordinierten Alkan-Ni(I) Komplex verläuft.

# 1 Introduction

## 1.1 Methanogenesis and Methane Oxidation

### 1.1.1 Methanogenic Archaea

Methanogenic archaea originated over 2 billion years ago[4] when the earth contained only trace amounts of molecular oxygen[5]. Archaea[6, 7] are single-celled microorganisms lacking a cell nucleus. They form the third phylogenetic domain next to bacteria and eukaryotes[8-10]. It is believed that in the Proterozoic ara (between 2500 and 542 million years ago) the atmosphere contained mainly $H_2$, $NH_3$, $CH_4$, CO, $CO_2$ $N_2$ and $H_2O$[11]. Already during that time cyanobacteria were producing molecular oxygen. However, until about 600 million years ago most of the oxygen was used up to oxidize inorganic material, in particular iron and sulfide[12]. At the same time, the greenhouse gas methane generated by methanogenic archaea and by geochemical processes was oxidized photochemically which led to a "snowball event", a dramatic decrease of the global temperature[13].

Nowadays, molecular oxygen makes up 21% of the atmosphere, so methanogenic archaea adapted to an oxygen-free atmosphere can only continue to exist in specific anaerobic environments, often under extreme conditions. Known habitats of methanogenic archaea include lake sediments, rice fields, guts of animals, sewage plants, marine sediments and hot springs[6].
Examples of extreme conditions include a growth optimum at 106 °C[14], very high salt concentrations[15], or very acidic environments (down to pH = 0.7)[16].
These extreme forms of living testify to the fact that archaea are highly evolved species since they repeatedly had to adjust to major global changes in atmospheric composition and temperature over the long

time period since their first appearance. Their biochemistry involves chemical transformations that are unknown in other organisms and, in some cases, also in laboratory chemistry. One such example is the methane forming and functionalizing reaction that is the topic of this thesis.

### 1.1.2 The global methane cycle

Most of the methane in the biosphere has been produced in an anaerobic environment by methanogenic archaea. The amount formed per year is estimated to be $10^9$ metric tons (1 Gt p.a.)[17]. In addition, methane is also generated geochemically and thermogenically which can be distinguished by relative depletion of $^{13}C$[18].
At present, the atmosphere contains 1.8 ppm (by volume) methane, a significant increase relative to the values of 250 years ago (0.7 ppm)[19], which is mainly due to human agricultural activity (rice fields and animal farming)[20]. Because methane is considered to be 21 times more active as a greenhouse gas than $CO_2$ (calculated for 100 years[19]) this has a large impact on climate-change.

In the atmosphere, the main sink of methane is the photochemical degradation to $CO_2$ by UV light[21]. However, microorganisms oxidize a significant amount of the newly generated methane before it reaches the atmosphere. This biological methane degradation is carried out at about 0.6 Gt per year by aerobic bacteria and to a slightly lesser extent by anaerobic methanotrophs[17] (**figure. 1.1**).
The anaerobic oxidation of methane[22] is mainly carried out with sulfate as the ultimate electron acceptor (figure 1.1, orange)[17]. This process appears to result from cooperation of sulfate reducing and methane oxidizing bacteria[1, 23]. The methane oxidizing archaea (so-called ANME[24, 25]) are genetically related to methanogenic archaea and are believed to carry out methane functionalization by using enzymes and pathways very similar to those used by the methanogens. This

"hypothesis of reverse methanogenesis" will be discussed in more detail in Chapter 2.

Additional anaerobic methane oxidation pathways utilize nitrate[26], Fe(III) and Mn(IV) as electron acceptors[17].

Methane formation by plant leaves was once considered to have a high impact on the methane budget[27] but experiments showing that plant leaves can form methane in large amounts[27] could not be reproduced[28].

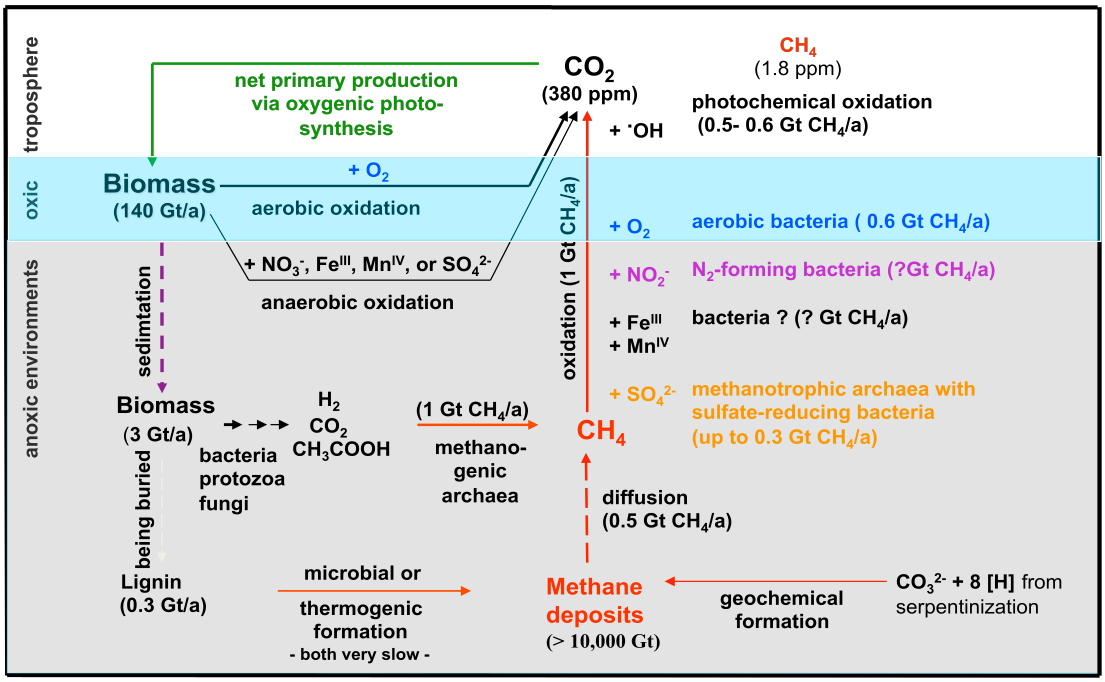


**Figure 1.1**: Important processes in the global methane cycle[17].

### 1.1.3 Biochemistry of methanogens

Biomass is fermented in anaerobic environments to $C_1$-compounds ($CO_2$, formate, dimethyl sulfide, methanethiol, methanol, methylamines) and to acetate. These compounds are the substrates for methanogens[29], which convert them by respiration with hydrogen to methane as the last step of biomass decomposition.

The reduction of $CO_2$ to methane represents the major pathway, where the carbon atom undergoes an 8-electron reduction to finally give methane (**figure 1.2**).

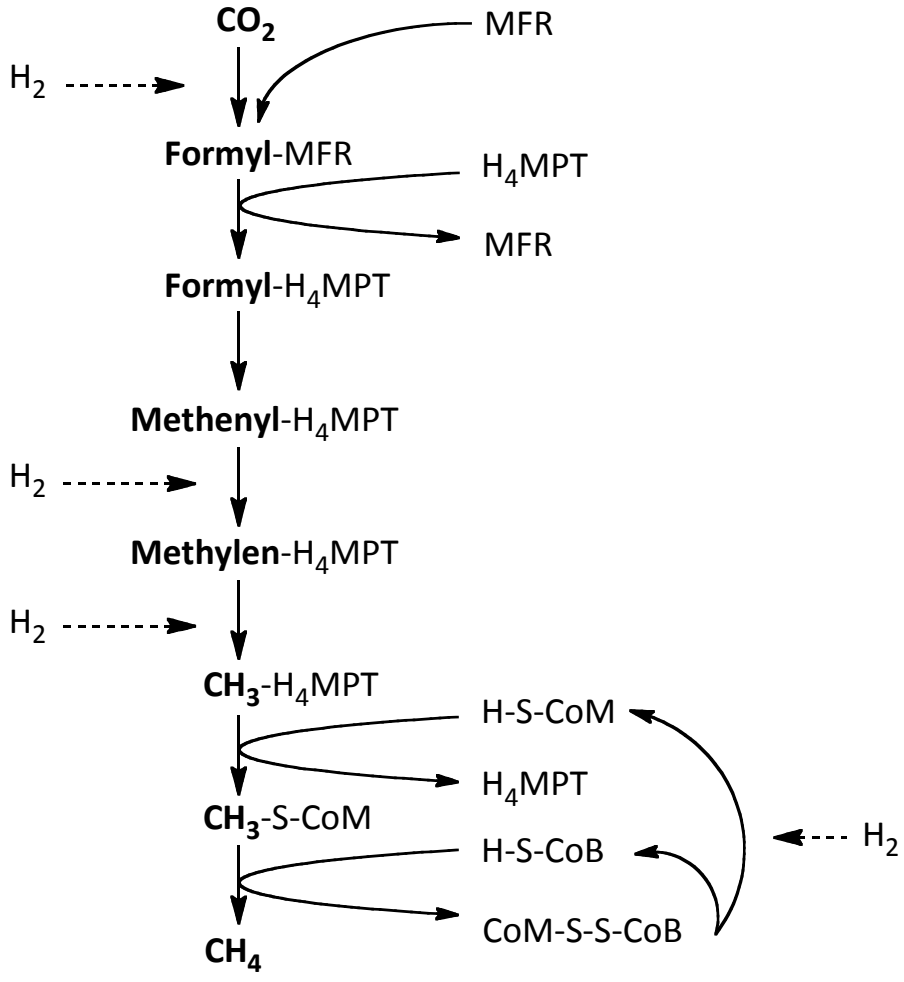


**Figure 1.2**: The 8-electron reduction pathway from carbon dioxide to methane.

The reduction of $CO_2$ to the level of formate is catalyzed by the molybdoenzyme formylmethanofuran dehydrogenase[30] in the first of four reduction steps. The formyl group is then transferred to tetrahydromethanopterin ($H_4$MPT)[31] at which, after cyclisation to methenyl-$H_4$MPT[32], two reduction steps occur to yield a *N*-methyl group[33]. This nitrogen-bound methyl group is transferred by coenzyme M methyl-transferase[34] to the thiol group of coenzyme M.

Methyl-coenzyme M reductase (MCR) is the nickel-containing enzyme that reduces the sulfur-bound methyl group to methane with the thiol coenzyme B as the reductant and the heterodisulfide of coenzymes M and B as the second product[35]. Coenzyme B is regenerated by heterodisulfide reductase[36] in an exergonic reaction ($\Delta G^{0'}$ = -39 kJ $mol^{-1}$ [37]) that plays a central role in energy gain and energy balance of the cells.

The overall reaction (see equation below) is exergonic and therefore allows the organism to live from this process as the sole energy source.

$$CO_2 + 4\ H_2 \ = \ CH_4 + 2\ H_2O \quad \Delta G^{0'} = -131\ kJ\ mol^{-1}\ [29]$$

The first step, namely the activation of $CO_2$, is endergonic by 16 kJ $mol^{-1}$. In order to overcome this first step a coupling to the exergonic reduction of the heterodisulfide was proposed[37, 38]. A protein complex containing all required enzymes together was identified recently which supports this hypothesis[39].

The exergonic reaction of the methyl transferase ($\Delta G^{0'}$ = -30 kJ $mol^{-1}$) is coupled to a sophisticated energy-accumulating system that is also linked with the heterodisulfide reductase used for ATP production[37]. The system involves $Na^+$ gradients[40] coupled to $H^+$ gradients and allows organisms to synthesize ATP from reactions where a single turnover would not be enough to produce one ATP molecule[41].

Substrates other than $CO_2$ can only be processed by members of the order *Methanosarcinales*[29]. They convert formate to $CO_2$ and to hydrogen prior to methanogenesis. Acetate is disproportionated to a methyl group and to $CO_2$, which undergoes the full reduction pathway. The methyl group is directly transferred to methyl-coenzyme M, as also seen for other methylated substrates (dimethyl sulfide, methanethiol, methanol, methylamines). Methyl-coenzyme M is therefore the central intermediate regardless of the initial substrate.

While there are different pathways towards methyl-coenzyme M, the last reactions are always the same: reduction with the thiol coenzyme B to methane (catalyzed by MCR) and regeneration of coenzyme B (catalyzed by heterodisulfide reductase). Hence, MCR is the key enzyme for methane formation and it is not a surprise that it represents about 10% of the total amount of protein[42].

## 1.2 The Enzyme Methyl-Coenzyme M Reductase (MCR)

### 1.2.1 Substrates and products of MCR

The reduction of an alkyl sulfide with a thiol to give an alkane and a disulfide is a reaction not known in non-enzymatic chemistry. MCR, however, catalyzes such a reaction. The reaction sequence (including the chemical structures of substrates and products) is shown in **figure 1.3**.

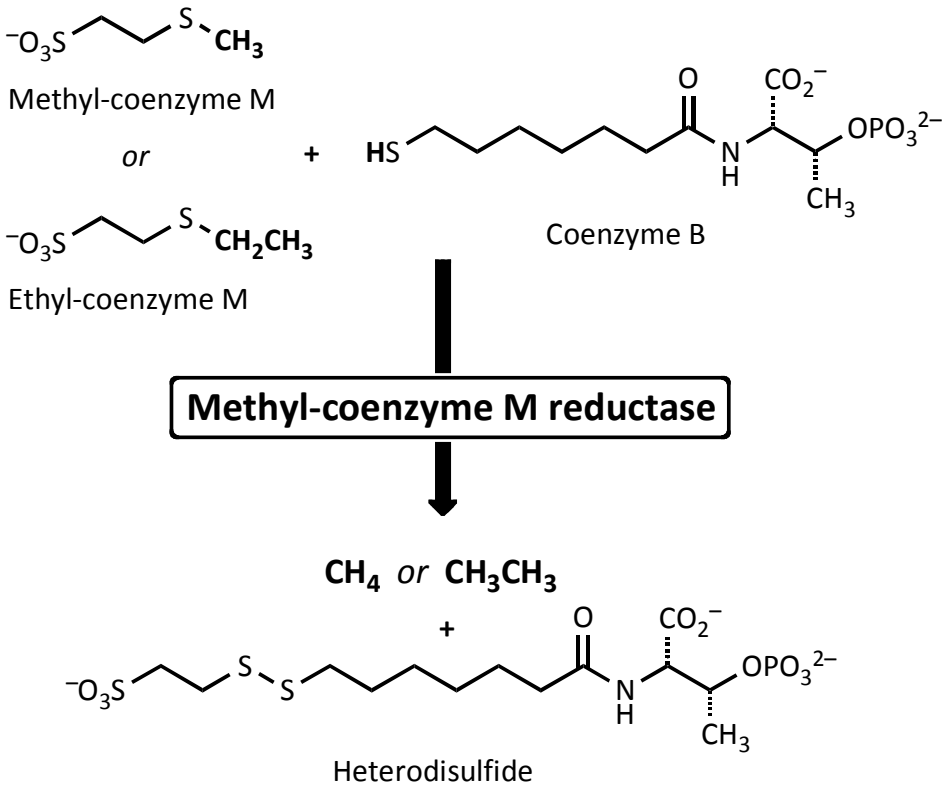


**Figure 1.3**: The catalytic reaction of MCR. Methyl- or ethyl-coenzyme M (Me-S-CoM or Et-S-CoM) is converted with the thiol coenzyme B (HS-CoB) to two products: the heterodisulfide (between coenzyme M and coenzyme B) and the corresponding alkane (methane or ethane).

*In vivo*, methyl-coenzyme M is produced by a methyl transferase. The second substrate coenzyme B is delivered by the heterodisulfide reductase. At the same time, heterodisulfide reductase removes the product heterodisulfide and regenerates the methyl group carrier coenzyme M. Methane is the final waste product generated by methanogenic archaea.

*In vitro* (with purified MCR), ethyl-coenzyme M can also serve as a substrate to give the corresponding product ethane[43, 44]. In order to remove the heterodisulfide, an external reductant (such as $Ti^{III}$-citrate) can be added instead of the heterodisulfide reductase, allowing coenzyme B to be used catalytically. Adding an excess of coenzyme B is another option if full conversion is required.

### 1.2.2 Structure of MCR

Crystal structures of MCR in the catalytically inactive $Ni^{II}$ state revealed the enzyme to be an $\alpha_2\beta_2\gamma_2$ hexamer with $C_2$ symmetry and two active sites[45] (**figure 1.4**).

**Figure 1.4**: The crystal structure of MCR ($MCR_{ox1\text{-}silent}$ form)[45]. Colors of the subunits: α (red), α‘ (orange), β (green), β‘ (light green), γ (blue), γ‘ (light blue). The two F430 prosthetic groups are highlighted in yellow.

The enzyme contains 5 post-translationally modified amino acids: 4 different methylated amino acids and a thioglycine (carbonyl oxygen replaced by sulfur)[45]. The benefit of these modifications is not known to date.

The nickel-containing coenzyme F430 (see section 1.2.3) is the prosthetic group; it is anchored tightly in the protein via its carboxylate side chains. **Figure 1.5** shows the active site containing coenzyme M (an inhibitor) and the substrate coenzyme B. Glutamine α147 coordinates via its carbamoyl-oxygen to the $Ni^{II}$ in cofactor F430 from the face where the propionic acid side chains are anchored to the protein (also called the α-side of free F430 or the distal face in the enzyme active site).

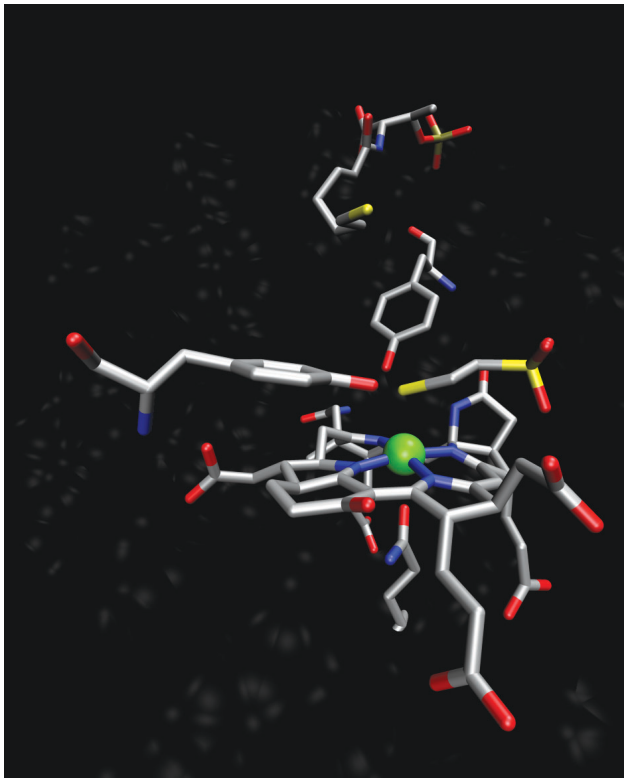

**Figure 1.5**: View into the active site of MCR in the $MCR_{ox1\text{-}silent}$ form. The nickel center is drawn in green, oxygen red, nitrogen blue and sulfur yellow. The inhibitor coenzyme M (coordinating with its thiolate group to the nickel center) and the second substrate coenzyme B are bound. Two tyrosine side chains are pointing into the active site with their OH groups.

The crystal structure of the $MCR_{ox1\text{-}silent}$ form of the enzyme with coenzyme M and coenzyme B bound displays a long channel leading from the enzyme surface towards the proximal face of F430 for both active sites. The channel is polar and wider near the surface and becomes very narrow and hydrophobic near the entrance into the hydrophobic cavity above the macrocycle of F430. A less well-resolved X-ray structure of MCR without substrates or inhibitors bound shows a wider and less ordered channel structure[46]. Although no crystal structures with only methyl-coenzyme M bound are available, it is reasonable to assume that the binding of the first substrate at the active enzyme leads to an ordering of the protein chains forming the channel. Such ordering can increase the affinity towards the second substrate

(coenzyme B), which binds in the channel, and would explain the kinetically observed ordered substrate binding. **Figure 1.6** depicts the described channel and the binding of substrates and inhibitors schematically.

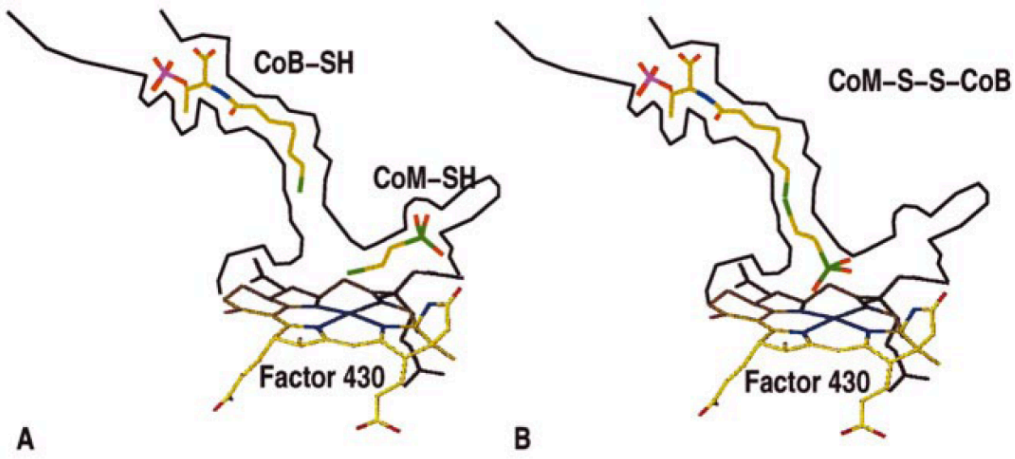


**Figure 1.6**: **A**) Inhibitor-substrate ternary complex ($MCR_{ox1\text{-}silent}$): inhibitor coenzyme M and the substrate coenzyme B bound (same crystal structure as in figure 1.5). **B**) Pseudo-ternary product complex ($MCR_{silent}$): the heterodisulfide is bound to the channel, but the other product methane is missing[46].

In the crystal structure mimicking the ternary substrate complex ($MCR_{ox1\text{-}silent}$, in the non-active Ni(II) valence form) the sulfur atom of coenzyme B is about 8 Å away from the nickel center. The threonine-phosphate moiety of coenzyme B is fixed at the entrance of the channel that is now closed and prevents coenzyme B from coming closer to the active site.

In experiments with the active enzyme (Ni(I)), the coenzyme B analog trifluormethyl-coenzyme B was used to form an inhibitor-inhibitor ternary complex. Determination of the distance between the fluorine atoms and the nickel center by $^{19}$F-ENDOR spectroscopy revealed that

the sulfur atom is 2 Å closer to the nickel center in this EPR-active Ni(I) form than in all crystal structures of Ni(II) forms[47].
This experiment is an important milestone demonstrating that the solved crystal structures show the enzyme in a conformation different from that of the active ternary complex. EPR experiments of a very similar state ("red2", see section 1.2.6) reveal that at least one nitrogen atom of the F430 hydrocorphin is further away from the nickel center than the others. Thus it is postulated that binding of coenzyme B induces a major conformational change, which distorts the macrocycle and allows coenzyme B to come closer to the active site.

Specific labeling within the hydrocorphin followed by reconstitution of the enzyme would be required to study which part of the macrocycle is distorted. Unfortunately, it has not yet been possible to obtain a reconstituted active enzyme. One reason might be that the two α-chains are entangled and contribute to both active sites. The protein may require unknown chaperones to fold correctly even if the post-translationally modified proteins are used. The other obstacle is that both nickel centers have to be in their Ni(I) oxidation state for the enzyme to be fully active (see 1.2.3 and 1.2.6) and re-reduction from Ni(II) to Ni(I) in the enzyme has not been achieved so far.

### 1.2.3 Coenzyme F430

The prosthetic group coenzyme F430[48] is non-covalently bound in the active site and can be liberated by denaturing the enzyme with dilute perchloric acid. The name F430 originates from the strong UV absorption maximum at 430 nm seen for the Ni(II) form.
Structure elucidation by biosynthethic $^{13}$C-labeling and NMR studies[49-51] identified coenzyme F430 as the most reduced tetrapyrrole found in nature (**figure 1.7**).

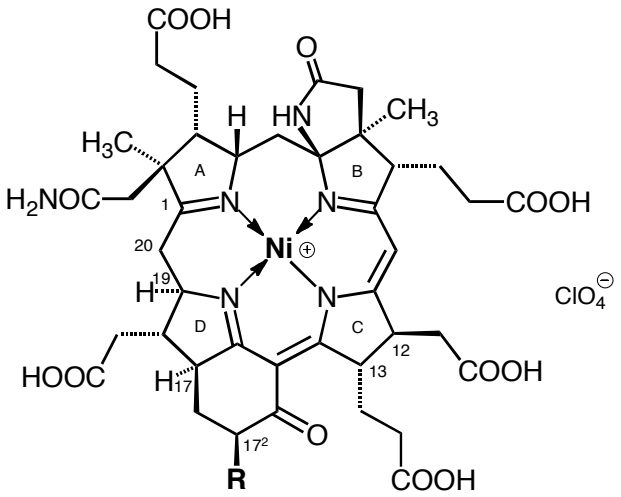


Coenzyme F430 (R = H)
Coenzyme F430X (R = $SCH_3$)

**Figure 1.7**: Structure of coenzyme F430 (found in all methanogenic archaea and in ANME-2). The modified form F430X is found in ANME-1.

The π-system of coenzyme F430 is interrupted between the A/B and D/A rings. Since the carbon atom at position 20 is still present, coenzyme F430 is called a hydrocorphin[52].

In order to study the isolated cofactor in aprotic solvents it is usually converted into the pentamethyl ester. Esterification of all side chain carboxylates allows electrochemical generation of the corresponding Ni(I)[53] as well as the Ni(III)[54] forms of the cofactor in the absence of protein (**figure 1.8**). The redox potentials (vs. NHE) are -0.65 V for Ni(II/I) and +1.41 V for Ni(III/II).

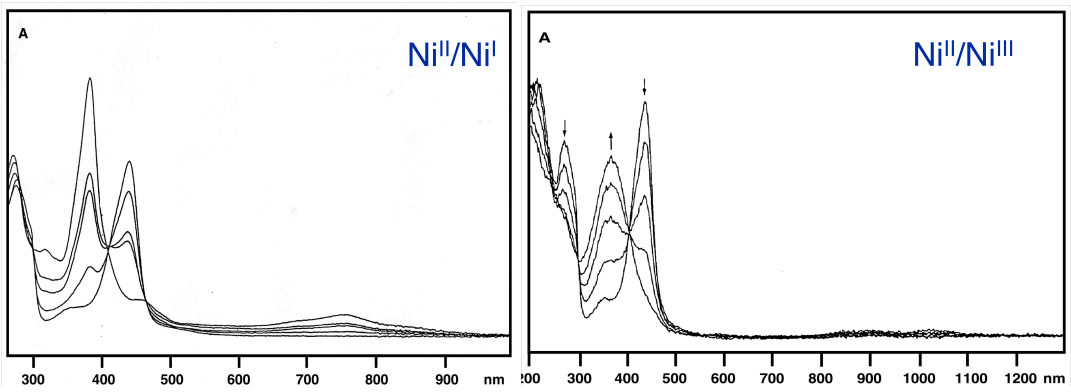


**Figure 1.8**: UV-Vis spectra of the electrochemically generated Ni(I) and Ni(III) oxidation states of esterified coenzyme F430 in acetonitrile[53, 54].

The high degree of saturation in the coenzyme F430 ligand is required for a metal-centered oxidation and reduction of Ni(II). Reduction of the only slightly less saturated 12,13-didehydro-coenzyme F430 pentamethyl ester, for example, proceeds at the ligand to form the corresponding π-radical[55].

The saturated carbon atoms between the A/B and D/A rings could serve as hinges to provide the flexibility needed to distort the ligand and may create a second adjacent coordination site. The fine-tuning of the saturation to allow Ni I, II and III oxidation states and the flexibility of the ligand illustrate the high degree of evolutionary optimization of MCR and its cofactor F430.

Proteins that are close homologs of MCR and also have nickel-containing prosthetic groups could be extracted from organisms known to carry out anaerobic oxidation of methane (ANME archaea[24]). In the ANME-2 subtype, the yellow cofactor is identical to coenzyme F430. In ANME-1, the cofactor is (17$^2$*S*)-17$^2$-$CH_3S$-coenzyme F430 (see figure 1.7). Its structure was recently elucidated in our group[56].

Experiments with isolated coenzyme F430 and its pentamethyl ester give important insights into the spectroscopic properties and reactivity of the nickel center in its different oxidation states. With methylating

agents such as methyl iodide or trimethylsulfonium ions methane formation catalyzed by Ni(I)F430 can be mimicked[57]. With the natural substrates of MCR, however, no methane formation catalyzed by free coenzyme F430 or its derivatives could be demonstrated so far.

### 1.2.4 Purification of highly active enzyme

Strictly anaerobic conditions are required to obtain pure MCR in the active Ni(I) oxidation state. A successful procedure was developed in the group of R. K. Thauer in Marburg[58-60] from cells of the organism *Methanothermobacter marburgensis*[61]. The addition of the inhibitor coenzyme M during all purification steps, for example, is mandatory since otherwise even trace amounts of oxygen inactivate the very sensitive empty active site. Here, only an overview of the purification procedure is given. Details can be found in section 6.1.

Before harvesting the cells, the cell-suspension is treated with pure hydrogen, cooled down, and centrifuged while still under hydrogen. After disrupting the cells (ultrasound) and removal of cell debris (centrifugation), proteins other than MCR can be precipitated with dilute ammonium sulfate. A final chromatography step allows the separation of the two isoenzymes[35] MCR-I and MCR-II.

All experiments described in this thesis were performed with purified MCR-I which was obtained routinely in more than 90% Ni(I) form.

### 1.2.5 Kinetic parameters of MCR-I

Investigation of the methane-forming rate (GC) by varying the concentration of the two substrates allowed elucidating the order of substrate binding already before the first crystal structure of MCR was solved[35].

The temperature optimum of methane formation is 65 °C[62] and the pH optimum 7.5[35]. An enzyme activity of about 20 U (µmol methane per minute) per mg protein was routinely obtained at 60 °C with the natural

substrates (section 6.1). Kinetic parameters for various substrates and inhibitors are listed in **table 1.1**.

**Table 1.1**: Kinetic parameters[44] for substrates (**A**) and selected inhibitors (**B**) of MCR. For the second substrate coenzyme B an apparent $K_M$ value of 0.2 mM was measured[62].

| **A**: substrates | app. $K_M$ [mM] | $V_{max}$ [U $mg^{-1}$] |
|---|---|---|
| $CH_3$-S-CoM | 5 | 30 |
| $CH_3CH_2$-S-CoM | 20 | 0.1 |

| **B**: reversible inhibitors | app. $K_i$ [mM] |
|---|---|
| H-S-CoM | 4 |
| $CH_3CH_2CH_2$-S-CoM | 2 |
| $CH_2$=$CHCH_2$-S-CoM | 0.1 |

| irreversible inhibitors | $[I]_{0.5V}$ [mM] |
|---|---|
| $BrCH_2CH_2SO_3^-$ | 0.002 |
| $BrCH_2CH_2CH_2SO_3^-$ | 0.0001 |

In early experiments (before 2002, when pure, highly active enzyme became accessible[59]) the enzyme was purified with a very low activity and "reactivated" by the addition of Ti(III)-citrate to increase the specific activity. In other experiments, cell-free extracts were used which contained all other soluble enzymes as well. The values of kinetic parameters obtained in these early experiments therefore have to be interpreted with care. However, they allowed screening a large number of possible substrates and inhibitors[43, 63].

With the pure and active enzyme, the reductant Ti(III)-citrate is still included stoichiometrically for some experiments (in combination with a catalytic amount of hydroxy-cobalamin) in order to cleave the heterodisufide that is formed during the reaction, thereby avoiding product inhibition and thus extending the range of linear enzyme activity (section 6.2).

### 1.2.6 Enzyme states

The amount of active cofactor Ni(I)F430 in an enzyme preparation can be deduced by UV-Vis spectroscopy. The active Ni(I) form has its absorption maximum at 385 nm, the inactive Ni(II) form at 420 nm. Both spectra are very similar to those of free cofactor 430 (see 1.2.3). Fully active enzyme exhibits a moss-green color due to the second absorption band at 720 nm. 10% of the inactive Ni(II) form is already apparent to the naked eye due to its yellow tint.

EPR spectroscopy proved to be a rewarding tool to obtain more details about the active site. With routine CW spectroscopy at X-band, 3 main categories of enzyme states can be easily distinguished: red1, red2 and ox1[64]. Sophisticated pulsed EPR methods (also at higher fields) and the use of ENDOR spectroscopy allowed resolving hyperfine couplings in order to prove binding of ligands or to determine distances to the nickel center.

Ni(I) states without the second substrate coenzyme B bound are named red1. The subscript indicates which substrate or inhibitor is bound (**table 1.2 A**). At W-band, two *g*-values of the red1a state (a for "absence" of substrates) can be resolved, depending on whether the other active site is occupied or not[65].

**Table 1.2**: EPR active enzyme states. The four nitrogen atoms of the tetrapyrrole symbolize the cofactor F430. **A**: red1 states (containing a Ni(I) center[65]); **B**: red2 states (containing a H-Ni(III) bond[66]); **C**: ox1 state (containing a S-Ni(III) bond[67]); **D**: states containing a C-Ni(III) bond[68-70].

| **A**: red1 states (coenzyme B not bound) | | |
|---|---|---|
| red1a (left)<br>red1c (R = H)<br>red1m (R = $CH_3$)<br>red1e (R = $CH_3CH_2$) | 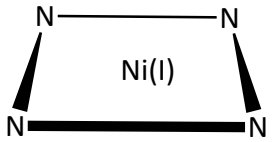 | 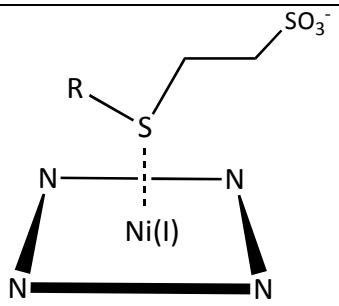 |
| **B**: red2 states (coenzyme M and coenzyme B bound) | | |
| red2a (left)<br>red2r (right) | 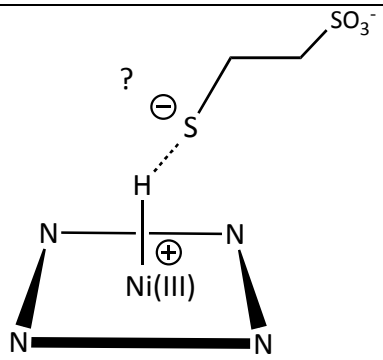 | 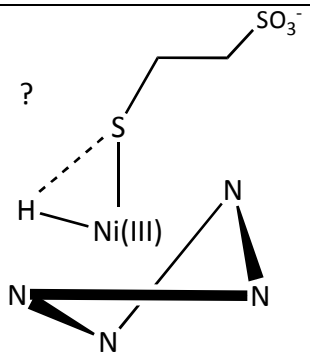 |
| **C**: ox1 state (coenzyme M and coenzyme B bound) | | |
| ox1 | 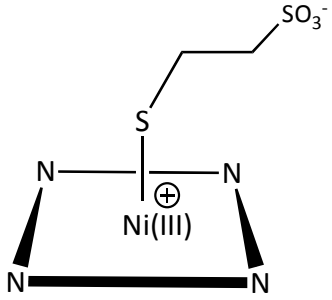 | |
| **D**: alkyl states (carbon nickel bond assured) | | |
| BPS (left)<br>BrMe (right) | 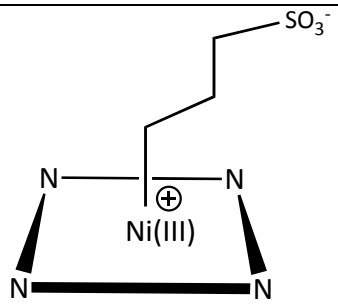 | 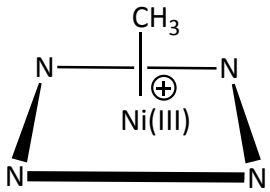 |

When both substrates are added to active MCR, methane formation occurs and only the red1m state can be detected. An analog of the ternary substrate complex can be observed when the inhibitor coenzyme M and the second substrate coenzyme B are added to $MCR_{red1a}$ giving the red2 state. This state can be induced only to 50%; the remaining active sites stay in the red1c form[62]. W-band EPR spectroscopy of the red2 form resolved two sub-states[66], a rhombic form with at least one of the nitrogen atoms of the tetrapyrrole being further away from the nickel center than the others (red2r) and an axial form (red2a) with a hydride bonded to the nickel (**table 1.2 B**). The red2 states are mechanistically very important, because a nickel-hydrogen bond was confirmed and this state is probably closest to the elusive ternary-substrate complex.

Treating the cells with $CO_2/N_2$ prior to harvest induces the ox1 state. Induction of this enzyme state with $^{33}$S-coenzyme M proved the existence of a Ni-sulfur bond[67]. Formally, a Ni(III)-thiolate is formed (**table 1.2 C**). The oxidation state of $MCR_{ox1}$ was a matter of debate for some time because its EPR spectra is very similar to Ni(I) states ($MCR_{red1}$) but it is now well established that $MCR_{ox1}$ is a Ni(III) species with the unpaired electron predominantly in the $d_{x2-y2}$ orbital[71]. Reaction of the isolated Ni(II) coenzyme F430 pentamethyl ester with thiyl radicals leads to an EPR spectrum almost identical to that of $MCR_{ox1}$[72] which further assures the formal Ni(III) oxidation state.

With the strong inhibitor 3-bromopropane sulfonate (BPS) and with methyl iodide or bromide (BrMe), the corresponding alkyl-Ni(III) species with authentic Ni-C bonds (**table 1.2 D**) can be prepared in the active site as verified by EPR spectroscopy[68-70].

The range of different enzyme states generated with substrates and inhibitors revealed the ability of the active site to form Ni-H, Ni-S, and Ni-C bonds. Further, the red2r state demonstrates that the prosthetic

group must be able to distort its ligand and may make two adjacent coordination sites available for the catalytic cycle.
It has to be emphasized, however, that no intermediate relevant to catalytic turnover with the natural substrates could be observed spectroscopically so far. Corresponding experiments are ongoing.

### 1.2.7 Possible mechanisms of MCR

The reaction mechanism of MCR is not known. Many different mechanisms have been proposed[45, 46, 54, 73-76] and diverse reactivity of the nickel center was discovered by spectroscopic analysis of different enzyme states. The reaction catalyzed by MCR involves the cleavage of the C-S bond and the S-H bond in the substrates and the formation of the S-S bond and a C-H bond in the products. Formally, the two involved sulfur atoms are oxidized to the disulfide and the methyl group is reduced from the –II to the –IV oxidation state in the product methane.
With enantioselectively prepared [1′-$^{2}$H, 1′-$^{3}$H]-ethyl-coenzyme M as the substrate, net inversion of configuration to give chiral ethane was reported[77]. This finding supports a mechanism starting with nucleophilic attack of the Ni(I) center on the methyl carbon of methyl-coenzyme M in an $S_N2$ fashion and excludes formation of a freely rotating methyl radical as an intermediate.
Based on DFT calculations, however, Siegbahn and coworkers proposed an $S_R2$ substitution by Ni(I) at sulfur. The leaving group, a free methyl radical, was proposed first as an intermediate[73] and later presented as a transition state, described as a "transient methyl radical"[74]. Alternatively, radical formation could occur in other elementary steps. The separation of mechanisms into "radical" and "non-radical", however, can be ambiguous since the enzyme states containing a Ni(III)-H, Ni(III)-C or Ni(III)-S bond can all be regarded to some extent as a Ni(II) center with an unpaired electron on the ligand. For the ox1 state, for example, a spin density of 7 ± 3% on the sulfur ligand was

calculated[71]. In order to give a comprehensive overview of the different reaction pathways possible, mechanisms involving only non-radical steps are described here as "corner stones" of possible electron distributions.

When dissecting the substrates in a formal, heterolytic way, the thiol group represents a proton source and the methyl-thioether a "$CH_3^{+"}$ source. Upon interaction with the Ni(I) center, a formal reassignment of electrons could give a Ni(III) center with either a hydride or $CH_3^-$ bound to it. Since formal Ni(III) oxidation states have been observed in the enzyme and in the free F430 cofactor, intermediates of this type are reasonable. Together with the redox abilities of the two sulfur atoms, a variety of different reaction mechanisms can be formulated by which methyl-coenzyme M could be reduced to methane (**Figure 1.9**).

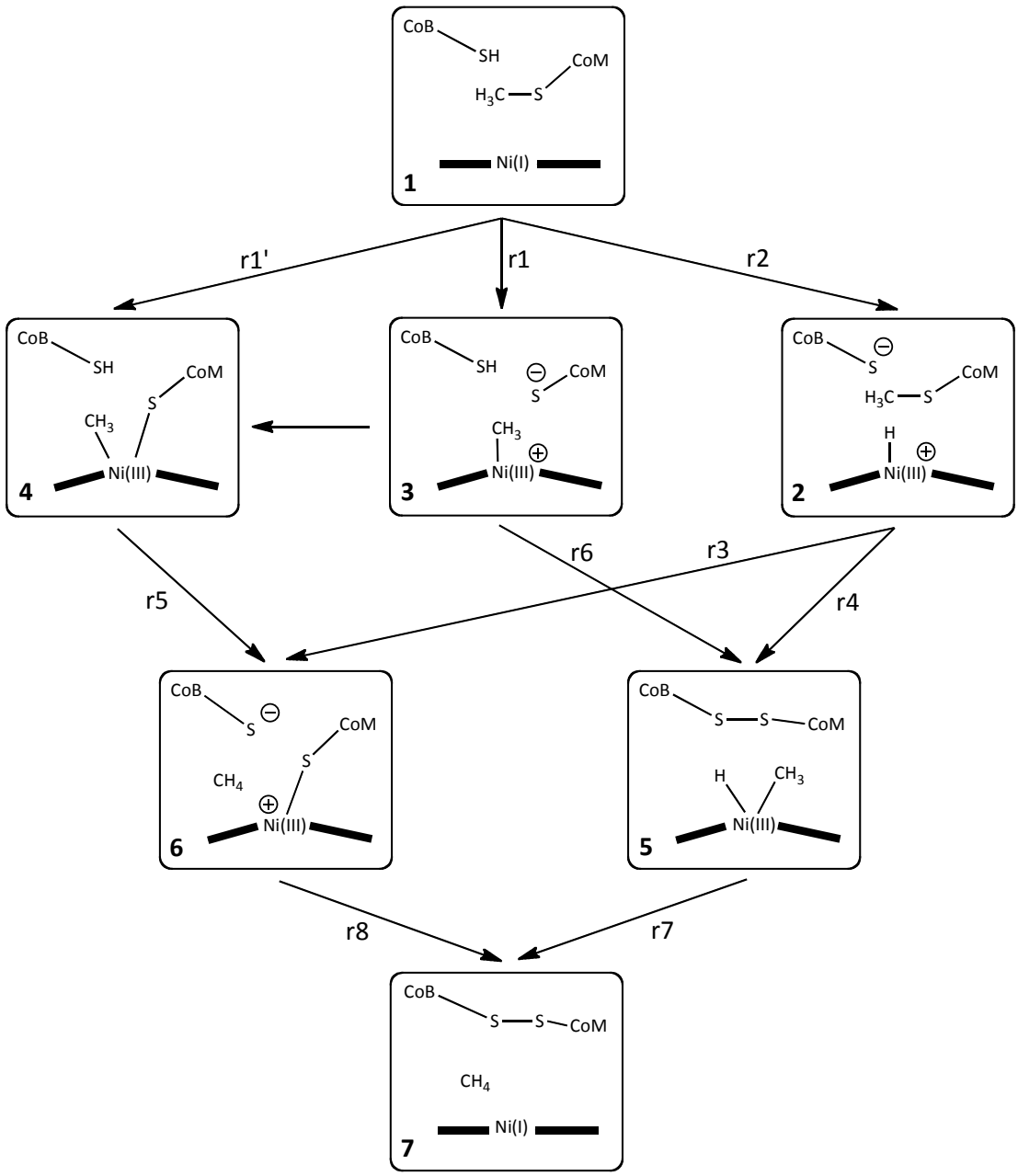


**Figure 1.9**: Schematic conceivable heterolytic reaction pathways for methane formation catalyzed by the Ni(I)-cofactor F430 (represented as bold lines) in the active site of MCR. The bend in the coenzyme F430 ligand symbolizes the possibility of two adjacent coordination sites that might be accessible for some intermediates.

The first step after formation of the ternary substrate complex (**1**) can be regarded as a nucleophilic substitution at carbon (r1) or a protonation at the nickel center (r2). After formation of the methyl-Ni(III) intermediate

(**3**), coordination of the thiolate could occur to give the intermediate (**4**) which is also obtained via a direct oxidative addition of the C-S bond (r1').

Formation of the second intermediate is less obvious for some of the depicted steps. The ox1-type intermediate (**6**) is formed by protonation (r5) of the methyl-Ni(III) complex (**4**). The same intermediate is obtained when the H-Ni(III) complex (**2**) reacts with methyl-coenzyme M. This reaction (r6) can be an $S_N2$ substitution of hydride at carbon followed by coordination of the resulting thiolate. A concerted mechanism (a σ-bond metathesis-type reaction) would lead to the same product. Formation of the hydrido methyl complex (**5**) would require reduction of the proton of coenzyme B to a hydride (r3) or the reduction of the *S*-methyl group of methyl-coenzyme M to a $CH_3^-$ ligand (r4), both using thiolate as the reductant.

The ternary product complex (**7**) is formed by reductive coupling of either the hydrido methyl complex (r7) or the complex containing two thiolates (r8).

The presence of two active sites in the enzyme evokes the question whether they operate independently or are in some way coupled. A "two-stroke engine" mechanism was postulated[62] in which the reaction steps at the two active sites are shifted in phase and thus allow an energetically uphill process to be coupled with an exergonic step. This hypothesis is supported by the fact that some enzyme states can only be obtained in 50% conversion and that the red1a-state exhibits two signals with different *g*-values in W-band EPR experiments, depending on whether the second active site is occupied or empty. A coupling might arise from a conformational change upon binding of substrates or by other mechanisms. So far, however, no hard experimental evidence for such a coupling has been obtained.

## 1.3 Mechanisms of Alkane C-H Bond Cleavage

### 1.3.1 General aspects

Since methane formation catalyzed by MCR is only slightly exergonic, its microscopic reverse (methane oxidation) must take place to some extent (see Chapter 2). However, alkane C-H bonds are inert and accordingly difficult to cleave. This is due to the absence of "functional groups" that could interact with the chemical reagents or stabilize potential intermediates and thus allow the reaction to proceed. Cleavage of an alkane C-H bond can be achieved by overcoming the bond dissociation energy (e.g. 439 kJ $mol^{-1}$ for methane[78], the alkane with the strongest C-H bond) either thermally or by H-atom abstraction to give a high-energy radical. If methane is oxidized this way to give methanol, the reaction does not stop there but overoxidation will happen because the C-H bond of methanol is 46 kJ $mol^{-1}$ weaker than that of methane.

In non-radical alkane oxidation reactions the C-H bond itself has to be the "functional group" that interacts with the reagent or the catalyst prior to cleavage. This process is observed with transition metal complexes where the alkane coordinates to the metal center. Examples of intramolecular (agostic) coordination of C-H bonds as ligands have been reported earlier (for a review see [79]). The characterization of complexes with alkanes as ligands (so-called σ-complexes) is a popular field of investigation at present[80-82]. To date, however, only very few such complexes could be characterized by NMR spectroscopy in solution[83-88] (**figure 1.10**).

A)

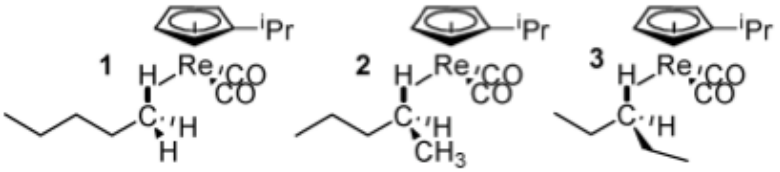


B)

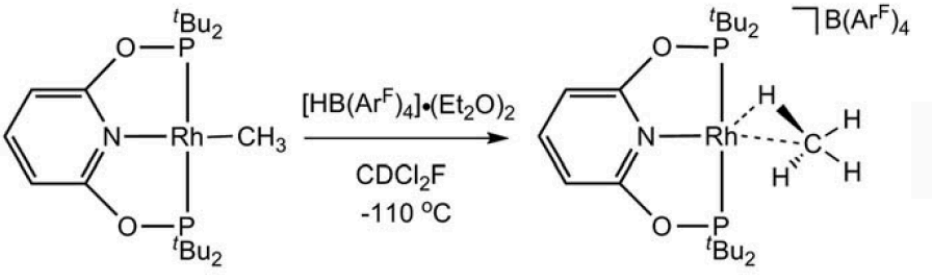


**Figure 1.10**: Examples of σ-alkane complexes characterized by NMR spectroscopy. **A**: An equilibrium between coordination at all different positions (isomers 1, 2 and 3) was found[84]; **B**: First characterization of a methane complex in solution[86].

In the solid state, a heptane complex of a modified Fe(porphyrin)[89] as well as a U(III) complex with different alkanes bound[90] have been characterized crystallographically.

In the case of MCR as the catalyst for the reverse reaction, a direct radical H-atom abstraction from methane is unlikely (see section 4.8.6). Thus a short review of methane activation by transition metals is given in this section. Alkane C-H bond cleavage events by transition metals are mechanistically divided into 5 different classes in the literature[91] (for a full review see [92]): electrophilic activation, oxidative addition, σ-bond metathesis, 1,2-addition and metalloradical activation as depicted in **figure 1.11**.

**oxidative addition**

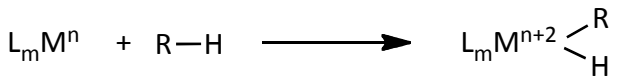

**σ-bond metathesis**

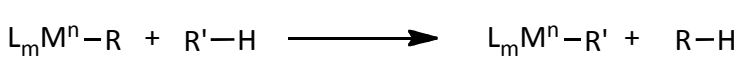

**1,2-addition**

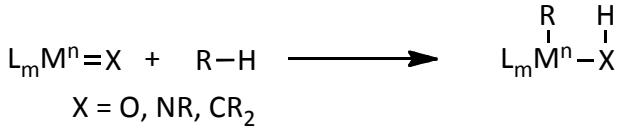

**electrophilic activation**

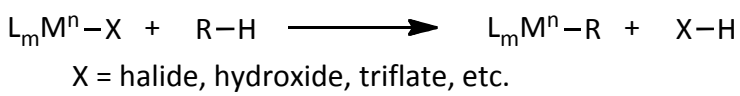

**metalloradical activation**

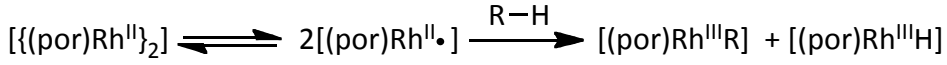

**Figure 1.11**: Summary of different types of C-H bond activation by transition metals[91].

### 1.3.2 The Shilov cycle

The first observation of alkane C-H bond activation by transition metals was published by Alexander Shilov and coworkers[93]. They detected deuterium incorporation into methane when it reacted with a boiling solution of a platinum(II) salt in acidic $D_2O$. Later they found that alkanes are oxidized by platinum(IV) compounds[94]. This led to a catalytic system with a Pt(II) catalyst able to activate methane in aqueous solution according to the following stoichiometry:

$$CH_4 + H_2O + [PtCl_6]^{2-} = CH_3OH + 2\,H^+ + PtCl_2 + 4\,Cl^-$$

Because Pt(IV) is used stoichiometrically as the oxidant in this cycle, the reaction has been further investigated and optimized to run with $SO_3$ or

oxygen as the oxidant. For a comprehensive review see [95] where 4 individual reaction steps are described (**figure 1.12**).

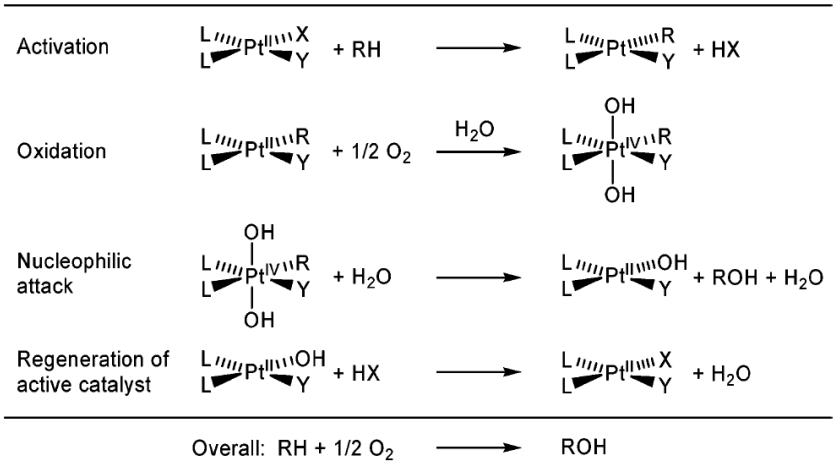


**Figure 1.12**: Individual steps in the functionalization of lower alkanes by platinum[95].

It is important to note that these steps are not necessarily elementary reactions. The actual mechanism may be dependent on the exact nature of the catalyst and the conditions. The methane activation step is assumed to involve coordination and deprotonation of methane at the Pt(II) center. Hence this type of chemistry can be called "electrophilic activation"[93] and stronger, more electron rich bonds are attacked preferentially. The coordination of the alkane may proceed dissociatively (leading to a three-coordinate 14-electron intermediate) or associatively (five-coordinate 18-electron intermediate). The latter is believed to be the case for most substitutions at Pt(II)[96].

### 1.3.3 Oxidative addition reactions

The process of oxidative addition is known for a wide range of different transition metals[97]. It was first discovered accidentally when a ruthenium(II) complex was reduced with sodium naphthalide[98]. The resulting ruthenium(0) complex contained one equivalent of

naphthalene which was concluded to be in equilibrium with the corresponding hydrido naphthyl complex[98, 99].
About 20 years later, in 1982, the first oxidative addition reactions of alkanes were reported for iridium centers by the groups of Bergman and Graham[100, 101].
Oxidative addition can be regarded as "nucleophilic activation" since a coordinatively unsaturated, low valent metal center donates electrons into the antibonding orbital of the C-H of the alkane that is coordinated to the metal. A hydride is formed to give the hydrido alkyl complex with an increase in the oxidation state of the metal center by two units.

As depicted in **figure 1.13**, the process of oxidative addition involves at least 2 elementary steps. First, the alkane coordinates to the metal center and a ligand is usually displaced. In a second step the σ-coordinated alkane undergoes oxidative cleavage to give the hydrido alkyl complex. In this reaction sequence, the association or dissociation of the alkane complex is often rate limiting.

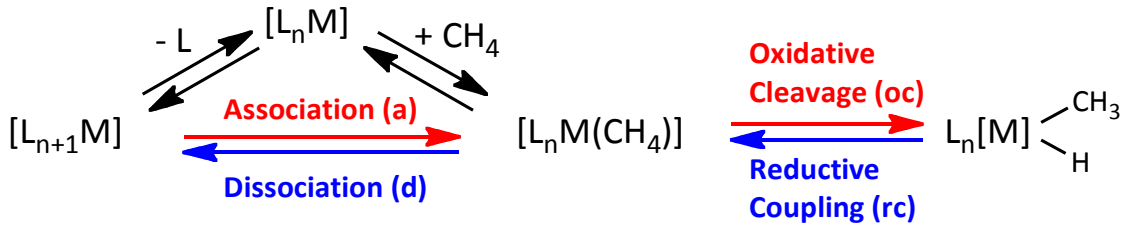


**Figure 1.13**: The elementary steps of oxidative addition (red) and reductive elimination (blue). The association of the alkane usually proceeds by a displacement of a ligand.

The reverse reaction is called reductive elimination and involves a composite of reductive coupling and dissociation of the alkane.

If the coordination or dissociation of the alkane is rate limiting, an equilibrium between the alkyl hydride and the alkane complex can be

established. If a deuterido alkyl complex is involved, exchange of deuterium into the alkyl group can be observed, as exemplified with a tungstenocene complex (**figure 1.14**).

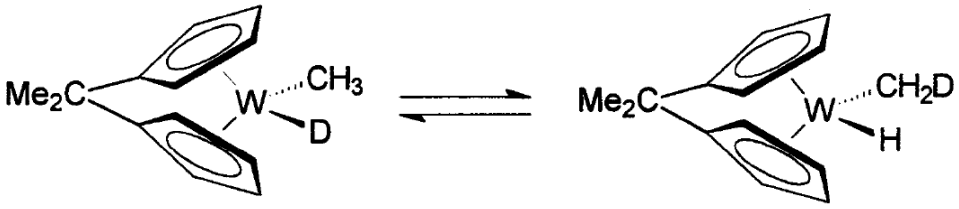


**Figure 1.14**: Deuterium exchange between the hydride position and the alkyl substituent via the unseen σ-complex[102].

### 1.3.4 Isotope effects of oxidative addition and reductive elimination

The measurement of isotope effects is an important tool in the investigation of reaction mechanisms[103]. In the case of alkane C-H bond cleavage deuterium labels can be used to observe kinetic and/or equilibrium isotope effects as described here for oxidative addition and its reverse reaction.

Kinetic isotope effects (KIE) on methane activation can be measured if $CH_2D_2$ is used as the substrate. The advantage of this methane isotopologue is the inherent presence of an equal number of hydrogen and deuterium isotopes within the same molecule and therefore the absence of an isotope effect on association. If the isotope exchange from the hydride to the methyl group (cf. W-complex in figure 1.14) can be prevented during the oxidative addition process, the isotope effect on oxidative cleavage (oc) can be directly determined by analyzing the ratio of M-$CH_2D$ versus M-$CHD_2$ product. For most conditions where oxidative addition occurs, however, isotope exchange from the hydride to the methyl group is faster than the association of methane (**figure 1.15 A**). In these cases only an equilibrium isotope effect (EIE) on oxidative cleavage and reductive coupling is observed.

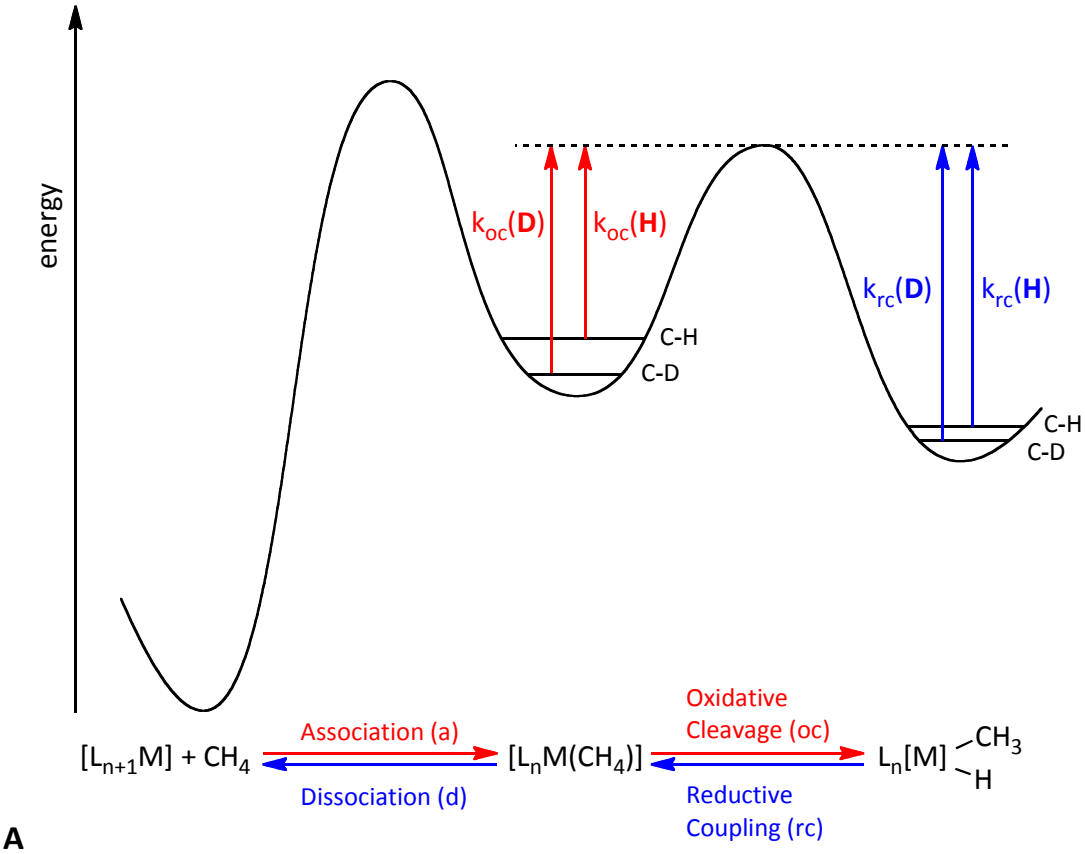


**A**

$$EIE_{ox.add.} = \frac{KIE_{oc}}{KIE_{rc}} > 1 \qquad KIE_{oc} = \frac{k_{oc}(H)}{k_{oc}(D)} >> 1$$

$$EIE_{red.el.} = \frac{KIE_{rc}}{KIE_{oc}} < 1 \qquad KIE_{rc} = \frac{k_{rc}(H)}{k_{rc}(D)} > 1$$

**B**

**Figure 1.15**: **A**: Schematic energy profile for the process of oxidative addition. **B**: Relation between the kinetic and the equilibrium isotope effects.

The kinetic isotope effects for the elementary reactions ($KIE_{oc}$ and $KIE_{rc}$) are coupled to give the observed equilibrium isotope effects ($EIE_{ox.add.}$ and $EIE_{red.el.}$) according to **figure 1.15 B**.

It is obvious that one of the two EIE, usually in the direction of reductive coupling ($EIE_{red.el.}$), is formally inverse (< 1), although all KIE

are normal. Hence, "it became common to associate an inverse isotope effect on alkane loss with the intermediacy of a σ-alkane complex"[104].

An elegant experiment that allows the isotope effects of all elementary reactions to be determined was carried out by W. Jones and coworkers with a very reactive rhodium complex[105]. After initiation with light, the coordinatively unsaturated rhodium center reacts at 5 °C with $CH_2D_2$ to give the corresponding hydrido methyl or deuterido methyl complex. At this temperature no significant reductive coupling occurs and thus the isotope effect of oxidative cleavage can be determined directly from the ratio of the two isotopomeric species (**figure 1.16**, red values).

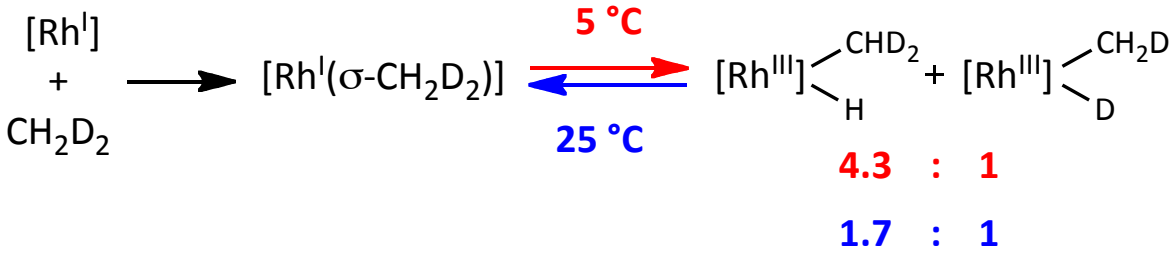


**Figure 1.16**: Experiment allowing to determine the kinetic isotope effect of oxidative cleavage ($KIE_{oc}$, red numbers) and the equilibrium isotope effect of oxidative addition ($EIE_{ox.add.}$, blue numbers).

Upon warming to room temperature, reductive coupling takes place and an equilibrium between the hydrido $d_2$-methyl and the deuterido $d_1$-methyl complex is established. From the ratio of their concentrations the equilibrium isotope effect can be directly obtained (**figure 1.16**, blue values) and the kinetic isotope effect of reductive coupling calculated:
$KIE_{rc} = KIE_{oc} / EIE_{ox.add.} = 4.3 \ / \ 1.7 = 2.5$

### 1.3.5 Sigma-bond metathesis-type reactions

Methane activation by early transition metals and rare-earth metals could be demonstrated by isotope exchange using a $^{13}C$ label[106] as depicted in **figure 1.17**.

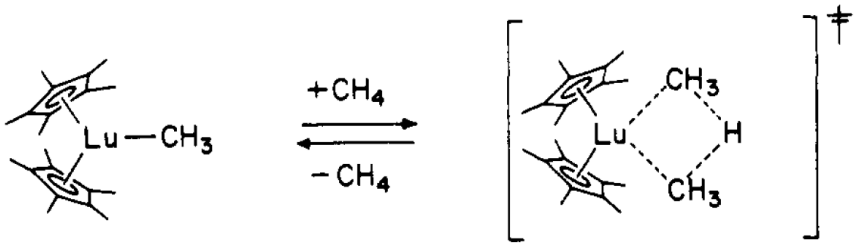


**Figure 1.17**: First observation of methane activation by a σ-bond metathesis reaction. The detection was achieved by the use of $^{13}CH_4$ and analysis of the label in the complex[106].

The fact that this reaction proceeds readily with $d^0$-metal centers such as scandium(III) and yttrium(III) rules out an oxidative addition pathway which would require a corresponding +V oxidation state that is not accessible to these complexes.

Thus a concerted mechanism is assumed and generally called sigma-bond metathesis[107]. This mechanism differs from the electrophilic activation by the fact that the group formally deprotonating the methane (the $CH_3^-$ group) is attached to the metal center. Coordination of the alkane prior to the reaction is assumed[107] (**figure 1.18**).

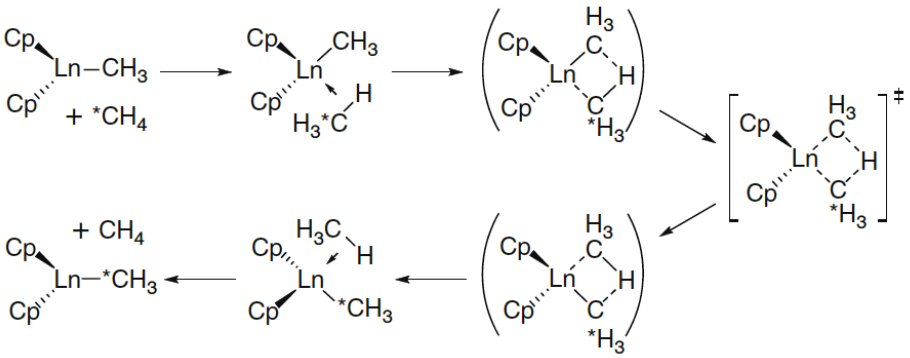


**Figure 1.18**: Assumed reaction mechanism for σ-bond metathesis. It involves coordination of the alkane prior to rearrangement[107].

For complexes containing permethylated cycopentadienyl ligands a "tuck-in" intermediate can represent a second reaction pathway[108] (**figure 1.19**), which then corresponds to an oxidative addition mechanism. Using fully deuterated ligands, this pathway could be verified or excluded by the formation of deuterium-labeled methane.

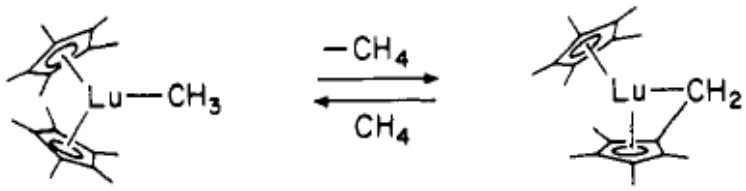


**Figure 1.19**: Formation of a "tuck-in" intermediate as second possible pathway for methane activation.

The corresponding sigma-bond metathesis reactions with ethane and propane are slower and more difficult to study because β-hydride elimination competes as a side reaction[109].

One catalytic cycle in which homogeneous methane activation is achieved by this chemistry has been reported. It involves "hydromethylation" of propene to give isobutane[110] (**figure 1.20**).

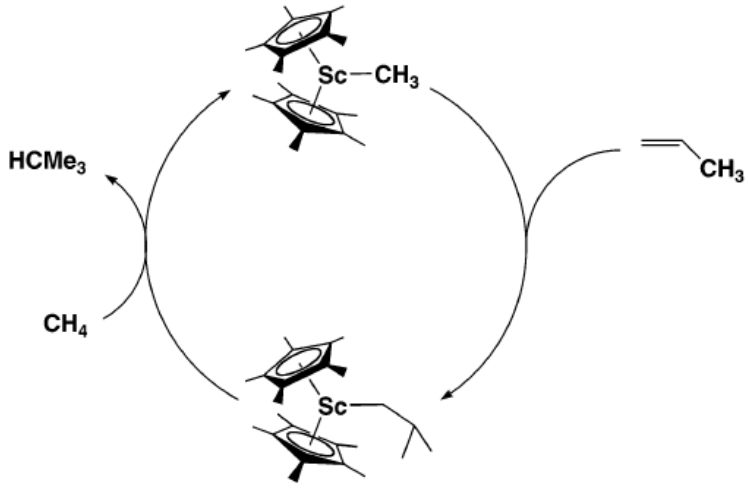


**Figure 1.20**: Catalytic cycle for a homogenous "hydromethylation" of an alkene with methane[110].

This cycle affords only 3 turnovers in 2 days, but it is an important precedent demonstrating that the activation of methane may occur by mechanisms other than oxidative addition and the Shilov cycle.

With nickel as the catalyst, a nickelocene-lithium aluminium hydride system in THF was able to activate methane[111]. For a transition metal center with an odd number of electrons (such as MCR), only nickel-mediated thermal activation of methane in the gas phase was reported[112].

The cleavage and formation of methane's C-H bond by MCR could proceed by one of the mechanisms discussed here or by some other mechanism that is not common in laboratory chemistry.

## 1.4 Outline of the Project

### 1.4.1 Starting point

In experiments with purified MCR in deuterated medium, the formation of about 7 mol% $CH_2D_2$ (in addition to the expected isotopologue $CH_3D$) was discovered in our group[113].
This finding was highly intriguing and led to the hypotheses described in the next two sections, which were the starting point of this project.

### 1.4.2 Reversibility of MCR

It is well known that the forth hydrogen of methane originates from solvent[114-116]. If the reverse reaction proceeds to a significant extent, $CH_2D_2$ could be formed by a "double-turnover" according to **figure 1.21**.

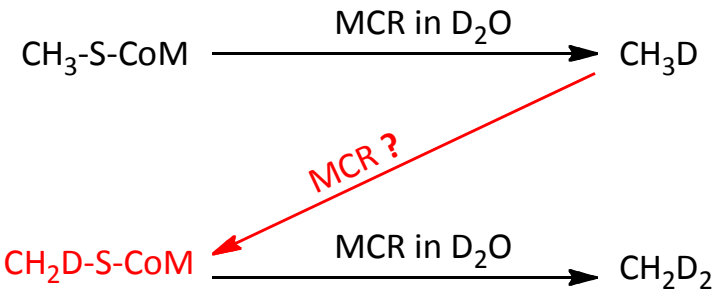


**Figure 1.21**. Formation of $CH_2D_2$ through methane activation catalyzed by MCR followed by a second turn over.

This hypothesis can be verified by the use of a $^{13}C$ label, which would allow alternative mechanisms for deuterium incorporation into the substrate to be excluded. Experiments can be performed using the $^{13}C$ label in the substrate under methane containing only natural abundance $^{13}C$ or according to the contrary setup with $^{13}CH_4$ and natural abundance substrate.

The rate of this reverse reaction is of biological relevance because consortia of methanotrophic archaea and sulfate reducing bacteria are known to oxidize methane anaerobically. It has been postulated that the methanotrophic archaea and methanogens use very similar enzymes but in the reverse direction. This hypothesis would be substantiated if MCR were able to activate methane at a significant rate.

### 1.4.3 Deuterium incorporation into the substrate methyl-coenzyme M

An intermediate along the catalytic cycle could also account for the observed formation of $CH_2D_2$. A "partial reversibility" of the reaction through which deuterium is incorporated into the substrate (**figure 1.22 A**) or into the intermediate (**figure 1.22 B**) would be an alternative explanation of the formation of $CH_2D_2$.

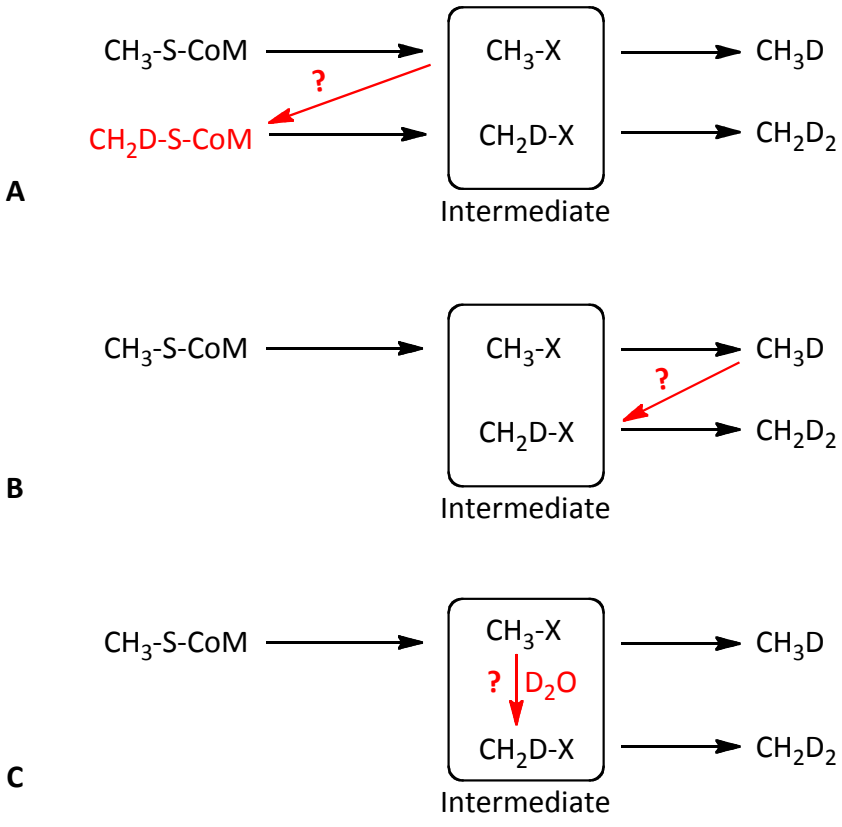


**Figure 1.22**: Mechanisms accounting for the formation of $CH_2D_2$. **A** and **B**: Partial reversibility through an intermediate. **C**: Intermediate able to exchange deuterium from the solvent into the methyl group.

The occurrence of an intermediate that can exchange deuterium from the solvent into the methyl group of the substrate is a third option that would account for the observed $CH_2D_2$ (**figure 1.22 C**).
The kinetics of this putative deuterium incorporation has to be measured and compared with the full reverse reaction. The rate of deuterium incorporation into the substrate relative to the rate of methane formation may allow a rough energy profile of the reaction to be deduced.

### 1.4.4 Isotope effects

It will be shown that the reverse reaction proceeds to some extent and that an intermediate is formed. This combination of reaction pathways offers the possibility of measuring $^{2}H$ and $^{13}C$ isotope effects for different steps and directions within the catalytic cycle.
In addition, utilizing the non-natural substrate ethyl-coenzyme M revealed more fascinating insights into the catalytic capabilities of MCR.

### 1.4.5 Collaboration

The enzyme MCR was purified from archaea cultures produced together with Meike Goenrich and Reinhard Boecher in the laboratory of R. K. Thauer at the Max Planck Institute for Terrestrial Microbiology in Marburg. The active enzyme was incubated using different assay conditions depending on the goal of the investigations. Analysis of the experiments was carried out at the ETH Zurich by extensive NMR studies of products and recovered substrates.

# 2 Methane Activation by MCR

## 2.1 Introduction: Anaerobic Oxidation of Methane (AOM) with Sulfate

1.5 billion metric tons per year (1.5 Gt p.a.) of methane is produced globally in anoxic environments[17]. Microorganisms using sulfate as the ultimate electron acceptor are estimated to oxidize up to 0.3 Gt p.a. of the methane that is formed to carbonate before it reaches the atmosphere[20, 117, 118]. This process represents the major anaerobic pathway of methane oxidation (cf. figure 1.1 in section 1.1.2) and thus has a significant effect on global warming since methane is estimated to be 21 times more active as a greenhouse gas than $CO_2$ (calculated for 100 years[19]).

A correlation between sulfate depletion and methane depletion in anoxic sea water was noticed quite a while ago by analysis of the corresponding concentration profiles[119]. It was postulated that methane is oxidized to $CO_2$ (or carbonate, respectively) and sulfate reduced at the same time to sulfide[2, 42, 120] according to the following stoichiometry:

$$CH_4 + SO_4^{2-} = CO_3^{2-} + H_2S + H_2O \qquad \Delta G^{\circ\prime} = -21 \text{ kJ mol}^{-1}$$

In the Black Sea at depths of 230 m, carbonate towers up to 4 m tall were discovered at methane springs[121] (**picture 2.1**).

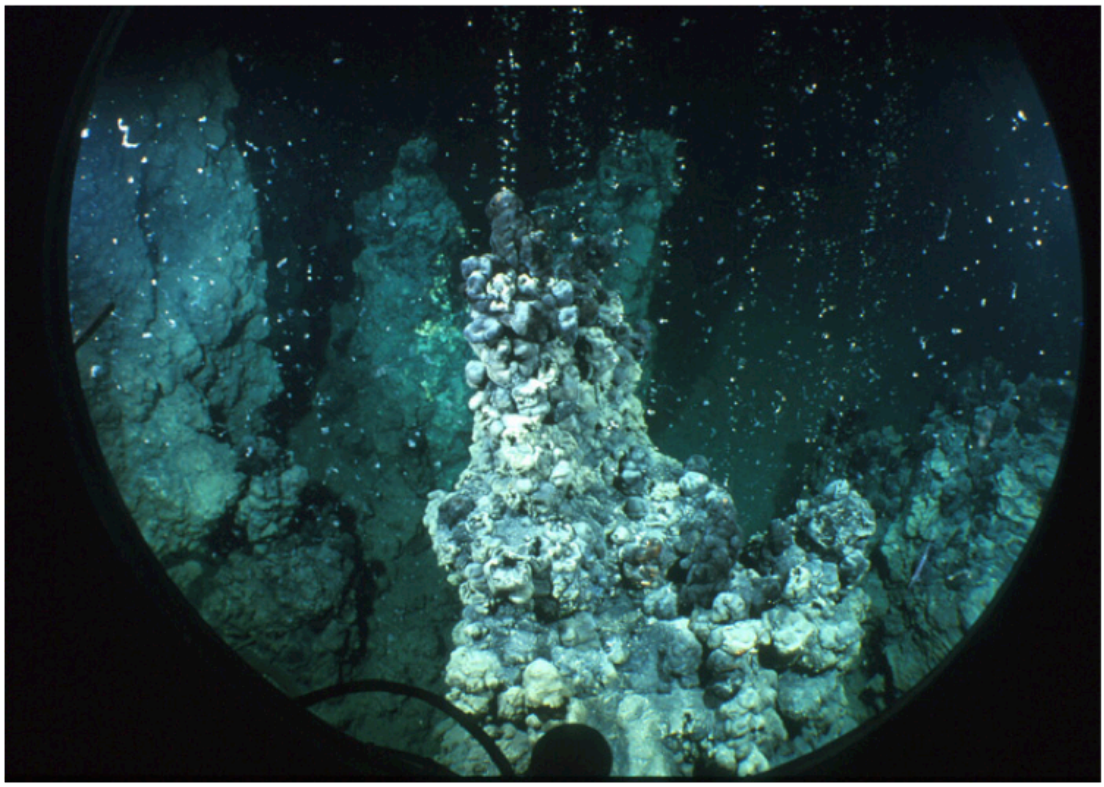

**Picture 2.1**: Carbonate built up 230 m deep in the Black Sea at methane springs. Picture from the porthole of a submarine: Expedition GHOSTDABS, 2001[121].

A consortium of different organisms was found embedded in such carbonate towers. Fluorescence in situ hybridization (FISH, for a review see [122]) was used to stain different types of organisms in a specific color[23] (**picture 2.2**).

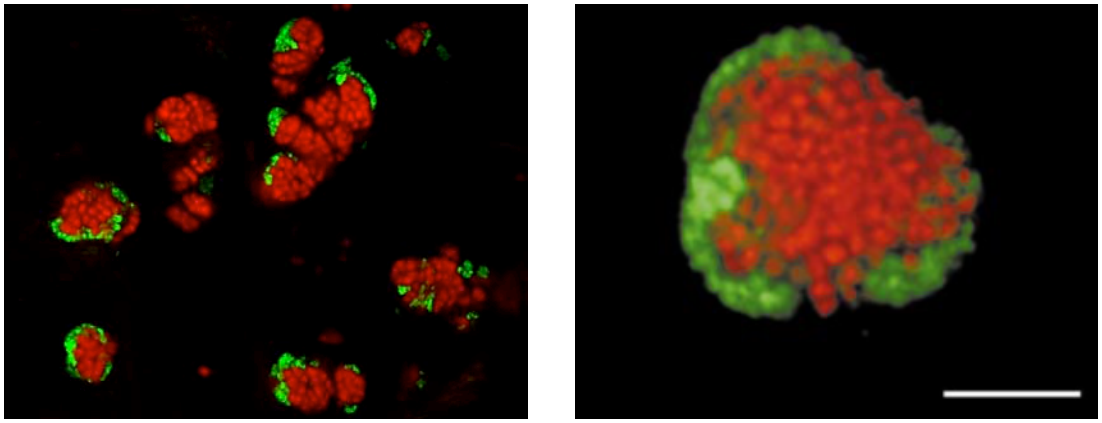

**Picture 2.2**: Fluorescence in situ hybridization (FISH) of microbial mats carrying out anaerobic oxidation of methane[23]. The scale bar (right picture) corresponds to 5 μm. Organisms related to methanogens are stained red; sulfate-reducing bacteria are stained green.

It could be demonstrated that the organisms stained red are genetically related to methanogens and contain genes homologous to those coding for MCR. These organisms were named ANME archaea and were divided into the subclasses ANME-1, 2 and 3[25, 123]. The organisms stained green were identified as sulfate-reducing bacteria[124].

Splitting the overall reaction into the two "half reactions" visualizes the 8-electron oxidation of methane and the 8-electron reduction of sulfate as shown below:

$$CH_4 + Ca^{2+} + SO_4^{2-} = CaCO_3 + H_2S + H_2O$$

$$CH_4 + 3\ H_2O = CO_3^{2-} + 8\ e^- + 10\ H^+ \quad \text{(ox.)}$$

$$SO_4^{2-} + 8\ e^- + 10\ H^+ = H_2S + 4\ H_2O \quad \text{(red.)}$$

Assigning the two half reactions to the two types of organisms according to **figure 2.1** could account for such a cooperation. However, the two types of organisms must exchange redox equivalents with each other and the nature of the compound(s) exchanged remains unknown. In addition, this simplified picture does not account for a carbon source on which the sulfate-reducing bacteria could grow. Formate or acetate as redox intermediates instead of hydrogen would be suitable carbon sources for the growth of the sulfate-reducers.

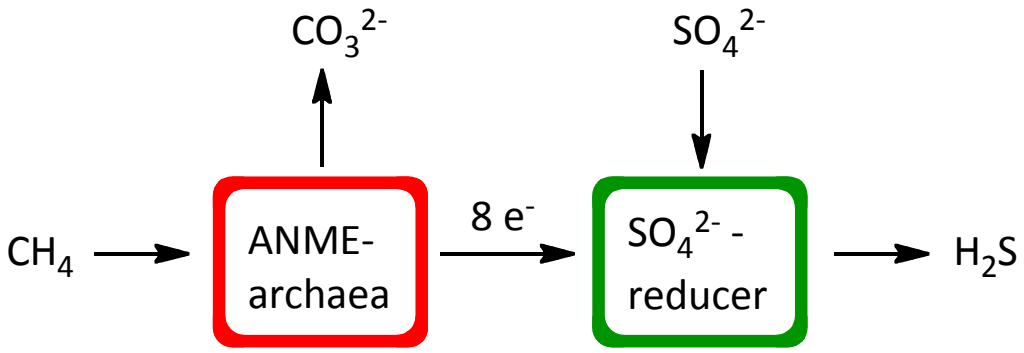


**Figure 2.1**: Simplified representation of the net reaction of anaerobic oxidation of methane with sulfate. The electron carrier between the two organisms is still unknown. A carbon source for the growth of the sulfate-reducing bacteria is not taken into account in this representation.

The hypothesis of reverse methanogenesis[2, 3] is the proposal that ANME archaea carry out the anaerobic oxidation of methane using enzymes very similar to those used in methanogenesis.

The number of oxidation steps performed by the ANME archaea is not known. According to the hypothesis of reverse methanogenesis, at least the first step, the oxidation of methane, must be performed by archaea. This assumption appears to be reasonable considering that 10% of proteins extracted from communities carrying out anaerobic oxidation of methane are homologous to MCR[42]. These proteins contain either coenzyme F430 (ANME-2) or its derivative "F430X"[56] (ANME-1) at their active sites (cf. section 1.2.3).

The microbial consortium present in the carbonate structures described above could be grown in the laboratory under strictly anaerobic conditions applying 14 bar methane pressure[125]. Kinetic analysis of substrate consumption confirmed the 1:1 stoichiometry of methane and sulfate. After cultivation for two years, a doubling time of about seven months was reached. The organisms exhibited a methane consumption rate of 0.23 mmol per day per gram dry sediment at 12 °C under 14 bar methane[1]. From this activity, a specific activity of 70 nmol methane per mg MCR homologue can be estimated (**table 2.1**).

**Table 2.1**: Estimation of the specific methane oxidation activity if the reaction were catalyzed by proteins homologous to MCR. The specific rate was calculated from the measured rate exhibited by communities of archaea and sulfate reducing bacteria grown in the laboratory at 12 °C under 14 bar $CH_4$ (21 mM dissolved $CH_4$)[1].

| $CH_4$ activated | per | by | assumption |
|---|---|---|---|
| **0.23 mmol** | **day** | **1 g dry sediment** | **measured**[1] |
| 5 mmol | day | 1 g dry cell mass | 4.6% dry cell mass in dry sediment[1] |
| 10 mmol | day | 1 g protein | 50% protein in the dry cell mass |
| 10 μmol | day | 1 mg protein | |
| 7 nmol | min | 1 mg protein | |
| **70 nmol** | **min** | **1 mg "MCR"** | 10% of proteins homologous to MCR[42] |

In order to test the first step of the reverse methanogenesis, the proteins homologous to MCR should be purified and tested for their activity.
Because the intermediate exchanged by the two organisms is not known, ANME cannot be grown in pure cultures. In addition, the doubling time of the organisms is too long for the production of a reasonable amount of protein.
The inaccessibility of pure ANME cultures prompted us to test the hypothesis of reverse methanogenesis with purified MCR from a methanogen as a model of the homologous protein present in ANME archaea (**figure 2.2**).

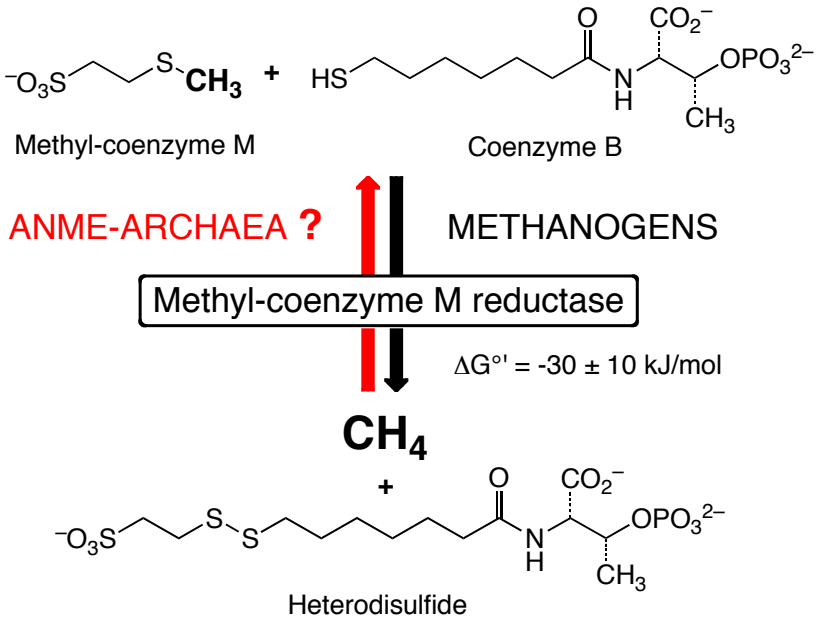


**Figure 2.2**: Reaction scheme for methane formation and methane activation. According to the hypothesis of reverse methanogenesis, ANME archaea should be able to activate methane (red arrow).

In the present study we used MCR (isoenzyme I) purified from *Methanothermobacter marburgensis* to measure the specific rate of anaerobic oxidation of methane.

## 2.2 Results

### 2.2.1 Detection of methane activation

Since methane formation from the substrates of MCR is exergonic, a direct reverse reaction is difficult to observe. If the products (methane and the heterodisulfide) are incubated with the enzyme, the reaction may only proceed to the thermodynamic equilibrium, which lies strongly on the product side. Corresponding experiments were performed with two different concentrations of the heterodisulfide (HDS) with and without methane (**table 2.2**).

**Table 2.2**: Observation of the direct reverse reaction catalyzed by 7.5 nmol MCR in 1.6 ml assay solution. Incubation time: 8 min at 60 °C. For further details see experimental section 6.2.2.

| | $CH_3$-S-CoM formed [nmol] | $CH_3$-S-CoM per HDS | HDS per $CH_3$-S-CoM |
|---|---|---|---|
| 8 μmol HDS | | | |
| 0 bar $CH_4$ | 0 | 0 | |
| 1.5 - 2 bar $CH_4$ | 14.477 | 0.00181 | 552.6 |
| 80 μmol HDS | | | |
| 0 bar $CH_4$ | 0 | 0 | |
| 1.5 - 2 bar $CH_4$ | 0 | 0 | |

In order to obtain precise data, higher rates of methane activation are needed. This can be achieved using isotopic labeling under equilibrium conditions where methyl-coenzyme M and the heterodisulfide are both present. The endergonic reaction **A** is driven by the exergonic reaction **B**.

**A** $\quad CoB\text{-}S\text{-}S\text{-}CoM + {}^{13}CH_4 = {}^{13}CH_3\text{-}S\text{-}CoM + CoB\text{-}SH$

**B** $\quad {}^{12}CH_3\text{-}S\text{-}CoM + CoB\text{-}SH = CoB\text{-}S\text{-}S\text{-}CoM + {}^{12}CH_4$

---

**A + B** $\quad {}^{12}CH_3\text{-}S\text{-}CoM + {}^{13}CH_4 = {}^{13}CH_3\text{-}S\text{-}CoM + {}^{12}CH_4$

The net reaction **A** + **B** is energetically neutral and allows observation of higher conversions. The incorporation of the $^{13}C$ label can be detected via $^{1}H$-NMR spectroscopy of the assay solution.

To enable the detection of small extents of methane activation, the first substrate methyl-coenzyme M was synthesized with the *S*-$CH_3$ group depleted in $^{13}C$ ($^{13}C$ content < 0.0014%). All experiments described in this chapter were done under equilibrium conditions. A premixed solution of $^{12}CH_3$-S-CoM (4.0 mM) and CoB-SH (2.0 mM) was supplemented with enzyme in an ice bath. After distribution to the vials, the headspace was replaced by the desired partial pressure of $^{13}CH_4$ and the reaction was started by incubation in a water bath shaker at 60 °C. At equilibrium, which was reached after less than a minute, the concentrations for $^{12}CH_3$-S-CoM and heterodisulfide were 2.0 mM each. The low concentration of CoB-SH drives the reaction towards the "substrate side". Additional incubation time allows $^{13}CH_4$ to be converted to $^{13}CH_3$-S-CoM. Thus the amount of measured $^{13}CH_3$-S-CoM formed corresponds to the amount of $^{13}CH_4$ activated.

An overview of the reaction parameters is given in **table 2.3**. For further details see the experimental section describing each set of experiments.

**Table 2.3**: Standard parameters for methane activation assays if not stated otherwise.

| | |
|---|---|
| Volume of assay solution | 1.6 ml |
| Volume of headspace | 5.0 ml |
| $^{12}CH_3$-S-CoM (initial) | 4.0 mM |
| CoB-SH (initial) | 2.0 mM |
| pH (50 mM phosphate buffer) | 7.6 |
| Enzyme (MCR) | 4.06 mg |
| $^{13}CH_4$-pressure | 1 bar |
| Incubation temperature | 60 °C |
| Incubation time | 30 min |
| Stop of the reaction | 100 °C |

After the desired incubation time, the reaction was stopped by immersion of the vials in boiling water for 2 min. Data analysis was carried out by $^{1}$H-NMR spectroscopy of the assay solution without further treatment (see experimental section 6.6 for details). **Figure 2.3** shows a typical $^{1}$H-NMR spectrum after incubation with $^{13}CH_4$.

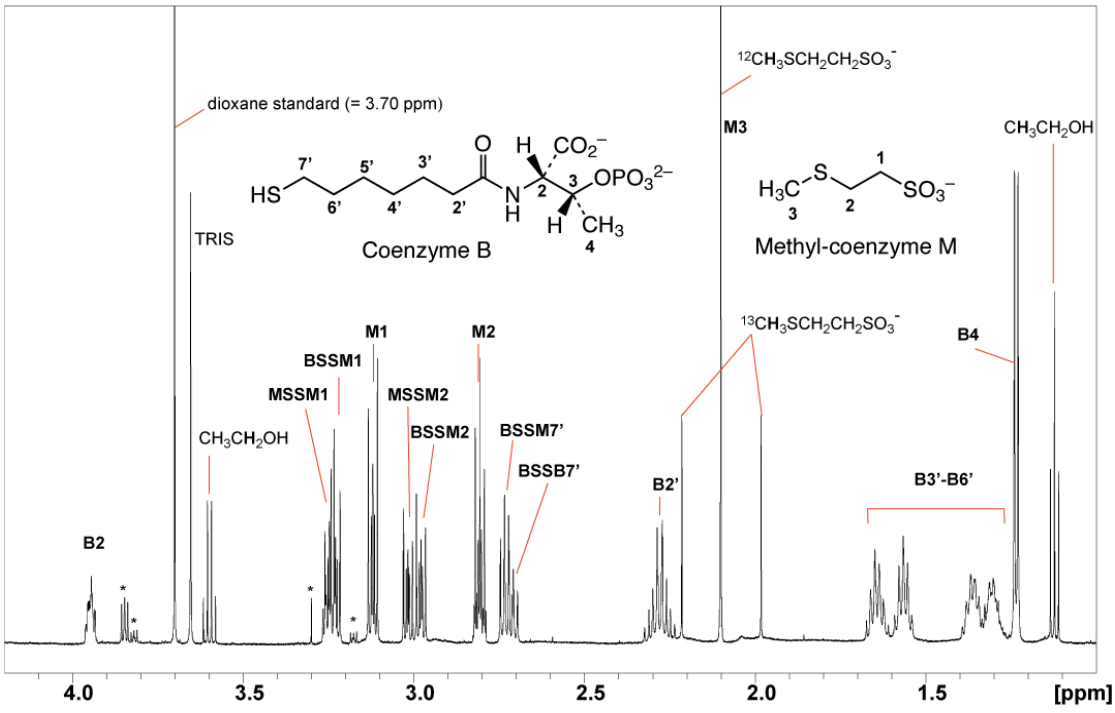


**Figure 2.3**: Expansion of the 600 MHz $^{1}$H-NMR spectrum of an assay solution after incubation with $^{13}CH_4$ without further treatment. The $^{13}$C-content of $CH_3$-S-CoM was determined by integrating the central peak and both $^{13}$C satellites of the methyl group (2.10 ppm). The conversion was calculated from the integral values of the signals at 3.12 and 1.57 ppm.

Assignment: M = methyl-coenzyme M; B = coenzyme B and signals that are indistinguishable for CoB and the CoB-containing disulfides; BSSM = heterodisulfide of CoM and CoB; MSSM = homodisulfide of CoM; BSSB = homodisulfide of CoB. *unassigned impurities. The homodisulfides of coenzyme B and coenzyme M are formed via thiol-disulfide exchange within hours. The signal of Tris-HCl buffer is due to the added enzyme solution. Signals of ethanol originate from a contamination of the atmosphere in the anaerobic tent due to unrelated experiments. For full range spectra before and after addition of enzyme, see experimental section 6.3.1.

### 2.2.2 Correlation of enzyme concentration and methane activation

To prove that methane activation is catalyzed by MCR, two series of experiments with increasing enzyme concentration and control experiments without enzyme were performed (**table 2.4**).

**Table 2.4**: Dependence of methane activation (measured as $^{13}CH_3$-S-CoM formed in 30 min) on enzyme concentration under standard conditions.

| Enzyme [mg] | Enzyme [nmol] | $CH_3$-CoM [Molar fraction] | $CH_3$-CoM [µmol] | $^{13}C$ in $CH_3$-CoM [Molar fraction] | $^{13}CH_3$-CoM formed [µmol] |
|---|---|---|---|---|---|
| Run 1 | | | | | |
| 0 | 0 | 1 | 6.4 | 0 | 0 |
| 2.03 | 7.3 | 0.523 | 3.349 | 0.105 | 0.350 |
| 4.06 | 14.5 | 0.494 | 3.161 | 0.240 | 0.759 |
| 8.12 | 29.0 | 0.445 | 2.845 | 0.476 | 1.354 |
| Run 2 | | | | | |
| 0 | 0 | 1 | 6.4 | 0 | 0 |
| 2.03 | 7.3 | 0.525 | 3.358 | 0.103 | 0.347 |
| 4.06 | 14.5 | 0.490 | 3.136 | 0.230 | 0.721 |
| 8.12 | 29.0 | 0.452 | 2.892 | 0.447 | 1.294 |

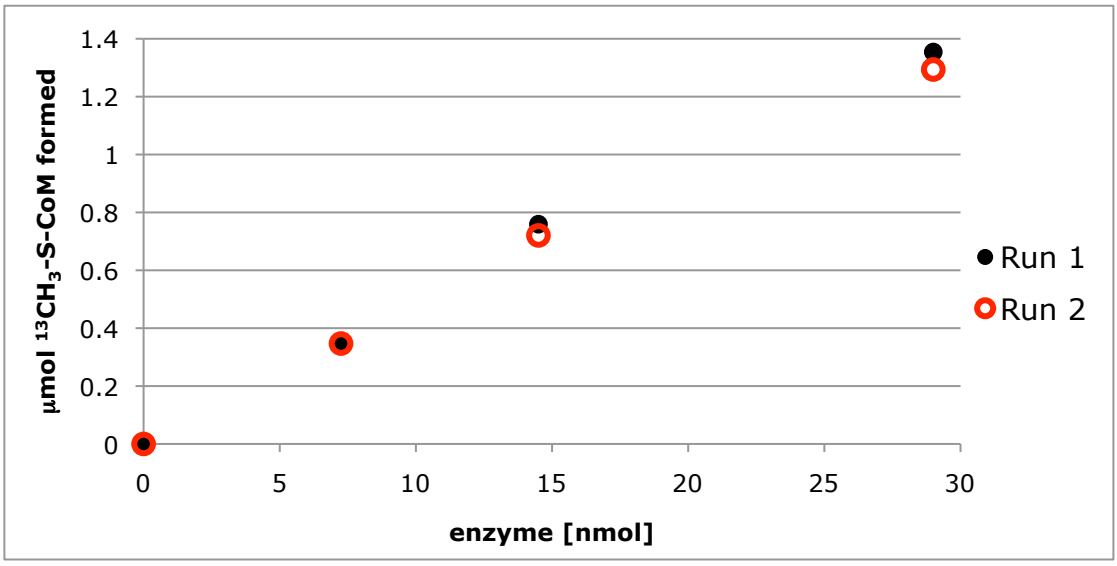


**Figure 2.4**: Dependence of methane activation on enzyme concentration (data from table 2.4).

### 2.2.3 Time dependence

Methane activation as a function of the incubation time was determined in two independent series (**table 2.5**).

**Table 2.5**: Time dependence of methane activation under standard conditions.

| Time [min] | $CH_3$-CoM [Molar fraction] | $CH_3$-CoM [μmol] | $^{13}C$ in $CH_3$-CoM [Molar fraction] | $^{13}CH_3$-CoM [μmol] | catalytic turnovers |
|---|---|---|---|---|---|
| Run 1 | | | | | |
| 8 | 0.526 | 3.365 | 0.110 | 0.370 | 25.5 |
| 15 | 0.514 | 3.289 | 0.151 | 0.497 | 34.3 |
| 30 | 0.510 | 3.261 | 0.232 | 0.757 | 52.2 |
| 60 | 0.499 | 3.193 | 0.285 | 0.911 | 62.9 |
| 120 | 0.471 | 3.012 | 0.363 | 1.095 | 75.5 |
| Run 2 | | | | | |
| 7.5 | 0.543 | 3.478 | 0.095 | 0.332 | 22.9 |
| 15 | 0.521 | 3.336 | 0.169 | 0.564 | 38.9 |
| 30 | 0.498 | 3.188 | 0.224 | 0.715 | 49.3 |
| 60 | 0.481 | 3.081 | 0.279 | 0.860 | 59.3 |

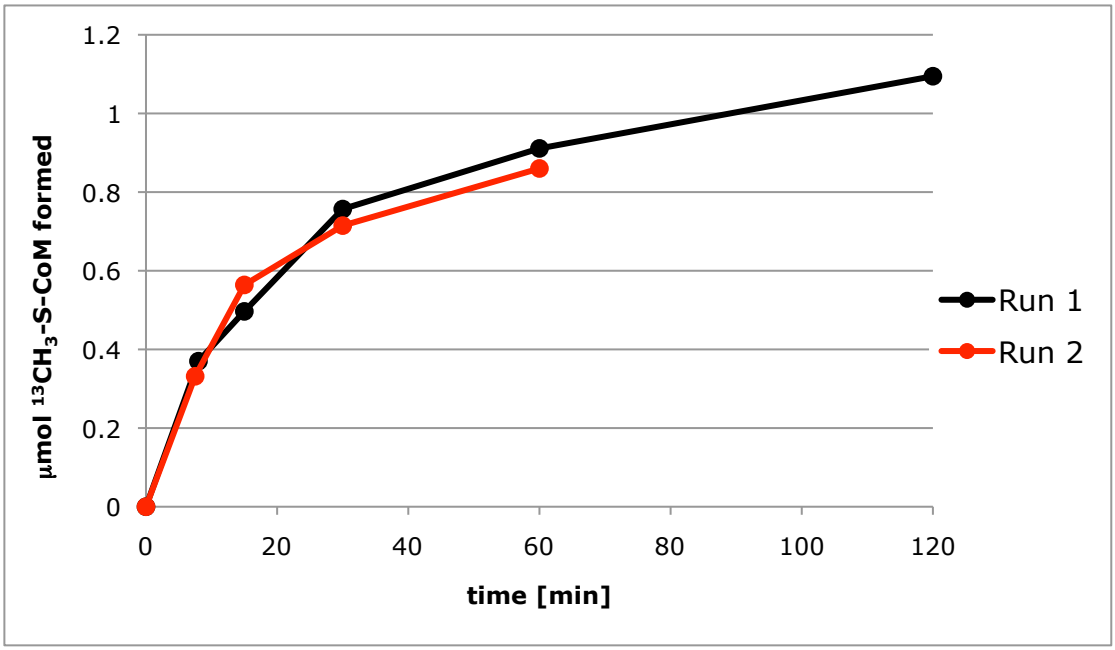


**Figure 2.5**: Methane activation as a function of incubation time (data from table 2.5).

### 2.2.4 Temperature dependence

Experiments at temperatures lower than 60 °C were stopped by injection of 1 ml of air in order to prevent uncontrolled additional activity during warming to 100 °C. **Table 2.6** displays methane activation at different temperatures. Values for 60 °C are taken from the time-dependence experiments, Run 1.

**Table 2.6**: Methane activation at different temperatures. For detailed incubation procedures see experimental part (6.3.2).

| Time [min] | $CH_3$-CoM [Molar fraction] | $CH_3$-CoM [μmol] | $^{13}C$ in $CH_3$-CoM [Molar fraction] | $^{13}CH_3$-CoM [μmol] | turn-overs |
|---|---|---|---|---|---|
| 60 °C | (Run 1) | | | | |
| 8 | 0.526 | 3.365 | 0.110 | 0.370 | 25.5 |
| 15 | 0.514 | 3.289 | 0.151 | 0.497 | 34.3 |
| 30 | 0.510 | 3.261 | 0.232 | 0.757 | 52.2 |
| 60 | 0.499 | 3.193 | 0.285 | 0.911 | 62.8 |
| 120 | 0.471 | 3.012 | 0.363 | 1.095 | 75.5 |
| 40 °C | | | | | |
| 30 | 0.564 | 3.612 | 0.172 | 0.620 | 42.8 |
| 60 | 0.545 | 3.485 | 0.291 | 1.013 | 69.9 |
| 22 °C | | | | | |
| 30 | 0.573 | 3.667 | 0.030 | 0.110 | 7.6 |
| 60 | 0.566 | 3.620 | 0.075 | 0.273 | 18.8 |
| 120 | 0.570 | 3.649 | 0.171 | 0.625 | 43.1 |
| 240 | 0.565 | 3.617 | 0.238 | 0.862 | 59.4 |
| 4 °C | | | | | |
| 30 | 0.576 | 3.683 | 0.00058 | 0.00213 | 0.1 |
| 60 | 0.569 | 3.643 | 0.00246 | 0.00897 | 0.6 |
| 120 | 0.579 | 3.707 | 0.00687 | 0.02546 | 1.8 |
| 240 | 0.577 | 3.692 | 0.01612 | 0.05952 | 4.1 |
| 1115 | 0.514 | 3.287 | 0.10742 | 0.35312 | 24.4 |

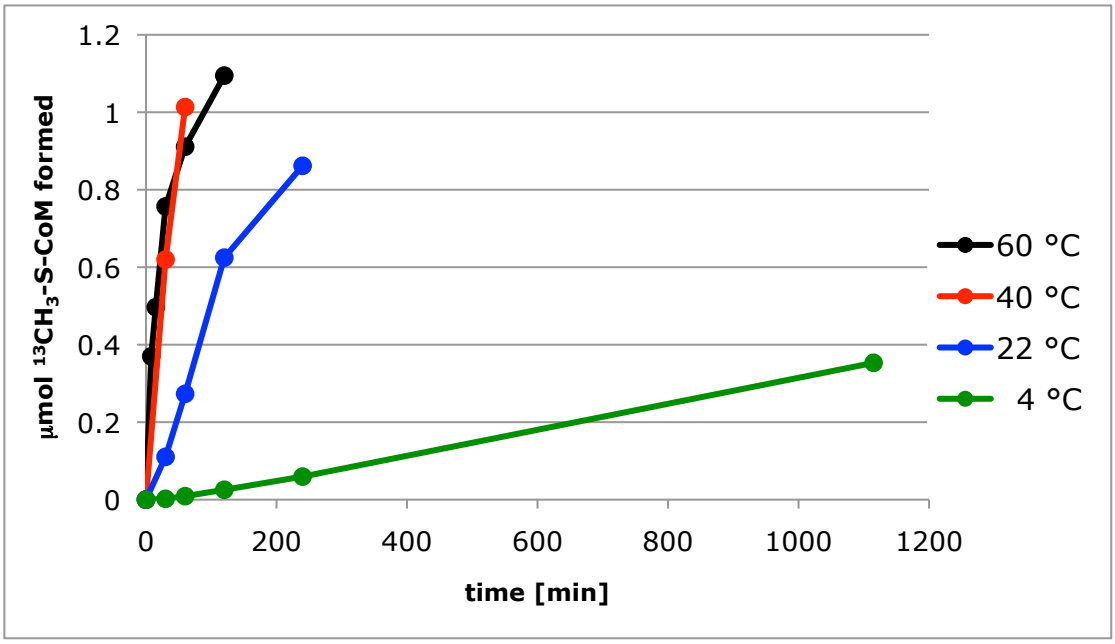


**Figure 2.6**: Time course of methane activation at the different temperatures employed (data from table 2.6).

For the determination of the specific activity, a temperature correction factor for the solubility and the pressure of methane was calculated relative to the standard temperature of 60 °C according to **table 2.7**.

**Table 2.7:** Calculation of correction factors for methane solubility and methane pressure (vials filled with $^{13}CH_4$ at 22 °C) relative to the standard temperature 60 °C.

| T [°C] | $CH_4$ solubility at 1 bar * [mM] | Correction for solubility | Pressure [bar] | Correction for pressure | Correction factor |
|---|---|---|---|---|---|
| 4 | 2.23 | 0.409 | 0.94 | 1.202 | 0.492 |
| 22 | 1.5 | 0.609 | 1 | 1.130 | 0.688 |
| 40 | 1.13 | 0.808 | 1.06 | 1.066 | 0.861 |
| 60 | 0.913 | 1.000 | 1.13 | 1.000 | 1.000 |

* According to [126], extrapolated to 50 mM potassium phosphate.

The calculated specific activities at the temperatures investigated are listed in **table 2.8**.

**Table 2.8**: Calculation of specific catalytic activities at the different temperatures corrected for the change of pressure and solubility.

| T [°C] | Initial rate uncorrected * [nmol $min^{-1}$] | factor | Initial rate corrected [nmol $min^{-1}$] | Specific activity corrected [nmol $min^{-1}$ $mg^{-1}$] |
|---|---|---|---|---|
| 4 | 0.071 | 0.492 | 0.035 | 0.0086 |
| 22 | 3.68 | 0.688 | 2.53 | 0.62 |
| 40 | 20.66 | 0.861 | 17.79 | 4.38 |
| 60 | 46.30 | 1.000 | 46.30 | 11.40 |

* The initial rate of $^{13}C$ incorporation from $^{13}CH_4$ at 1 bar into $CH_3$-S-CoM was determined from the first data point at each temperature (8 min for 60 °C, 30 min for 4, 22, and 40 °C).

For an Arrhenius plot see **figure 2.7**. The specific activity of 11.4 nmol $min^{-1}$ $mg^{-1}$ at 60 °C corresponds to a turnover frequency of 3.2 $min^{-1}$ or 0.053 $s^{-1}$.

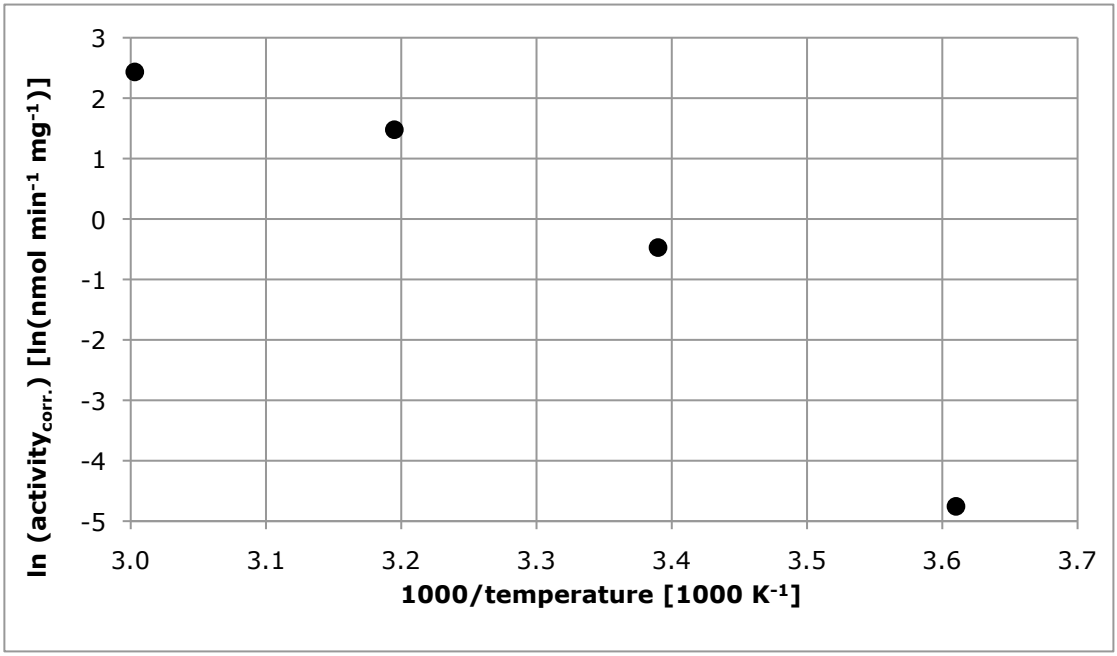


**Figure 2.7**: Arrhenius plot of the corrected initial rates of methane activation at the different temperatures employed.

### 2.2.5 Dependence on methane pressure

Experiments at different partial pressures of methane up to 2 bar were performed with standard equipment (**table 2.9**).

**Table 2.9**: Methane activation during incubation for 30 min at different partial pressures of $^{13}CH_4$. For detailed procedures see experimental section 6.3.3.

| Pressure [bar] | $CH_3$-CoM [Molar fraction] | $CH_3$-CoM [μmol] | $^{13}C$ in $CH_3$-CoM [Molar fraction] | $^{13}CH_3$-CoM [μmol] | turn-overs |
|---|---|---|---|---|---|
| Run 1 | | | | | |
| 0.05 | 0.480 | 3.070 | 0.0106 | 0.033 | 2.1 |
| 0.1 | 0.486 | 3.110 | 0.0239 | 0.074 | 4.8 |
| 0.2 | 0.503 | 3.219 | 0.0476 | 0.153 | 9.9 |
| 0.5 | 0.480 | 3.070 | 0.1483 | 0.455 | 29.4 |
| 1.0 | 0.501 | 3.208 | 0.2283 | 0.732 | 47.3 |
| 2.0 | 0.499 | 3.196 | 0.3851 | 1.231 | 79.4 |
| Run 2 | | | | | |
| 0.2 | 0.495 | 3.165 | 0.0501 | 0.159 | 10.2 |
| 0.5 | 0.501 | 3.206 | 0.1395 | 0.447 | 28.9 |
| 1.0 | 0.507 | 3.245 | 0.1980 | 0.642 | 41.4 |
| 2.0 | 0.506 | 3.238 | 0.4073 | 1.319 | 85.1 |

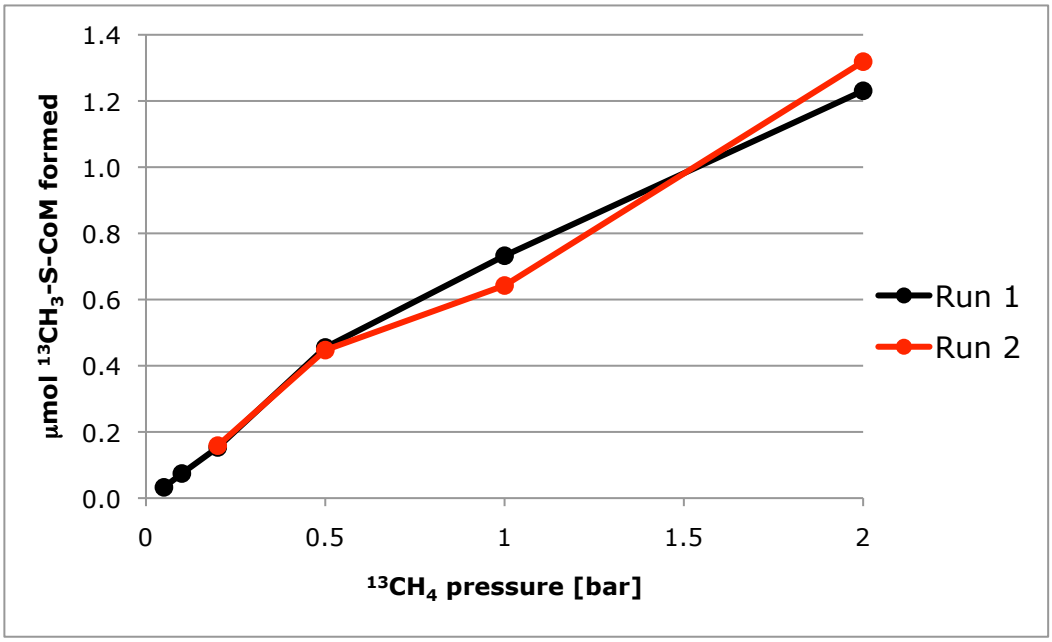


**Figure 2.8**: Correlation of the partial pressure of $^{13}CH_4$ and methane activation (data from table 2.9).

Experiments under higher pressures of $^{13}CH_4$ were performed in a modified French press (for details see experimental section 6.3.4). The preheated French press cell (60 °C) was introduced into the anaerobic tent, charged with 5.0 ml of assay solution (identical to the one for the experiments described above). The cell was immediately closed and charged via the outlet with 1 bar $^{13}CH_4$ (the initial height of the headspace column was 6.6 cm). The plunger was pushed down and fixed at a height yielding the desired pressure. The cell was incubated further at 60 °C. Corresponding experiments at 0.5 bar were performed in the French press containing 1 bar of a mixture of $^{13}CH_4$/forming gas at ca. 1:1 v/v. Collecting the assay solution aerobically from the outlet after 30 min stopped the reaction.

The results of all 12 independent runs are given in **table 2.10**.

**Table 2.10**: Methane activation during incubation for 30 min at different pressures of $^{13}CH_4$ performed in a modified French press cell catalyzed by 12.69 mg (45.3 nmol) enzyme. For detailed procedures see experimental section 6.3.4.

| Pressure [bar] | $CH_3$-CoM [Molar fraction] | $CH_3$-CoM [μmol] | $^{13}C$ in $CH_3$-CoM [Molar fraction] | $^{13}CH_3$-CoM [μmol] | turn-overs |
|---|---|---|---|---|---|
| 0.5 | 0.542 | 10.842 | 0.035 | 0.375 | 8.3 |
| 1 | 0.565 | 11.297 | 0.054 | 0.610 | 13.5 |
| 2 | 0.562 | 11.239 | 0.075 | 0.846 | 18.7 |
| 4 | 0.528 | 10.556 | 0.190 | 2.008 | 44.3 |
| 8 | 0.570 | 11.395 | 0.328 | 3.740 | 82.5 |
| ca. 100 | 0.542 | 10.836 | 0.517 | 5.597 | 123.5 |
| 0.5 | 0.555 | 11.095 | 0.031 | 0.349 | 7.7 |
| 1 | 0.526 | 10.527 | 0.046 | 0.487 | 10.7 |
| 2 | 0.575 | 11.503 | 0.091 | 1.043 | 23.0 |
| 4 | 0.560 | 11.209 | 0.156 | 1.749 | 38.6 |
| 8 | 0.558 | 11.154 | 0.339 | 3.780 | 83.4 |
| 16 | 0.558 | 11.163 | 0.458 | 5.109 | 112.7 |

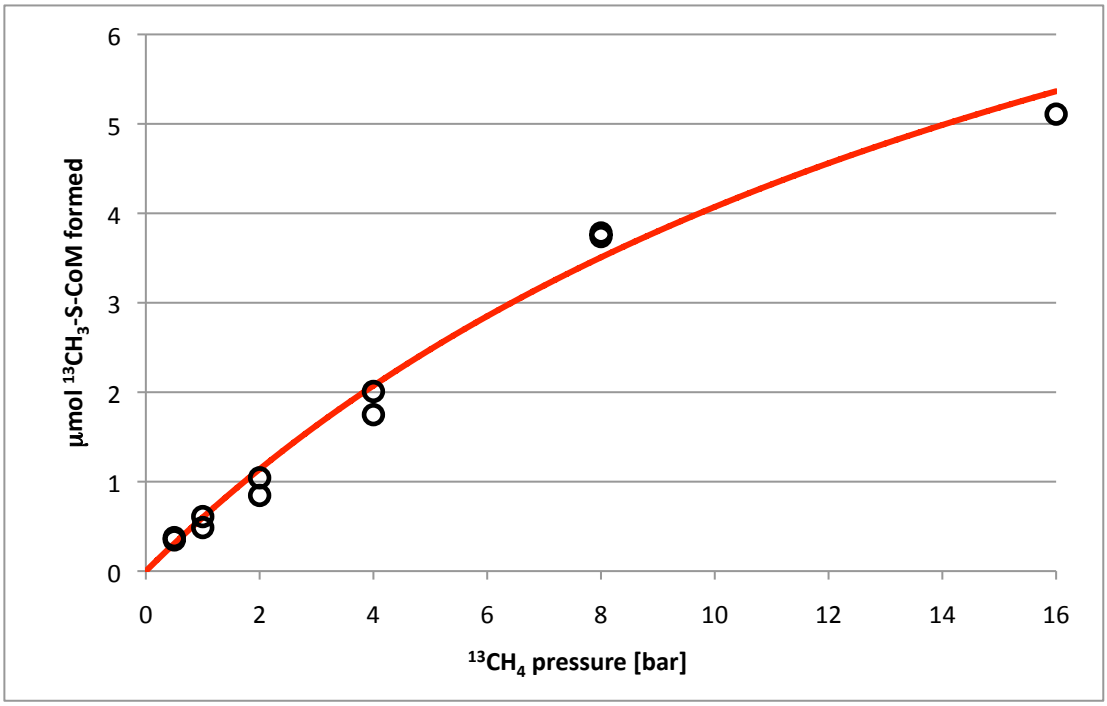


**Figure 2.9**: Correlation of the pressure of $^{13}CH_4$ and methane activation. The experiment with estimated 100 bar $^{13}CH_4$ is omitted in this graph because the precise pressure is not known. **Black circles**: data from table 2.10 without "100 bar" value. **Red line**: Least squares fitting to Michaelis–Menten kinetics (KaleidaGraph version 4.1.2): $K_M(^{13}CH_4)$ = 18 ± 4 bar; $v_{max}$ = 11 ± 2 µmol $^{13}CH_3$-S-CoM formed in 30 min.

### 2.2.6 Influence of the heterodisulfide concentration

The influence of the heterodisulfide (HDS) concentration on the activity of methane activation was determined by varying its concentration at equilibrium. In order to have x mM heterodisulfide and 2 mM methyl-coenzyme M present at equlibrium, x mM coenzyme B and (x + 2) mM $^{13}CH_3$-S-CoM were premixed at different concentrations x. In this set of experiments the $^{13}C$ label was in the substrate and methane with natural abundance $^{13}C$ was used. For each set of experiments one aliquot of each premixed solution was complemented with enzyme and the desired pressure of methane (for details see experimental section 6.3.5). **Table 2.11** shows the amount of methane activated according to $^{12}CH_3$-S-CoM formed.

**Table 2.11**: Activation of methane using different amounts of heterodisulfide at equilibrium. The incubation time was 15 min with an average of 2.04 mg (7.27 nmol) enzyme, determined for each data point by $^{1}$H-NMR integration of the signal of Tris-HCl buffer that is proportional to enzyme concentration. Values are corrected for initial 1.0% $^{12}$C in the substrate. For detailed procedures and additional comments see experimental section 6.3.5.

| | 0.2 bar $CH_4$ | | | 1 bar $CH_4$ | | |
|---|---|---|---|---|---|---|
| HDS [mM] | $^{12}CH_3$-S-CoM formed [μmol] | E [nmol] | turn-overs | $^{12}CH_3$-S-CoM formed [μmol] | enzyme [nmol] | turn-overs |
| Run 1 | | | | | | |
| 0.2 | 0.048 | 6.776 | 7.0 | 0.291 | 6.554 | 44.4 |
| 0.5 | 0.065 | 6.342 | 10.3 | 0.551 | 7.664 | 72.0 |
| 1 | 0.035 | 7.041 | 4.9 | 0.413 | 6.721 | 61.4 |
| 2 | 0.113 | 8.272 | 13.6 | 0.455 | 7.122 | 63.9 |
| 4 | 0.127 | 7.379 | 17.2 | 0.696 | 7.413 | 93.8 |
| 8 | 0.105 | 7.631 | 13.7 | 0.569 | 7.271 | 78.2 |
| Run 2 | | | | | | |
| 0.2 | 0.048 | 7.149 | 6.7 | 0.289 | 6.910 | 41.8 |
| 0.5 | 0.085 | 9.525 | 9.0 | 0.454 | 7.405 | 61.4 |
| 1 | 0.106 | 6.931 | 15.3 | 0.547 | 6.550 | 83.5 |
| 2 | 0.164 | 7.928 | 20.6 | 0.612 | 7.265 | 84.3 |
| 4 | 0.129 | 7.378 | 17.5 | 0.643 | 7.259 | 88.6 |
| 8 | 0.102 | 7.805 | 13.0 | 0.454 | 6.449 | 70.4 |

The rate of methane activation decreases at higher concentrations of heterodisulfide (**figure 2.10**).

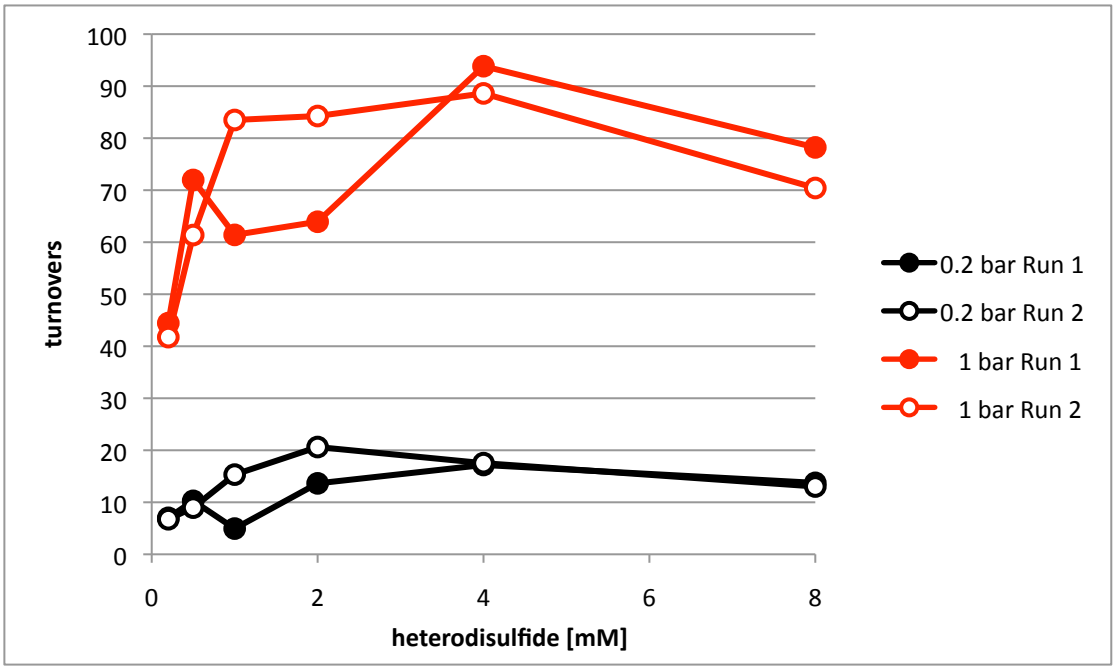


**Figure 2.10**: Dependence of the rate of methane activation (displayed in turnovers) on the heterodisulfide concentration present at equilibrium (data from table 2.11).

Possible explanations for the activity decrease at higher concentrations of heterodisulfide will be discussed in section 2.4.3.

In order to obtain a first estimation of the kinetic parameters related to the heterodisulfide concentration, only the data points of each "Run 2" from 0.2 to 2 mM heterodisulfide were evaluated (**figure 2.11**).

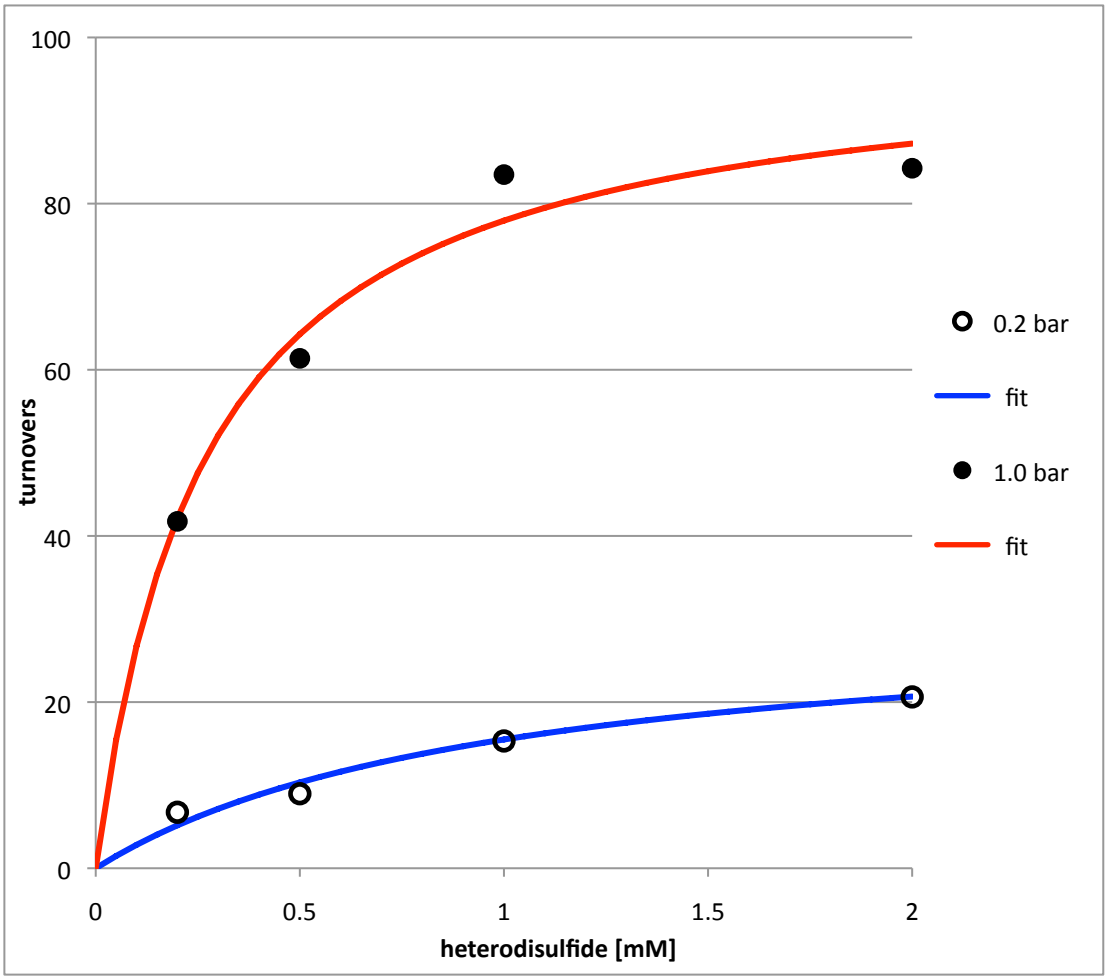


**Figure 2.11**: Dependence of methane activation rate (displayed in turnovers) on the heterodisulfide (HDS) concentration present at equilibrium. Only data points from "Run 2" between 0.2 mM and 2 mM heterodisulfide are evaluated for the two pressures of methane employed. Colored lines: Least squares fitting to Michaelis–Menten kinetics (KaleidaGraph version 4.1.2). **Red line**: $K_M$(HDS) for 1 bar methane = 0.27 ± 0.07 mM; $v_{max}$ = 99 ± 7 turnovers in 15 min. **Blue line**: $K_M$(HDS) for 0.2 bar methane = 1.0 ± 0.4 mM; $v_{max}$ = 31 ± 5 turnovers in 15 min.

The different kinetic behavior of the two runs of experiments (denoted as "Run 1" and "Run 2") for both methane pressures applied could be related to the different sample preparation order for the two experiments as described more in detail in section 6.3.5.

## 2.3 Implication of the Results for AOM with Sulfate

The *in vitro* experiments with purified MCR from *M. marburgensis* displayed a methane activation rate of 11.4 nmol $min^{-1}$ $mg^{-1}$ at 60 °C under 1 bar methane pressure (about 1 mM dissolved methane). The rate *in vivo* was estimated to be 70 nmol $min^{-1}$ $mg^{-1}$ (at 12 °C and 21 mM dissolved methane, cf. table 2.1)

Considering the different methane concentrations present and that the apparent $K_M$ value for methane is above 10 mM, these two specific rates are in reasonable agreement. The *in vitro* experiment at lower temperatures displayed a specific activity lower than that observed *in vivo*. But, since the temperature optimum of the process carried out by the ANME archaea is 12 °C and the optimum for MCR from *M. marburgensis* is 65 °C, the two enzymes should be compared at their temperature optimum.

The results described here demonstrate that MCR is able to activate methane at a rate high enough to fully support the hypothesis of reverse methanogenesis.

From a chemical point of view, the result that methane activation occurs at temperatures down to 4 °C in neutral aqueous solvent without the involvement of oxygen-derived radicals is remarkable and unprecedented in laboratory chemistry. Besides the biological relevance of this process, understanding how MCR operates at a molecular level could stimulate the design of more sophisticated synthetic catalysts for the selective functionalization of unactivated C-H bonds.

## 2.4 Discussion of Experiments and Outlook

### 2.4.1 Dependence on enzyme concentration, time and temperature

The rate of methane activation depends linearly on the amount of enzyme added, and no $^{13}C$ incorporation occurs without enzyme. This correlation proves that the C-H bond activation of $^{13}C$-labeled methane is catalyzed by the enzyme.

The decrease in methane activation activity during incubation at 60 °C is consistent with earlier experiments performed in the forward direction. Deactivation is caused by oxidation of the nickel center to the more stable Ni(II) form. However, it is not clear if this oxidation is caused by residual oxygen reacting with the enzyme or by another source of oxidant within the protein. Experiments at lower temperatures display a lower rate of enzyme deactivation.

The highest rate of methane activation occurs at 60 °C, which corresponds to the temperature optimum of methane formation. The specific rate of methane activation (11.4 nmol $min^{-1}$ $mg^{-1}$) is about 1,750 times lower than that of methane formation (20 μmol $min^{-1}$ $mg^{-1}$).

Since the reactions catalyzed by MCR are multistep reactions (ternary complexes have to be formed), the Arrhenius plot of the rate of methane activation is not expected to be linear. In the laboratory, the highest number of turnovers might be achieved at around 40 °C, since enzyme deactivation is slower at this temperature.

### 2.4.2 Dependence on methane pressure

The experiments using lower partial pressures of methane (0.05 bar to 2 bar), as well as the high-pressure series (up to 8 bar) done in the French press cell, show a linear correlation between pressure and the rate of methane activation. Fitting of the high-pressure data from 1 to 16 bar $^{13}CH_4$ to the Michaelis-Menton equation results in an apparent $K_M$ value of 18 ± 2 bar, corresponding to about 20 mM dissolved methane at 60 °C.

Although both the low-pressure series of experiments as well as the high-pressure series in the French press cell show a remarkably linear behavior between methane pressure and the rate of methane activation, the specific rates of the high-pressure experiments are consistently lower than the low-pressure experiments by a factor of 4 (compare corresponding turnover numbers). The cause of this significant difference could not be identified with certainty. Besides the different reaction containers and the fact that the French press cell is not shaken or stirred during incubation, the main difference is that, in the French press experiments, the equilibrium of methyl-coenzyme M and heterodisulfide is reached before the assay is treated with $^{13}CH_4$, because the assay solution is added into the preheated French press cell and not mixed with the substrates on ice, as in the experiments under standard conditions. If this difference in the moment of methane treatment were the reason for the different activities observed, the enzyme would be less stable with the heterodisulfide present and methane absent. Either this methane-free enzyme state is more sensitive to oxygen, or the enzyme may adopt a "blocked" state. Such a state might be caused if all coenzyme B is consumed (because the missing methane drives the reaction to complete conversion of coenzyme B), but the enzyme requires the presence of coenzyme B in one active site so that the other active site can activate methane.

Experiments varying the moment of methane introduction following establishment of the methyl-coenzyme M / heterodisulfide equilibrium would be required to test this hypothesis.

### 2.4.3 Influence of the heterodisulfide concentration

A higher concentration of heterodisulfide in the equilibrium causes a higher rate of methane activation until a maximum is reached between 2 and 4 mM. In all experiments, the highest concentration employed (8 mM) resulted in a decrease of activity. The heterodisulfide (which is formed in these experiments *in situ*) either has a negative effect on enzyme stability or it is able to inhibit the enzyme if its concentration is too high. A mechanism of inhibition could be that methane activation is not possible if both active sites of the enzyme are occupied with heterodisulfide.

### 2.4.4 Order of substrate binding for methane activation

The order of substrate binding in the methane activating direction is a central issue in the elucidation of the still unknown reaction mechanism. It is not known whether the Ni(I) center of the empty active site is able to react with methane or if it has to be converted first to another enzyme state with the heterodisulfide. The preliminary experiments varying the concentration of the heterodisulfide at 0.2 bar and at 1 bar methane pressure were intended to give an answer to this question. Because of the decrease of activity at higher concentrations of heterodisulfide only a first rough estimate of the apparent $K_M$ values for the heterodisulfide at the two partial pressures of methane can be deduced. According to fitting to the Michaelis-Menton equation the apparent $K_M$ values for the heterodisulfide are 1.0 mM for the 1 bar experiments and 0.3 mM for the 0.2 bar experiments. Since it is not understood why activity decreases at higher heterodisulfide concentrations and data for the dependence of apparent methane $K_M$ values at different heterodisulfide concentrations are lacking, no

conclusive statement on the order of substrate binding can be made at this time. To distinguish the three different possibilities (methane first, heterodisulfide first or random), more data are required, and since the experiments are performed under equilibrium conditions, they have to be evaluated using a simulation that also includes the methane forming direction.
However, the experiments at different pressures of methane and the experiments at different concentrations of heterodisulfide allowed a first rough estimate of the two $K_M$ values.

### 2.4.5 Direct reverse reaction

With 8 μmol heterodisulfide and methane, a direct reverse reaction could be observed. The formation of an equal amount of methyl-coenzyme M relative to the active sites present (15 nmol) might be a coincidence. Further studies with different enzyme concentrations would be required to establish a direct correlation. In the experiments with a high concentration of heterodisulfide (50 mM, 80 μmol), no methyl-coenzyme M was formed at all. This result could be due to impurities in the synthesized heterodisulfide that quenched the enzyme. In order to verify that the thermodynamic equilibrium was reached in the 5 mM heterodisulfide experiment, further studies are required. The equilibrium constants, together with the $K_M$ values, would allow the $\Delta G'^0$ value of the reaction (which is estimated to be -30 ± 10 kJ $mol^{-1}$ towards methane formation) to be determined using the Haldane equation. However, in the preliminary experiments described here, the concentration of the coenzyme B formed was low and could not be determined (probably due to oxidation prior to measurement). Experiments at a defined concentration of added coenzyme B will be needed to determine equilibrium constants.

### 2.4.6 Implications for the reaction mechanism

The results described in this chapter provided a more comprehensive thermodynamic picture of the overall reaction since at least approximate $K_M$ values are now known for all the natural substrates. The finding that MCR is able to activate methane at a significant rate allows us to rule out some of the reaction mechanisms proposed earlier for methanogenesis because they are not reasonable for the reverse reaction. An example is the proposed generation of methane by protonation of $CH_3$-Ni(II)F430 which, in the reverse direction, would require the deprotonation of free methane.

The formation of about 7% $CH_2D_2$ in the methane forming direction cannot be caused by a "double-turnover" alone (the hypothesis proposed in section 1.4.2) since the rate of methane activation is far too low. The process of $CH_2D_2$ formation is analyzed in the next chapters through detailed studies with deuterium and $^{13}C$ labels.

# 3 Detection of Intermediates by Isotope Exchange

## 3.1 Introduction: The Formation of $CH_2D_2$

The formation of $CH_2D_2$ from $CH_3$-S-CoM catalyzed by MCR in deuterated medium was discovered earlier in our group[113]. These experiments with purified MCR also proved that the formation of $CH_2D_2$ is indeed catalyzed by MCR whereas in older experiments[114-116] a cell-free extract containing all soluble enzymes was used.

A "double turnover" (formation of $CH_3D$, reverse reaction to $CH_2D$-S-CoM followed by formation of $CH_2D_2$), as proposed in section 1.4.2, cannot account for all $CH_2D_2$ formed, because the reverse reaction proceeds at a much lower rate (cf. Chapter 2). Accordingly, the formation of $CH_2D_2$ requires at least one intermediate, and could occur along one of the pathways A-C in **figure 3.1**.

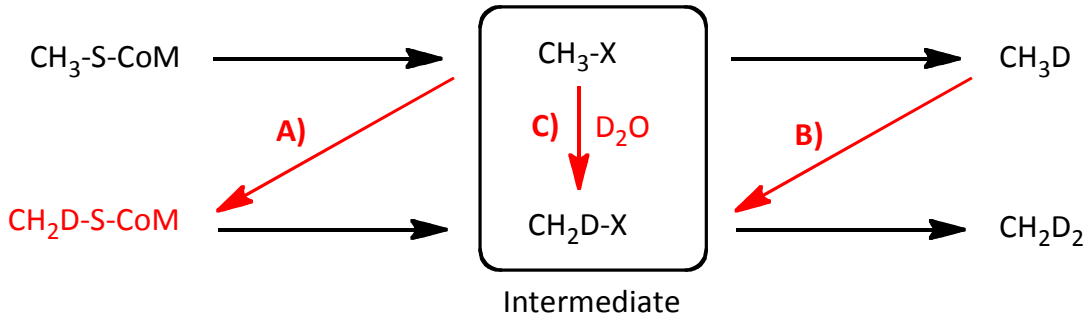


**Figure 3.1**: Additional reaction pathways (**A**, **B** and **C**) proceeding via an intermediate that account for the formation of $CH_2D_2$.

In order to probe the different reaction pathways described above, the substrate was analyzed in the assay solution before complete conversion and checked for the amount of $CH_2D$-S-CoM formed. A kinetic analysis comparing the rates of $CH_2D$-S-CoM and $CH_2D_2$ formation was carried out as well as an experiment probing methane activation in deuterated medium.

The analysis of the different methane isotopologues was performed by $^1$H-NMR spectroscopy after dissolving the methane in $CDCl_3$, as exemplified with a synthetic mixture (section 6.4.1) containing all possible H/D isotopologues of methane (**figure 3.2**).

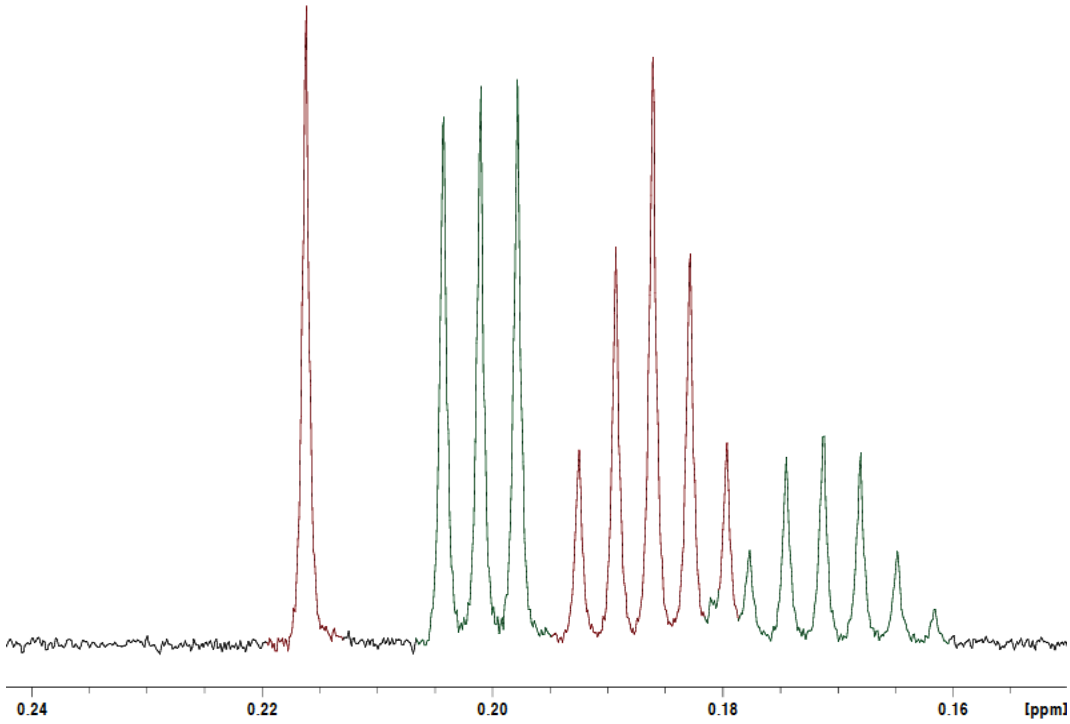


**Figure 3.2**: 600 MHz $^1$H-NMR spectrum of a gas mixture containing all H/D isotopologues of methane. From left to right: $CH_4$ (red), $CH_3D$ (green), $CH_2D_2$ (red) and $CHD_3$ (green).

## 3.2 Deuterium Incorporation into Methyl-Coenzyme M

### 3.2.1 Correlation of $CH_2D$-S-CoM and $CH_2D_2$ formation

Methyl-coenzyme M (4 mM) and coenzyme B (2 mM) were incubated at 60 °C with MCR (0.47 μM) in deuterated medium. Analysis of the aqueous phase by $^1$H-NMR spectroscopy after 4 min revealed that a significant amount of deuterium had been incorporated into the *S*-methyl group of methyl-coenzyme M (**figure 3.3**).

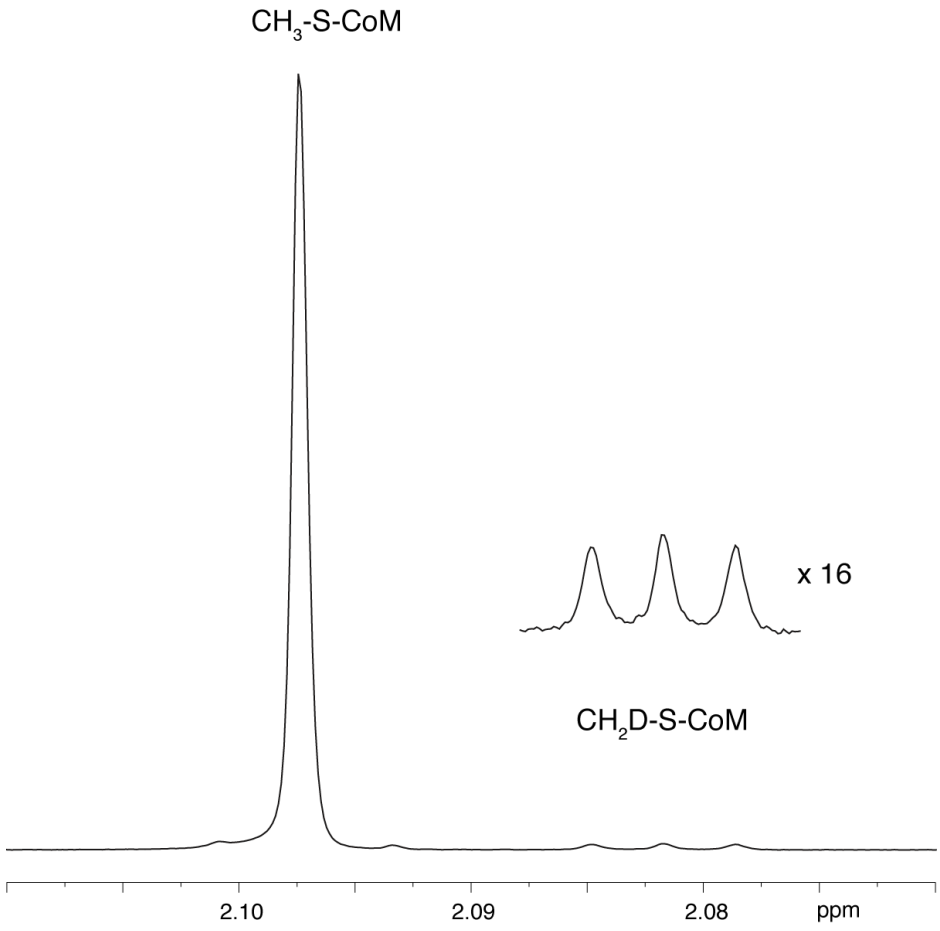


**Figure 3.3**: Expansion of the $^1$H-NMR spectrum in the region of the *S*-methyl group of methyl-coenzyme M. After incubation with MCR (0.47 μM) in deuterated medium (assay: section 6.2.4), deuterium is introduced into the methyl group (triplet with intensity ratio 1:1:1, $J$ = 1.9 Hz). The two satellites around the signal of the $CH_3$ group ($J$ = 4.4 Hz) are due to the natural abundance of $^{13}$C at carbon 2 ($CH_3$-S-***C***$H_2CH_2SO_3^-$).

In order to correlate the observed deuterium incorporation into the substrate with the formation of $CH_2D_2$, assays containing Ti(III)-citrate (see 6.2.6) were used, which allowed 10 mM substrate to be converted to methane. **Table 3.1** displays the formation of $CH_4$ (due to incomplete labeling of the medium), $CH_3D$, $CH_2D_2$ and deuterium incorporation into the substrate as a function of time.

**Table 3.1**: Formation of different isotopologues of methane and incorporation of deuterium into the substrate methyl-coenzyme M as a function of time. Catalyzed by 2.4 nmol (0.48 mg) MCR in deuterated medium using an assay (1.6 ml) with Ti(III)-citrate (6.2.6).

| Time [min] | $CH_4$ [μmol] | $CH_3D$ [μmol] | $CH_2D_2$ [μmol] | $CH_3$-S-CoM [μmol] | $CH_2D$-S-CoM [μmol] |
|---|---|---|---|---|---|
| 0 | 0 | 0 | 0 | 16 | 0 |
| 0.5 | 0.039 | 1.135 | 0.042 | 10.341 | 0.107 |
| 1 | 0.085 | 3.121 | 0.087 | 8.677 | 0.176 |
| 2 | 0.173 | 6.951 | 0.201 | 4.836 | 0.243 |
| 4 | 0.289 | 12.574 | 0.562 | 2.905 | 0.366 |
| 8 | 0.335 | 14.728 | 1.054 | 0.000 | 0.000 |

The time course of all isotopologues of the product and substrate is plotted in **figure 3.4 A**. Expansion of the plot containing only the two species of interest, $CH_2D_2$ and $CH_2D$-S-CoM (**figure 3.4. B**), shows that $CH_2D$-S-CoM is formed initially and $CH_2D_2$ is formed after a delay.

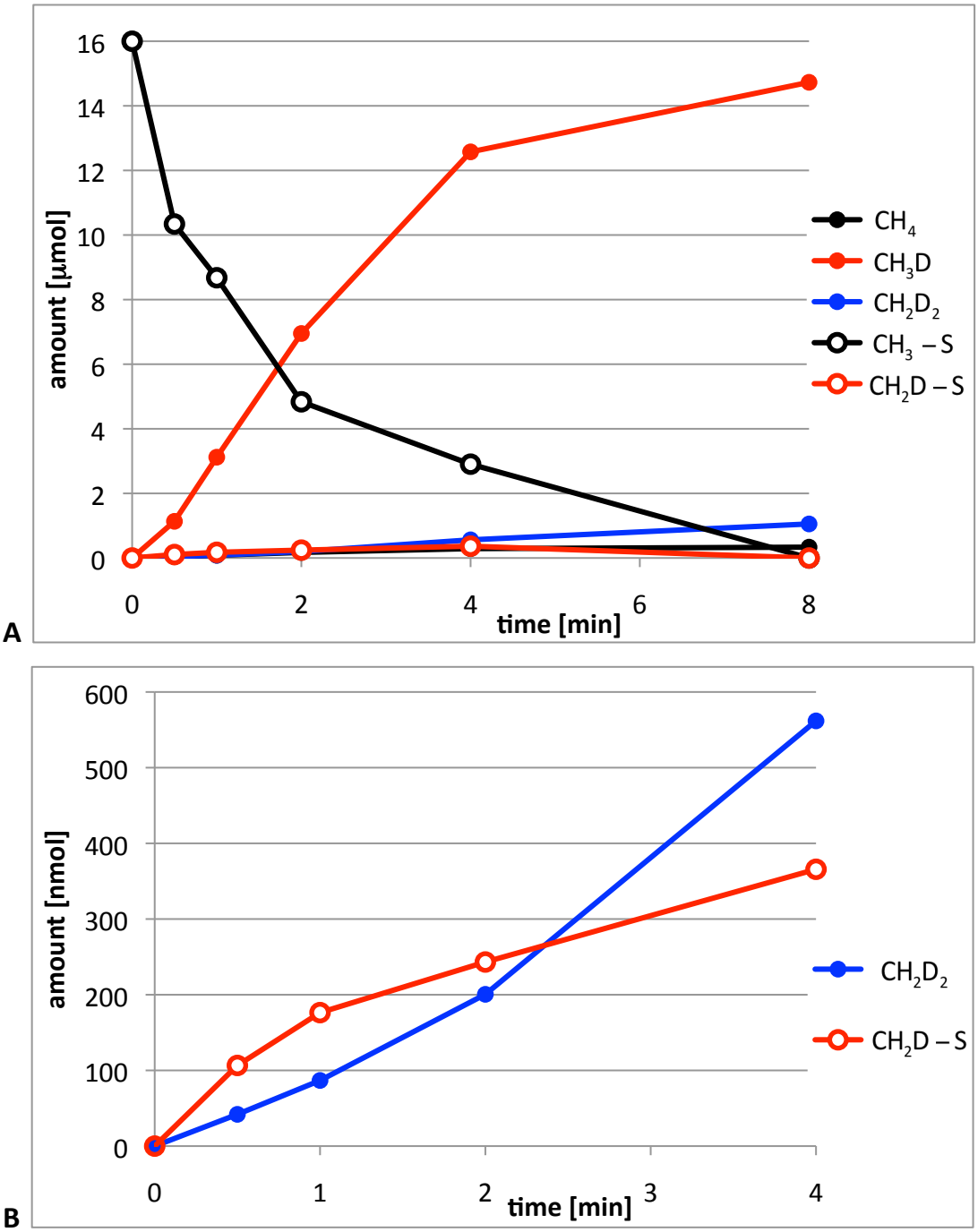


**Figure 3.4**: Formation of different methane isotopologues and deuterated substrate (data from table 3.1). **A**: Time course until completion of the reaction. **B**: Expansion until 4 min showing only the deuterated substrate and the doubly labeled methane.

### 3.2.2 Isotope exchange under equilibrium conditions

Without the second substrate coenzyme B no deuterium incorporation into the substrate could be observed.

In order to compare deuterium incorporation into methyl-coenzyme M under different conditions (e.g. different temperatures), the conversion to methane should be constant.

4 mM methyl-coenzyme M and 2 mM coenzyme B in the assay (section 6.2.4) resulted in a constant conversion of about 50%. An experiment to confirm the constant conversion was carried out by stopping the reaction after different incubation times after equilibrium was reached.

No significant incorporation of deuterium into the substrate occurs anymore after reaching equilibrium when the concentration of coenzyme B is very low (**figure 3.5**).

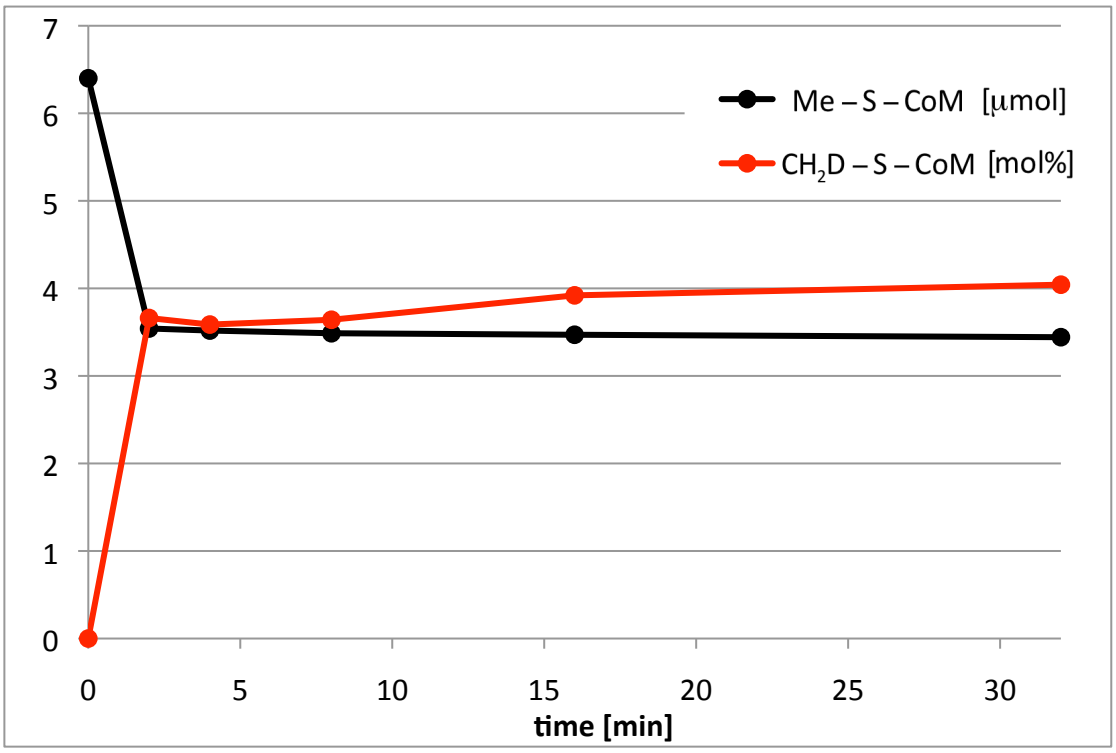


**Figure 3.5**: Conversion to methane and the molar fraction of deuterated substrate as a function of the incubation time. No significant deuterium incorporation occurs after coenzyme B is used up (numerical data given in section 6.4.2).

### 3.2.3 Temperature dependence of isotope exchange

The correlation between product formation and substrate deuteration was investigated at different temperatures. The method of limiting the amount of the second substrate coenzyme B in order to obtain 50% conversion within 4 min in all experiments, as described above, was used. Because the rate of methane formation is dependent on the temperature, different concentrations of enzyme were used (**table 3.2**).

**Table 3.2**: Deuterium incorporation into methyl-coenzyme M after 4 min incubation time at different temperatures.

| T [°C] | Enzyme [nmol] | Me-S-CoM [μmol] | $CH_2D$-S-CoM [molar fraction] | $CH_2D$-S-CoM [μmol] | methane [μmol] |
|---|---|---|---|---|---|
| 4 | 21.4 | 3.552 | 0.0860 | 0.305 | 2.848 |
| 22 | 8.6 | 2.898 | 0.0728 | 0.211 | 3.502 |
| 40 | 2.1 | 2.931 | 0.0536 | 0.157 | 3.469 |
| 60* | 1.1 | 3.462 | 0.0342 | 0.118 | 2.938 |

* Values for 60 °C were taken from another set of experiments with the same enzyme preparation (performed to measure the D incorporation into Me-S-CoM dependent on the concentration of $D_2O$ in the medium, see 4.6.3).

For comparison of the different temperatures employed, the absolute amount of deuterated substrate had to be used because the assay incubated with enzyme at 4 °C proceeded only to 45% conversion (22 °C and 40 °C assays proceeded to 55% conversion) and the assay at 60 °C was taken from another set of experiments.

The ratio of deuterated substrate formed versus methane formed is plotted logarithmically against the inverse of the temperature (**figure 3.6)**.

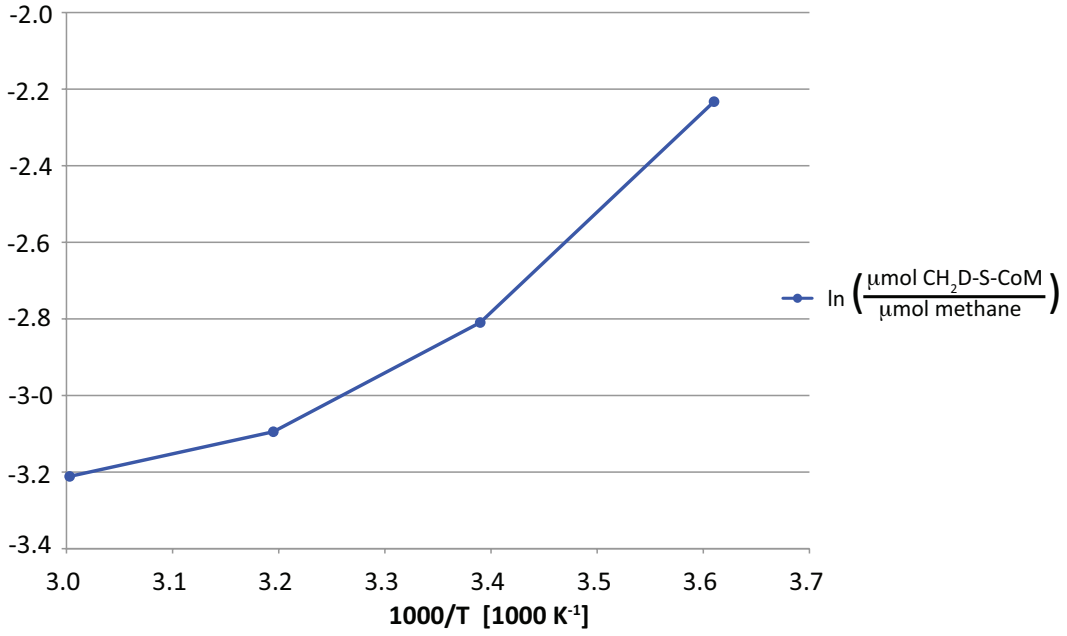


**Figure 3.6**: Correlation of substrate deuteration versus methane formation. Ln ($CH_2D$-S-CoM formed / methane formed) versus 1000/T. For numerical values see section 6.4.3.

### 3.2.4 $CH_4$ activation in $D_2O$

Methane activation in deuterated medium and analysis of the gas phase allows deuterium incorporation into methane (pathway B in figure 3.1) to be probed. At the same time, deuterium incorporation into the intermediate (pathway C in figure 3.1) can be studied. This experiment was performed with $^{13}CH_3$-S-CoM and methane with natural abundance $^{13}C$. Analysis of both the assay solution and the headspace gas allowed all different isotopologues of methane and substrate from the same assay to be quantified (**table 3.3**).

**Table 3.3**: Activation of $CH_4$ in $D_2O$ catalyzed by 15 nmol (4.2 mg) enzyme under equilibrium conditions containing $^{13}CH_3$-S-CoM. Analysis of species after 32 min incubation time was done by integration of the $^1$H-NMR spectra of the aqueous phases and of the gas phase. For the headspace a total amount 200 μmol methane (5 ml) was assumed and not corrected for the additional methane formed from the substrate (3 μmol). For t = 0, 99.0% $^{13}$C enrichment was used for the substrate to calculate the amount of $^{12}CH_3$-S-CoM. A natural abundance of 1.1% for $^{13}$C and 150 ppm for deuterium (600 ppm $CH_3D$ in $CH_4$ and 450 ppm $^{13}CH_2D$-S-CoM in $^{13}CH_3$-S-CoM) was assumed.

| Species | t = 0 min | t = 32 min | Formed by MCR |
|---|---|---|---|
| solution | | | |
| $^{13}CH_3$-S-CoM [nmol] | 6 336 | 2 586 | |
| $^{13}CH_2D$-S-CoM [nmol] | 3 | 413 | 410 |
| $^{13}CHD_2$-S-CoM [nmol] | 0 | 26 | 26 |
| $^{12}CH_3$-S-CoM [nmol] | 64 | 384 | 320 |
| $^{12}CH_2D$-S-CoM [nmol] | 0 | 6 | 6 |
| headspace | | | |
| $^{12}CH_4$ [nmol] | 197 800 | 195 241 | |
| $^{12}CH_3D$ [nmol] | 119 | 140 | 21 |
| $^{13}CH_4$ [nmol] | 2 200 | 2 247 | 47 |
| $^{13}CH_3D$ [nmol] | 1 | 2 123 | 2 122 |
| $^{13}CH_2D_2$ [nmol] | 0 | 249 | 249 |

## 3.3 Isotope Exchange in the Substrate Ethyl-Coenzyme M

### 3.3.1 Introduction: The non-natural substrate ethyl-coenzyme M

When ethyl-coenzyme M is used as a substrate of MCR[43] ethane is formed at a specific rate that is 200 times lower than the rate of methane formation from methyl-coenzyme M. The apparent $K_M$ value of ethyl-coenzyme M was determined previously to be 20 mM[44].

Ahn, Krzycki and Floss reported that incubation of the chiral substrate [1′-$^2$H, 1′-$^3$H]-ethyl-coenzyme M with cell free extracts from *Methanosarcina barkeri* results in the formation of chiral ethane ($CH_3CHDT$) with a net inversion of configuration[77].

The conversion to ethane was 28% for the (*R*)-substrate and 10% for the (*S*)-substrate. After chemical conversion of the ethane that is formed to acetate (2-3% radiochemical yield), the absolute configuration of the methyl group was determined using an established method[127, 128]. A partial net inversion of the configuration corresponding to 41% ee from the (*S*)-substrate and 51% ee from the (*R*)-substrate was found[77].

In the present study, ethyl-coenzyme M was incubated in deuterated medium in order to check whether isotope exchange occurs as for the native substrate methyl-coenzyme M.

### 3.3.2 Deuterium incorporation into ethyl-coenzyme M

Incubation of ethyl-coenzyme M with MCR in deuterated medium (assay described in section 6.2.5) resulted in deuterium incorporation at *both* carbon centers within the ethyl-group. $^1$H-NMR spectroscopy with broadband deuterium decoupling ($^1$H{$^2$H}-NMR) identified the different isotopologues present (**figure 3.7**). After 32 min, a mixture containing all 12 possible isotopologues was found. The tetra-deuterated isotopologues, for example, were present at 10.8% (for $CHD_2CD_2$-S-CoM) and 4.9% (for $CD_3CHD$-S-CoM). **Figure 3.8** displays a time course for all 11 isotopologues that can be distinguished by $^1$H{$^2$H}-NMR spectroscopy.

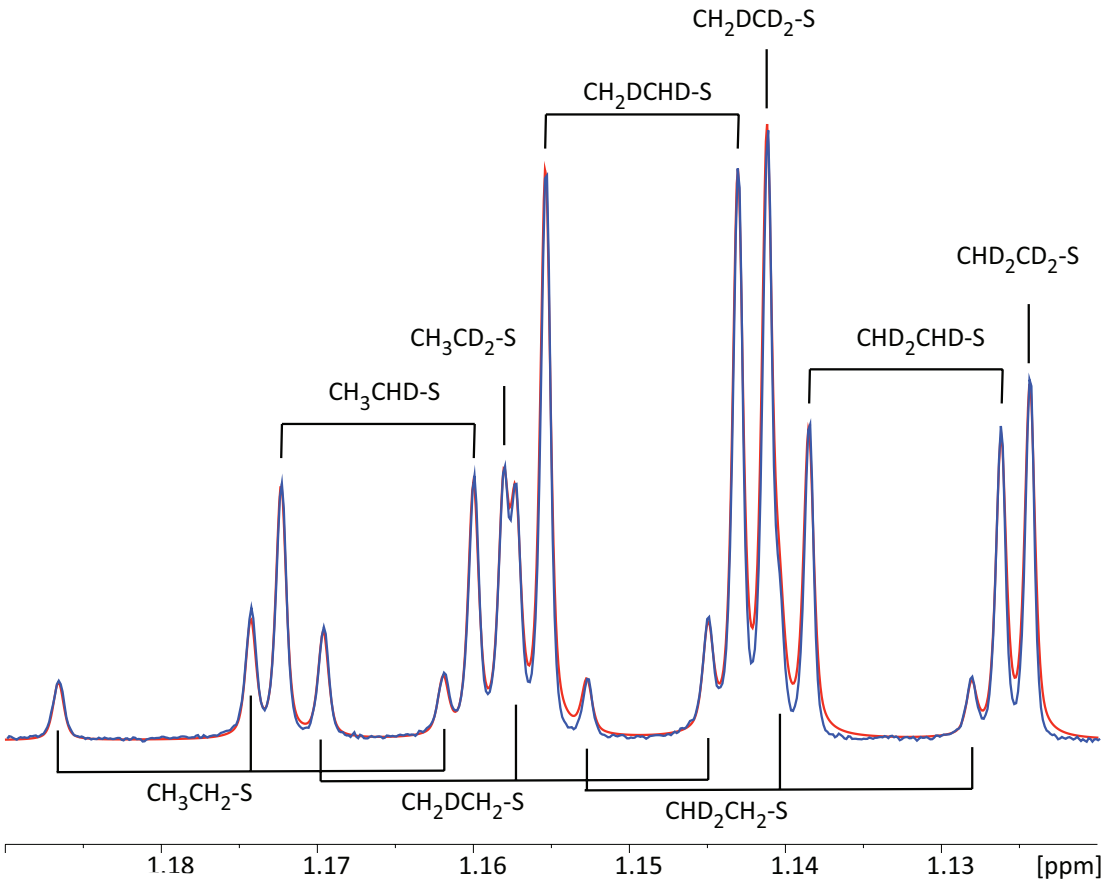


**Figure 3.7**: Expansion of the 600 MHz $^{1}H\{^{2}H\}$-NMR spectrum (acquired with broadband deuterium decoupling) showing the region of the methyl group of ethyl-coenzyme M (**C*H*$_3$**-$CH_2$-S-CoM). Ethyl-coenzyme M and coenzyme B were incubated with MCR (1.5 nmol, 0.42 mg) in $D_2O$ until 5% conversion to ethane was reached (32 min). Blue line: acquired spectrum, red line: fitted with iNMR (section 6.6.5). The brackets indicate peaks belonging to the same isotopologue. Expansion of the region of the corresponding methylene group of ethyl-coenzyme M ($CH_3$-**C*H*$_2$**-S-CoM), including the fitting, is shown in the experimental section 6.4.4. "-CoM" is omitted in the designation of the Et-S-CoM signals.

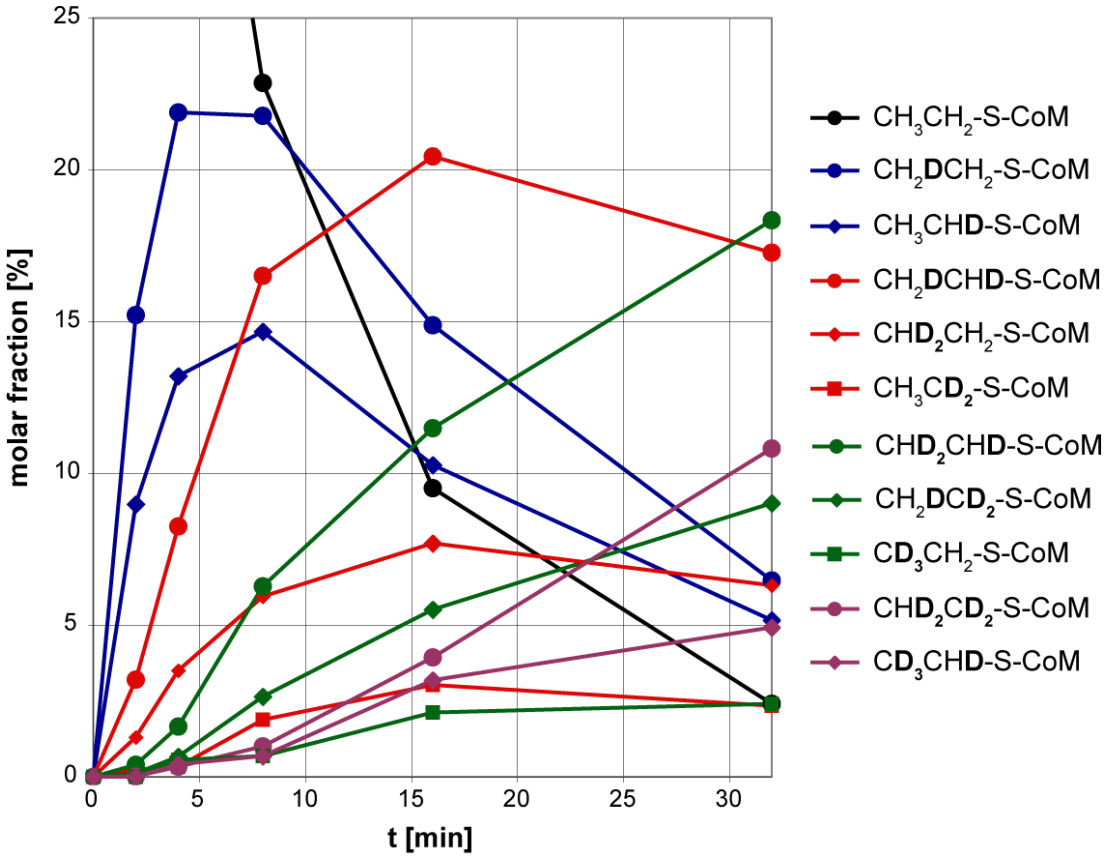


**Figure 3.8**: Formation of all 11 isotopologues of ethyl-coenzyme M that can be distinguished by $^{1}H\{^{2}H\}$-NMR spectroscopy as a function of the incubation time with MCR (1.5 nmol, 0.42 mg). Numerical values from fitted NMR spectra are given in 6.4.4.

### 3.3.3 Carbon-center scrambling within the ethyl group

Observing deuterium incorporation in the methyl group of ethyl-coenzyme M led us to consider an interchange of the two carbon atoms within the ethyl group. This possibility was tested by the synthesis of ethyl-coenzyme M labeled with one $^{13}C$ within the ethyl group ($CH_3{}^{13}CH_2$-S-CoM) followed by incubation with MCR in a non-deuterated assay solution. **Figure 3.9** shows the scrambling of the $^{13}C$ label within the ethyl group as a function of incubation time.

Incubation of ethyl coenzyme M with MCR in the absence of coenzyme B did not give any $^{13}C$ isotope exchange within the ethyl group.

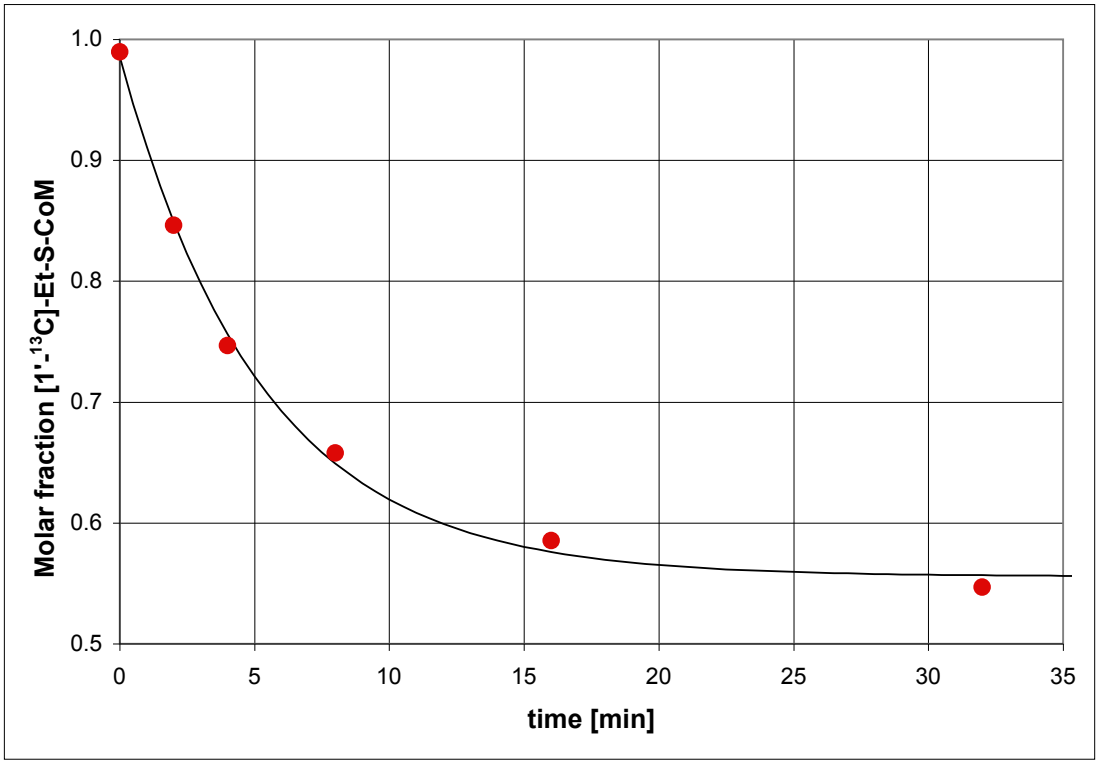


**Figure 3.9**: Scrambling of the $^{13}C$ label in ethyl-coenzyme M. Molar fractions of the starting isotopologue $CH_3{}^{13}CH_2$-S-CoM as a function of incubation time. Conditions: $CH_3{}^{13}CH_2$-S-CoM (10 mM) and CoB (2 mM) in 1.6 ml aqueous buffer, incubated with 1.5 nmol (0.42 mg) enzyme at 60 °C. The drawn curve represents an exponential fit to the data points assuming first order establishment of equilibrium kinetics ($t_{1/2}$ for scrambling = 3.63 min).

### 3.3.4 Correlation of carbon-center scrambling and deuterium incorporation

In order to obtain more detailed information about the process of isotope exchange within the ethyl group, ethyl-coenzyme M with one $^{13}C$ label in the ethyl group was incubated with MCR in deuterated medium. $^{1}H\{^{2}H\}$-NMR spectroscopy and fitting of the spectra (see section 6.4.5 for expansions of the spectra and fitting) allowed the deuterium incorporation and the interchange of the two carbon centers to be correlated. The time course of the formation of the different isotopologues (**figure 3.10**) shows that deuterium is introduced only at the carbon center bound to sulfur in the substrate. After 2 min reaction time, the only mono-deuterated isotopologues found were $CH_3{}^{13}CHD$-S-CoM (8.2%) and $^{13}CH_2DCH_2$-S-CoM (12.9%) (figure 3.10, blue curves).

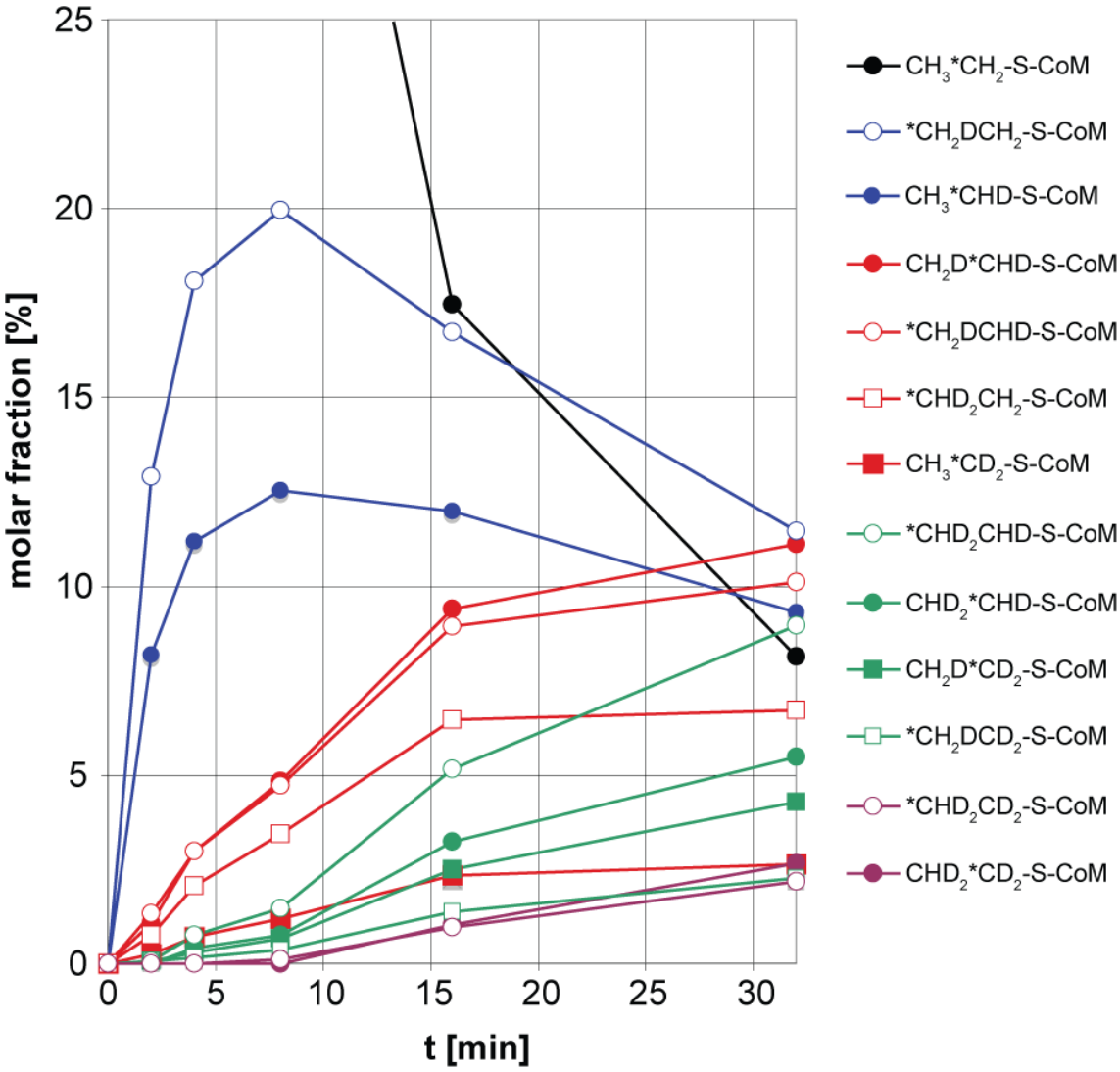


**Figure 3.10**: Incubation of $CH_3{}^{13}CH_2$-S-CoM and CoB-SH with 1.5 nmol (0.42 mg) MCR in $D_2O$. $^1H\{^2H\}$-NMR spectroscopy and fitting of the spectra allowed the concentrations of the 13 most abundant isotopologues to be measured. For numerical values see 6.4.5.

As the second "generation", the following *di*-deuterated species (red) were found: $CH_3{}^{13}CD_2$-S-CoM (1.18%), $^{13}CHD_2CH_2$-S-CoM (3.43%), and $^{13}CH_2DCHD$-S-CoM (4.71%), $CH_2D^{13}CHD$-S-CoM (4.84%).

$^{13}$C-NMR spectroscopy using simultaneous broadband proton and deuterium decoupling ($^{13}C\{^1H\}\{^2H\}$-NMR) allowed observation of all possible isotopologues present to more than 0.1 mol%, including the isotopologues containing a fully deuterated ethyl group (**figure 3.11**).

**Table 3.4** shows the molar fraction of all possible isotopologues obtained from integration of the $^{13}C\{^1H\}\{^2H\}$-NMR spectra.

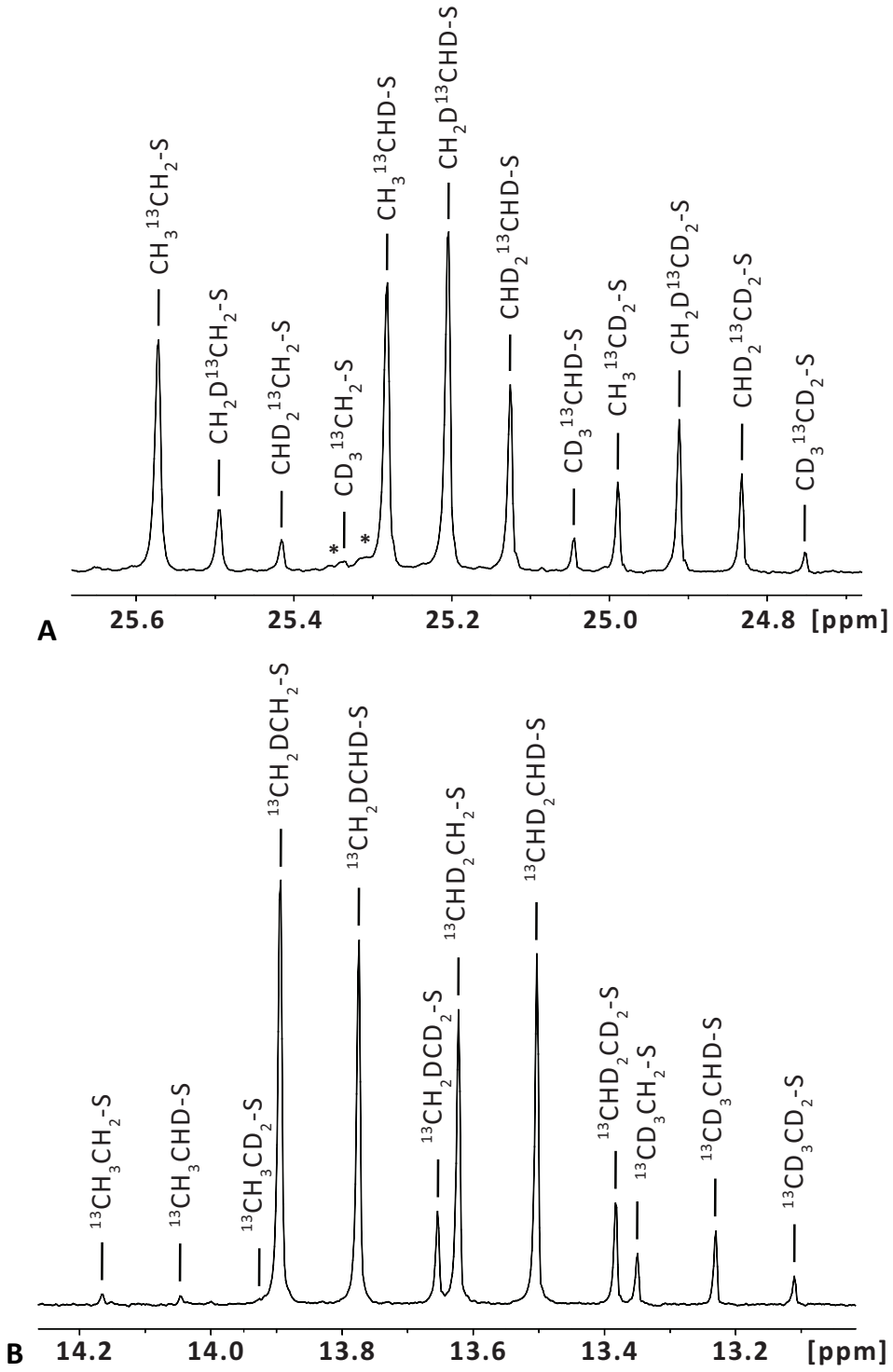


**Figure 3.11**: Expansions of the 150 MHz inverse-gated $^{13}C\{^{1}H\}\{^{2}H\}$-NMR spectrum from the assay correlating deuterium incorporation and carbon center scrambling after 32 min incubation time. **A**: Expansion containing the signals of isotopologues labeled in the methylene group. **B**: Signals of isotopologues labeled in the methyl group. *****: Signals due to natural abundance of $^{13}C$ at carbon 2 (Et-S-***C***$H_2CH_2SO_3^-$).

**Table 3.4**: Molar fraction [%] of all 24 isotopologues of [$^{13}$C]-ethyl-coenzyme M at different incubation times according to integration of the inverse-gated $^{13}$C-NMR spectrum (relaxation delay: 60 s). A plot is given in section 4.5.3, figure 4.8.

| $^{13}$C in $CH_2$ | | | | | | | | | | | | |
|---|---|---|---|---|---|---|---|---|---|---|---|---|
| min | $CH_3{}^{13}CH_2$-S-CoM | $CH_2D{}^{13}CH_2$-S-CoM | $CHD_2{}^{13}CH_2$-S-CoM | $CD_3{}^{13}CH_2$-S-CoM | $CH_3{}^{13}CHD$-S-CoM | $CH_2D{}^{13}CHD$-S-CoM | $CHD_2{}^{13}CHD$-S-CoM | $CD_3{}^{13}CHD$-S-CoM | $CH_3{}^{13}CD_2$-S-CoM | $CH_2D{}^{13}CD_2$-S-CoM | $CHD_2{}^{13}CD_2$-S-CoM | $CD_3{}^{13}CD_2$-S-CoM |
| 2 | 73.3 | 0.6 | 0 | 0 | 7.9 | 1.2 | 0.1 | 0 | 0.2 | 0.1 | 0 | 0 |
| 4 | 56.9 | 0.8 | 0 | 0 | 11.6 | 2.4 | 0.1 | 0 | 0.5 | 0.2 | 0 | 0 |
| 8 | 43.3 | 1.4 | 0.2 | 0 | 13.3 | 5.0 | 0.7 | 0 | 1.0 | 0.5 | 0.1 | 0 |
| 16 | 19.2 | 2.2 | 0.7 | 0 | 12.3 | 9.8 | 3.2 | 0.3 | 2.1 | 2.4 | 1.0 | 0.1 |
| 32 | 9.1 | 2.2 | 0.9 | 0 | 9.2 | 10.9 | 5.5 | 0.9 | 2.1 | 4.1 | 2.6 | 0.6 |

| $^{13}$C in $CH_3$ | | | | | | | | | | | | |
|---|---|---|---|---|---|---|---|---|---|---|---|---|
| min | $^{13}CH_3CH_2$-S-CoM | $^{13}CH_3CHD$-S-CoM | $^{13}CH_3CD_2$-S-CoM | $^{13}CH_2DCH_2$-S-CoM | $^{13}CH_2DCHD$-S-CoM | $^{13}CH_2DCD_2$-S-CoM | $^{13}CHD_2CH_2$-S-CoM | $^{13}CHD_2CHD$-S-CoM | $^{13}CHD_2CD_2$-S-CoM | $^{13}CD_3CH_2$-S-CoM | $^{13}CD_3CHD$-S-CoM | $^{13}CD_3CD_2$-S-CoM |
| 2 | 0.3 | 0 | 0 | 13.9 | 1.4 | 0 | 1.1 | 0.1 | 0 | 0 | 0 | 0 |
| 4 | 0.4 | 0 | 0 | 20.9 | 3.1 | 0.1 | 2.1 | 0.8 | 0 | 0 | 0 | 0 |
| 8 | 0.8 | 0.1 | 0 | 22.6 | 5.2 | 0.3 | 3.6 | 1.5 | 0.1 | 0.2 | 0.1 | 0 |
| 16 | 0.4 | 0.3 | 0 | 19.6 | 9.6 | 1.3 | 7.1 | 5.8 | 1.1 | 0.8 | 0.8 | 0.1 |
| 32 | 0.2 | 0.2 | 0 | 13.6 | 10.7 | 2.8 | 8.2 | 9.6 | 2.9 | 1.2 | 1.8 | 0.8 |

### 3.3.5 Check for enantioselectivity in the formation of chiral isotopologues

Isotopologues containing one deuterium and one hydrogen atom in the methylene group are chiral (**figure 3.12**).

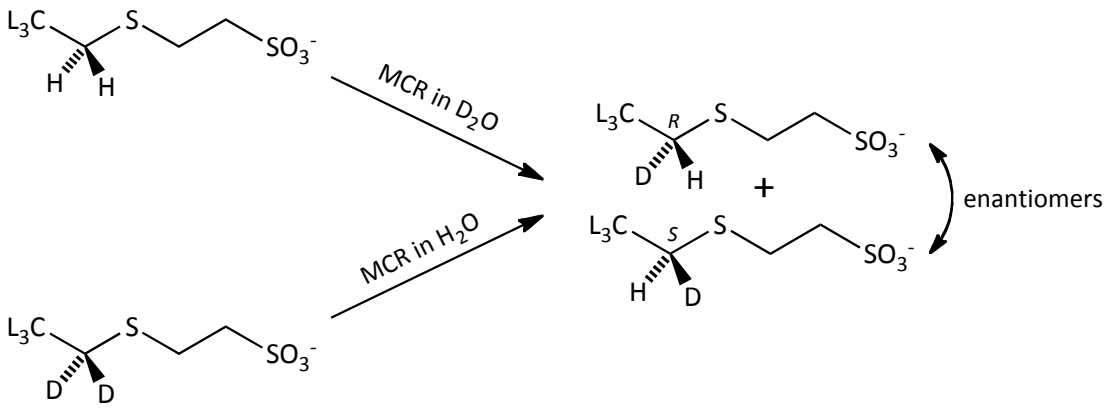


**Figure 3.12**: Formation of chiral isotopologues. L = hydrogen or deuterium. 4 different pairs of enantiomers can be formed: $CL_3$ = $CH_3$, $CH_3D$, $CHD_2$ or $CD_3$.

Since isotopologues containing multiple hydrogen atoms result in a large number of lines in the $^1$H-NMR spectrum, the enantioselectivity of the isotope exchange was determined by investigating $CD_3CHD$-S-CoM. This isotopologue was obtained by incubation of $CD_3CD_2$-S-CoM with MCR in $H_2O$. Because spectroscopic enantiomeric resolution of $CD_3CHD$-S-CoM was not successful, the corresponding sulfoxides of ethyl-coenzyme M ($CH_3CH_2$-(S=O)-CoM) were investigated. After oxidation of a mixture of the two enantiomers of ethyl-coenzyme M, 4 different stereoisomers of sulfoxides are expected (**figure 3.13**).

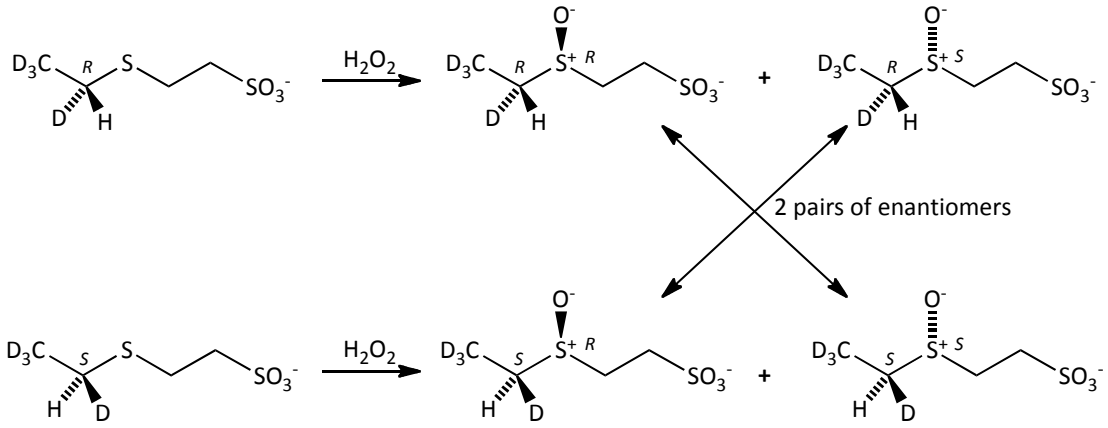


**Figure 3.13**: Two diastereomeric pairs of enantiomers of sulfoxides are formed after oxidation of the substrate $CD_3CHD$-S-CoM.

The R/S ratio at the carbon center corresponds to the ratio of enantiomers of any of the two pairs of enantiomeric sulfoxides (denoted in figure 3.13), if the oxidation to the sulfoxide produces equal amounts of R and S configuration at the sulfur center. A diastereoselectivity of the oxidation due to a chiral induction caused by a secondary isotope effect would have no effect on the ratio within one pair of enantiomeric sulfoxides. If the oxidation to the sulfoxide would proceed with any other type of stereoinduction, analysis would have to be performed by taking into account all 4 isomers of sulfoxides (comparing the sums of the two diastereomeric sulfoxides formed from one enantiomer of ethyl-coenzyme M).

Quinine sulfate as a chiral auxillary was found to cause an effective optical resolution of synthetic ethyl-coenzyme M-sulfoxide in various different solvents (**table 3.5**). Dihydroquinine was finally used since the signal of the proton allylic to the terminal double bond of quinine interfered with the signals of interest. The optical resolution is demonstrated with $CD_3NO_2$ as the solvent in **figure 3.14**.

**Table 3.5**: Splitting of the signal of ***CH₃***$CH_2$-(S=O)-CoM in the $^1$H-NMR spectrum due to chiral resolution with quinine sulfate in different solvents. (1 ppm = 1000 ppb)

| Solvent | Splitting [ppb] | Splitting [Hz] at 600 MHz |
|---|---|---|
| $CD_2Cl_2$ | 78.0 | 46.8 |
| $CD_3NO_2$ | 59.2 | 35.5 |
| $CDCl_3$ | 46.2 | 27.7 |
| acetonitril-$d_3$ | 44.5 | 26.7 |
| acetone-$d_6$ | 36.0 | 21.6 |
| methanol-$d_4$ | 0.6 | 0.34 |
| $D_2O$ | 0.4 | 0.25 |

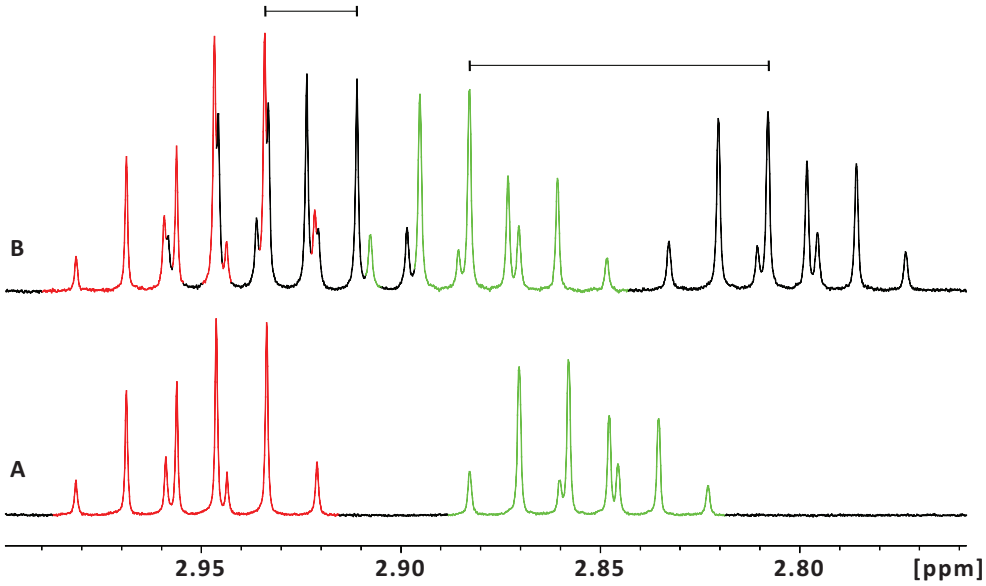


**Figure 3.14**: Optical resolution of ethyl-coenzyme M-sulfoxide demonstrated by 600 MHz $^1$H-NMR spectroscopy. Expansion of the region of the signals due to $CH_3$***CH₂***-(S=O)-CoM. **A**: 600 MHz $^1$H-NMR spectrum of the pure sulfoxide (10 mM) in $D_2O$ (dioxane = 3.70 ppm). **B**: Measurement in $CD_3NO_2$ (5 μmol) including dihydroquinine sulfate (50 μmol). The chemical shift is adjusted for the signal highlighted in red (TMS at 0.1517 ppm). Colored signals belong to one enantiomer, black signals belong to the other enantiomer. The magnitude of the relative shift due to the alkaloid is marked with scale bars (23.1 ppb and 74.8 ppb).

Acetonitrile-$d_3$ was chosen as the solvent because it can be diluted stepwise with $D_2O$ to control the magnitude of the splitting.

The solution from the MCR assay containing about 5% $CD_3CHD$-S-CoM in the remaining ethyl-coenzyme M was oxidized to the sulfoxide with hydrogen peroxide (**figure 3.15**).

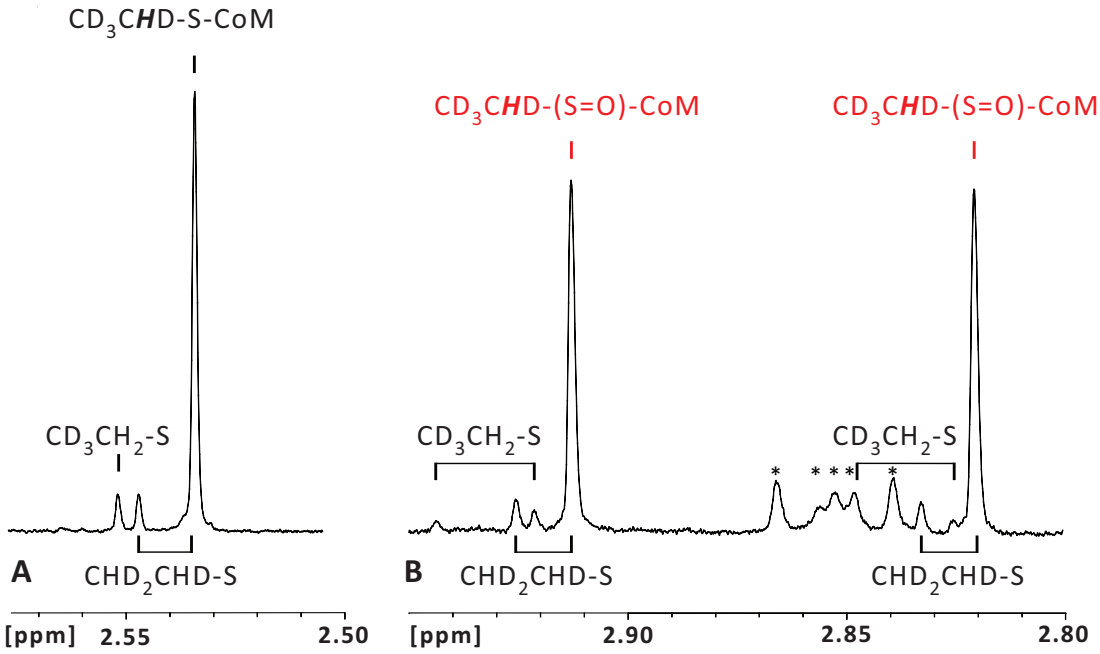


**Figure 3.15**: Expansion of $^1H\{^2H\}$-NMR spectra of the methylene group with assignments (dioxane = 3.70 ppm). Peaks originating from one H are indicated with brackets. **A**: Assay solution without any treatment. **B**: Solution after oxidation to the sulfoxide. The signal marked with 5 * is due to an unrelated methylene group.

Optical resolution of the sulfoxides with dihydroquinine sulfate in actonitrile-$d_3$ / $D_2O$ is shown in **figure 3.16** (for experimental procedures see section 6.4.6).

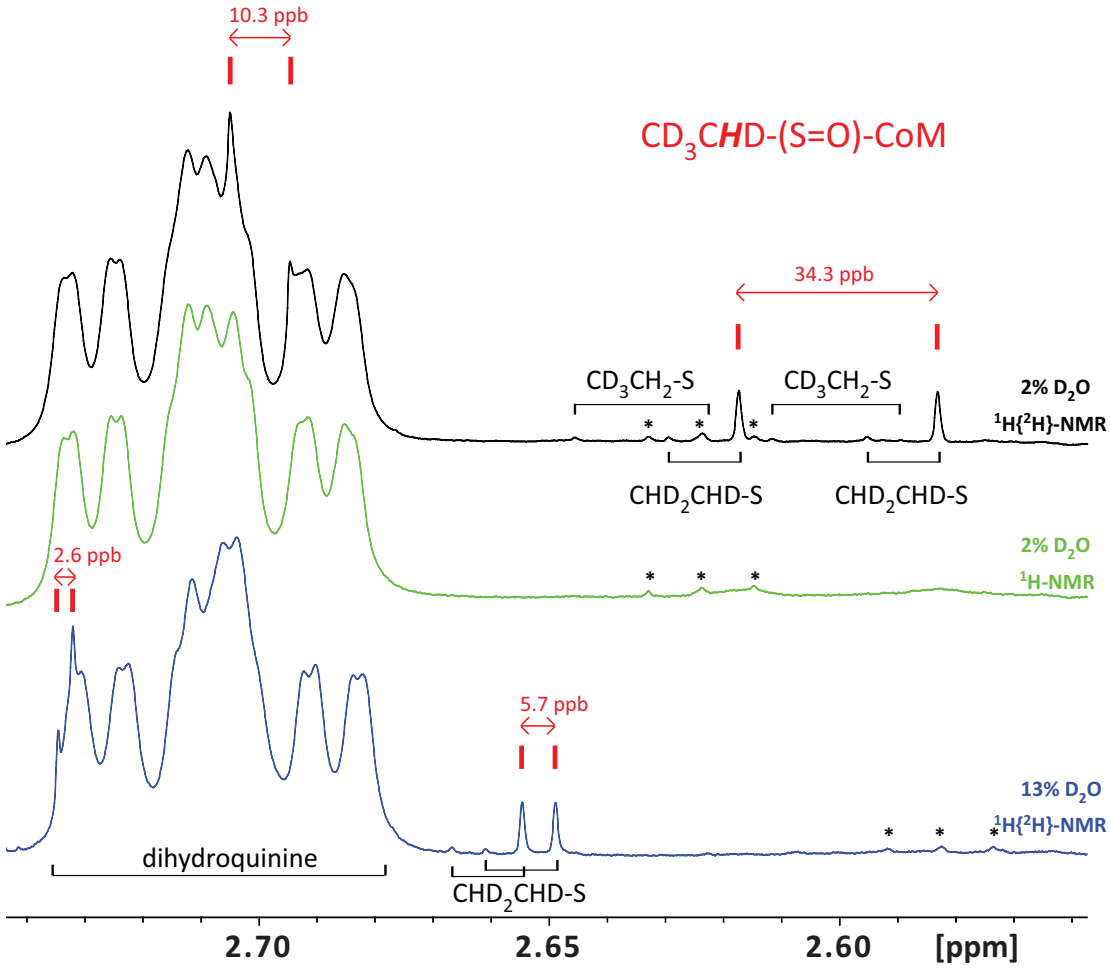


**Figure 3.16**: 600 MHz $^{1}$H-NMR spectra demonstrating the optical resolution of the assay containing $CD_3CHD$-(S=O)-CoM (highlighted in red) in acetonitrile-$d_3$/$D_2O$. **Black**: 2% $D_2O$ in the solvent (v/v), acquired with deuterium decoupling (TMS = 0 ppm). **Green**: Same sample without deuterium decoupling. **Blue**: After addition of $D_2O$ to a concentration of 13% (v/v). The chemical shifts were adjusted for the signal from dihydroquinine (TMS at -0.038 ppm). The relative shifts of the two enantiomers of $CD_3CHD$-(S=O)-CoM are highlighted with red red arrows (10.3 / 34.3 ppb in 2% $D_2O$ and 2.6 / 5.7 ppb in 13% $D_2O$). Integral ratio of the signals of the $H_{upfield}$ of $CD_3CHD$-(S=O)-CoM is not significantly different from 1:1.

The lines marked with * are not due to the ethyl group as verified in the measurement without deuterium decoupling (green).

The identity of the signals was verified by adding $D_2O$ stepwise until the signals due to one pair of enantiomers converged (**table 3.6**).

**Table 3.6**: Optical resolution of the signals from $CD_3C\boldsymbol{H}D$-(S=O)-CoM due to dihydroquinine after increasing the concentration of $D_2O$ in the solvent acetonitril-$d_3$ from 2% to 50%.

| $D_2O$ [vol%] | Relative shift of $H_{downfield}$ [ppb] | Relative shift of $H_{upfield}$ [ppb] |
|---|---|---|
| 2.0 | 10.3 | 34.3 |
| 3.4 | 7.4 | 24.0 |
| 7.3 | 4.2 | 10.4 |
| 13 | 2.6 | 5.7 |
| 23 | 1.1 | 1.9 |
| 50 | < 0.5 | < 0.5 |

### 3.3.6 Activation of ethane

The experiment to determine the rate of ethane activation was performed with the substrate $^{12}CH_3$-S-CoM under ethane at conditions analogous to those for the experiments to study methane activation. The amount of ethane activated corresponds to the amount of ethyl-coenzyme M formed. An experiment with pure ethane and a large amount of enzyme as well as a competitive experiment using ethane and $^{13}CH_4$ was performed (**table 3.7**).

**Table 3.7**: Activation of ethane catalyzed by MCR (for spectra see section 6.4.7).

| species | 1 bar ethane, 40.6 mg MCR | 0.5 bar ethane + 0.5 bar $^{13}CH_4$, 4.06 mg MCR |
|---|---|---|
| remaining substrate [μmol] | 2.195 | 2.842 |
| $^{13}CH_3$-S-CoM formed [μmol] | 0 | 0.410 |
| Et-S-CoM formed [μmol] | 0.580 | 0.027 |
| ratio $^{13}CH_3$-S-CoM / Et-S-CoM | | 15.3 |

In the competitive experiment, the ratio of methane versus ethane activation was 15.3 : 1. From the specific rate of methane activation (11.4 nmol $min^{-1}$ $mg^{-1}$, cf. Chapter 2), the rate of ethane activation can be calculated to be 0.75 nmol $min^{-1}$ $mg^{-1}$, which corresponds to 0.0035 $s^{-1}$ or 0.21 $min^{-1}$.

### 3.3.7 Probing propyl- and allyl-coenzyme M for isotope exchange

The two known competitive inhibitors propyl- and allyl-coenzyme M were also tested for deuterium incorporation. After incubation in deuterated medium with MCR, no significant deuterium incorporation into these two inhibitors could be detected (see section 6.4.9 for details).

## 3.4 Discussion

### 3.4.1 Reaction pathway of $CH_2D_2$ formation

Analysis of the assay solution before full conversion to methane revealed a significant amount of deuterium incorporation in the substrate. Hence, formation of $CH_2D_2$ results from conversion of the deuterated substrate to methane (**figure 3.17, A**).

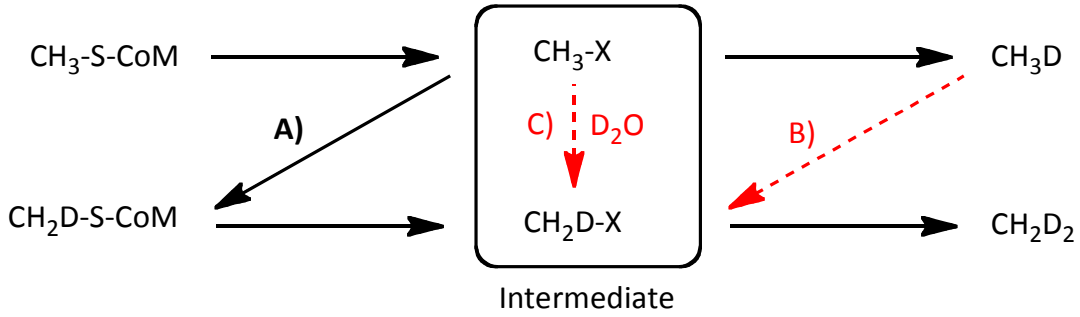


**Figure 3.17**: Reaction pathway (**A**) catalyzed by MCR in deuterated medium leads to the observed methane isotopologue $CH_2D_2$. Pathways drawn in red (**B** and **C**) do not contribute to the formation of $CH_2D_2$.

Methane activation in deuterated medium did not show deuterium incorporation into methane (pathway B in figure 3.17). The small amount of $^{12}CH_3D$ formed by MCR (21 nmol, cf. table 3.4) is due to methane formation from the unlabeled starting material (1.0%). The same experiment also allows us to rule out deuterium exchange between the medium and the intermediate (pathway C in figure 3.17), because the activated methane was found to be converted to the undeuterated isotopologue exclusively ($^{12}CH_3$-S-CoM). The small amount of $^{12}CH_2D$-S-CoM formed by MCR (6 nmol, cf. table 3.4) is explained by deuterium incorporation into the small amount of unlabeled starting material.

### 3.4.2 Energy barriers prior and after intermediates for methyl- and ethyl-coenzyme M

The finding that isotope incorporation into the substrate is much faster than the full reverse reaction (activation of methane) can only be explained by the formation of an intermediate. The existence of an intermediate is even more obvious considering the scrambling of the $^{13}C$ label within the ethyl group of ethyl-coenzyme M, which goes along with the activation of its chemically inert $CH_3$ group. Further evidence for an intermediate comes from the different relative rates of deuterium incorporation into the substrate methyl-coenzyme M and of methane formation at different temperatures. Upon lowering the temperature, the rate of methane formation decreases more than the rate of deuterium incorporation into the substrate.

From the relative rate of isotope exchange into the substrate ($k_b$) and product formation ($k_f$), the difference in height of the energy barriers from intermediate to product versus intermediate to substrate can be deduced (**figure 3.18**). In the case of the natural substrate methyl-coenzyme M, formation of the intermediate is rate limiting, whereas for the slower substrate ethyl-coenzyme M formation of ethane from the intermediate is rate limiting. However, no information on the energy of the intermediates relative to the initial ternary complex can be deduced from the described experiments.

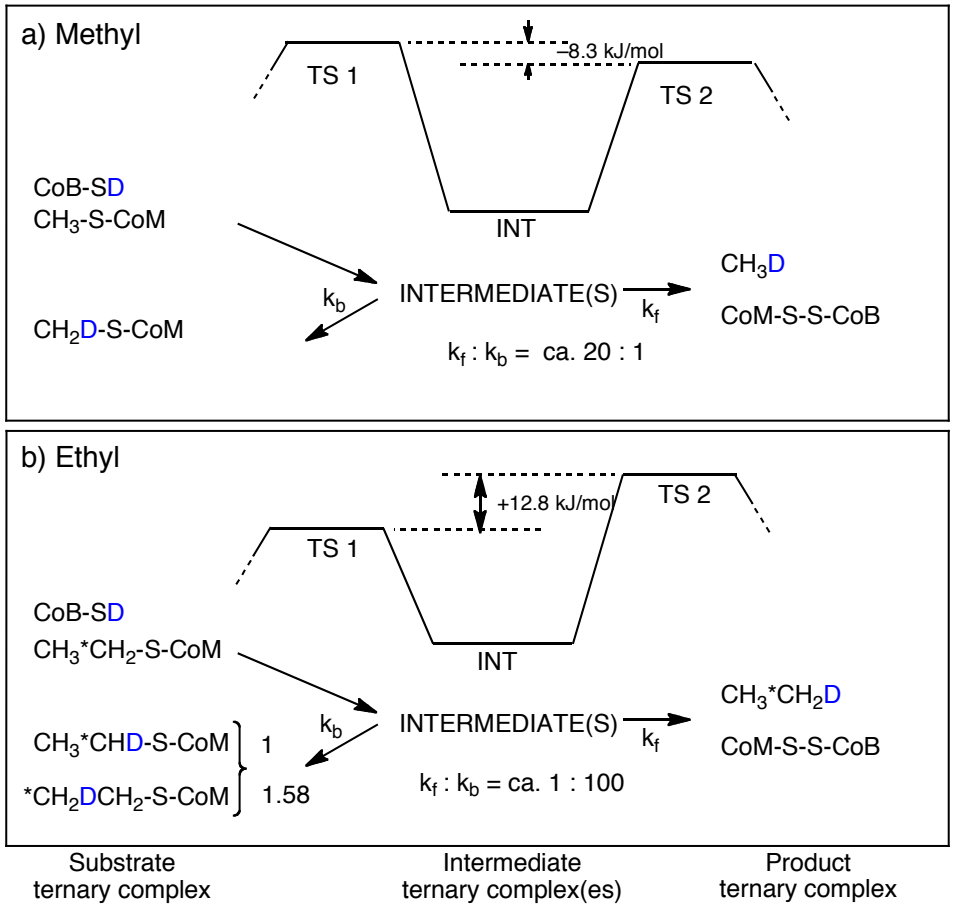


**Figure 3.18**: Schematic energy profiles from intermediates back to substrates (TS 1) and towards alkane formation (TS 2). The energy differences were calculated from the corresponding relative rates at 60 °C.

The specific rate of isotope exchange in ethyl-coenzyme M is 7.3 μmol $min^{-1}$ (mg enzyme)$^{-1}$ = 7.3 U $mg^{-1}$ according to the specific rate of $^{13}C$ scrambling in non-deuterated medium (see section 6.4.10 for calculation). Taking into account that the concentration of the substrate (10 mM) was only half of the $K_M$ value (20 mM[44]), the specific activity at saturation would be 21.8 U $mg^{-1}$ (see section 6.4.10). Within experimental error, this value is equal to the rate of methane formation (20 U $mg^{-1}$), which means that the C-S bond is broken at the same rate in methyl- and in ethyl-coenzyme M.

Thus the low rate of reaction towards ethane is caused by a higher transition state after formation of the intermediate. A higher energy

barrier between intermediate and ethane (denoted as "TS 2" in figure 3.18) than for the native substrate is also expected since the rate of ethane activation is 15 times lower.

The non-natural substrate ethyl-coenzyme M is slower in ethane formation and in ethane activation. In the direction of alkane formation, the reaction rate of ethyl-coenzyme M is slowed down more relative to the native substrate methyl coenzyme M than it is the case in alkane activation, which is in agreement with the reaction being less exergonic for ethyl-coenzyme M.

### 3.4.3 Pattern of isotope exchange in ethyl-coenzyme M

Each interchange of the carbon atoms within the ethyl group is accompanied by introduction of deuterium into the methyl group if the reaction is carried out in deuterated medium. The exchange pattern formally corresponds to a replacement of sulfur by deuterium and it appears that all C-H and C-D bonds of the prospective alkane are already set up in the intermediate (**figure 3.19**).

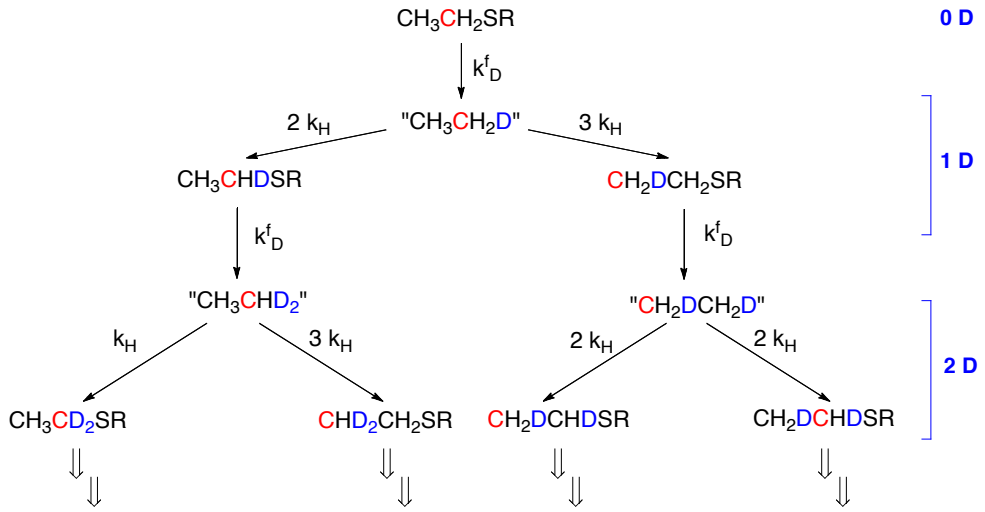


**Figure 3.19**: Isotope exchange pattern of $^{13}$C-labeled (red) ethyl-coenzyme M in deuterated medium. Only the first two "generations" of isotopologues are shown. The intermediates with all C-H/C-D bonds of the prospective alkane set up are in quotation marks. The comprehensive isotope exchange pattern will be given in section 4.5.1.

In the first generation, the ratio of the isotopologues that are formed (8.2% for $CH_3{}^{13}CHD$-S-CoM and 12.9% for $^{13}CH_2DCH_2$-S-CoM) roughly corresponds to the statistical ratio expected (2:3). The same can be verified for the second generation: 1.18% $CH_3{}^{13}CD_2$-S-CoM / 3.43% $^{13}CHD_2CH_2$-S-CoM ≈ 1:3; 4.71% $^{13}CH_2DCHD$-S-CoM / 4.84% $CH_2D{}^{13}CHD$-S-CoM ≈ 2:2. A more detailed analysis for deriving the isotope effects is given in section 4.5.

### 3.4.4 Implications for the experiment with chiral ethyl-coenzyme M

The published experiment performed to determine the stereochemical course of the reaction of [1′-$^2$H, 1′-$^3$H]-ethyl-coenzyme M to chiral ethane ($CH_3CHDT$)[77] is discussed here in light of the new finding that the substrate undergoes fast isotope exchange.

It is assumed that the intermediate contains all C-H/C-D bonds of the prospective alkane already set up with an inverted configuration at the carbon center as published for ethane formation. The isotope exchange scheme for [1′-$^2$H, 1′-$^3$H]-ethyl-coenzyme M in $H_2O$ neglecting any isotope effects is depicted in **figure 3.20**.

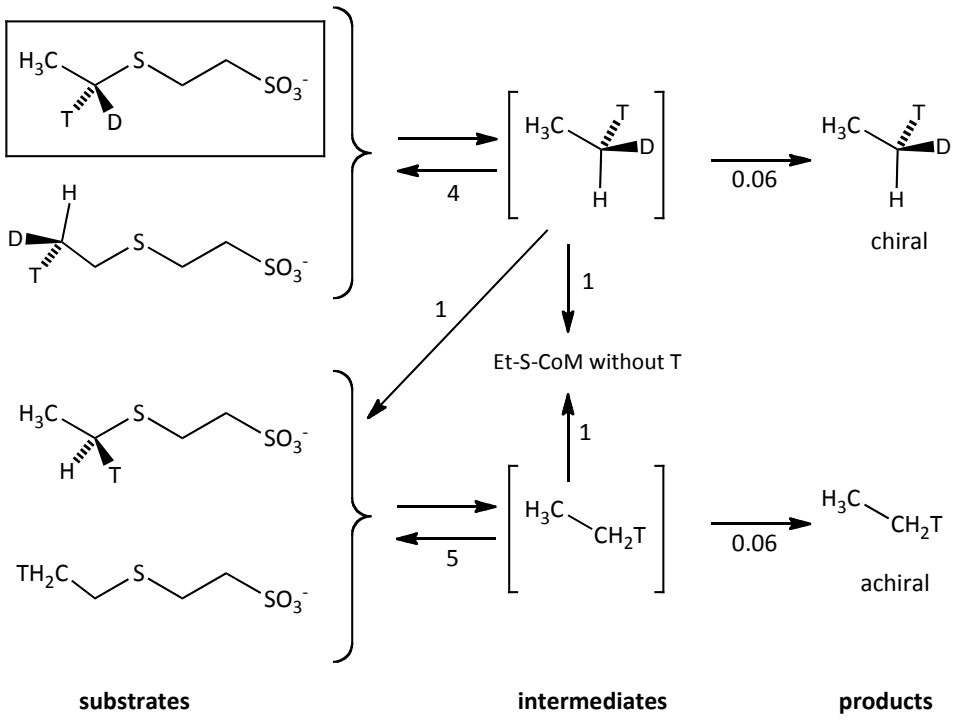


**Figure 3.20**: Isotope exchange in the substrate [1'-$^{2}$H, 1'-$^{3}$H]-ethyl-coenzyme M (highlighted in the box) in $H_2O$. Intermediates are denoted in brackets and are assumed to have the same configuration of the C-H, C-D and C-T bonds present as in the product formed from it. The ratio of ethane formation versus back reaction from the intermediate is about 1:100 (section 3.4.2, figure 3.18). The ratio of C-H/C-D/C-T bond activation versus ethane formation is 4/1/1 versus 0.06 if all isotope effects are neglected.

Without isotope effects, the ratio of C-H, C-D and C-T bond activation in [1'-$^{2}$H, 1'-$^{3}$H]-ethyl-coenzyme M corresponds to the statistical ratio 4/1/1. Since only the tritium-labeled molecules were analyzed and most of the substrate used was not tritium-labeled, loss of tritium has no influence on the determination of the stereochemical course and can be neglected. Hence stereoinformation is lost only when deuterium is abstracted from the intermediate containing the chiral ethane. The ratio of chirality loss to ethane formation from the intermediate containing the chiral ethane corresponds to 1 : 0.06 = 17 : 1. A correlation of ethane formation and loss of stereoinformation is depicted in **figure 3.21**, which includes only the ratio of 1:17 for ethane formation versus loss of stereoinformation.

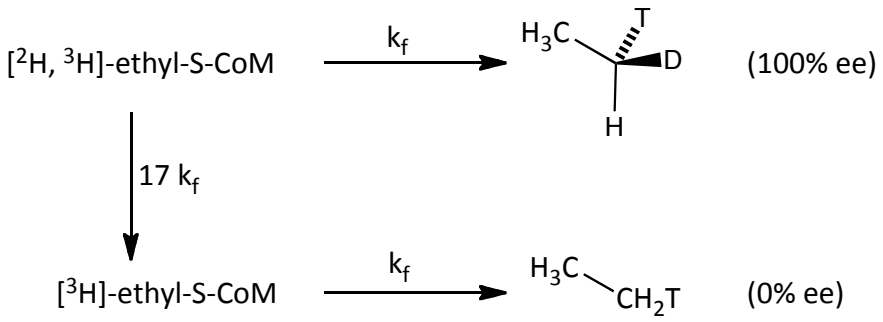


**Figure 3.21**: Simplified representation of stereoinformation loss in tritiated ethane neglecting any isotope effects. The steps involving intermediate formation are omitted in this representation.

The percentage of chiral ethane in the total amount of tritiated ethane corresponds to the enantiomeric excess (ee). From this simplified representation the ratio of chiral ethane versus achiral, tritiated ethane can be calculated analytically (see experimental section 6.4.11). The correlation between conversion and enantiomeric excess is shown in **figure 3.22**.

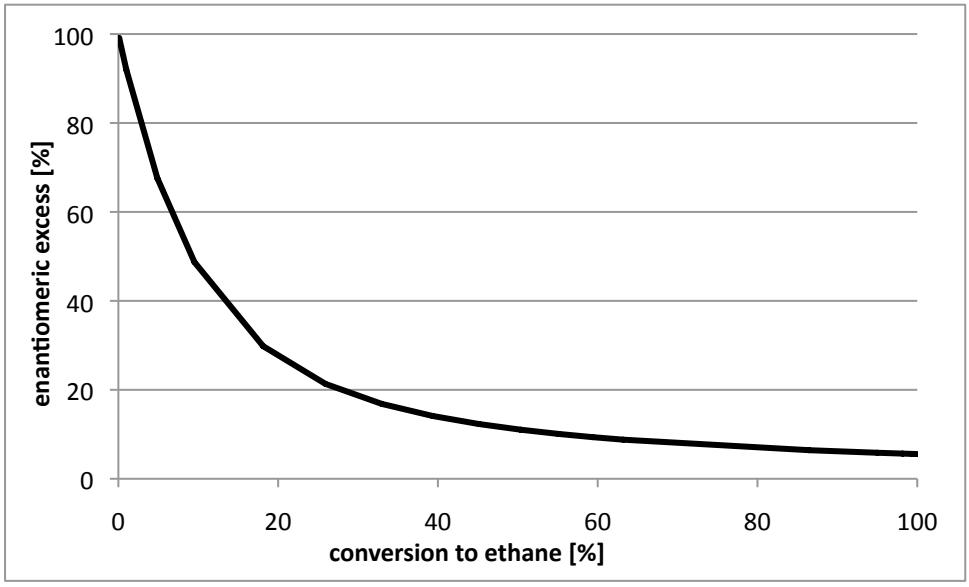


**Figure 3.22**: Enantiomeric excess as a function of the fraction of conversion towards ethane.

10% conversion to ethane gives 47% ee, 28% conversion 20% ee and full conversion 5.6% ee (6.4.11).

Floss and coworkers published an enantiomeric excess of 51% for the (*R*)-substrate (at 28% conversion) and 41% ee for the (*S*)-substrate (at 10% conversion)[77]. The magnitude of these reported ee values is reasonable. The isotope exchange described in this chapter explains why only partial inversion of configuration to ethane was found. It can be assumed that the conversion of ethyl-coenzyme M to ethane would proceed without loss of stereoinformation if the isotope exchange in the substrate would not happen.
The finding that the (*R*)-substrate exhibited a higher fraction of conversion to ethane relative to the (*S*)-substrate might only reflect variation in enzymatic activity during the long incubations.
The finding that the (*R*)-substrate gives a higher ee even though the conversion was higher cannot be explained and is assumed to be within the error of the reported experiments.
The isotope effects for the measured label exchange in ethyl-coenzyme M catalyzed by MCR are deduced in the next chapter. A kinetic simulation determining the effective loss of stereoinformation that takes into account the relevant isotope effects will be given section 4.5.4.

The finding that proton incorporation into $CD_3CD_2$-S-CoM to yield $CD_3CHD$-S-CoM proceeds without significant enantiomeric excess supports the interpretation that all C-H/C-D bonds of the alkane are already set up in the intermediate "$CD_3CHD_2$", which reverts to $CD_3CHD$-S-CoM. Although the two deuterium atoms in the intermediate are enantiotopic (diastereotopic at the chiral active site), only a large steric secondary isotope effect H/D could give a result that is significantly different from the result with a homotopic methyl group, namely a 1:1 ratio of the two enantiomers of $CD_3CHD$-S-CoM.

### 3.4.5 Implications for the reaction mechanism

The isotope exchange pattern we observed for $^{13}$C-labeled ethyl-coenzyme M in deuterated medium is congruent with the isotope exchange reported by Periana and Bergman for a labeled hydrido ethyl rhodium complex[129]. These authors found that the deuterido [1-$^{13}$C]-ethyl complex rearranges to the hydrido [1-$^{13}$C, 1-$^{2}$H]-ethyl complex upon warming to -80 °C. Further warming to -25 °C led to a rearrangement of the $^{13}$C label to the β-position whereby deuterium remained attached to the labeled carbon (**figure 3.23**).

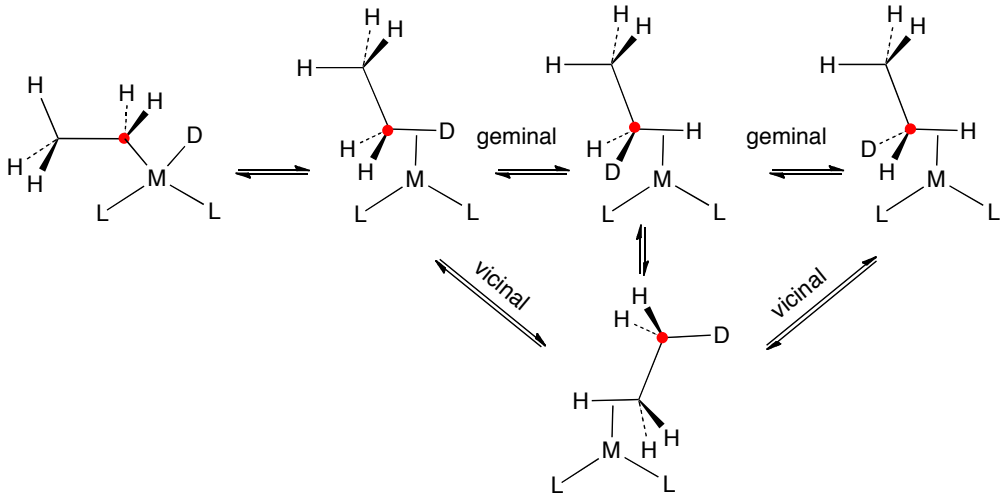


**Figure 3.23**: Rearrangement in the deuterido [1-$^{13}$C]-ethyl complex via the unseen σ-ethane complex. Deuterium remains attached to the $^{13}$C-labled position (red) during rearrangement from the α to the β-position.

According to the authors, formation of a σ-coordinated ethane complex, which rearranges by rapid geminal and slightly slower vicinal bond shifts, seems to be the most economical explanation for these findings.

Because our experiments show that all C-H/C-D bonds of the prospective alkane are already present in the intermediate, a σ-alkane nickel complex in the active site of MCR would explain all aspects of the observed isotope exchange.

Assuming such an alkane complex as the intermediate, the second step would be dissociation of the alkane. The slow reaction of the non-natural substrate ethyl-coenzyme M would signify a tighter binding of ethane at the nickel center.

If the alkane that is formed would be trapped at the active site, the same pattern of isotope exchange could be detected. Trapping could occur if the channel to the active site remains blocked by the threonine-phosphate moiety of coenzyme B, or the corresponding portion in the heterodisulfide, and no separate channel for methane to escape exists. If such trapping would prevent alkane loss, the alkane would not necessarily have to be bonded to the nickel center. Blocking of the channel could originate from a very tight binding of the heterodisulfide, or from a significant energy barrier for heterodisulfide formation whereby coenzyme B remains tightly bound until the S-S bond is formed.
In the case of a blocked channel, the slower reaction with ethyl-coenzyme M as the substrate would signify either a tighter binding of the heterodisulfide or a slower rate of heterodisulfide formation caused by a steric effect.

Although a species with the alkane bonded to the nickel center seems to be the most reasonable intermediate, its exact nature has to remain open as long as no intermediates can be identified spectroscopically.

# 4 Isotope Effects

## 4.1 Introduction

### 4.1.1 Different types of isotope effects

A different reaction rate or a shift of an equilibrium caused by an isotopic substitution is called an isotope effect.
If the bond to the isotope varied is broken or formed, the change in the rate of the reaction is called a primary kinetic isotope effect (KIE). If the isotope varied is not directly involved in the reaction but still affects the reaction (for example via a change in geometry involving a bond to the isotope), the change in the rate of the reaction is called a secondary kinetic isotope effect. The kinetic isotope effect is defined by the ratio of the reaction rate with the light isotope versus the rate with the heavy isotope. For hydrogen and deuterium, for example, the KIE is defined as:

$$KIE = \frac{k_H}{k_D}$$

An isotope effect larger than 1 is called "normal", an isotope effect smaller than 1 is called "inverse".

An equilibrium isotope effect (EIE) is observed if the two kinetic isotope effects of the forward and backward reactions differ. An example of such a situation is often found in oxidative addition/reductive elimination reactions (cf. introduction, 1.3.4).
Hydrogen sulfide in deuterated water serves as a second example:

$$H_2S + HOD = HSD + H_2O$$

Protonation of the hydrosulfide exhibits a larger isotope effect than deprotonation, hence the equilibrium is on the left side (K = 0.42[130]). From this solvent isotope effect, the fractionation factor Φ, i.e. the amount of D present at an exchangeable position as a function of the concentration of D present in the solvent, can be deduced. For aqueous solutions, the fractionation factor Φ is defined as follows[131]:

$$\Phi = \frac{[XD]}{[XH]} \frac{[H_2O]}{[D_2O]}$$

where X represents the functional group able to undergo proton/deuterium exchange.
OH and NH groups usually have a fractionation factor close to 1, which means that the ratio OH/OD or NH/ND is equal to the ratio $H_2O/D_2O$. For a thiol, however, the fractionation factor equals 0.4 - 0.5. Thus the ratio CoB-SH/D (conezyme B) in a 50%/50% mixture of $H_2O$ and $D_2O$ is 0.42[113], which corresponds to a molar fraction of CoB-SD of only 30%.

### 4.1.2 Measurement of isotope effects

Hydrogen/deuterium isotope effects are usually large enough to be determined by measuring the reaction rate with hydrogen ($k_H$) and the reaction rate with deuterium ($k_D$) independently. If a competitive measurement is possible whereby the product ratio is measured, the results are more accurate. Especially in experiments with MCR, which is very sensitive to traces of oxygen, competitive reactions were used whenever possible in order to cancel out effects due to enzyme deactivation.

For heavy atom isotope effects, such as the $^{12}C/^{13}C$ KIE, a direct measurement of the product ratio is difficult because these isotope effects are all smaller than 1.1. Singleton and coworkers established a

method for analyzing the unreacted starting material before full conversion in order to calculate the isotope effect[132]. The enrichment of the heavier isotope ($R/R_0$) corresponds to the ratio $^{13}C/^{12}C$ (R) at a given conversion divided by the initial ratio $^{13}C/^{12}C$ ($R_0$). The enrichment increases at high conversion (F) according to the equation shown below[133] and mathematically nearly reaches infinity for the last molecule to be converted:

$$\frac{R}{R_0} = (1-F)^{\frac{1}{KIE}-1}$$

The isotope effect can be calculated from this relation if the conversion and the enrichment are known:

$$KIE_{calcd} = \frac{\ln(1-F)}{\ln[(1-F)\bullet\frac{R}{R_0}]}$$

This method allows the $^{12}C/^{13}C$ KIE to be determined even at natural abundance[132]. After 99% conversion, for example, a $^{13}C$ enrichment of 25% is obtained with a KIE of 1.05.

### 4.1.3 Representation of data

The isotope effects measured in this work were evaluated assuming a t-distribution of the data. The probable errors of the mean were calculated[134] and the corresponding 95% confidence intervals are given.

## 4.2 Methane Formation

### 4.2.1 $^{12}C/^{13}C$ kinetic isotope effect on methane formation

Singleton's method, based on analysis of the enriched remaining starting material at high conversion, was used to determine of the isotope effect on $^{12}CH_3$-/$^{13}CH_3$-S-CoM conversion to methane. Instead of natural abundance, a 1:1 mixture of $^{12}CH_3$- and $^{13}CH_3$-S-CoM was used. The reaction was stopped after different incubation times and the remaining substrate analyzed for enrichment of $^{13}C$ by $^{1}H$-NMR spectroscopy (**figure 4.1**).

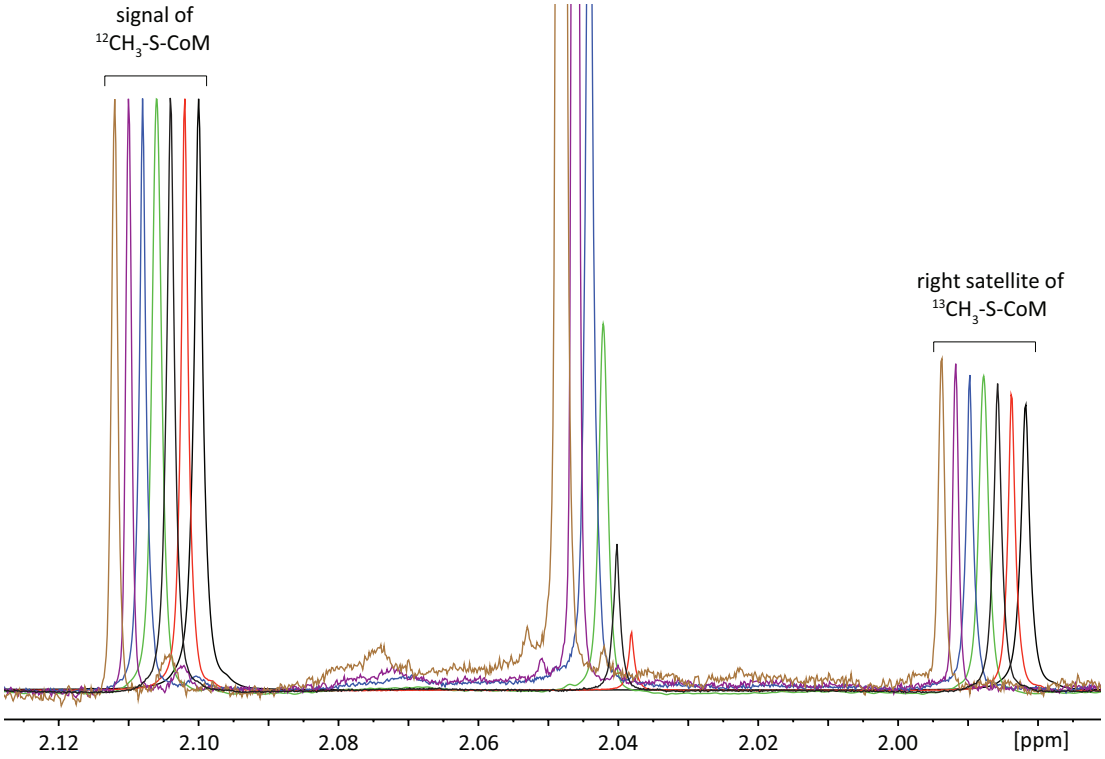


**Figure 4.1**: Expansion of the 600 MHz $^{1}H$-NMR spectra of the *S*-methyl group of methyl-coenzyme M after incubation times of 0, 2, 3, 4, 5, 5.5 and 6 min (from right to left, spectra shifted by 0.002 ppm per assay for better visibility). The signals at 2.10 ppm ($^{12}CH_3$ group) are adjusted to have the same height. Peaks at 1.98 ppm are due to the right $^{13}C$ satellite originating from the $^{13}CH_3$ group. The signal at 2.04 ppm is unrelated to methyl-coenzyme M and about constant in absolute height, therefore increasing relative to the remaining substrate with increasing conversion.

With increasing conversion, the specific $^{13}C$ content of the *S*-methyl carbon in the remaining substrate increased as shown in **figure 4.2**.

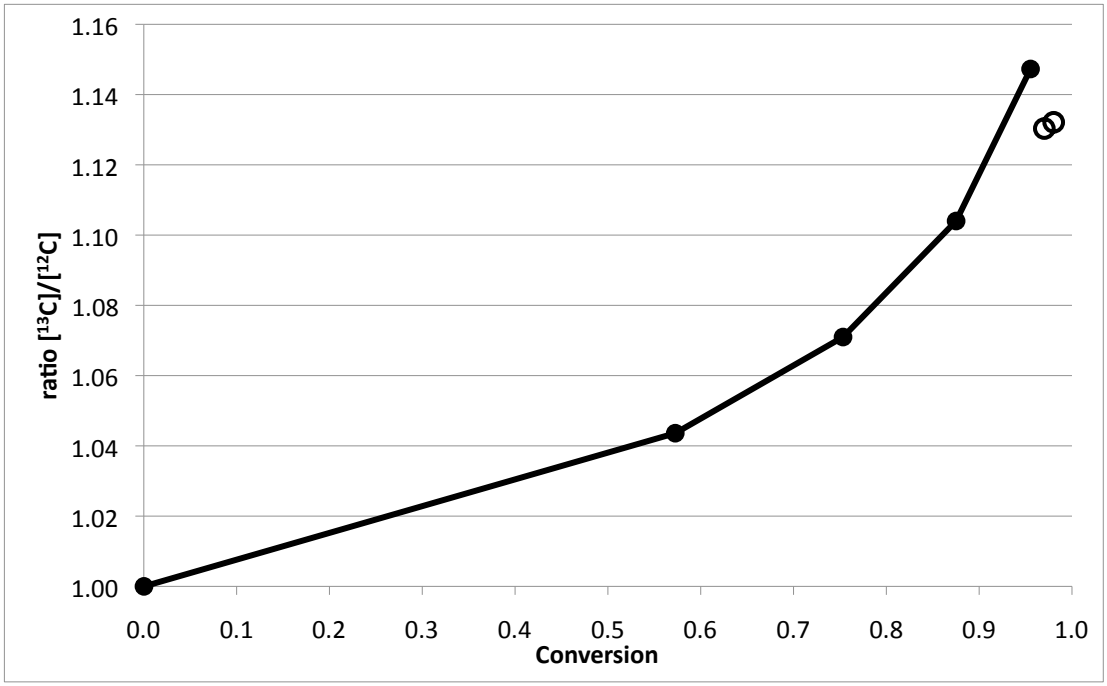


**Figure 4.2**: Ratio of $^{13}C$ and $^{12}C$ substrate as a function of the conversion. The data points drawn in circles are classified as outliers since the integral ratio $^{13}C/^{12}C$ decreases although the height of the peaks still increased (cf. figure 4.1).

The kinetic isotope effect was determined according to the equation given in the introduction (**table 4.1**).

**Table 4.1**: Measurement of $^{13}CH_3$-S-CoM enrichment relative to $^{12}CH_3$-S-CoM at high conversion towards methane in an assay containing Ti(III)-citrate. The kinetic isotope effect was calculated with the formula described in 4.1. For details of the calculation see experimental section 6.5.1.

| Time [min] | Substrate [μmol] | 1-conversion = 1-F | $[^{13}C]/[^{12}C]$ = $R/R_0$ | KIE |
|---|---|---|---|---|
| 0 | 16 | 1.000 | 1.0000 | |
| 2 | 6.839 | 0.427 | 1.0436 | 1.0529 |
| 3 | 3.947 | 0.247 | 1.0710 | 1.0515 |
| 4 | 1.997 | 0.125 | 1.1040 | 1.0499 |
| 5 | 0.714 | 0.045 | 1.1473 | 1.0462 |
| 5.5 | 0.477 | 0.030 | 1.1303 | 1.0361 |
| 6 | 0.315 | 0.020 | 1.1321 | 1.0326 |

Statistical analysis of the KIE from the 2 to 5 min data results in a value of $\mathbf{k_{12}/k_{13} = 1.050 \pm 0.005}$. The data points at 5.5 and 6 min were excluded because the integral ratio $^{13}C/^{12}C$ decreases although the height of the peaks still increases (cf. figures 4.1 and 4.2).

### 4.2.2 $H_2O/D_2O$ primary solvent isotope effect on the rate of methane formation

The influence of the deuterium content of the buffer medium on the rate of methane formation had been investigated previously[113]. Using GC as the analytical method, a slightly lower rate of methane formation found in deuterated buffer was not statistically significant because the mean error was rather large (outliers, presumably because of introduction of oxygen during gas sampling with a syringe)[113].
Therefore, we attempted to determine this important solvent isotope effect again by comparing the rate of methane formation in $H_2O$ and in $D_2O$ via $^1$H-NMR analysis of the remaining substrate and formation of the heterodisulfide (**table 4.2**).

**Table 4.2:** Rate of methane formation in $H_2O$ and in $D_2O$ catalyzed by the amount of enzyme indicated. 1.6 ml assay containing 2 mM of methyl-coenzyme M and 2 mM coenzyme B.

| | Time [min] | Conversion in $H_2O$ [%] | Conversion in $D_2O$ [%] | KIE [ratio of conversion] |
|---|---|---|---|---|
| 0.428 nmol MCR | | | | |
| Run 1 | 2 | 74.71 | 66.44 | 1.12 |
| | 4 | 84.02 | 81.23 | 1.03 |
| Run 2 | 2 | 76.08 | 46.85 | 1.62 |
| | 4 | 83.03 | 76.27 | 1.09 |
| 0.107 nmol MCR | | | | |
| Run 1 | 2 | 33.06 | 27.86 | 1.19 |
| | 4 | 47.37 | 43.99 | 1.08 |
| Run 2 | 2 | 35.34 | 22.00 | 1.61 |
| | 4 | 52.07 | - * | |

* sample broken, no measurement possible.

### 4.2.3 Secondary kinetic H/D isotope effect on methane formation

The secondary isotope effect on methane formation was investigated by an intermolecularly competitive experiment with a mixture of $^{13}CH_3$-S-CoM and $CD_3$-S-CoM. The assay solution contained ca. 5 mM of each of the two isotopologues of methyl-coenzyme M and 2 mM coenzyme B. This substrate ratio limited conversion to 20%. As a consequence, the rates of formation determined for the different methane isotopologues can be used as a good approximation for the initial rates of reaction. The isotopologues of methane were characterized by $^1$H-NMR spectroscopy (**table 4.3**). The sum of $CHD_3$ and $CH_2D_2$ (originating from incomplete labeling and H incorporation into $CD_3$-S-CoM) corresponds to the amount of $CD_3$-S-CoM consumed; $^{13}CH_4$ corresponds to the amount of $^{13}CH_3$-S-CoM consumed.

**Table 4.3**: Different isotopologues of methane formed from a mixture of $^{13}CH_3$-S-CoM and $CD_3$-S-CoM.

| Time [min] | $^{13}CH_4$ [mol %] | $CH_2D_2$ [mol %] | $CHD_3$ [mol %] | $CH_2D_2 + CHD_3$ [mol %] |
|---|---|---|---|---|
| Run 1 | | | | |
| 2 | 56.14 | 1.66 | 42.20 | 43.86 |
| 4 | 55.97 | 1.53 | 42.49 | 44.03 |
| Run 2 | | | | |
| 2 | 55.83 | 1.75 | 42.43 | 44.17 |
| 4 | 56.30 | 1.58 | 42.12 | 43.70 |

The isotope effect $^{13}CH_3$-/$CD_3$-S-CoM was determined by taking into account the measured exact ratio of substrates present in the assay solution (**table 4.4**).

**Table 4.4**: Ratio of different isotopologues of methane corrected for the measured ratio of $^{13}CH_3$-S-CoM to $CD_3$-S-CoM (44.22% / 55.78%, see experimental section 6.5.2). The ratio of these values corresponds to the isotope effect of $^{13}CH_3$-S-CoM consumption versus $CD_3$-S-CoM consumption. Average isotope effect: 1.609 ± 0.021.

| Time [min] | $^{13}CH_4$ formed per $^{13}CH_3$-S-CoM (44.22%) | $CH_2D_2$ + $CHD_3$ formed per $CD_3$-S-CoM (55.78%) | ratio |
|---|---|---|---|
| Run 1 | | | |
| 2 | 126.95 | 78.63 | 1.6145 |
| 4 | 126.57 | 78.93 | 1.6036 |
| Run 2 | | | |
| 2 | 126.24 | 79.20 | 1.5940 |
| 4 | 127.30 | 78.35 | 1.6247 |

For reasons of detection, the protium-containing isotopologue had to be labeled with $^{13}C$. Taking into account the $k_{12}/k_{13}$ IE of 1.05 (see section 4.2.1), the experimental secondary KIE has to be corrected giving $k_{CH3}/k_{CD3} = 1.69$ The correction assumes that the carbon and deuterium isotope effects are independent of each other and follow the product rule. This is justified if both isotope effects act on the transition state of the same rate determining step and the lowering of the rate by deuterium substitution does not cause another step to become partially rate determining as well.

The secondary isotope effect per deuterium equals the cubic root of 1.69. From statistical analysis an isotope effect of **1.191 ± 0.005 per D** is obtained.

## 4.3 Methane Activation

### 4.3.1 Intermolecular kinetic isotope effect: $CH_4$ / $CD_4$ activation

A premixed gas mixture of $CH_4$ and $CD_4$ (1:1) was used to measure the intermolecularly competitive kinetic isotope effect on methane activation. Experiments were done in $H_2O$ and in $D_2O$ buffer (**table 4.5**).

**Table 4.5**: Activation of a mixture of $CH_4$ and $CD_4$ catalyzed by 10.7 nmol (3.0 mg) enzyme during 30 min reaction time. The ratio of $CH_4$ to $CD_4$ activation is displayed relative to the added standard containing equal amounts of acetonitrile-$d_0$ and acetonitrile-$d_3$ (ACN-$d_0$ and ACN-$d_3$). Assay conditions analogous to methane activation experiments described in section 2 (see section 6.2.3).

| | Remaining Substrate [μmol] | $CH_4$ act. [μmol] | $CH_4$ act. per ACN-$d_0$ | $CD_4$ act. per ACN-$d_3$ |
|---|---|---|---|---|
| $H_2O$, Run 1 | 2.956 | 0.414 | 0.858 | 0.206 |
| $H_2O$, Run 2 | 2.920 | 0.451 | 1.130 | 0.251 |
| $D_2O$ * | 3.031 | 0.466 | 1.027 | 0.220 |

* Measured with presaturation of the $D_2O$ signal. Influence of presaturation on the integral ratio was excluded by comparison with the signal of dioxane-$d_0$/-$d_8$ present as an internal standard at the same time.

The isotope effect was calculated taking into account the measured ratio of $CH_4/CD_4$ present in the gas mixture used (**table 4.6**).

**Table 4.6**: Calculation of the kinetic isotope effect on methane activation (ratio of [$CH_4$ act per $CH_4$ present] per [$CD_4$ act. per $CD_4$ present]). The relative values per internal standard are corrected for the measured ratio of $CH_4$ : $CD_4$ (53.57% : 46.43%, see experimental section 6.5.3) present in the gas mixture used.

| | $CH_4$ act. per ACN-$d_0$ | $CH_4$-act. per $CH_4$ (53.57%) | $CD_4$ act. per ACN-$d_3$ | $CD_4$ act. per $CD_4$ (46.43%) | KIE |
|---|---|---|---|---|---|
| $H_2O$, Run 1 | 0.858 | 1.601 | 0.206 | 0.443 | 3.613 |
| $H_2O$, Run 2 | 1.130 | 2.110 | 0.251 | 0.540 | 3.906 |
| $D_2O$ | 1.027 | 1.917 | 0.220 | 0.473 | 4.054 |

From the three measurements, an isotope effect of **3.9 ± 0.6** was deduced.

### 4.3.2 Intramolecular competitive kinetic isotope effect: $CH_2D_2$ activation

Since the methane isotopologue $CH_2D_2$ contains an equal number of C-H and C-D bonds within the same molecule, any isotope effect on substrate binding is irrelevant. The activation of the C-H bond involves two secondary isotope effects, the activation of the C-D bond a primary and one secondary isotope effect. Hence, the measured isotope effect for C-H versus C-D bond activation corresponds to the ratio of primary to secondary isotope effect. Since it was shown that no deuterium or hydrogen is introduced from the solvent into the methyl-coenzyme M formed (cf. section 3.2.2 and 3.2.4), the isotope effect of $CH_2D_2$ activation was determined directly by comparing the ratio of the two isotopologues $CHD_2$-S-CoM and $CH_2D$-S-CoM that are formed (**table 4.7**).

**Table 4.7**: Measurement of the kinetic isotope effect on $CH_2D_2$ activation in $H_2O$ and $D_2O$. 1 bar pressure of $CH_2D_2$ in the headspace, catalyzed by 22 nmol (6.2 mg) enzyme in 15 min. Values of $CH_2D$-S-CoM formed are corrected for a contribution from incompletely $^{13}C$-labeled starting material (see experimental section 6.5.4). Experiment in $D_2O$, Run 3 (marked with *) was performed with 44 nmol enzyme but only 0.2 bar $CH_2D_2$. Data are not corrected for the incomplete labeling of $CH_2D_2$ (containing 3.70 mol% $CH_3D$, see experimental part).

| | Remaining substrate [μmol] | $CH_2D_2$ activated [μmol] | $CHD_2$-S-CoM formed per $CH_2D$-S-CoM formed = KIE |
|---|---|---|---|
| $H_2O$, Run1 | 2.656 | 0.892 | 2.160 |
| $H_2O$, Run2 | 2.681 | 0.791 | 2.233 |
| $D_2O$, Run1 | 2.862 | 0.678 | 2.038 |
| $D_2O$, Run2 | 2.967 | 0.384 | 1.922 |
| $D_2O$, Run3* | 2.560 | 0.290 | 2.091 |

Statistical evaluation of all experiments results in a kinetic isotope effect of **2.09 ± 0.15**.

### 4.3.3 Calculation of the primary and secondary isotope effect of methane activation

If one assumes that no equilibrium isotope effects are involved in the steps before the rate determining one (e.g. methane and heterodisulfide substrate binding), the primary and secondary kinetic isotope effects can be calculated from the two measured isotope effects for $CH_4/CD_4$ activation and $CH_2D_2$ activation.

The activation of $CD_4$ involves the primary isotope effect and a triple secondary isotope effect; the activation of $CH_4$ has no isotope effect. Hence the measured isotope effect of 3.9 ± 0.6 corresponds to $KIE_{prim} \bullet (KIE_{sec})^3$.

The activation of C-D in $CH_2D_2$ involves a primary and a single secondary isotope effect, whereas activation of the C-H bond is only subject to a double secondary isotope effect. Hence the measured isotope effect of 2.09 ± 0.15 corresponds to $(KIE_{prim} \bullet KIE_{sec})/(KIE_{sec})^2 = KIE_{prim} / KIE_{sec}$.

The following values are obtained for the two isotope effects after using these two equations:

**Prim KIE = 2.44 ± 0.22**

**Sec KIE = 1.17 ± 0.05**

The calculation including the error propagation is given in the experimental section 6.5.5.

## 4.4 Isotope Exchange in Methyl-Coenzyme M

### 4.4.1 Design of the experiments

The experiments described in this section were designed to study the isotope effects on C-H/C-D bond activation in the intermediate(s).
Different isotopologues of the intermediate(s) are formed from reaction of the substrates in $H_2O$- or $D_2O$-based medium and can react backwards to the substrates ("re-formed substrates") either by C-H or C-D bond cleavage (**figure 4.3**).

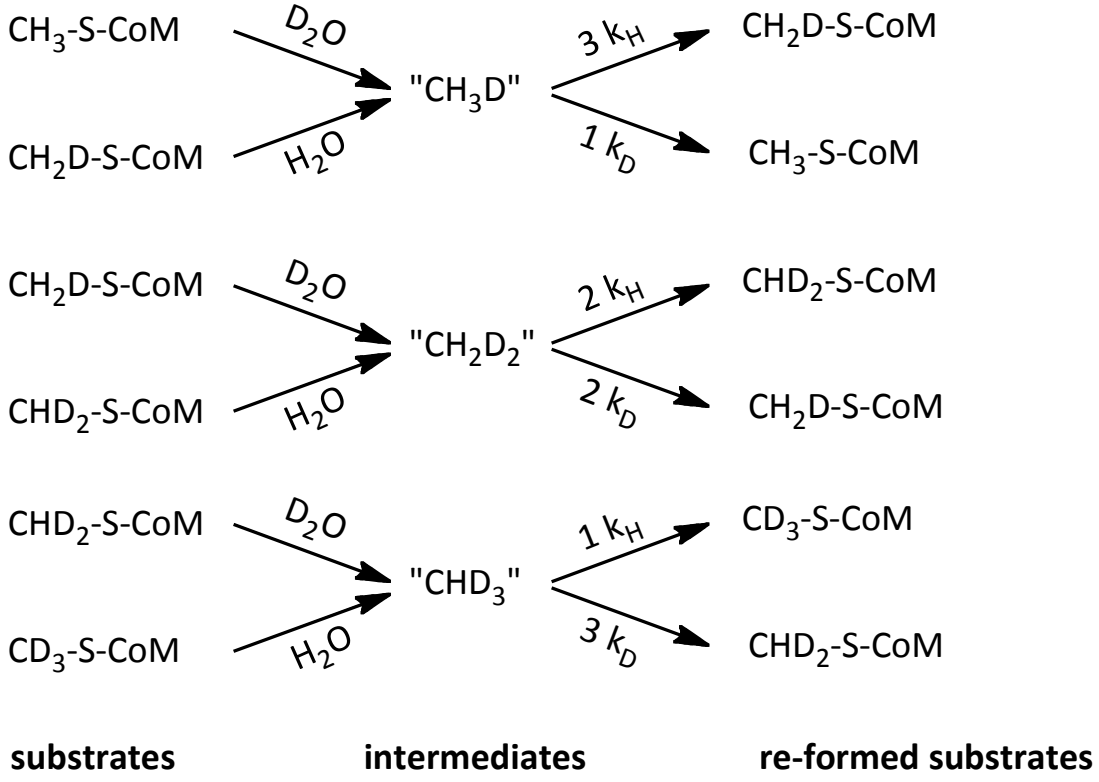


**Figure 4.3**: Isotope exchange via intermediates in the reaction of methyl-coenzyme M. $k_H$ indicates the rate constant of C-H bond cleavage, $k_D$ the rate of C-D bond cleavage.

If the reaction is carried out in deuterated medium (e.g. $CH_3$-S-CoM in $D_2O$), the substrate re-formed from the intermediate ("$CH_3D$") by C-H bond cleavage can be observed ($CH_2D$-S-CoM). The re-formed substrate from C-D bond cleavage, however, is identical to the initial substrate and cannot be quantified. The reaction in non-deuterated medium leading to the same intermediate ($CH_2D$-S-CoM in $H_2O$ giving "$CH_3D$") allows quantification of the substrate re-formed by C-D bond cleavage but not the substrate re-formed through C-H bond cleavage.
Hence in order to measure the isotope effect for C-H/C-D bond cleavage of a particular isotopologue of the intermediate, two separate complementary experiments, one in $H_2O$ and one in $D_2O$, are required.
Because these experiments are not intramolecularly competitive, the ratio of H incorporation in $H_2O$ and D incorporation in $D_2O$ for the two complementary substrates only reflects the intrinsic primary kinetic isotope effect for C-H/C-D bond activation in the intermediate if the partitioning of the intermediate between forward and backward reactions (commitment) is the same in $H_2O$ and in $D_2O$.

### 4.4.2 Analysis from isotope exchange into methyl-coenzyme M

The method of analyzing the substrate before full conversion was performed with 4 mM of mono- or di-deuterated methyl-coenzyme M and 2 mM of the second substrate coenzyme B in order to obtain a constant conversion (50%). It was shown that after consumption of the second substrate coenzyme B no significant isotope exchange occurs (section 3.2.2).
$CH_2D$-S-CoM in $D_2O$ was used to measure the rate $k_H$ of C-H activation from the intermediate "$CH_2D_2$" and $CHD_2$-S-CoM in $H_2O$ to measure the rate $k_D$ of C-D activation from the same intermediate "$CH_2D_2$" (**table 4.8 A and B**).

**Table 4.8**: **A**) Deuterium incorporation into $CH_2D$-S-CoM compared to **B**) protium incorporation into $CHD_2$-S-CoM after 50% conversion to methane catalyzed by 1.07 nmol enzyme. All values are corrected for the small amount of other isotopologues present in the starting material (incomplete labeling and natural abundance of deuterium, see experimental section 6.5.6).

| **A**) Exp. with $CH_2D$-S-CoM in $D_2O$ | | | **B**) Exp. with $CHD_2$-S-CoM in $H_2O$ | | |
|---|---|---|---|---|---|
| time [min] | substrate [μmol] | $CHD_2$-S-CoM [mol %] | time [min] | substrate [μmol] | $CH_2D$-S-CoM [mol %] |
| Run 1 | | | Run 1 | | |
| 0 | 6.4 | 0 | 0 | 6.4 | 0 |
| 2 | 3.386 | 2.246 | 2 | 3.189 | 0.990 |
| 4 | 3.366 | 2.237 | 4 | 3.183 | 0.961 |
| Run 2 | | | Run 2 | | |
| 0 | 6.4 | 0 | 0 | 6.4 | 0 |
| 2 | 3.365 | 2.158 | 2 | 3.343 | 0.904 |
| 4 | 3.319 | 2.332 | 4 | 3.307 | 0.833 |
| average (2, 4 min) | | **2.243 ± 0.113** | average (2, 4 min) | | **0.922 ± 0.110** |

The ratio of deuterium incorporation versus protium incorporation ($2 \bullet k_H / 2 \bullet k_D$ = apparent kinetic isotope effect) equals **2.43 ± 0.32**.

### 4.4.3 Analysis from isotopologues of methane

Analysis of the methane isotopologues formed via isotope exchange into the substrate represents a second option for the measurement of the isotope effect on intermediate C-H/C-D bond activation (**figure 4.4**).

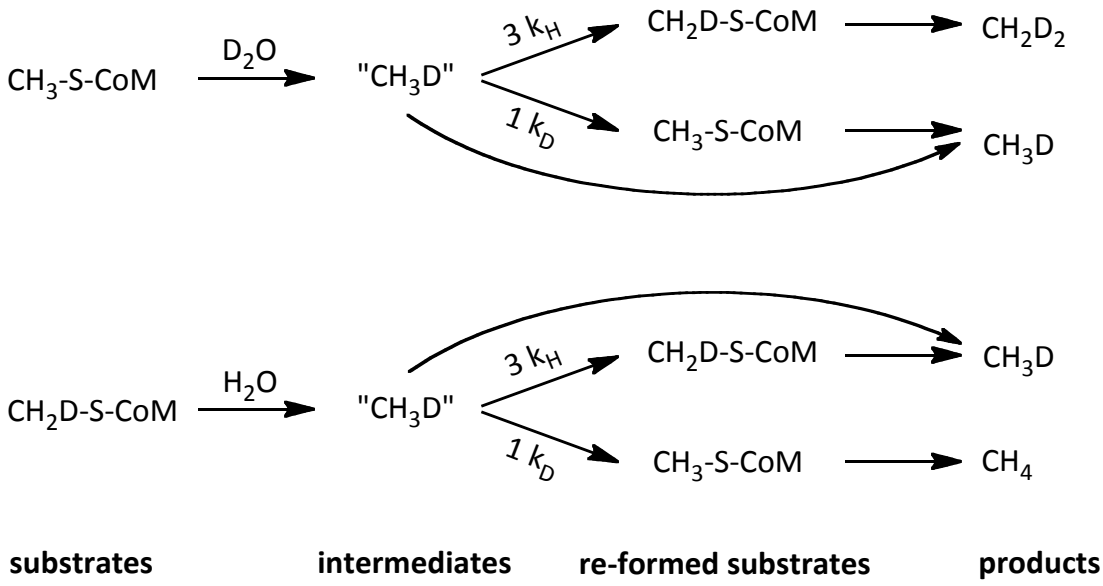


**Figure 4.4**: Isotope exchange via intermediates in the reaction of methyl-coenzyme M observed by analysis of the final product methane as exemplified with "$CH_3D$" as the intermediate.

The amount of $CH_2D_2$ formed from $CH_3$-S-CoM substrate ($D_2O$ experiment) is proportional to 3 • $k_H$ of "$CH_3D$" activation; the amount of $CH_4$ formed from $CH_2D$-S-CoM substrate ($H_2O$ experiment) is proportional to $k_D$ of "$CH_3D$" activation. The results of these experiments are shown in **table 4.9**. The analogous experiments for activation of the "$CH_2D_2$" intermediate are presented in **table 4.10**.

**Table 4.9**: Fraction of isotopologues of interest for the calculation of the isotope effect of "$CH_3D$" activation. Values are corrected for incomplete labeling of the starting material (see experimental section 6.5.6 for the fractions of all isotopologues measured).

| | Molar fraction of the 2 isotopologues of interest [%] | | |
|---|---|---|---|
| Isotopologue formed | $CH_4$ | $CH_3D$ | $CH_2D_2$ |
| **A**) $CH_3$-S-CoM in $D_2O$ | | 92.3195 | 7.6805 |
| **B**) $CH_2D$-S-CoM in $H_2O$ | 0.9887 | 99.0113 | |
| ratio $CH_2D_2$ formed per $CH_4$ formed | 7.7680 | | |
| KIE per C-H/C-D (divided by 3 ) | **2.59** | | |

**Table 4.10**: Fraction of isotopologues of interest for the calculation of the isotope effect of "$CH_2D_2$" activation. Values are corrected for incomplete labeling of the starting material (see experimental section 6.5.6 for the fractions of all isotopologues).

| | Molar fraction of the 2 isotopologues of interest [%] | | |
|---|---|---|---|
| Isotopologue formed | $CH_3D$ | $CH_2D_2$ | $CHD_3$ |
| **A**) $CH_2D$-S-CoM in $D_2O$ | | 95.6967 | 4.3033 |
| **B**) $CHD_2$-S-CoM in $H_2O$ | 1.7736 | 98.2264 | |
| ratio $CHD_3$ formed per $CH_3D$ formed | **2.43** | | |

## 4.5 Isotope Exchange in Ethyl-Coenzyme M

### 4.5.1 Isotope exchange pattern for [1′-$^{13}$C]-ethyl-coenzyme M in $D_2O$

The sequential formation of isotopologues of ethyl-coenzyme M with increasing deuterium content and concomitant scrambling of the $^{13}$C label corresponds formally to a substitution of the sulfur of coenzyme M by deuterium to give an intermediate (cf. section 3.4.3, figure 3.19) with all carbon-hydrogen bonds of the prospective ethane already present. In the reaction back to the substrate, any of the C-H or C-D bonds at the labeled or unlabeled carbon can be cleaved. This leads to the isotope exchange pattern depicted in **figure 4.5**.

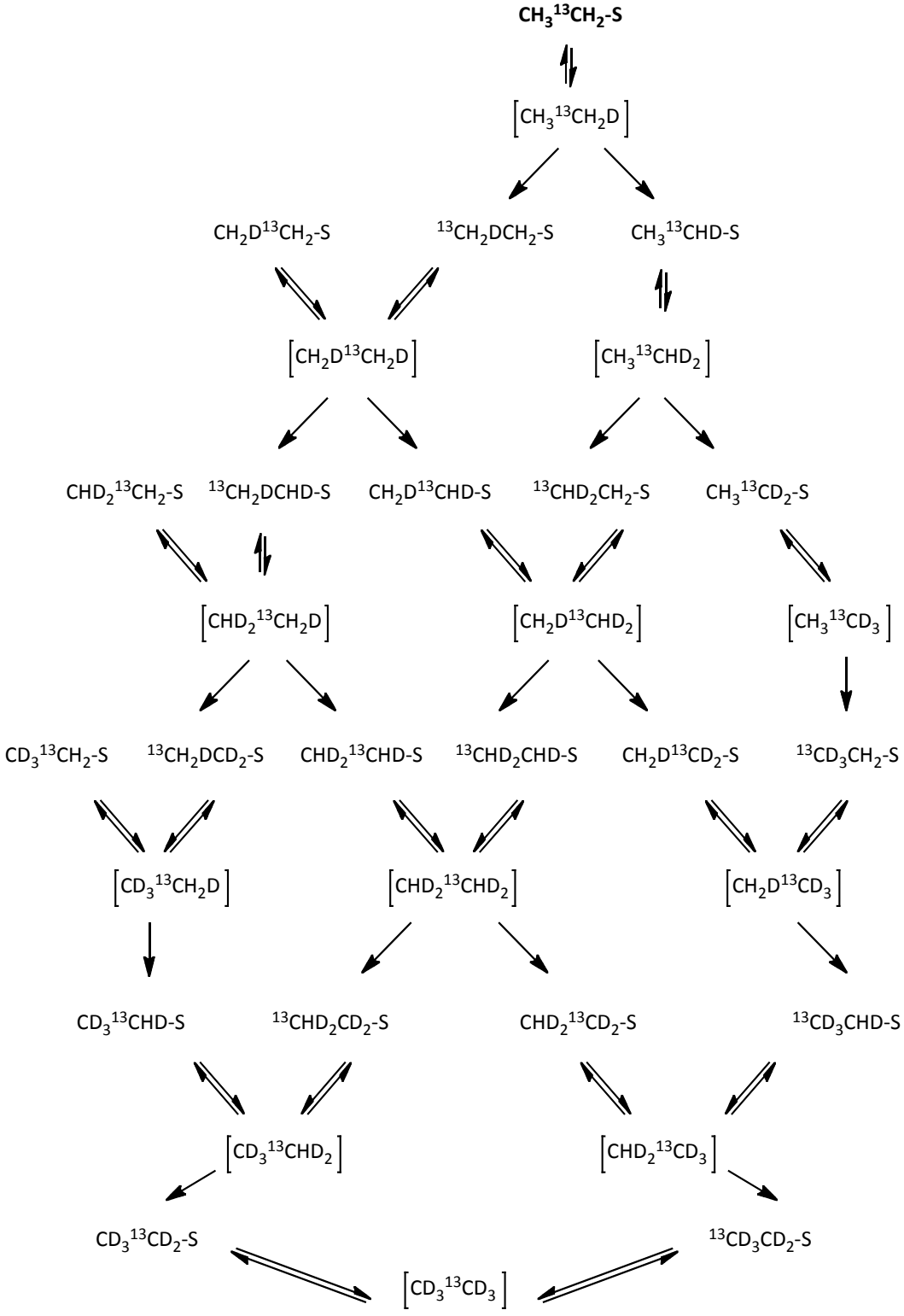


**Figure 4.5**: Comprehensive isotope exchange pattern for [1'-$^{13}$C]-ethyl-coenzyme M (top, highlighted bold) in fully deuterated buffer after incubation with MCR. Intermediates are drawn with square brackets; "-CoM" is omitted in the representation of Et-S-CoM.

### 4.5.2 Extraction of isotope effects for label exchange in ethyl-coenzyme M in $D_2O$ by kinetic simulation

In order to extract the isotope effects from the experimentally determined concentration vs. time profile of the 24 isotopologues, the kinetic scheme in figure 4.5 was simulated numerically with the program COPASI[135]. To keep the number of free parameters manageable, the following approximations were introduced into the kinetic model:

For the crucial isomerization of ternary complexes, two basic rate constants were introduced, one for the forward reaction (formal substitution of S by H) to the intermediate and one for the reaction of the intermediate back to the substrates ternary complex (C-H activation). Substrate binding in the known order was fully simulated whereas all steps leading from the intermediate ternary complex to free ethane and heterodisulfide were lumped together in a single irreversible reaction step with one rate constant, which was adjusted to give the experimentally observed conversion of 5% within 32 min.

The SH group of free coenzyme B was assumed to exchange rapidly with deuterium from the solvent according to the known fractionation factor of $\Phi = 0.42$ but no H/D exchange with solvent in the ternary complexes was allowed (shielded active site). The slow partial deactivation of the enzyme during the 32 min runs at 60 °C was introduced into the model through an irreversible first-order deactivation reaction of free enzyme.

Each individual rate constant for the different reactions leading to and from a particular isotopologue of the intermediate was modeled by dividing the basic forward ($k^0_{fwd}$) or back ($k^0_{bck}$) rate constants by the corresponding isotope effects at the appropriate power:

$$k_{fwd}^{H,n,m} = \frac{k_{fwd}^{0}}{(KIE_{fwd}^{\alpha\text{-sec}})^{n}(KIE_{fwd}^{\beta\text{-sec}})^{m}}$$

$$k_{fwd}^{D,n,m} = \frac{k_{fwd}^{0}}{(KIE_{fwd}^{prim})(KIE_{fwd}^{\alpha\text{-sec}})^{n}(KIE_{fwd}^{\beta\text{-sec}})^{m}}$$

n = number of D atoms in α
m = number of D atoms in β
α: position where "substitution" occurs

$$k_{bck}^{H,i,j} = \frac{k_{bck}^{0}}{(KIE_{bck}^{\alpha\text{-sec}})^{i}(KIE_{bck}^{\beta\text{-sec}})^{j}}$$

statistical weight: 3-i

$$k_{bck}^{D,i,j} = \frac{k_{bck}^{0}}{(KIE_{bck}^{prim})(KIE_{bck}^{\alpha\text{-sec}})^{i}(KIE_{bck}^{\beta\text{-sec}})^{j}}$$

statistical weight: i

i = number of D atoms in α
j = number of D atoms in β
α: position where C-H/D activation occurs

Assuming independence of the different isotope effects (product rule) and taking into account the statistical factors for the back reaction reduced the number of independent isotope effects to be determined to six: one primary, one α-secondary and one β-secondary KIE for each direction. Potential isotope effects on the release of the product ethane and on the substrate binding steps, as well as $^{13}C$ isotope effects were neglected. As an example, the different rate constants for the partition of the very first intermediate formed are illustrated in **figure 4.6**.

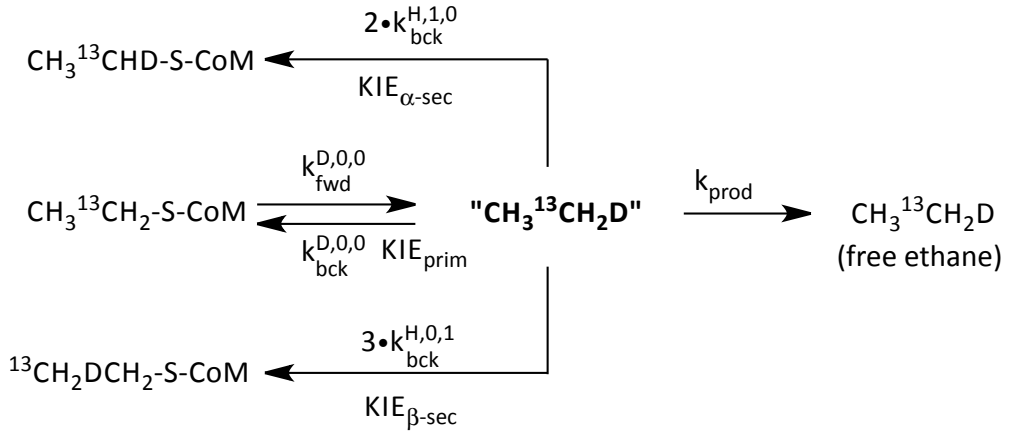


**Figure 4.6**: Isotope effects of the isomerization of the intermediate complex (ethane bound, highlighted bold) back to the ternary substrate complex.

### 4.5.3 Adjusting isotope effects in the simulation of label exchange in [1′-$^{13}$C]-ethyl-coenzyme M in $D_2O$ to approach the experimental time course of isotopologues

The model was first adjusted without any isotope effects to match the amount of ethane formed (5% after 32 min reaction time) and monodeuterated substrate formed. Since the concentrations of the mono- and dideuterated species were found to drop too fast, the parameter for irreversible first-order deactivation of free enzyme was adjusted to compensate for this effect (experimental section 6.8.2, figure 6.17 A). A more detailed description is given in the experimental section 6.8.2.
The main discrepancies still present compared to the experimental data are now mostly due to isotope effects.

The secondary isotope effect on intermediate formation could be deduced from the relative rate constants of different isotopologues undergoing exchange. In order to match the experimental time course, the α-secondary isotope effect has to be about 1.25 and the β-secondary isotope effect must be close to 1.
The primary isotope effect on intermediate formation (about 1.1) was deduced from comparing the rate of isotope exchange in the model with the one obtained from the $^{13}$C label scrambling experiment in water (cf. section 3.3.3, figure 3.9).
Isotope effects on C-H/C-D bond activation were deduced from the proportions of the re-formed substrates. For the determination of the ratio α to β secondary isotope effect, the determination of the initial rate of monodeuterated substrates formed from the intermediate "$CH_3{}^{13}CH_2D$" (**figure 4.7**, black intermediate) represents one option.
Monitoring the isotopologue $CH_2D{}^{13}CH_2$-S-CoM, formed from the intermediate "$CH_2D{}^{13}CH_2D$" (**figure 4.7**, red intermediate) is a valuable source of data to determine the primary isotope effect of intermediate activation. The mentioned intermediate contains 2 deuterium atoms

symmetrically distributed and thus the C-H/C-D activation rate of the $^{13}$C-labeled methyl group (red arrows) corresponds to the primary isotope effect (with a statistical correction since two hydrogen atoms and only one deuterium atom are present). The pathways via the intermediate "$CH_2D^{13}CHD_2$" (highlighted blue) re-connect the two branches formed after the first intermediate. Thus the time course of the different dideuterated species allowed fine-tuning the model further.

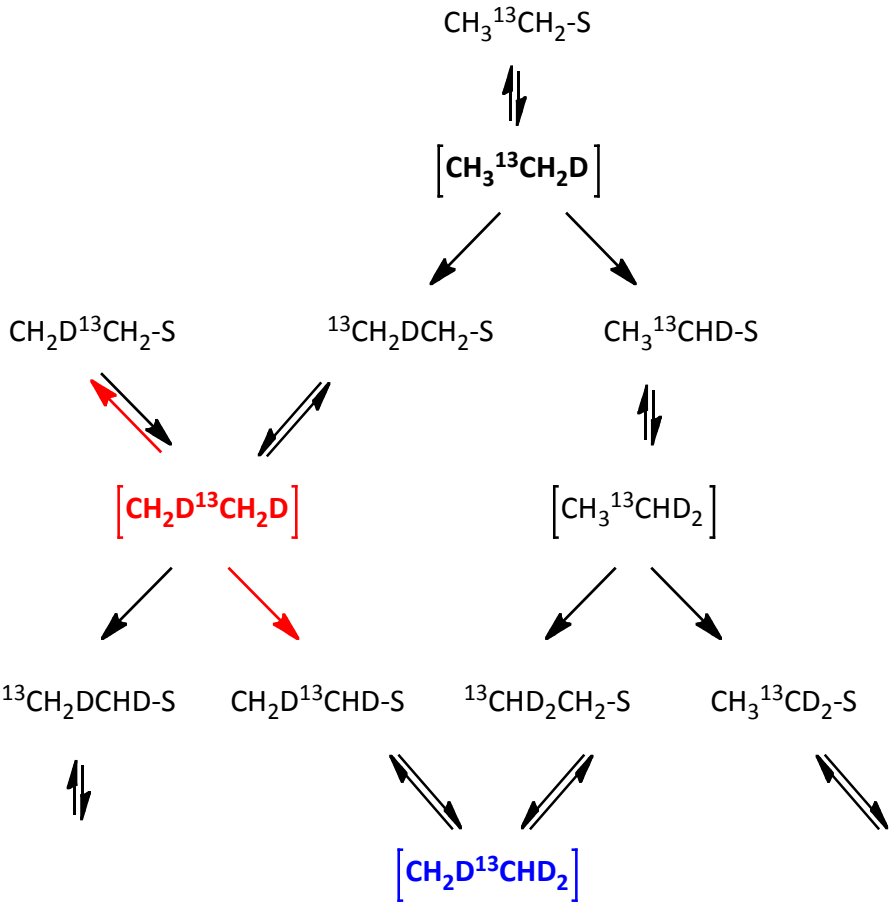


**Figure 4.7**: Selection from the isotope exchange pattern that proved to be very valuable for the determination of the isotope effects on C-H/C-D bond activation.

The simulation that matches the measured time course (**figure 4.8**) best is displayed in **figure 4.9.**

The isotope effects applied in the simulation were:

| Isotope effect (IE) | Intermediate formation | C-H / C-D activation from intermediate |
|---|---|---|
| primary IE | **1.1 ± 0.1** | **2.5 ± 0.1** |
| $\alpha$ secondary IE (per D) | **1.25 ± 0.10** | **1.25 ± 0.10** |
| $\beta$ secondary IE (per D) | **1.00 ± 0.05** | **1.00 ± 0.05** |

The robustness of these values was investigated by changing each value and trying to re-obtain a reasonable fit to the experimental data. A good match to the experimental result by applying the simulation described, however, was only possible with the values for the isotope effects (including the error limits given) presented here.

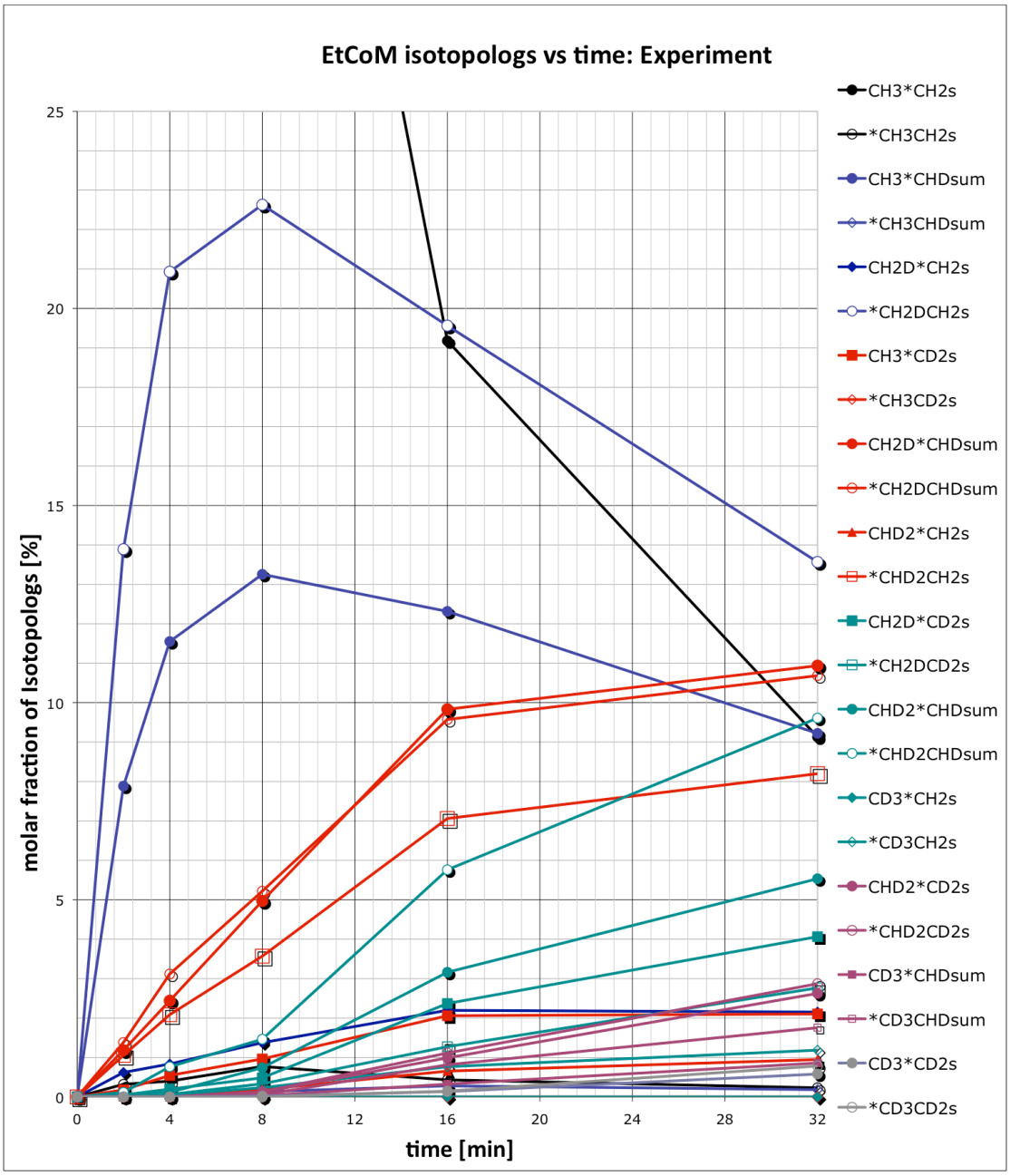


**Figure 4.8**: Measured time course of all isotopologues of ethyl-coenzyme M during incubation of [1'-$^{13}$C]-ethyl-coenzyme M with MCR in a deuterated assay (data from section 3.3.4, cf. table 3.4 for numerical values). "$CL_3CHDsum$" denotes the sum of the corresponding two enantiomeric isotopologues.

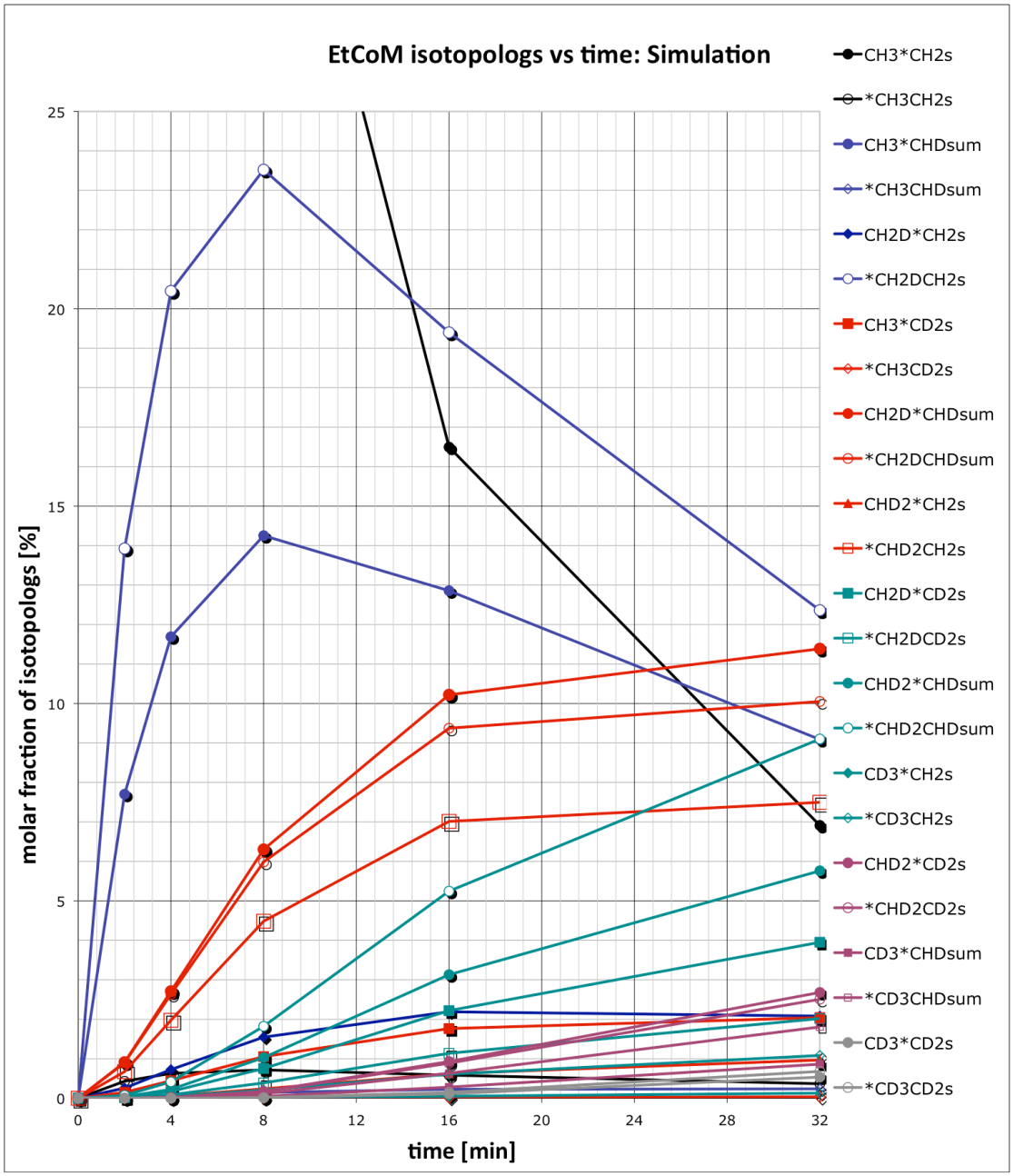


**Figure 4.9**: Optimized simulation of the time course of all isotopologues of ethyl-coenzyme M during incubation of [1'-$^{13}$C]-ethyl-coenzyme M with MCR in a deuterated assay. Isotope effects were adjusted in the model to give the best match to the experimentally measured time course of all isotopologues.

### 4.5.4 Simulation of the reported experiments for the determination of the steroechemical course of ethyl-coenzyme M to ethane

The experiment to determine the stereochemical course of the reaction of [1′-$^{2}$H, 1′-$^{3}$H]-ethyl-coenzyme M to chiral ethane published by Floss and coworkers[77] (cf. section 3.3.1) was already discussed in light of fast isotope exchange (cf. section 3.4.4).

Here, the experiment was simulated with the values for the isotope effects determined in our experiments. The tritium isotope effects were calculated from the deuterium isotope effects according to Swain-Schaad with an exponent of 1.442[136]. A chemical model was used without taking into account substrate binding and product release.

Both reactions, the forward substitution of S by H and its reverse (activation of H/D/T and replacement by S), are assumed to occur with pure inversion of configuration. A more comprehensive description is given in experimental section 6.8.4.

After 28% conversion to ethane, an enantiomeric excess of 44.5% was obtained from a starting material with 75% ee. (Floss et al. reported 51% ee). After 10% conversion, the ee was simulated to be 58% (Floss et al.: 41% ee)[77].

## 4.6 Proton Inventory Studies

### 4.6.1 Introduction to proton inventory experiments

A proton inventory experiment investigates the solvent isotope effect as a function of the deuterium content of the solvent[137]. It represents an extension to the measurement of the reaction rate in pure non-deuterated solvent and fully deuterated solvent. The purpose is to examine if the solvent isotope effect is linear, or, if not, to draw conclusions from the type and extent of the non-linearity.

Because the proton or deuterium from the solvent involved in the reaction with MCR ends up in the product methane, the isotope distribution in the product ($CH_4$ versus $CH_3D$) can be studied in addition to the "classical" proton inventory experiment (which measures the suppression of the reaction rate as a function of the deuterium content in the solvent).
The resulting curve proceeds from only $CH_4$ formed at 0% $D_2O$ to only $CH_3D$ formed at 100% $D_2O$ in the solvent (neglecting the doubly labeled methane discussed in Chapter 3). Without any isotope effect, a linear correlation is expected.
The shape of the measured curve originates from a composite of the kinetic isotope effect (H or D being selected in the rate limiting step to give methane) and of the equilibrium concentration of H or D present in the hydrogen donating species (fractionation factor $\Phi$) before the rate-limiting step. Hence an apparent fractionation factor ($\Phi_{app}$) is obtained.

### 4.6.2 Proton inventory experiment on methane formation carried out previously with MCR

S. Mayr in our group investigated the proton inventory experiment on the isotopologue distribution of the formed methane together with the group of R. K. Thauer in Marburg.

A curve corresponding to an apparent fractionation factor ($\Phi_{app}$) of 0.27 was found (**figure 4.10**).

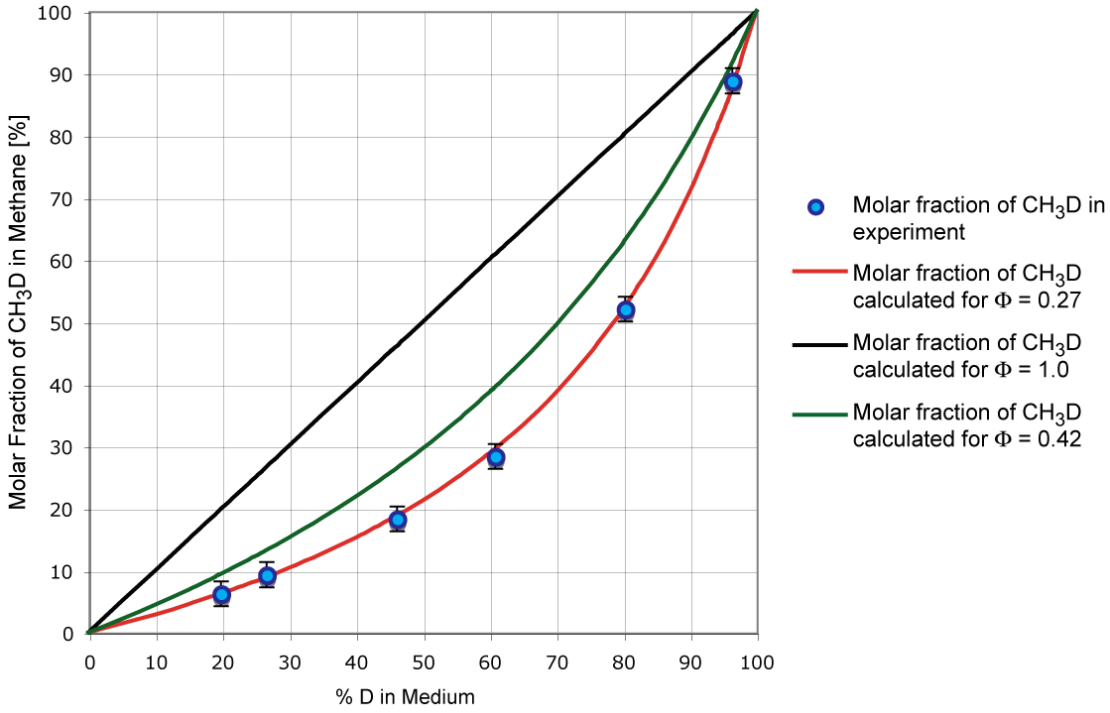


**Figure 4.10**: Proton inventory on product composition ($CH_4/CH_3D$) as determined for MCR by S. Mayr in collaboration with the group of R. K. Thauer. A Ti(III)-citrate assay was used which led to full conversion of the substrate employed. The fit corresponds to an apparent fractionation factor of 0.27[113].

### 4.6.3 Combined proton inventory studies on methane formation and substrate deuteration

Here, the proton inventory on deuterium incorporation into methyl-coenzyme M is examined in combination with the proton inventory on the isotopologue distribution of the methane that is formed. 4 mM methyl-coenzyme M and 2 mM coenzyme B (assay condition 6.2.4) were used in order to ensure a constant fraction of remaining methyl-coenzyme M. From each vial, the headspace (methane) and the assay solution were analyzed by $^1$H-NMR spectroscopy, which allowed comparison of deuterium incorporation into the substrate and the isotopologue distribution in the methane formed from each identical experiment (**table 4.11**).

**Table 4.11**: Formation of different methane isotopologues and substrate isotopologues after reaction with MCR buffer medium containing different concentrations of $D_2O$. Catalyzed by 1.07 nmol MCR after incubation for 2 min at 60 °C. The concentration of residual protons was determined by $^1$H-NMR spectroscopy (experimental section 6.5.8).

| $D_2O$ [%] | $CH_3$-S-CoM [μmol] | $CH_2D$-S-CoM [μmol] | $CH_4$ [μmol] | $CH_3D$ [μmol] | $CH_2D_2$ [μmol] |
|---|---|---|---|---|---|
| 97.30 | 3.364 | 0.1166 | 0.236 | 2.634 | 0.049 |
| 97.30 | 3.483 | 0.1168 | 0.224 | 2.482 | 0.094 |
| 72.97 | 3.389 | 0.0629 | 1.620 | 1.302 | 0.026 |
| 72.97 | 3.188 | 0.0615 | 1.733 | 1.382 | 0.036 |
| 48.65 | 3.431 | 0.0316 | 2.309 | 0.629 | 0 |
| 48.65 | 3.419 | 0.0286 | 2.300 | 0.653 | 0 |
| 24.32 | 3.503 | 0.0139 | 2.624 | 0.259 | 0 |
| 24.32 | 3.375 | 0.0135 | 2.756 | 0.255 | 0 |

The proton inventory curve for the distribution of isotopologues in the product methane is shown in **figure 4.11**.

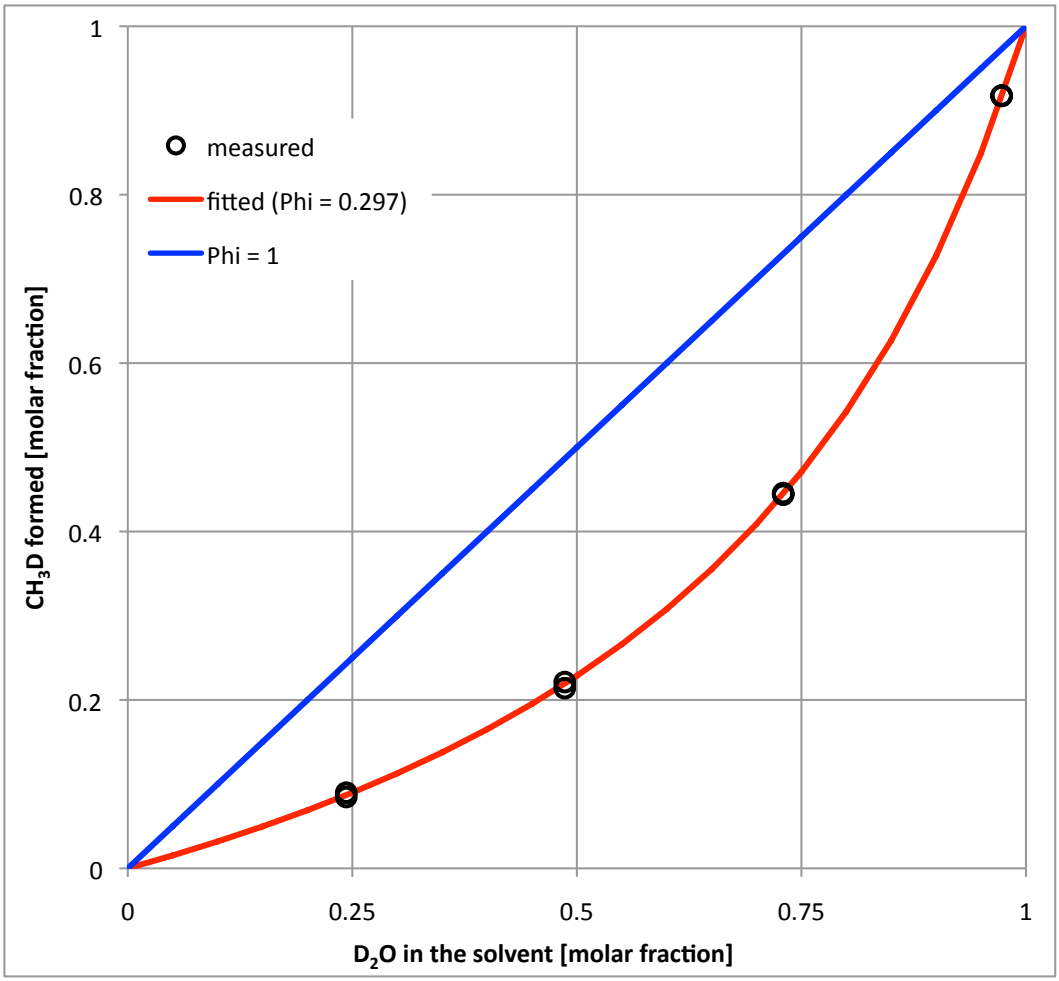


**Figure 4.11**: Proton Inventory curve of the fraction $CH_3D/CH_4$ formed. The small amount of $CH_2D_2$ formed is not taken into account in this curve.

The proton inventory curve for deuterium incorporation into the substrate is given in **figure 4.12**.

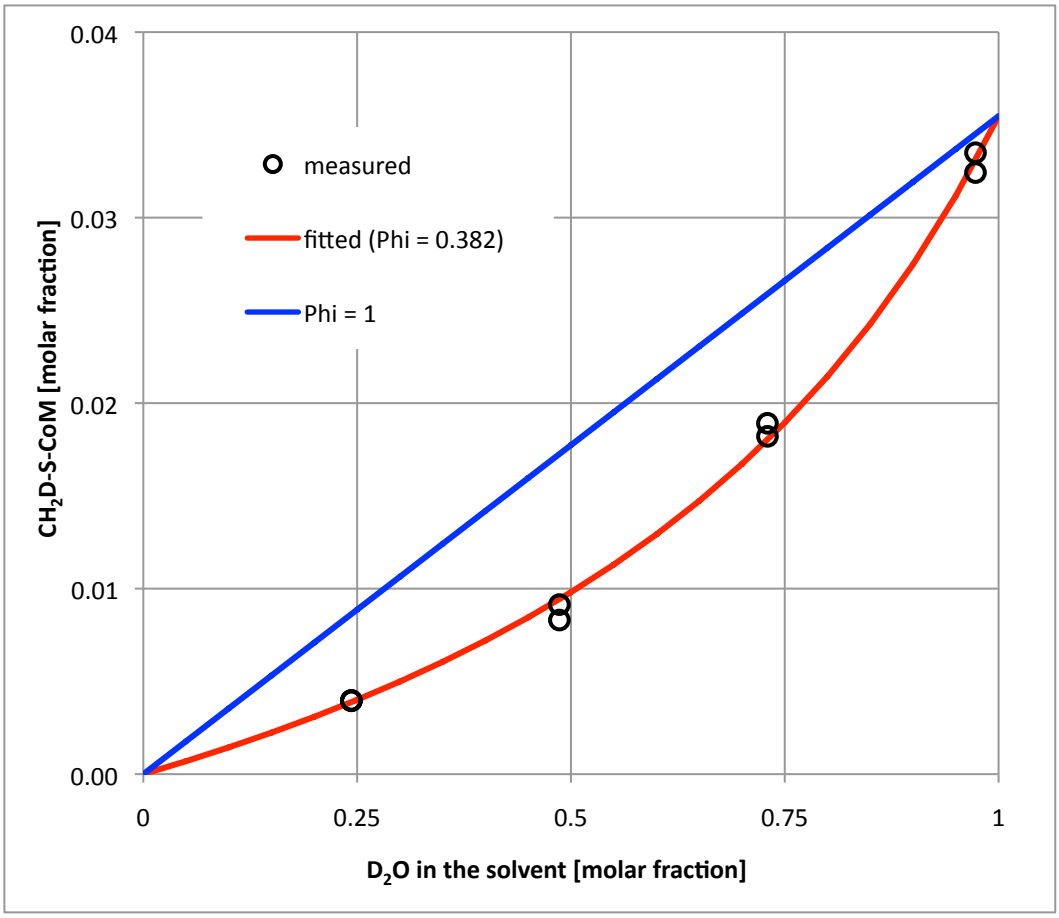


**Figure 4.12**: Proton Inventory curve of the fraction of $CH_2D$-S-CoM present in the remaining substrate. The red curve was obtained from a least square fit varying the fractionation factor and the unknown amount of $CH_2D$-S-CoM formed at hypothetical 100% $D_2O$ in the medium (0.03547).

## 4.7 Summary of the Measured Isotope Effects

**Methane formation:**

- $^{12}CH_3$-/$^{13}CH_3$-S-CoM: 1.050 ± 0.005
- Sec. KIE per D: 1.191 ± 0.005
- Prim. solvent IE ($H_2O/D_2O$): 1.0 to 1.6

**Methane activation:**

- Prim. KIE = 2.44 ± 0.22
- Sec. KIE (per D) = 1.17 ± 0.05

**Activation of the methane intermediate:**

- "$CH_3D$" intermediate: 2.59 per H/D (single measurement)
- "$CH_2D_2$" intermediate: 2.43 (identical value measured in two independent experiments)

**Formation of the ethane intermediate and C-H/C-D bond activation of the ethane intermediate:**

| Isotope effect (IE) | Intermediate formation | C-H / C-D activation from intermediate |
|---|---|---|
| primary IE | 1.1 ± 0.1 | 2.5 ± 0.1 |
| α secondary IE (per D) | 1.25 ± 0.10 | 1.25 ± 0.10 |
| β secondary IE (per D) | 1.00 ± 0.05 | 1.00 ± 0.05 |

**Apparent fractionation factor ($\Phi_{app}$) of methane formation:**

- $\Phi_{app}$ = 0.30, very small dispersion

**Apparent fractionation factor ($\Phi_{app}$) of $CH_2D$-S-CoM formation:**

- $\Phi_{app}$ = 0.38, with larger dispersions than measured for product isotopologue distribution

## 4.8 Discussion of the Measured Isotope Effects

### 4.8.1 Isotope effects on methane formation

The carbon isotope effect of 5.0 ± 0.5% for $^{12}CH_3$-S-CoM/$^{13}CH_3$-S-CoM is substantial (among the largest reported $^{12}C/^{13}C$ isotope effects are those for nucleophilic substitution of methyl iodide by cyanide with $k_{12}/k_{13}$ = 6.9% at 58 °C[138] and that for hydrogen abstraction from methane by chlorine atoms $k_{12}/k_{13}$ = 6.6% at 24 °C[139]). This result proves that the S-C bond is broken on the way to the intermediate. In addition, it confirms that formation of the intermediate is rate limiting for the native substrate methyl-coenzyme M.

The occurrence of a secondary isotope effect of 1.191 ± 0.005 per D present in the methyl group of methyl-coenzyme M points to a geometry change at the methyl carbon during the rate-limiting step. Secondary isotope effects[140] in this range are observed for $S_N1$-type nucleophilic substitution reactions with a partial change from $sp^3$ to $sp^2$ hybridization upon going to the carbenium-ion-like transition state, and, with a similar geometric rearrangement, for hydrogen atom abstraction from a $sp^3$-hybridized carbon to give a planar carbon-centered radical. $S_N2$-type nucleophilic substitutions on the other hand, usually show smaller α-secondary KIE in the range 0.95 to 1.05.

The primary $H_2O/D_2O$ solvent isotope effect on the methane formation rate was too small to be measured accurately (no competitive measurement possible). The experiments led to an estimated isotope effect of about 1.1 to 1.2, which would also qualitatively agree with the primary KIE for the forward reaction of $k_H/k_D$ = 1.1 determined for ethyl-coenzyme M. Unfortunately, the quality of the data available so far does not allow us to exclude with certainty that this isotope effect could be as large as 1.5. This is important for the following reason: If methane were formed from the bound substrates coenzyme B and methyl-coenzyme M via a single transition state, a kinetic isotope effect

of ca. 1.5 would be required in addition to the low fractionation factor of $\Phi = 0.42$ for the SH group of coenzyme B to explain the even lower fractionation factor observed in the distribution of produced methane isotopologues (cf. also discussion 4.8.6). If, by acquiring better data, one could definitely exclude that the solvent isotope effect on the rate of methane formation is as large as 1.5, such a one-step mechanism with a direct transfer of the 4$^{th}$ hydrogen from the SH group of coenzyme B to the methyl carbon (as e.g. proposed by Siegbahn and coworkers[74]) could be excluded.

Two scenarios would be consistent with the absence of a significant solvent kinetic isotope effect $k_{H2O}/k_{D2O}$ on the rate of methane formation: a) the product determining step (H or D incorporation) is not rate limiting or b) product determining and rate limiting step are identical but the hydrogen is transferred from a position with a very low fractionation factor, so that the ratio of $\Phi^{\neq}/\Phi_{reactant}$ is close to one. In view of the significant primary KIE of 2.44 observed in the reverse reaction (see 4.8.2 below), scenario b) where the rate determining and product determining steps are identical would have to exhibit a large inverse equilibrium isotope effect of $K_H/K_D = 0.4\text{-}0.44$ in the direction of methane formation.

### 4.8.2 Isotope effects on C-H/C-D bond activation

The isotope effects measured for methane activation (primary KIE = 2.44, secondary KIE = 1.19) are in good agreement with the isotope effects found for the activation of the bound ethane present in the intermediate formed from ethyl-coenzyme M (primary KIE = 2.5, α-secondary KIE = 1.25).

In contrast to the experiments studying C-H/C-D bond activation in the methyl-coenzyme M intermediate (cf. "$CH_2D_2$" activation, section 4.4.2), a direct determination from one experiment was possible for the ethyl-coenzyme M intermediate, because the scrambled re-formed substrate

is distinguishable from the unreacted substrate (cf. section 4.5.3, figure 4.7).

The ratios of primary/secondary isotope effects for $CH_2D_2$ activation ($KIE_{prim}/KIE_{sec}$ = 2.07) and the corresponding ratio in the activation of the "$CH_2D_2$" intermediate ($KIE_{prim}/KIE_{sec}$ = 2.43), however, do not match, although the activation of $CH_2D_2$ must proceed via the "$CH_2D_2$" intermediate according to the principle of microscopic reversibility. The measurement of the isotope effect on the "$CH_2D_2$" intermediate activation was complicated by the fact that no competitive measurement was possible. With $CH_2D$-S-CoM as the substrate in $D_2O$, the activation of the C-H bond in the intermediate could be measured; with $CHD_2$-S-CoM as the substrate in $H_2O$, the activation of the C-D bond could be measured (cf. section 4.4.1, figure 4.3). Calculation of the isotope effect was based on the assumption that the ratio of methane formation versus methyl-coenzyme M formation from the intermediate (commitment) is equal in $H_2O$ and $D_2O$. A higher commitment of the intermediate to methane formation (versus back reaction) in $H_2O$ relative to $D_2O$ would lead to a calculated isotope effect that is larger than the intrinsic one. Analysis of the proton inventory on deuterium incorporation into methyl-coenzyme M, however, points rather to the opposite effect (a slightly higher commitment to methane formation in $D_2O$, see discussion in section 4.8.5). Hence a correction for the difference in the commitment would make the intrinsic isotope effect even higher. Taking into account the incomplete deuteration of the medium (approx. 98% $D_2O$) combined with the low apparent fractionation factor in the product (and therefore intermediate), a correction for residual protons would lead to more C-H bond activation observed and therefore also slightly increase the intrinsic isotope effect.
Accordingly, both considered sources of error in the experiments designed for the measurement of the isotope effect on "$CH_2D_2$" intermediate activation do not explain the difference to the experiment

of activation of free $CH_2D_2$ but point to an even higher intrinsic isotope effect.

In order to explain the difference between the two isotope effects, the following hypothesis involving a hydrido methyl nickel complex is presented.

### 4.8.3 Hypothesis accounting for the different isotope effects observed in activation of free $CH_2D_2$ and "$CH_2D_2$" intermediate

In the case of activation of $CH_2D_2$ under equilibrium conditions (very low concentration of coenzyme B), an equilibrium between the hydrido $d_2$-methyl complex and deuterido $d_1$-methyl complex is established (**figure 4.13**). Dissociation of $CH_2D_2$ from the "$CH_2D_2$" intermediate has no influence on the outcome of the reaction, because it is also in equilibrium by association.

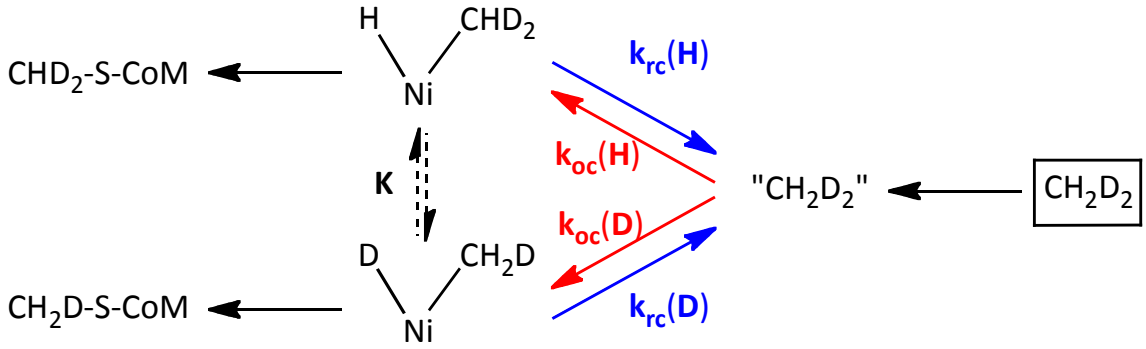


**Figure 4.13**: Assumption that the observed ratio of isotope effects in methane activation (primary/secondary = 2.07) corresponds to an equilibrium isotope effect K (dashed arrows) in an oxidative addition reaction.

If one assumes that the formation of methyl-coenzyme M from the hydrido methyl complexes does not exhibit a H/D isotope effect, the ratio of $CHD_2$-S-CoM to $CH_2D$-S-CoM corresponds to the equilibrium constant (K) of the two isotopomeric hydrido methyl complexes. This equilibrium constant corresponds to the ratio of the kinetic isotope

effects for oxidative cleavage and reductive coupling (EIE = $KIE_{oc}/KIE_{rc}$ = 2.07).

In the experiments performed to measure the ratio of isotope effects in the activation of the "$CH_2D_2$" intermediate, no equilibrium is established during the 4 min incubation time. Hence, after formation of the intermediates, dissociation of $CH_2D_2$ from "$CH_2D_2$" is the dominant pathway (**figure 4.14**).

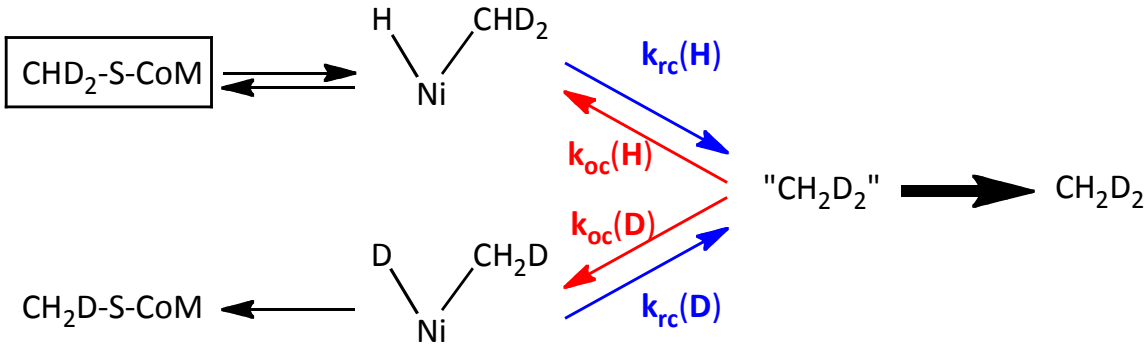


**Figure 4.14**: Assumption of hydrido methyl complexes as intermediates. Before the equilibrium conditions are reached, dissociation of the bound methane isotopologue dominates the decay of the intermediate (bold arrow).

The equilibrium of the two isotopomeric hydrido methyl complexes is disturbed by the dissociation of the "$CH_2D_2$" intermediate and cannot be fully established. Assuming that only an infinitesimal amount of the "$CH_2D_2$" intermediate would react back to the hydrido- methyl complex (because nearly all "$CH_2D_2$" would dissociate), the isotope effect of reductive coupling would lose its influence, because the re-formed "$CH_2D_2$" intermediate would react to free $CH_2D_2$. The observed ratio of $CHD_2$-S-CoM to $CH_2D$-S-CoM would correspond to the isotope effect on oxidative cleavage (red arrows), which is obviously larger than the ratio of oxidative cleavage to reductive coupling (all isotope effects of these elementary reactions are "normal", cf. section 1.3.4).

Under the experimental conditions employed, dissociation of $CH_2D_2$ cancels the influence of the isotope effect of reductive coupling only

partly, which would lead to an isotope effect in the range between the equilibrium isotope effect and the isotope effect for oxidative cleavage.
For this effect to be significant, the reaction from the hydrido methyl complex back to methyl-coenzyme M would have to be competitive with the reaction of reductive coupling.
For the substrate ethyl-coenzyme M, dissociation of the alkane (or a reaction coupled with dissociation of the alkane) is rate limiting and, as a consequence, the equilibrium is always established. The simulation therefore allowed determination of the equilibrium isotope effect accurately (primary KIE = 2.5, α-secondary KIE = 1.25), but no information about the isotope effect on ethane formation could be obtained (only 5% conversion to ethane after the longest incubation period employed).
Periana and Bergman reported an isotopomeric distribution of 1 : 4.5 for the equilibrium of the deuterido [1-$^{13}$C]-ethyl rhodium complex and the hydrido [1-$^{2}$H, 1-$^{13}$C]-ethyl rhodium complex[129]. Statistical correction for the two hydrogen atoms present yields an equilibrium isotope effect of 2.25, which is in close agreement to the isotope effects we observed in the reactions catalyzed by MCR: 2.07 for $CH_2D_2$ and 2.0 (2.5/1.25) in case of the "ethane" intermediate.

### 4.8.4 Implication of the discovered isotope exchange and its isotope effects on the stereochemical course of ethane formation

Floss, Krzycki and coworkers[77] reported a long time ago that cell extracts of *M. barkeri* converted chiral $CH_3CDT$-S-coenzyme M to chiral ethane ($CH_3CHDT$) under (partial) net inversion of configuration. This result had a large impact on the discussion of possible catalytic mechanisms of MCR over the years. At first sight, our finding that MCR-catalyzed hydrogen isotope exchange and carbon scrambling in ethyl-coenzyme M are much faster than the reaction to ethane seemed to be in contradiction with survival of configurational information in

the product ethane. This prompted us to simulate the experiments of Floss et al. using the relative rates (partitioning of intermediate "ethane") and isotope effects found in our experiments with pure MCR enzyme ($^3$H isotope effects were calculated from $^2$H KIE using the Swain-Schaad relationship). In these simulations it was assumed that both the formation of the intermediate from ethyl-coenzyme M and the reverse C-L activation back to the substrate are completely stereospecific with inversion of configuration.

The observation of an enantiomeric excess of 41% (from (*S*)-ethyl-coenzyme M, after 10.3% conversion) and 51% (from (*R*)-ethyl-coenzyme M, after 28% conversion) in the product ethane is fully compatible with the isotope exchange and carbon scrambling reported here. At the low conversions reached in the experiment of Floss et al., the simulation predicts still significant but smaller ee values even in the absence of any isotope effects. Only the detection of a higher ee at the higher conversion (51% ee for 28% conversion and 41% ee for 10.3% conversion) is curious and judged to be within the experimental error.

This analysis not only confirms that the reported experiment would be compatible with the observed isotope exchange and isotope effects, it also means that if product formation is stereospecific the stereochemical information must be conserved in the intermediate. With a freely rotating ethyl radical as the intermediate, for example, isotope exchange in the substrate would result in racemic ethane.

### 4.8.5 Proton inventory studies

The apparent fractionation factor ($\Phi_{app}$) for the $CH_3D/CH_4$ distribution in the product methane (depending of the concentration of $D_2O$ present in the solvent) from 4 mM methyl-coenzyme M and 2 mM coenzyme B was found to be 0.30. This result shows that the conditions with limiting coenzyme B to give only 50% conversion lead to a comparable result as the experiments performed with the reductant Ti(III)-citrate leading to full conversion ($\Phi_{app} = 0.27$[113]).

Deuterium incorporation into the remaining substrate was evaluated and correlated to the fraction of $D_2O$ present in the medium in the same sets of experiments from which the fractionation factor on methane formation was deduced. An apparent fractionation factor of $\Phi_{substrate}$ = 0.382 was obtained from least square fitting. Since all C-H and C-D bonds are set up in the intermediate and no exchange of the intermediate with the solvent occurs (3.2.4), it would be expected that the deuterium incorporation into methyl-coenzyme M should proceed with the same fractionation factor as for product formation.

The experiments to measure the amount of deuterium incorporated into the substrate, as a function of the concentration of $D_2O$ present in the solvent, are dependent on the partitioning from the intermediate (reaction to methane versus re-formation of substrates).

If in fully deuterated medium a higher proportion of the intermediate would react back to the substrates, the values of $CH_2D$-S-CoM would have to be corrected down to match the proton inventory curve due to the fractionation factor.

If a lower proportion of the intermediate would react back to the substrates in fully deuterated medium, too little $CH_2D$-S-CoM would be detected and would have to be corrected up to match the proton inventory curve due to the fractionation factor.

Such a correlation could originate from a non-specific solvent isotope effect (e.g. by weakening of hydrogen bonding within the enzyme through exchange of NH by ND in the protein). According to the literature, however, such effects have been found to be remarkably small and would mainly arise at high concentrations of $D_2O$ in the medium[131]. **Figure 4.15** displays the measured values of $CH_2D$-S-CoM formed combined with a fit of the apparent fractionation factor determined for methane formation ($\Phi_{app}$ = 0.297).

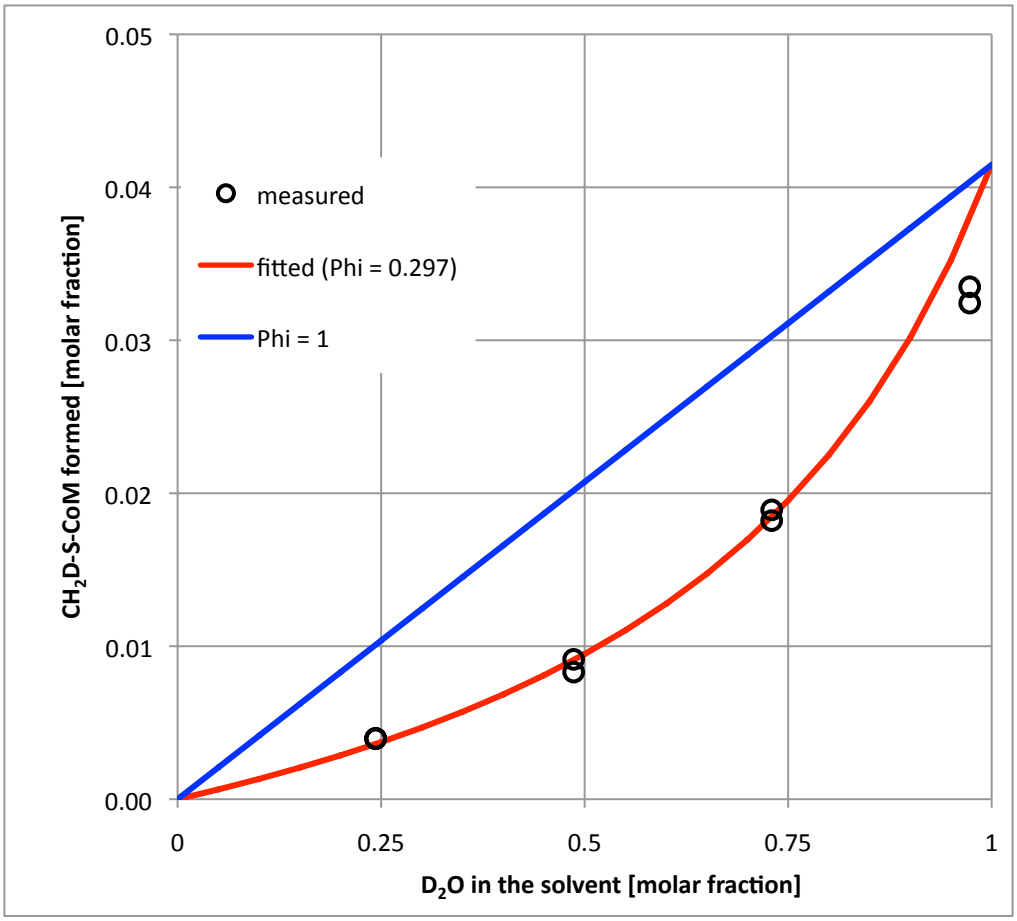


**Figure 4.15**: Proton Inventory curve for $CH_2D$-S-CoM formation with the apparent fractionation factor determined from product formation ($\Phi_{app}$ = 0.297). The red curve was obtained by fitting the amount of $CH_2D$-S-CoM formed at hypothetical 100% $D_2O$ in the medium for the data points at 24%, 49% and 73% $D_2O$ only.

It can be deduced from figure 4.15 that the commitment at high concentrations of $D_2O$ is rather higher (less substrate re-formation compared to methane formed) than lower.

Although the data do not appear to be very accurate, they rule out the difference observed in the isotope effect on activation of free $CH_2D_2$ and "$CH_2D_2$" intermediate being attributable to a difference in the commitment (methane formation versus substrate re-formation), assuming that the apparent fractionation factor for product formation and substrate deuteration is equal.

If the difference in the mentioned isotope effects (cf. section 4.8.2) were explained by a difference in the commitment, the apparent fractionation factor on substrate deuteration would have to be larger than 0.45, resulting in a poorer match to the measured data points.

### 4.8.6 Implications of the measured isotope effects on the mechanism proposed by Siegbahn and coworkers [73, 74, 141]

The mechanism Siegbahn and coworkers[73, 74], which is based on DFT calculations, assumes an $S_R2$ substitution of Ni(I) at the thioether sulfur to liberate a "transient methyl radical" that synchronously abstracts a hydrogen atom from the SH group of coenzyme B (**figure 4.16 bottom,** TS I). The only intermediate (INT) contains free methane, the thiolate of coenzyme M bound to Ni(II) and coenzyme B thiyl radical. The second step (TS 2) represents formation of the disulfide and regeneration of the nickel center in the Ni(I) oxidation state.

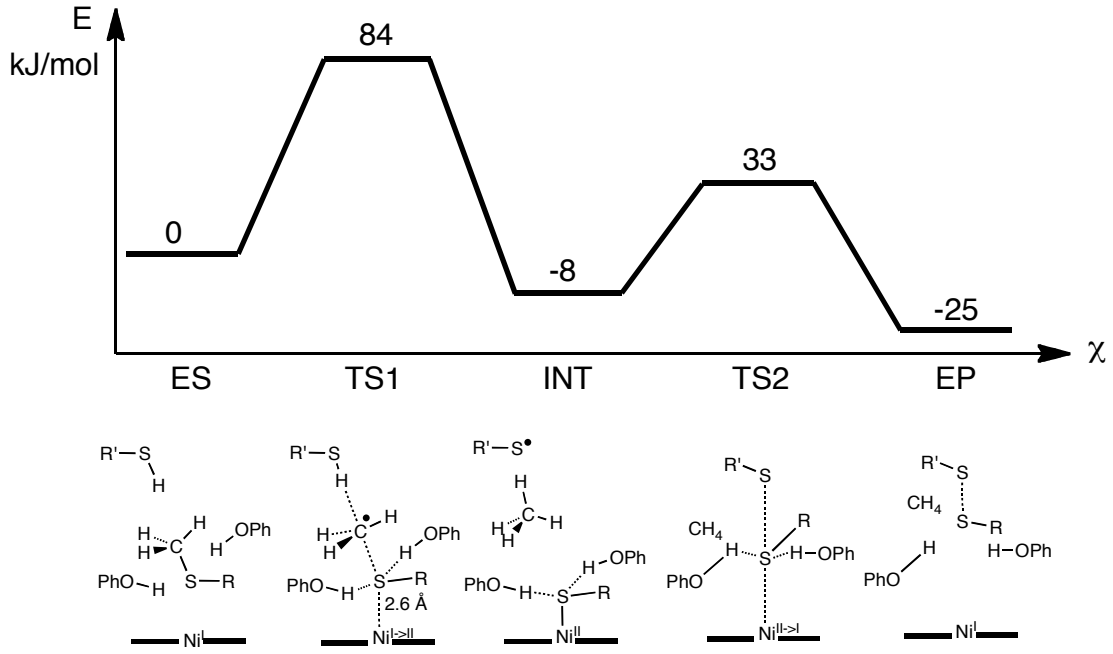


**Figure 4.16**: Mechanism and corresponding energy profile as reported based on DFT calculations by Siegbahn and coworkers[73, 74].

The calculated energy profile does not match the experimental finding of the observed isotope exchange in either methyl-coenzyme M or ethyl-coenzyme M. The authors calculated the second transition state to be 51 kJ $mol^{-1}$ lower than that of the rate-limiting step. From our experiments, the second transition state is only 8.3 kJ $mol^{-1}$ lower than that for the rate-limiting step for the native substrate methyl-coenzyme M; for ethyl-coenzyme M, the second transition state is even 12.8 kJ $mol^{-1}$ higher than the first transition state (as discussed in section 3.4.2, cf. figure 3.18). With the energy profile from Pelmenschikov's DFT calculations shown above, the isotope exchange we observed cannot be explained (partitioning of the intermediate between back and forward reaction would be on the order of $1 : 6 \bullet 10^7$).

The qualitative pattern of isotope exchange in the calculated mechanism, however, is in agreement with the experimental finding since sulfur is directly replaced by the forth hydrogen and all C-H bonds of the alkane are set up in the intermediate.

The absence of a significant isotope effect depending on whether hydrogen or deuterium is introduced in the rate limiting step to form methane is difficult to reconcile with this step being rate limiting. The kinetic isotope effect on S-H/S-D hydrogen atom abstraction from *tert*-Bu-SH by a methyl radical, for example, was reported to be 2.71[142]. In the mechanism proposed by Siegbahn and coworkers, however, a "transient methyl radical" is proposed and the H⋯C distance is still very long (2.57 Å) in TS I, which would reduce the KIE dramatically. It has to be considered, however, that in the starting structure used by Pelmenschikov *et al.* all coenzymes were positioned according to the X-ray structure of the inactive Ni(II) form $MCR_{ox1\text{-}silent}$. If one considers that the sulfur of coenzyme B is now known to move almost 2 Å nearer to the nickel when coenzyme B binds to active MCR, this overlong distance in TS I might well be an artifact of the model used by Pelmenschikov *et al.* In any case, it is very difficult, if not impossible, to qualitatively predict isotope effects in a reaction step in which, at the

same time, 2 bonds are broken, 2 bonds are formed, and 5 different atoms (Ni, S, C, H, S) have to be arranged in a more or less linear array.

Because the fourth hydrogen atom of the formed methane is delivered directly from a thiol in the rate-limiting step, the fractionation in $CH_3D/CH_4$ (measured to be 0.30) corresponds to the fractionation factor of coenzyme B (measured to be 0.42[113]) divided by the isotope effect. Hence the isotope effect has to be at least 1.4 to be consistent with the mechanism calculated by DFT calculations. As discussed above, we cannot exclude this with certainty from the experiments described here, although the best estimate is $k_H/k_D$ = 1.1 to 1.2.

### 4.8.7 Catalytic mechanisms accounting for all measured isotope effects

The very low fractionation factor of 0.30 on product isotopologue distribution combined with the absence of a significant $H_2O/D_2O$ solvent isotope effect is most economically explained by the formation of a species containing a weakly bound hydrogen prior to the rate limiting step, such as a transition metal hydride (which is expected to have a very low fractionation factor). The absence of a significant solvent isotope effect on the rate of methane formation would be consistent with a reaction profile in which the prospective fourth hydrogen of methane does not participate in bond formation or cleavage in the rate-limiting step. Hence the new C-H bond of methane should be formed after the rate-limiting step, as is the case in the oxidative addition/ reductive elimination pathway described in section 4.8.3.

Combining the mentioned steps (nickel-hydride formation, C-S bond breaking in the rate limiting step and formation of the new C-H bond to give the intermediate with methane bound) leads to the reaction mechanism depicted in **figure 4.17**, which does not include any radical intermediates.

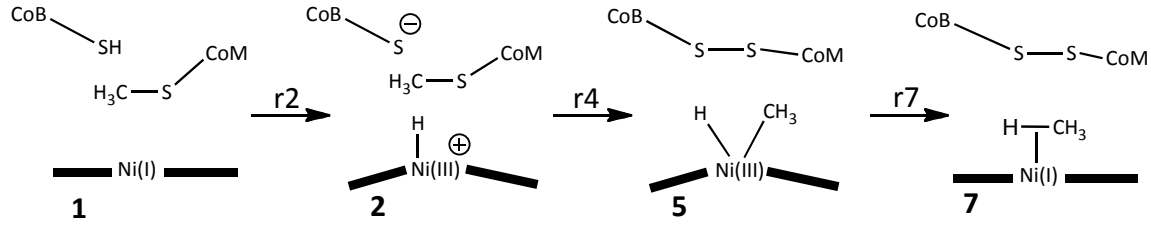


**Figure 4.17**: Schematic representation of a non-radical reaction mechanism accounting for all measured isotope effects. The numbering of reactions and intermediates corresponds to the scheme described in the introduction (figure 1.9).

After binding of the second substrate coenzyme B, protonation of the nickel center occurs (figure 4.17, r2). The hydride that is formed (**2**) is responsible for the low fractionation factor. In the rate-limiting step (r4), the C-S bond is broken and the hydrido methyl complex (**5**) is formed (discussed in the next paragraph). Formation of the new C-H bond (r7) corresponds to a reductive coupling to give the σ-coordinated methane complex (**7**) and does not result in an isotope effect since it occurs after the rate-limiting step.

The nature of the rate-limiting step (r4) remains nebulous.

The $^{12}CH_3$-/$^{13}CH_3$-S-CoM isotope effect is in accordance with this step being rate limiting, and the secondary isotope effect points to a geometry change in the methyl group during the rate-limiting step. Assuming that reductive coupling proceeds with retention of configuration, the transformation from intermediate **2** to **5** (r4) has to proceed with inversion of configuration.

It is tempting to draw a one-step mechanism in which the thiolate of coenzyme B attacks the thioether sulfur of methyl-coenzyme M to release the methyl group ("$CH_3^-$", which is simultaneously bound to the Ni(III) center) in order to account for all measured isotope effects and for the inversion of stereochemistry.

Such a reaction, however, lacks precedent. But its reverse reaction, nucleophilic attack at dimethyl disulfide to give a methyl-sulfide and methyl thiolate, has been reported for acetone enolate and nitromethane anion as nucleophiles in the gas phase[143]. On the other hand, it is difficult to see why the formal Ni(III) center should interact with the methyl group of methyl-coenzyme M rather than with its thioether sulfur. Hence, it is likely that this transformation represents a more complex multistep reaction, in which the hydrido-Ni(III) species (**2**) first interacts with the thioether sulfur of coenzyme M.

### 4.8.8 Discussion of further catalytic mechanisms proposed in the literature in light of the measured isotope effects

Ragsdale and coworkers performed experiments with analogues of coenzyme B that varied in the length of their alkyl chain[144]. By replacing the native second substrate coenzyme B (chain of 7 carbon atoms) by its analogue with only 6 carbon atoms, radical formation could be detected[145]. The exact nature of these reported radicals remains open. Isotopic labeling studies with [$^2H_6$]-*p*-hydroxyphenylacetic acid, however, ruled out the possibility of tyrosine radicals[145]. These findings, together with earlier reports of radical formation caused by suicide inhibitors of methyl-coenzyme M[44, 76], demonstrate that radical formation can occur if the catalytic reaction is prevented from reacting along the native pathway.

Concluding that methane formation proceeds via a radical pathway, however, is not possible from these findings, because radical formation might be a side reaction leading to the observed deactivation of the enzyme *in vitro*.

Many catalytic mechanisms proposed in the literature assume an $S_N2$ reaction of the Ni(I) center at the methyl group of methyl-coenzyme M[45, 46, 54, 76], which is the most economical way to account for the reported inversion of the configuration. But the low fractionation factor ($\Phi_{app}$ = 0.30) found for the methane isotopologue distribution is not in accordance with such a reaction step being rate limiting.

A mechanism involving protonation prior to the rate-limiting step has been proposed by Duin and McKee based on DFT calculations[75]. Although the mode of protonation is controversial from a chemical point of view (one nitrogen atom of the macrocycle of F430 is protonated from the distal face), it was the first proposal that coenzyme F430 is activated by protonation in order to cleave the C-S bond of methyl-coenzyme M.

# 5 Conclusion and Outlook

A more detailed understanding of the reaction profiles for the native substrate methyl-coenzyme M and for the non-natural substrate ethyl-coenzyme M was obtained from the studies presented here.
The rate of anaerobic oxidation of methane catalyzed by MCR from a methanogen was found to be comparable to the rate observed *in vivo* for communities of ANME archaea and sulfate reducing bacteria. This finding is not only important in the biological context by supporting the "hypothesis of reverse methanogenesis", but it is also a precedent for chemists demonstrating that activation of methane in neutral, cold, aqueous solution without oxygen-derived radicals is possible. Stating that chemists are not able to perform a comparable reaction in water, however, might be unfair, because the active site of MCR is very apolar and thus approximates the environment present in a classical organic solvent. Nevertheless, establishing the right chemical conditions to activate methane (the alkane with the strongest C-H bond) anaerobically, including the highly optimized nickel catalyst coenzyme F430 in the active site of enzyme MCR, is a remarkable achievement by Nature.

We could show that at least one intermediate exists in the catalytic cycle for the native substrate methyl-coenzyme M and for the non-natural substrate ethyl-coenzyme M. For both substrates, the difference in height of the energy barriers for the forward reaction to products versus backward reaction to substrates from the intermediate could be determined through isotope exchange experiments.
However, the reaction mechanism of MCR is still unknown. It could be shown that the intermediates contain all C-H bonds of the prospective alkane. The structure of this intermediate, in particular the question whether the alkane is bonded to the nickel center or just trapped in the

active site, remains open because all attempts to detect and characterize intermediates spectroscopically have failed so far. The deeper insight into the shape of the different reaction profiles for the two substrates gained in this work may help to select conditions under which the steady state concentration of an intermediate is large enough to be detected spectroscopically.

The set of isotope effects measured in this work results in additional boundary conditions that have to be fulfilled by every mechanism proposed in the future. Proposing a mechanism that accounts for all findings observed previously and in this work is challenging, because the reaction catalyzed by MCR lacks a direct analogy from non-enzymatic reactions. None of the mechanisms proposed earlier seems to account for the combined findings of all experiments done with MCR.

It is still unknown which product, the alkane or the heterodisulfide, leaves the active site first, or whether there might even be a separate channel for methane to exit/enter the enzyme leading to a random type mechanism. In order to study (endergonic) methane activation, equilibrium conditions are required to observe a significant amount of conversion. Moreover, this is a complex system because all substrates and products are present in concentrations that are difficult to measure during the course of the reaction. Studying product inhibition of alkane formation requires high pressures of methane (or ethane), conditions that are technically difficult to achieve in a reproducible manner.

A central question that still remains is whether free carbon- or sulfur-centered radicals are involved as true intermediates or not. The mechanism proposed by Siegbahn, despite inconsistencies and an unprecedented concerted multi-radical-substitution, cannot be definitely ruled out based on the evidence available.

Protein-based radicals were found when active MCR was reacted with a certain class of irreversible inhibitors[44, 145].
The fact that persistent protein radicals are generated when catalysis goes wrong due to inhibitors or substrate analogs has no evidentiary value with regard to the native catalytic cycle. The (partial) mechanism proposed in section 4.8.7, on the other hand, is consistent with all data and does not involve any free radicals.

Potential cooperation of the two active sites present in the enzyme (proposed as a "two-stroke mechanism" by R. K. Thauer and coworkers[62]) needs to be investigated experimentally in depth.
The fact that some enzyme states can be induced to 50% only, and the slight difference in the *g*-value in the W-band EPR spectrum of the empty active site depending on whether the other active site is occupied or not, support such a hypothesis. The UV-Vis spectrum of the enzyme in the equilibrium state where anaerobic oxidation of methane could be measured showed a Ni(I) content very close to 50%, which remained constant during at least one hour (experimental section 6.3.6). The remaining 50% resembles the spectrum of the inactive Ni(II) form, which, however, is difficult to distinguish from the spectrum of some of the Ni(III)-X species observed with inhibitors[44, 146].
Hard evidence for cooperation of the two active sites, however, is not available and, so far, considering each finding separately seemed not to require cooperation of both active sites.
It appears that MCR still holds important secrets that need to be unmasked in order to understand the low reaction rate of ethane formation and to bring in line all other experimental facts discovered up to now.

# 6 Experimental Section

## 6.1 Purification of MCR

### 6.1.1 Equipment

**Fermenter**:

14 L glass fermenter: New Brunswick, Michigan

Temperature control bath: Haake

**Growth medium (10 L)**:

| | |
|---|---|
| $NH_4Cl$ | 65 mM |
| $KH_2PO_4$ | 50 mM |
| $Na_2CO_3$ | 30 mM |
| $MgCl_2$ x 6 $H_2O$ | 300 µM |
| Nitrilotriacetic acid | 240 µM |
| $FeCl_2$ x 4 $H_2O$ | 75 µM |
| $NiCl_2$ x 6 $H_2O$ | 7.5 µM |
| $CoCl_2$ x 6 $H_2O$ | 1.5 µM |
| $Na_2MoO_4$ x 2 $H_2O$ | 1.5 µM |

**Gases**:

Forming gas ($N_2/H_2$ = 95%/5%), growth gas ($H_2$/ $CO_2$ = 80%/20%), hydrogen (99.9995%): Messer, Griesheim (Siegen)

Hydrogen sulfide: Pan Gas

**Centrifuges**:

Continuous anaerobic centrifugation 15000 rpm: Hettich, Contifuge 17RS

Ultracentrifugation 40000 rpm: Sorvall Ultra pro 80, rotor Ti-45, Sorvall, Bad Homburg

**Anaerobic tent**:
Filled with forming gas, equipped with a palladium catalyst: Coy Instruments

**Ultra sonic rod**: Ultrasonic disintegrator Sonoplus HD200 with sonotrode TT 100, Bandelin, Berlin

**Chromatography**:
FPLC: Amersham Pharmacia Biotech, Freiburg
Column: Q-sepharose (high load, high performance, 3.58 $cm^2$ x 15 cm)

**Concentration cells**:
100 kDa cut off: Amicon (Millipore, Bedford MA)

**UV/Vis spectroscopy**:
Diode array photometer: Specord S10 (Zeiss, Jena)

### 6.1.2 Growth of *Methanothermobacter marburgensis* and *in vivo* induction of the red1 state

The fermenter filled with 10 L growth medium was stirred (1000 rpm), treated with $H_2/CO_2$ (80%/20%, 1200 ml $min^{-1}$) including $H_2S$ (approx. 10 bubbles $min^{-1}$) and heated to 65 °C.
After 2 h it was inoculated with 60 or 120 ml of a fresh cell suspension ($OD_{578}$, optical density at 578 nm = 10) grown before. In the beginning the cells grew exponentially (doubling time about 2 h), later at a rate approximately proportional to the gas flow. After $OD_{578}$ = 5-6 was reached (15-16 h growth time) the cells were ready for harvest.
In order to induce the red1 state *in vivo*, the gas was switched to pure hydrogen. After 20 min treatment with hydrogen the medium was cooled with a temperature control bath filled with ice water. The outside of the fermenter was additionally cooled with ice as rapidly as

possible. After reaching a temperature below 10 °C (ca. 20 min) the cell suspension was transferred through a hose (previously flushed with anaerobic buffer) into the continuous centrifuge cooled to 4 °C at a flow rate of approx. 300 ml $min^{-1}$. The rotor containing the cell pellet was closed and transferred into the anaerobic tent in which all following operations were performed.

### 6.1.3 Purification of MCR isoenzyme I

The cell pellet (about 70 g) was suspended in 100 ml Tris-HCl buffer (10 mM, pH 7.6, containing 10 mM coenzyme M) and sonicated in a rosette vessel in an ice bath (4 times 7 minutes applying 200 W, with 3 min delay in between in order to avoid warming up). Cell debris, intact cells, and membranes were removed by ultracentrifugation.

Under stirring and ice cooling, ammonium sulfate (aq., sat., containing 10 mM coenzyme M) was added until a final concentration corresponding to 60% saturation was reached. Precipitated proteins (mostly other than MCR) were removed by ultracentrifugation. Under stirring and ice cooling solid ammonium sulfate was added to the supernatant until some of the salt remained undissolved. The suspension containing precipitated MCR was decanted from the solid ammonium sulfate and centrifuged.

The supernatant was decanted and disposed. The remainig crude MCR was dissolved in 100 ml Tris-HCl buffer (50 mM, pH 7.6, containing 10 mM coenzyme M) and applied to a Q-sepharose column (3.6 $cm^2$ x 15 cm) at room temperature with a syringe.

MCR isoenzyme I was eluted using an increasing concentration of sodium chloride in Tris-HCl buffer (50 mM, pH 7.6, containing 10 mM coenzyme M). The flow rate was 4 ml $min^{-1}$ and the concentration of sodium chloride was increased from 360 mM to 600 mM; MCR eluted at approx. 480 mM NaCl. The proteins were detected at 280 nm. MCR isoenzyme II eluted before isoenzyme I. In cases where complete separation of the two isoenzymes could not be achieved, mixed

fractions were rejected. The pooled fractions containing isoenzyme I (about 80 ml) were concentrated in a stirred Amicon concentration cell (100 kDa cut off) using 3 bar overpressure until the enzyme solution became viscous. About 1-1.5 ml of a dark moss-green enzyme solution was obtained.

### 6.1.4 Determination of enzyme activity

The fraction of active enzyme (Ni(I) form) was determined by UV/Vis spectroscopy. **Figure 6.1** (black line) shows the spectrum of fully active enzyme (> 95% Ni(I)).

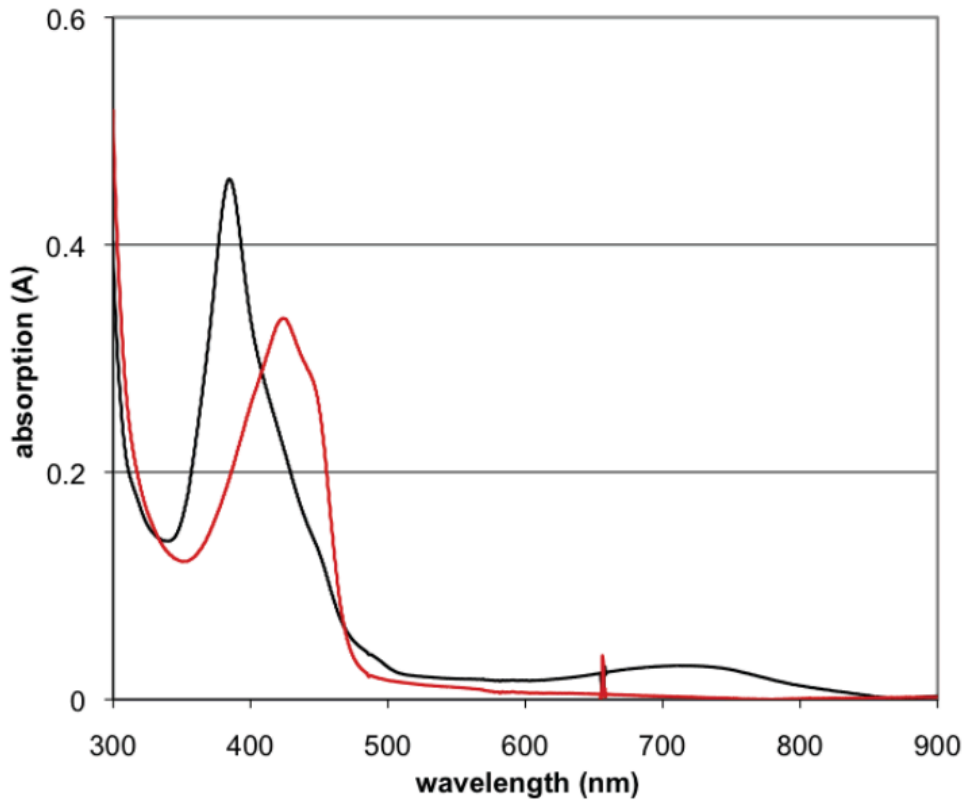


**Figure 6.1**: UV/Vis spectrum of fully active enzyme (black line) and inactive enzyme (red line, obtained after oxidation with air to the Ni(II) form), 1 cm cell, dilution 1:100.

The concentration of the enzyme (around 1 mM) was determined from the inactive Ni(II) form (**figure 6.1** red line), obtained by removing the rubber stopper of the cell for some seconds. A molar extinction coefficient at 420 nm of 44 000 l $mol^{-1}$ $cm^{-1}$ (22 000 l $mol^{-1}$ $cm^{-1}$ per active site) was used. Amounts of enzyme in mg units were calculated assuming a molar mass of 280 kDa of the protein. Enzyme concentrations were not corrected for the amount of inactive enzyme (0 – max. 10%) present in the samples.

Enzyme activity was measured by GC analysis of the methane that is formed. An assay involving the reductant Ti(III)-citrate (described in section 6.2.6) was used in order to avoid product inhibition. The enzyme solution was diluted and added to the assay solution on ice. After starting the reaction in a water bath shaker at 60 °C, 100 µl of the headspace gas was injected every 3 min into the GC (**figure 6.2**). The integral values were calibrated by injecting 5, 10 and 15 µl (2 times each) of pure methane into the GC prior to measurement (44 nmol methane per µl methane injected).

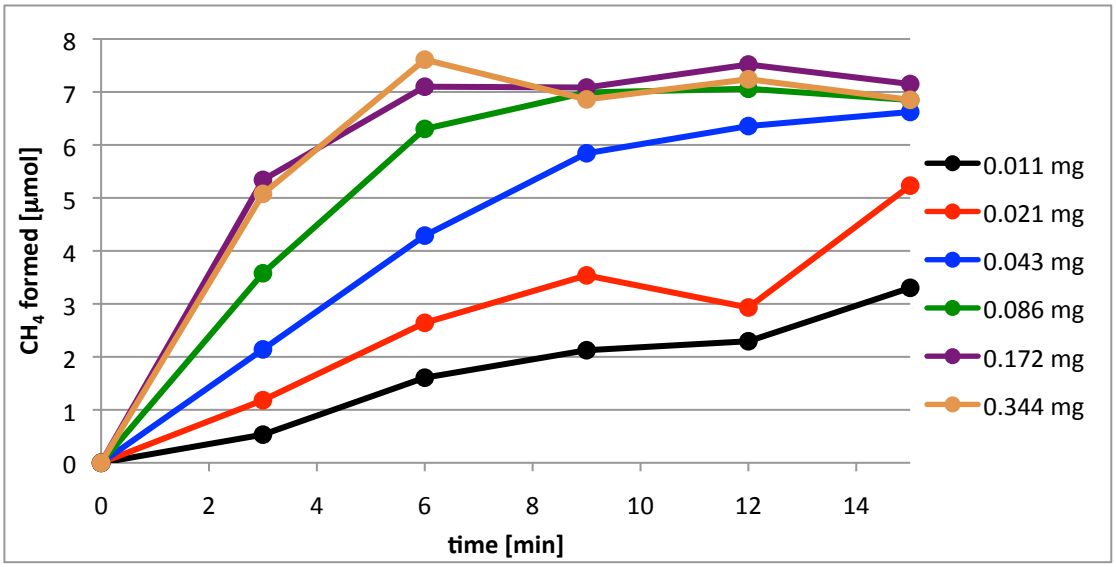


**Figure 6.2**: Methane formation from 800 µl assay solution containing 10 mM methyl-coenzyme M, 1 mM coenzyme B, 25 mM Ti(III)-citrate, 0.3 mM hydroxycobalamin and 10 µl enzyme solution (0.6136 mM = 171.8 mg $ml^{-1}$) diluted 1:4, 1:9, 1:19, 1:39, 1:79 and 1:159, respectively at 60 °C.

In assays containing high concentrations of enzyme the rate was limited by the regeneration of coenzyme B through reduction of the heterodisulfide by Ti(III)citrate/hydroxycobalamin as shown by experiments in which the concentration of Ti(III)-citrate was varied (data not shown).

The specific activity was calculated in μmol $min^{-1}$ $mg^{-1}$ for each data point (**table 6.1**).

**Table 6.1:** Specific enzyme activity displayed as μmol $min^{-1}$ $mg^{-1}$ obtained from the GC data (cf. Figure 6.2).

| Enzyme [mg] | time [min] | | | | |
|---|---|---|---|---|---|
| | 3 | 6 | 9 | 12 | 15 |
| 0.011 | 16.5 | 24.9 | 22.0 | 17.8 | 20.5 |
| 0.021 | 18.3 | 20.5 | 18.3 | 11.4 | 16.2 |
| 0.043 | 16.6 | 16.6 | 15.1 | 12.3 | 10.3 |
| 0.086 | 13.9 | 12.2 | 9.0 | 6.8 | 5.3 |
| 0.172 | 10.4 | 6.9 | 4.6 | 3.6 | 2.8 |
| 0.344 | 4.9 | 3.7 | 2.2 | 1.8 | 1.3 |

A maximum specific activity of about 20 μmol $min^{-1}$ $mg^{-1}$ protein (20 U $mg^{-1}$) can be deduced, which corresponds to a turnover frequency of about 100 $s^{-1}$.

## 6.2 Assay Conditions

### 6.2.1 Material and Methods

All experiments up to 2 bar methane pressure were performed in glass vials with a volume of 6.6 ml once sealed with a rubber stopper. The amount of assay solution was 1.6 ml (potassium phosphate buffer; 50 mM, pH 7.6) if not stated otherwise. Buffers in $H_2O$ and $D_2O$ were prepared outside the tent by weighting the required amount of $KH_2PO_4$ and $K_2HPO_4$ and the pH was checked by a pH meter. The buffers were boiled under a stream of nitrogen, evacuated during cool-down, introduced into the anaerobic tent and stirred without a rubber stopper under tent atmosphere (forming gas) overnight. This stirring procedure caused an ethanol contamination in the assay since some ethanol vapor was present in the anaerobic tent from unrelated experiments. Substrates were dissolved in the anaerobic buffers in $H_2O$ and $D_2O$ to give a concentration of 50 mM for coenzyme B and 100 mM for the derivatives of coenzyme M.

For one run of n experiments, (n + 1.5) times 1.6 ml of assay solution without enzyme was mixed on ice. 1.6 ml of this solution was removed and kept as a reference. The desired amount of enzyme was added, mixed, and 1.6 ml aliquots were transferred to the pre-cooled vials. After closing the vials with a rubber stopper, methane was applied to the headspace at a gas manifold connected to a vacuum pump all inside the anaerobic tent. The manifold was equipped with a rack allowing six samples to be treated with gas at the same time via a needle through the rubber stopper.

The samples were immediately incubated in a water bath shaker (New Brunswick; GYROTORY, Model G76) after preparation.

### 6.2.2 Assay for methane activation with heterodisulfide

Synthesized heterodisulfide (see end of section 6.7.2) was dissolved in cold buffer (Run 1: 5 mM, Run 2: 50 mM). The required amount of enzyme was added and the solution distributed to two vials. After sealing with a rubber stopper, the headspace of one sample was exchanged by methane. 5 ml of methane was additionally injected into the vial with a syringe in order to obtain an absolute pressure of about 2 bar. Both samples were incubated at 60 °C and stopped by denaturing the enzyme in boiling water for two minutes.

### 6.2.3 Assay for methane activation under equilibrium conditions

The equilibrium conditions of 2 mM methyl-coenzyme M and 2 mM heterodisulfide were obtained by reacting 4 mM methyl-coenzyme M with 2 mM coenzyme B in the presence of the enzyme. For all experiments intended for $^{13}CH_4$ activation, a premixed stock solution of methyl-coenzyme M depleted in $^{13}C$ in the *S*-methyl group and coenzyme B was used.

### 6.2.4 Assay for detection of isotope exchange in methyl-coenzyme M

For the detection of isotope exchange in methyl-coenzyme M 2 mM coenzyme B and 4 mM of the desired isotopologue of methyl-coenzyme M was used, identical to the assay for methane activation. This led to 50% conversion during which the isotope exchange of interest occurred.

### 6.2.5 Assay for detection of isotope exchange in ethyl-coenzyme M

2 mM coenzyme B and 10 mM of the desired isotopologue of ethyl-coenzyme M was used.

### 6.2.6 Assay for full conversion using Ti(III)-citrate as a reductant

The assays contained 10 mM coenzyme M derivative, 0.5 mM coenzyme B homodisulfide, 0.3 mM hydroxycobalamin and 25 mM Ti(III)-citrate mixed together in this order.
The advantage of this method is that only catalytic amounts of coenzyme B are needed and full conversion can be easily reached. In addition, methane formation is more linear because the product heterodisulfide is continuously cleaved to the second substrate coenzyme B and the weaker inhibitor coenzyme M. One disadvantage of these conditions is the presence of numerous additional signals in the $^{1}$H-NMR spectrum due to hydroxycobalamin and citrate.

Ti(III)-citrate was synthesized by adding sodium citrate (8.8 g dihydrate, 30 mmol) to a solution of titanium trichloride (20.4 g of a 15% solution, 20 mmol) in the anaerobic tent. The suspension was diluted with approx. 12 ml water and neutralized to pH = 7 by slowly adding sodium hydrogen carbonate (approx. 8.5 g, 100 mmol).
The concentration of Ti(III) was determined by twofold titration with methylene blue (equivalence point: turquoise color) and one time by titration with $KI_3$ as an independent method. Concentrations varying between 500 and 800 mM Ti(III) were obtained with this method. For assays in deuterated medium, 10 ml of the Ti(III)-citrate solution was frozen in an acetone/dry ice bath, lyophilized overnight, and re-dissolved in the same volume of $D_2O$.

### 6.2.7 Assay for high conversion without Ti(III)-citrate

For experiments to measure the $^{12}$C/$^{13}$C kinetic isotope effect, 6 mM coenzyme B and 2 mM of the desired $^{12}$C/$^{13}$C isotopologues of methyl or ethyl-coenzyme M were used. The advantage of these conditions is that the reaction slows down with increasing conversion, which allows generation of samples with a conversion between 80 and 95%. Besides the small amount of remaining substrate, the presence of excess

coenzyme B results in a mixture of both thiols (coenzyme B and coenzyme M) as well as the 3 disulfides through thiol-disulfide interchange.

### 6.2.8 Stopping the reaction

The reaction was stopped by deactivation of the enzyme. Immersion of the vials in boiling water for 2 min is a suitable way of denaturing the enzyme. The advantage of this method is that vials remain anaerobic and no other substances are added. In order to prevent the rubber stoppers from popping off during incubation or denaturation of the enzyme, the stopper was secured to the vial by a specific clip designed by R. Boecher in Marburg. Stopping the reaction by removing the rubber stopper or injection of 1 ml air (if the headspace gas had to be analyzed) proved to be the most convenient method, as the enzyme is immediately oxidized to the inactive Ni(II) form. More accurate and shorter incubation times are the main advantage of the rapid quench. In addition, this procedure was used for experiments at lower temperatures since thermal denaturation of the enzyme in boiling water would lead to an artificial activation as the sample was heated to 100 °C.

In some experiments, the assays were stopped by the injection of 20 to 50 µl of $DClO_4$ (68% in $D_2O$) or $HClO_4$ (70%), which had the advantage that the protein precipitates and can be removed by centrifugation. In combination with Ti(III)-citrate, however, it was found that some of the substrate is oxidized to the corresponding sulfoxide.

If Ti(III)-citrate and perchloric acid were added anaerobically to a pure solution of methyl-coenzyme M, formation of methyl-coenzyme M sulfoxide could be detected. Adding only perchloric acid or only Ti(III)-citrate to methyl-coenzyme M did not show formation of the sulfoxide. The identity of the sulfoxide was verified by selective synthesis of methyl- and ethyl-coenzyme M sulfoxides as well as the corresponding sulfones (see 6.7.4).

## 6.3 Experimental Procedures and Raw Data for Chapter 2

### 6.3.1 Full range spectra demonstrating methane activation

**Figure 6.3** shows the full range spectrum before addition of enzyme (4 mM $^{12}CH_3$-S-CoM and 2 mM coenzyme B).

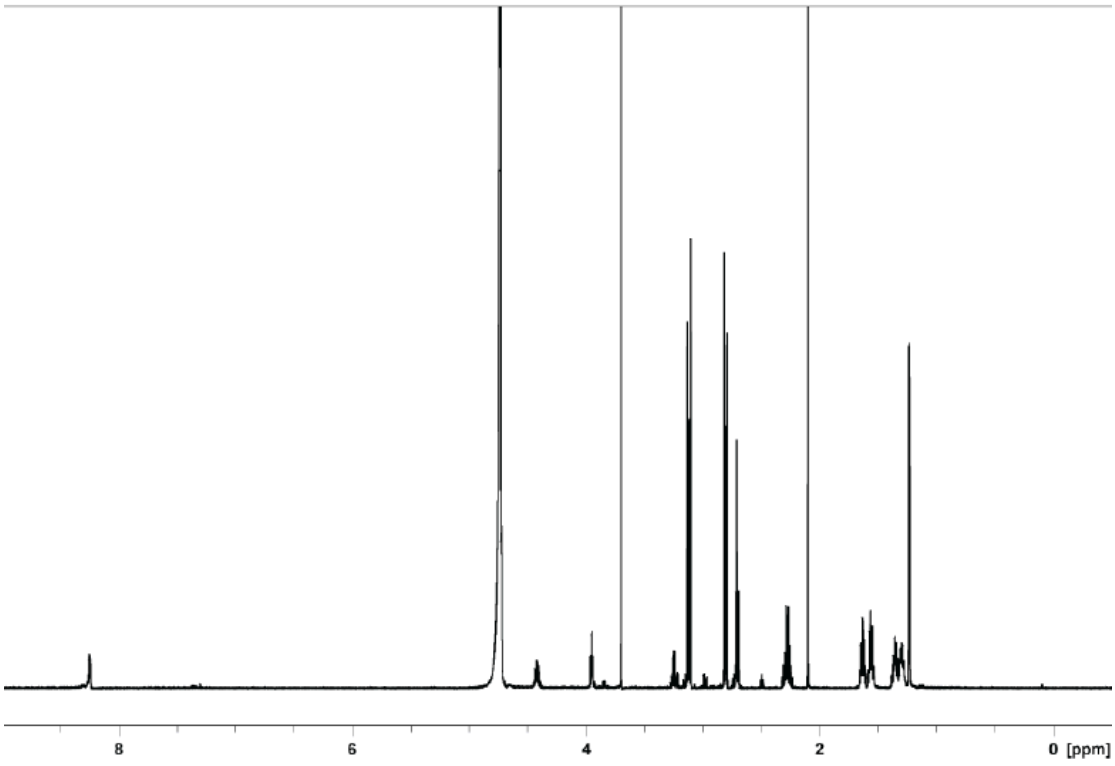


**Figure 6.3**: $^{1}$H-NMR spectrum of the assay solution before addition of enzyme, solvent suppression by presaturation.

After incubation with 4.06 mg enzyme for 30 min at 60 °C an equilibrium containing 2 mM coenzyme M and 2 mM heterodisulfide was reached (**figure 6.4**). The amount of $^{13}CH_4$ activated was calculated from the $^{13}$C content of the methyl group by integration of the central peak and the two $^{13}$C satellites (**figure 6.5**).

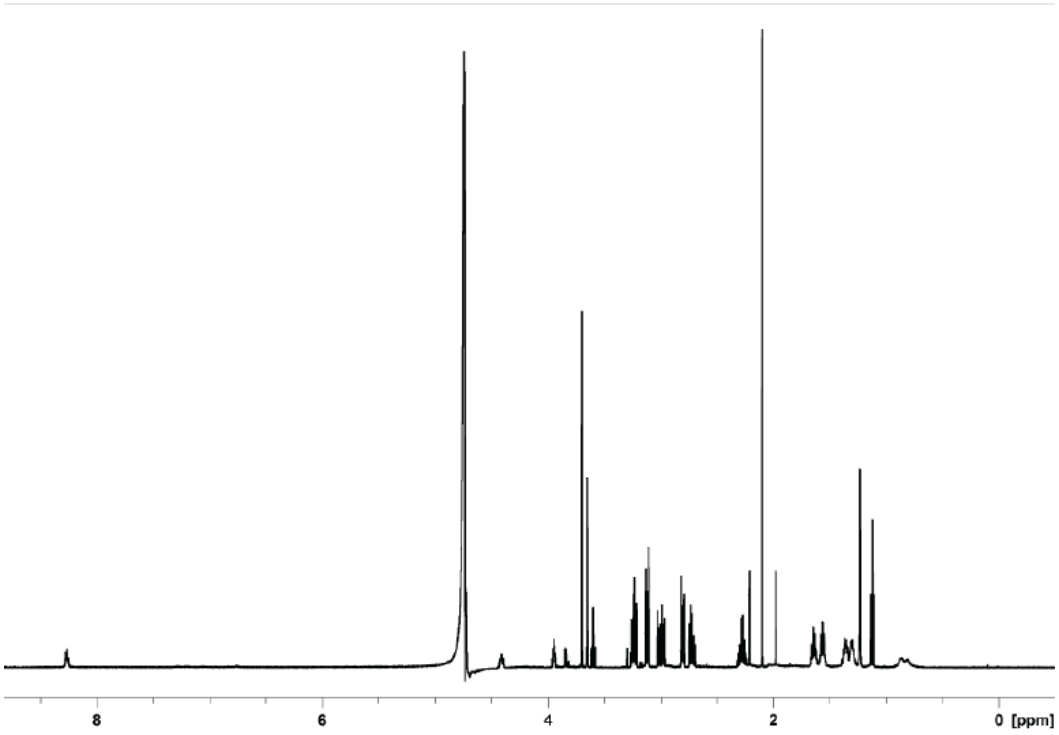


**Figure 6.4**: $^{1}$H-NMR spectrum of the assay solution after addition of enzyme, solvent suppression by presaturation.

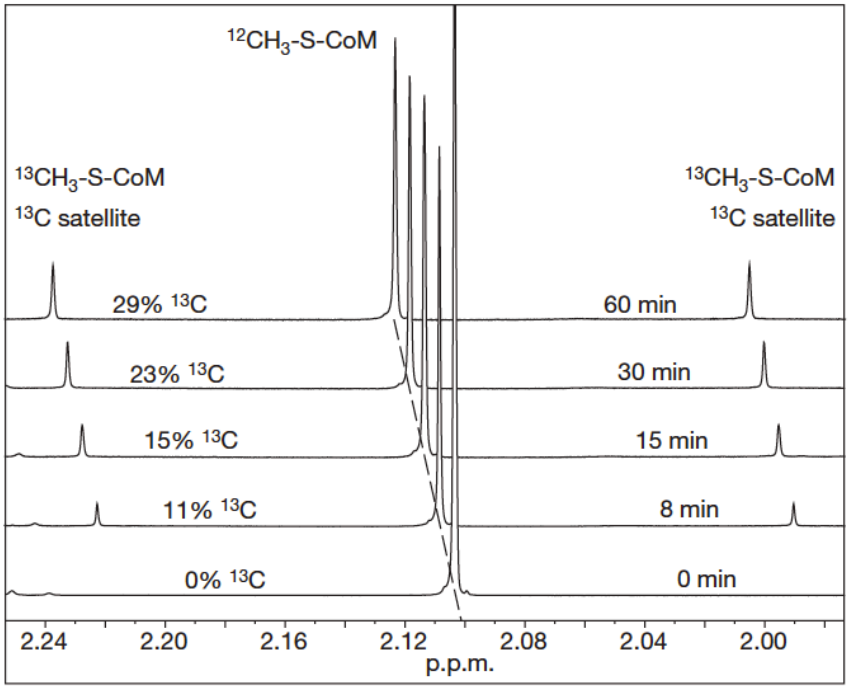


**Figure 6.5**: Expansion of the $^{1}$H-NMR spectrum showing the *S*-methyl group of methyl-coenzyme M with solvent suppression by presaturation. The molar fraction of $^{13}$C present was deduced from the ratio of the integrals (central peak / sum of both $^{13}$C satellites).

### 6.3.2 Methane activation at different temperatures

Experiments at lower temperature were stopped by addition of air into the vial in order to deactivate the enzyme.
Experiments at 40 °C were performed analogous to the standard experiments. Experiments at 22 °C were removed from the ice bath and agitated on the bench (22 °C) for the incubation times desired. Experiments at 4 °C were placed in a shaker in the 4 °C room for the desired time.

### 6.3.3 Methane activation at different pressures up to 2 bar

Partial pressures of 0.05, 0.1 and 0.2 bar were obtained by injecting 0.25, 0.5 and 1.0 ml, respectively, of $^{13}CH_4$ into the headspace with a syringe. For experiments at 0.5 bar, 5 ml $^{13}CH_4$ was injected into the headspace and the overpressure was released through a syringe needle. Samples at 1 bar $^{13}CH_4$ were prepared with the gas manifold. For experiments at 2 bar, the headspace was exchanged as for the 1 bar samples but 5 ml $^{13}CH_4$ was injected additionally.

### 6.3.4 Experiments under high pressures of $^{13}CH_4$

Experiments at pressures above 2 bar were performed in a modified French press cell (designed by R. Boecher, MPI Marburg, see **figure 6.6**). The preheated cell was charged with the assay solution and filled with 1 bar $^{13}CH_4$, height of headspace before compression: 66 mm. After taking the cell out of the anaerobic tent, the plunger was pushed down by rotating the threaded rod until the desired pressure was obtained. The cell was incubated in the oven at 60 °C for the 30 min and the reaction stopped by collecting the assay solution via the outlet.

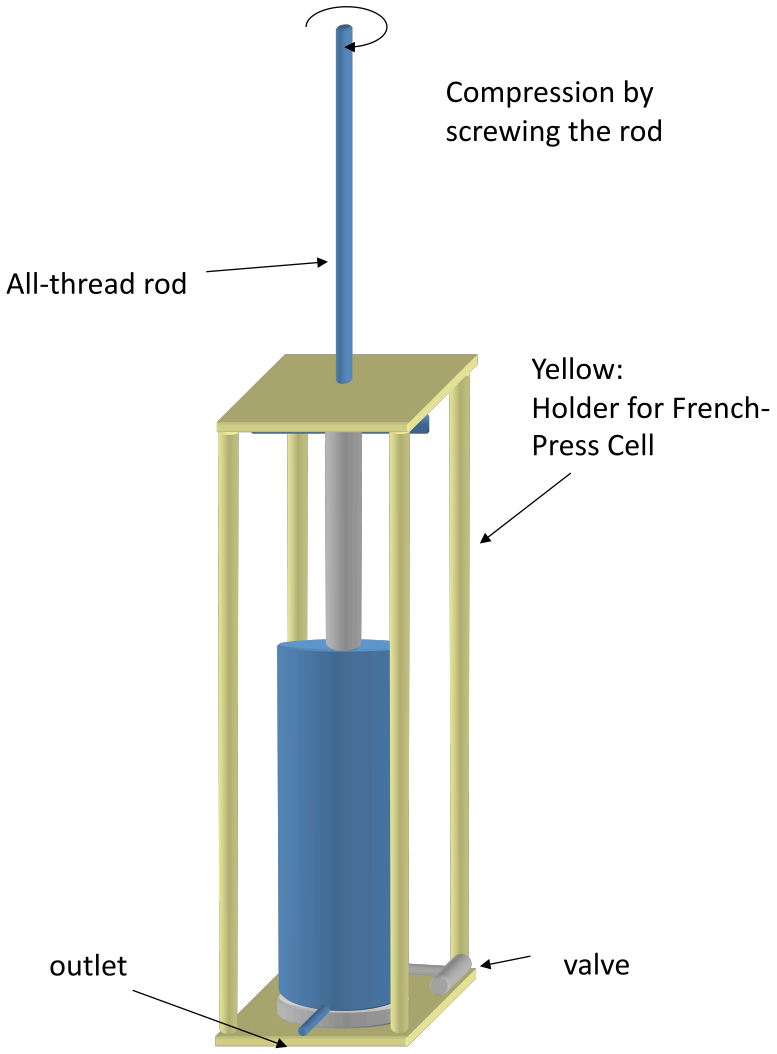


**Figure 6.6**: Modified French press cell to generate high pressures of $^{13}CH_4$.

### 6.3.5 Experiments varying the concentration of the heterodisulfide

The amount of activated methane was calculated from the amount of $^{12}CH_3$-S-CoM formed. Since the substrate ($^{13}CH_3$-S-CoM) only contained 99% $^{13}C$ in the methyl group, the amount of $^{12}CH_3$-S-CoM due to incomplete labeling was calculated and subtracted for the calculation of the amount of $^{12}CH_3$-S-CoM formed (**table 6.2**). The amount of methyl-coenzyme M was assumed to be 2.0 mM times 1.6 ml = 3.2 µmol. The amount of enzyme was calculated from the integral value of Tris-HCl buffer normalized to give an average amount of enzyme of 2.04 mg, which was the intended amount.

**Table 6.2**: Calculation of $^{12}CH_4$ activated taking the incomplete $^{13}C$ enrichement into account.

| HDS [mM] | Integral both $^{13}C$ sat. | Integral $^{12}CH_3$ | Integral $^{12}C$ from substrate | Integral $^{12}CH_3$ corr. | $^{12}CH_4$ act. [molar fraction] | $^{12}CH_4$ act. [μmol] |
|---|---|---|---|---|---|---|
| 0.2 bar methane, Run 1 | | | | | | |
| 0.2 | 169.6 | 4.28 | 1.6963 | 2.582 | 0.015 | 0.048 |
| 0.5 | 194.2 | 6.02 | 1.9423 | 4.078 | 0.020 | 0.065 |
| 1 | 198.8 | 4.20 | 1.9875 | 2.209 | 0.011 | 0.035 |
| 2 | 203.3 | 9.54 | 2.0335 | 7.506 | 0.035 | 0.113 |
| 4 | 181.7 | 9.38 | 1.8165 | 7.564 | 0.040 | 0.127 |
| 8 | 172.3 | 7.62 | 1.7234 | 5.895 | 0.033 | 0.105 |
| 0.2 bar methane, Run 2 | | | | | | |
| 0.2 | 163.2 | 4.15 | 1.6323 | 2.521 | 0.015 | 0.048 |
| 0.5 | 199.5 | 7.52 | 1.9949 | 5.528 | 0.027 | 0.085 |
| 1 | 155.0 | 6.92 | 1.5501 | 5.374 | 0.033 | 0.106 |
| 2 | 159.7 | 10.28 | 1.5971 | 8.686 | 0.051 | 0.164 |
| 4 | 181.1 | 9.51 | 1.8107 | 7.699 | 0.040 | 0.129 |
| 8 | 174.7 | 7.54 | 1.7473 | 5.795 | 0.032 | 0.102 |
| 1 bar methane, Run 1 | | | | | | |
| 0.2 | 155.6 | 17.29 | 1.5559 | 15.738 | 0.091 | 0.291 |
| 0.5 | 156.6 | 34.50 | 1.5661 | 32.937 | 0.172 | 0.551 |
| 1 | 198.1 | 31.61 | 1.9813 | 29.631 | 0.129 | 0.413 |
| 2 | 218.6 | 38.82 | 2.1864 | 36.638 | 0.142 | 0.455 |
| 4 | 149.0 | 43.28 | 1.4896 | 41.789 | 0.217 | 0.696 |
| 8 | 144.6 | 33.02 | 1.4462 | 31.570 | 0.178 | 0.569 |
| 1 bar methane, Run 2 | | | | | | |
| 0.2 | 159.5 | 17.56 | 1.5948 | 15.962 | 0.090 | 0.289 |
| 0.5 | 167.6 | 29.70 | 1.6761 | 28.022 | 0.142 | 0.454 |
| 1 | 156.9 | 34.23 | 1.5687 | 32.660 | 0.171 | 0.547 |
| 2 | 154.0 | 38.33 | 1.5401 | 36.794 | 0.191 | 0.612 |
| 4 | 149.8 | 39.57 | 1.4984 | 38.070 | 0.201 | 0.643 |
| 8 | 152.5 | 26.99 | 1.5246 | 25.466 | 0.142 | 0.454 |

All assays from one run were mixed on ice and incubated together. In the "Run 1" series (for 0.2 and 1 bar methane) the assays were mixed in the order of increasing heterodisulfide concentration; in the "Run 2" series the assays were premixed in the opposite order. Afterwards, all assays were treated together with methane and incubated in the same order as mixing with a delay of 30 seconds between two samples.
The samples with 1 mM and 2 mM heterodisulfide in "Run 1" at both methane pressures showed a lower methane activation rate (cf. figure 2.10). The reason for this effect (if they are not statistical outliers) could be connected to the different delays between premixing and methane treatment. Such an effect was also considered as a possible reason for the difference between the high pressure and low pressure experiments as discussed in section 2.4.2.

### 6.3.6 UV/Vis spectrum under equilibrium conditions

2.5 ml of an assay solution containing 4 mM $^{13}CH_3$-S-CoM and 2 mM CoB-SH was mixed in a 1 cm UV/Vis cell on ice. 62 µl enzyme solution (0.75 mM, 46.5 nmol, 13.0 mg) was added and the headspace of the cell was replaced by methane at the gas manifold. The cell was immediately placed into the cell bracket connected to a temperature control bath at 30 °C. UV/Vis spectra were recorded immediately after placement into the cell (assay still cold) followed by a measurement every minute (**figure 6.7**).

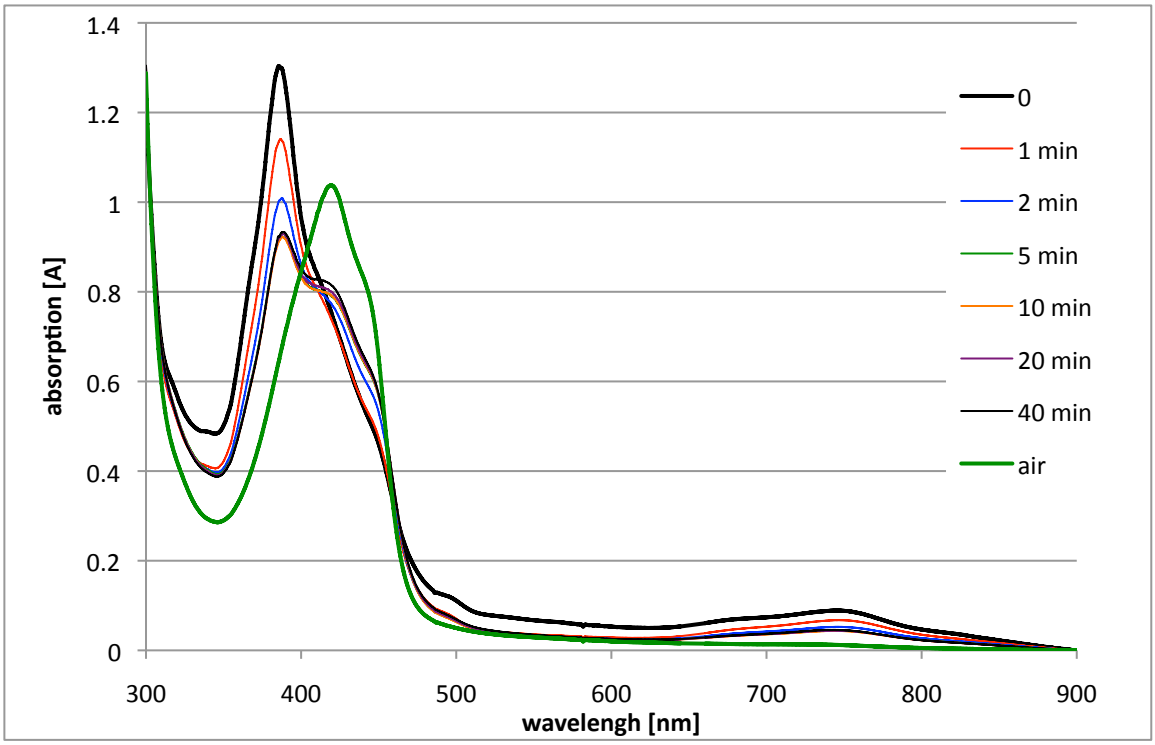


**Figure 6.7 A**: UV spectra under equilibrium conditions where methane activation occurs (offset adjusted to A = 0 for 900 nm).

After 50 min the cell was opened in order to oxidize the enzyme to the Ni(II) form (bold green curve).
From the difference spectrum (**figure 6.7 B**) it can be deduced that the equilibrium state contains 50% of the Ni(I) form.

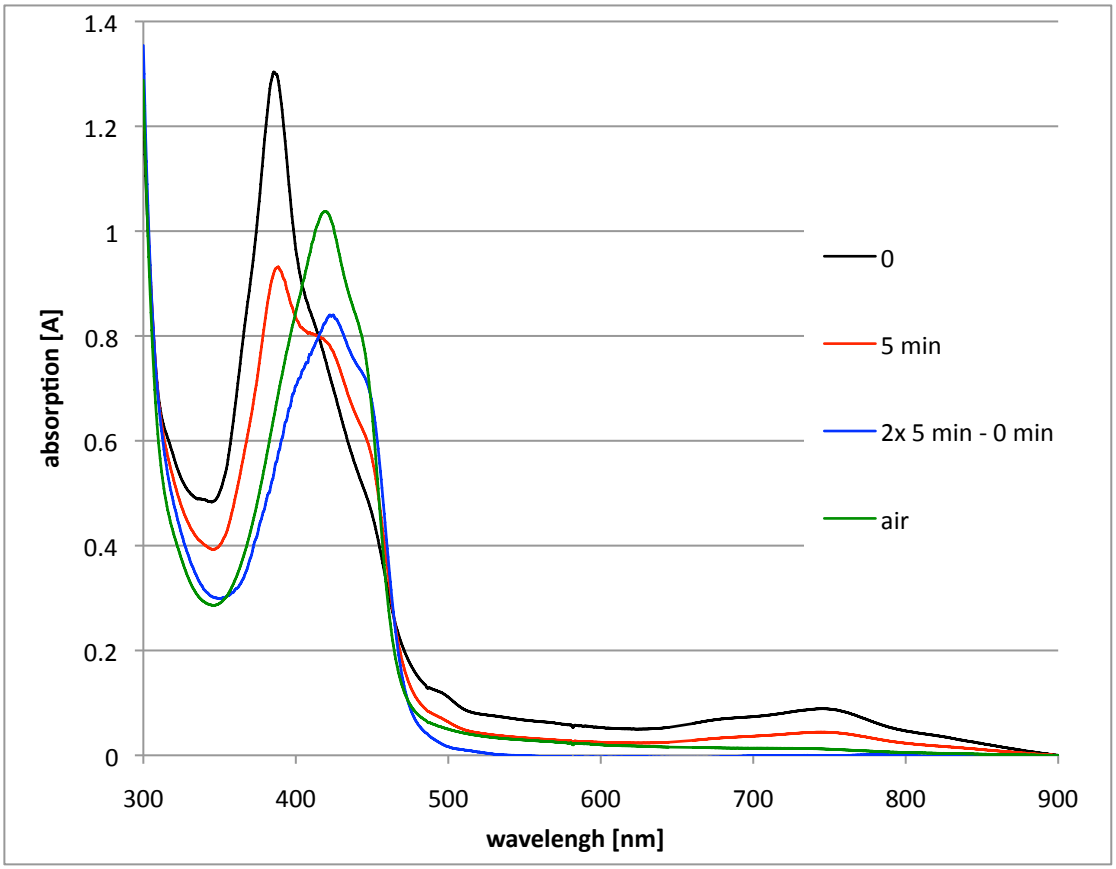


**Figure 6.7 B**: UV spectra from figure 6.7 A after 0 and 5 min including a difference spectrum (2 • 5min – 0min, blue line).

## 6.4 Experimental Procedures and Raw Data for Chapter 3

### 6.4.1 Preparation of a mixture of $CH_4$, $CH_3D$, $CH_2D_2$, $CHD_3$ and $CD_4$

$Al_4C_3$ was dissolved under vacuum in a solution of HCl in $D_2O$ (ca. 80-90% deuterium) giving about atmospheric pressure of the generated methane. 2 ml of this gas mixture was bubbled through $CDCl_3$ in an NMR tube.

### 6.4.2 Conversion and deuterium incorporation after the equilibrium of substrates and products is reached

**Table 6.3**: Set of experiments designed to verify that no significant deuterium incorporation into the substrate occurs after reaching the equilibrium. Assay: 4 mM methyl-coenzyme M, 2 mM coenzyme B catalyzed by 0.75 nmol (0.21 mg) enzyme at 60 °C.

| time [min] | Me-S-CoM [molar fraction] | Me-S-CoM [μmol] | $CH_2D$-S-CoM [%] | $CH_2D$-S-CoM [nmol] |
|---|---|---|---|---|
| 0 | 1 | 6.4 | 0 | 0 |
| 2 | 0.553 | 3.542 | 3.661 | 129.7 |
| 4 | 0.550 | 3.518 | 3.587 | 126.2 |
| 8 | 0.545 | 3.487 | 3.641 | 127.0 |
| 16 | 0.542 | 3.470 | 3.920 | 136.0 |
| 32 | 0.538 | 3.442 | 4.042 | 139.1 |

### 6.4.3 Temperature dependence of substrate deuteration and methane formation

**Table 6.4**: Inverse of the temperature and logarithm of the ratio of product and $CH_2D$-S-CoM formed.

| T [K] | 1000/T [1000 $K^{-1}$] | $k_b/k_f$ [μmol/μmol] | $\ln(k_b/k_f)$ |
|---|---|---|---|
| 277 | 3.61011 | 0.1072 | -2.2327 |
| 295 | 3.38983 | 0.0602 | -2.8095 |
| 313 | 3.19489 | 0.0453 | -3.0947 |
| 333 | 3.00300 | 0.0403 | -3.2113 |

### 6.4.4 Additional expansion of NMR spectra demonstrating deuterium incorporation into ethyl-coenzyme M and numerical data of species

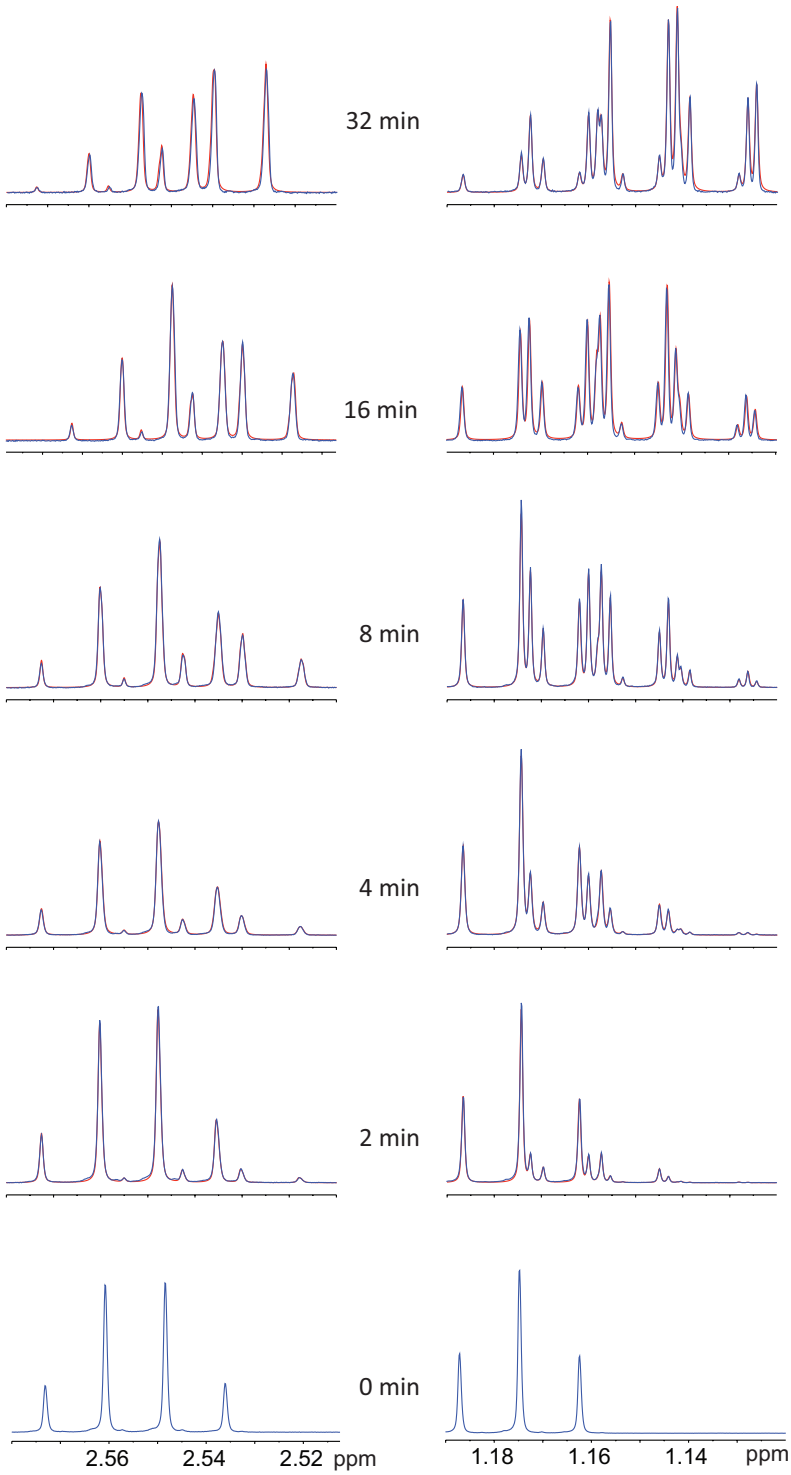


**Figure 6.8**: 600 MHz $^{1}H\{^{2}H\}$-NMR spectra of the $CH_2$ (left) and the $CH_3$ (right) group of ethyl-coenzyme M. Blue: measured, red: fitted with iNMR.

**Table 6.5**: Molar fraction of different isotopologues determined from fitting of $^{1}H\{^{2}H\}$-NMR spectra.

| time [min] | $CH_3CH_2SR$ | $CH_3CHDSR$ | $CH_3CD_2SR$ | $CH_2DCH_2SR$ | $CH_2DCHDSR$ | $CH_2DCD_2SR$ |
|---|---|---|---|---|---|---|
| 0 | 100.0 | 0.0 | 0.0 | 0.0 | 0.0 | 0.0 |
| 2 | 62.0 | 9.0 | 0.2 | 15.2 | 3.2 | 0.1 |
| 4 | 42.2 | 13.2 | 0.3 | 21.9 | 8.3 | 0.7 |
| 8 | 22.9 | 14.7 | 1.9 | 21.8 | 16.5 | 2.6 |
| 16 | 9.5 | 10.3 | 3.0 | 14.9 | 20.4 | 5.5 |
| 32 | 2.4 | 5.2 | 2.3 | 6.5 | 17.3 | 9.0 |

| time [min] | $CHD_2CH_2SR$ | $CHD_2CHDSR$ | $CHD_2CD_2SR$ | $CD_3CH_2SR$ | $CD_3CHDSR$ | $CD_3CD_2SR$ | tot pop |
|---|---|---|---|---|---|---|---|
| 0 | 0.0 | 0.0 | 0.0 | 0.0 | 0.0 | 0.0 | 100.0 |
| 2 | 1.3 | 0.4 | 0.0 | 0.0 | 0.0 | 8.6 | 91.4 |
| 4 | 3.5 | 1.7 | 0.3 | 0.6 | 0.4 | 6.9 | 93.1 |
| 8 | 5.9 | 6.3 | 1.0 | 0.7 | 0.7 | 5.1 | 94.9 |
| 16 | 7.7 | 11.5 | 3.9 | 2.1 | 3.2 | 7.9 | 92.1 |
| 32 | 6.3 | 18.3 | 10.8 | 2.4 | 4.9 | 14.5 | 85.5 |

### 6.4.5 $^{1}$H-NMR spectra of deuterium incorporation into $^{13}$C-labeled ethyl-coenzyme M and numerical data of species

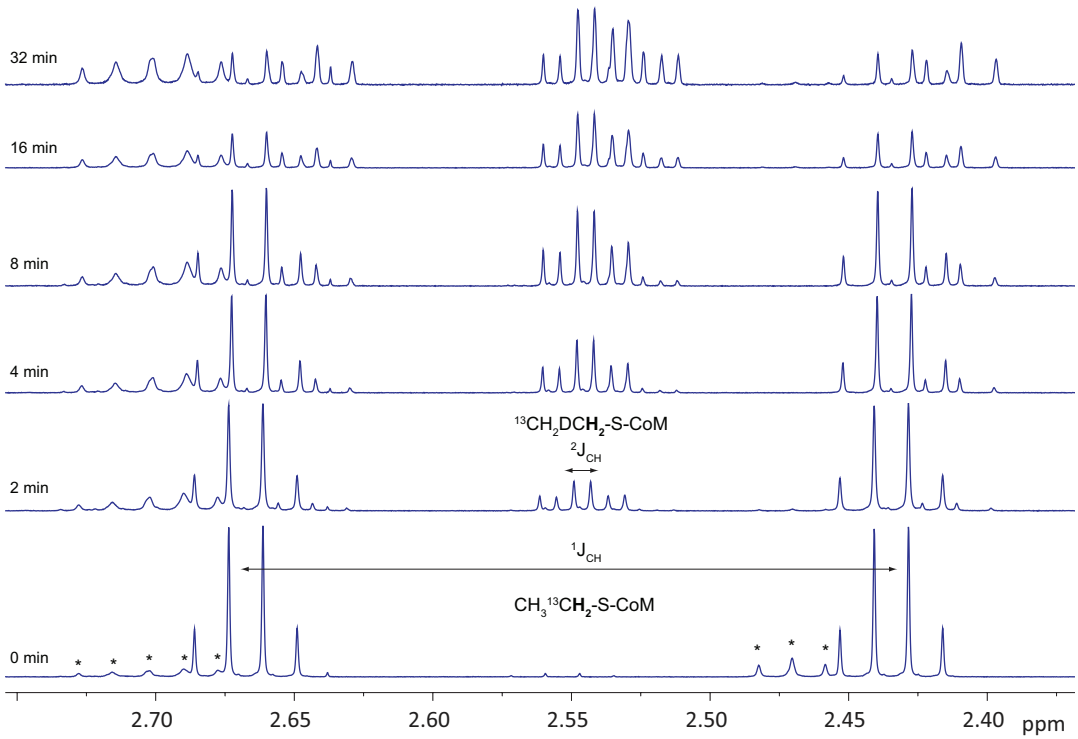


**Figure 6.9**: Expansion of the $CH_3\boldsymbol{CH_2}$-S-region of the $^{1}H\{^{2}H\}$-NMR spectra (600 MHz) with increasing incubation times. The signals labeled by * are not due to Et-S-CoM.

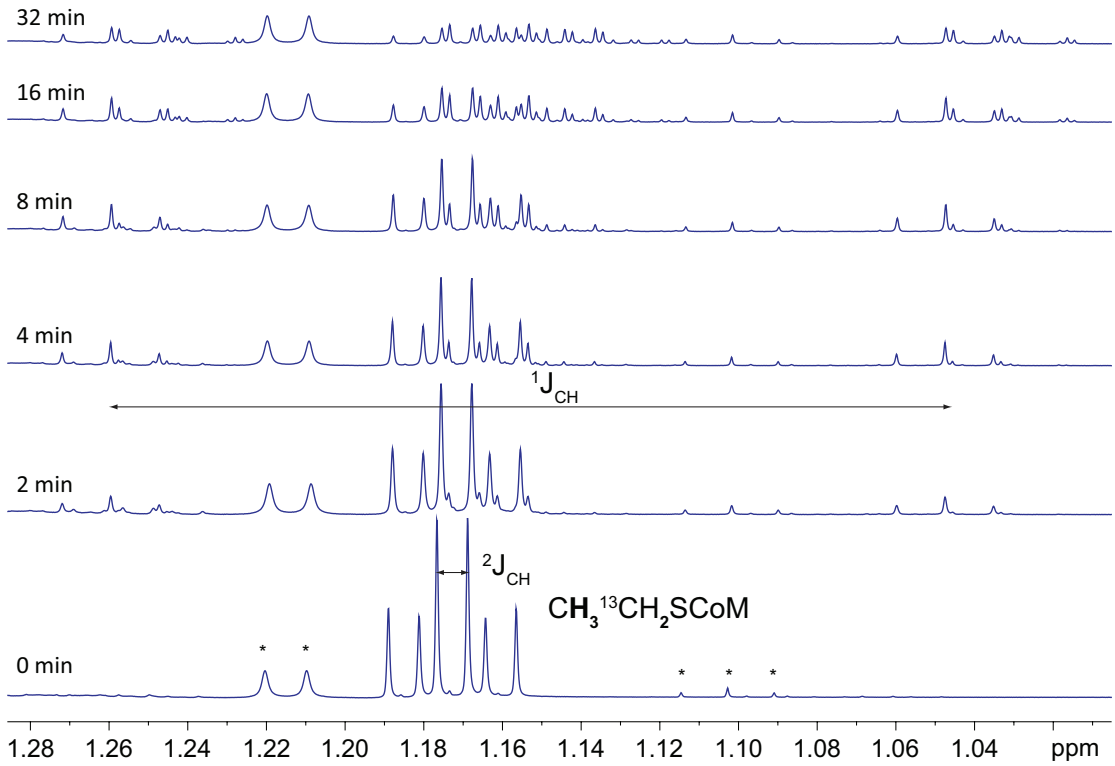


**Figure 6.10**: Expansion of the ***CH₃***$CH_2$-S-region of the $^1H\{^2H\}$-NMR spectra (600 MHz) with increasing incubation times. The signals labeled by * are not due to Et-S-CoM.

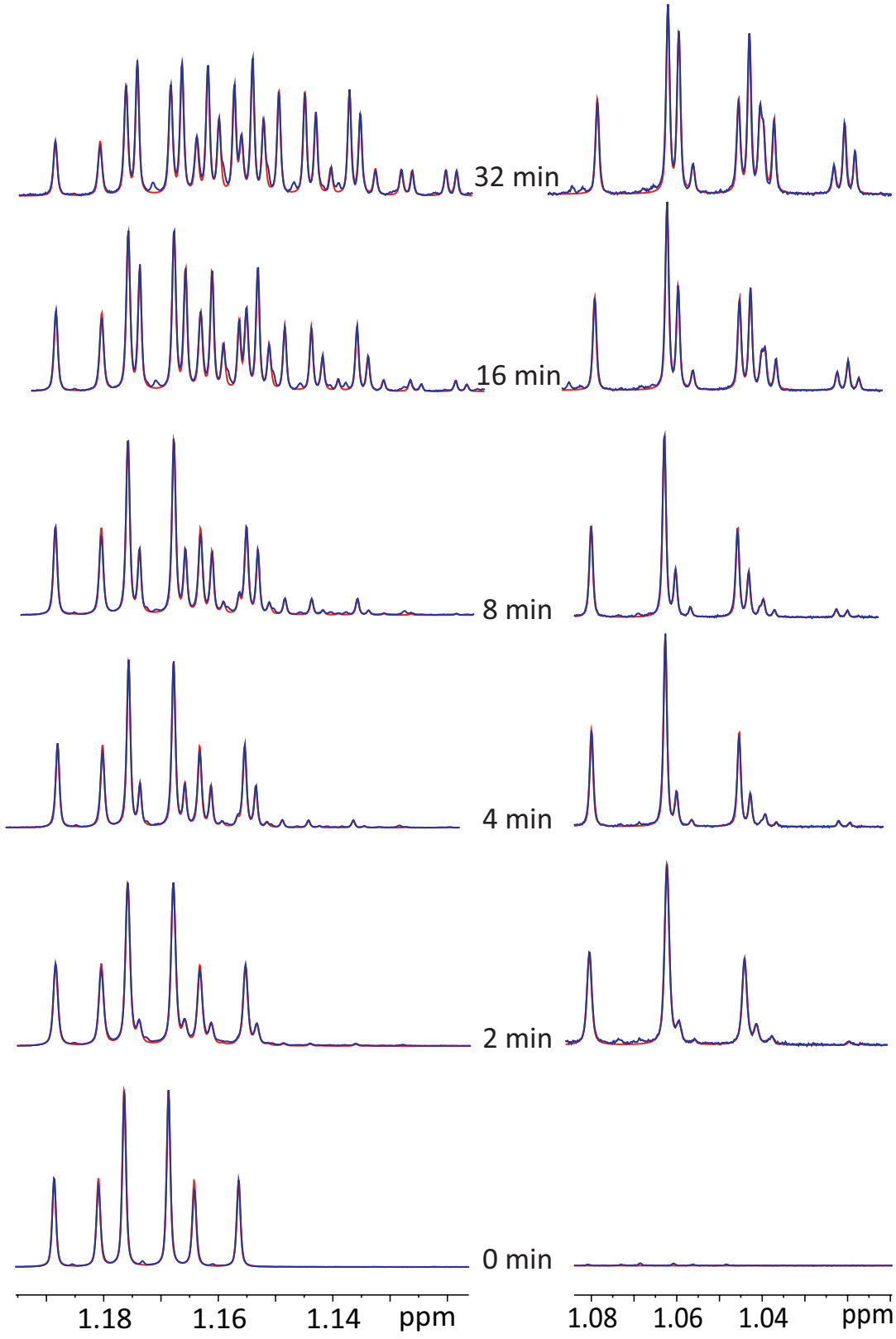


**Figure 6.11**: 600 MHz $^{1}H\{^{2}H\}$-NMR spectra and fitting of the $\mathbf{C}\boldsymbol{H_3}CH_2$-S group of ethyl-coenzyme M containing one $^{13}C$ label. Blue: measured, red: fitted with iNMR.

**Table 6.6**: Molar fraction of different isotopologues of mono-$^{13}$C-Et-CoM determined from fitting of $^{1}H\{^{2}H\}$-NMR spectra.

| time min | $CH_3$*$CH_2$ | $CH_3$*CHD | $CH_3$*$CD_2$ | $CH_2D$*CHD | $CH_2D$*$CD_2$ | $CHD_2$*CHD | $CHD_2$*$CD_2$ |
|---|---|---|---|---|---|---|---|
| 0 | 100.0 | 0.0 | 0.0 | 0.0 | 0.0 | 0.0 | 0.0 |
| 2 | 66.2 | 8.2 | 0.2 | 1.1 | 0.1 | 0.0 | 0.0 |
| 4 | 50.4 | 11.2 | 0.7 | 3.0 | 0.3 | 0.4 | 0.0 |
| 8 | 39.3 | 12.5 | 1.2 | 4.8 | 0.7 | 0.8 | 0.0 |
| 16 | 17.5 | 12.0 | 2.3 | 9.4 | 2.5 | 3.2 | 1.0 |
| 32 | 8.1 | 9.3 | 2.6 | 11.1 | 4.3 | 5.5 | 2.7 |

| time min | *$CH_2DCH_2$ | *$CH_2DCHD$ | *$CH_2DCD_2$ | *$CHD_2CH_2$ | *$CHD_2CHD$ | *$CHD_2CD_2$ | others |
|---|---|---|---|---|---|---|---|
| 0 | 0.0 | 0.0 | 0.0 | 0.0 | 0.0 | 0.0 | 0.0 |
| 2 | 12.9 | 1.3 | 0.1 | 0.8 | 0.1 | 0.0 | 2.9 |
| 4 | 18.1 | 3.0 | 0.2 | 2.1 | 0.8 | 0.0 | 3.9 |
| 8 | 20.0 | 4.7 | 0.4 | 3.4 | 1.5 | 0.1 | 6.0 |
| 16 | 16.7 | 8.9 | 1.4 | 6.5 | 5.2 | 1.0 | 8.8 |
| 32 | 11.4 | 10.1 | 2.3 | 6.7 | 9.0 | 2.2 | 11.3 |

### 6.4.6 ee Determination with $CD_3CHD$-S-CoM

The chiral auxiliary dihydroquinine sulfate was prepared from the free base dihydroquinine (Fluka). 1.0 mmol Dihydroquinine was dissolved in ethanol (10 ml). $H_2SO_4$ (0.50 ml of a 1.0 mM solution diluted in 5 ml ethanol) was added and the solution was evaporated to dryness under high vacuum.

After measurement of the assay solution of interest (containing 16 μmol ethyl-coenzyme M, about 5% of which was $CD_3CHD$-S-CoM), 5.0 μl $H_2O_2$ (30%, 44 μmol) was added to the NMR tube. The sample was shaken and heated in boiling water for 5 min in order to reach >95% conversion to the sulfoxide without formation of the corresponding sulfone ($^{1}$H-NMR measurement).

The sample solution was mixed with a solution of dihydroquinine sulfate (20 mg, 53 μmol, in 0.50 ml acetonitrile and 1.00 ml water) and lyophilized. The residue was suspended in the ultrasonic bath in a mixture of acetonitrile-$d_3$/$D_2O$ (1000 μl/20 μl) and heated briefly to about 45 °C. The solution was filtered, a small amount of TMS added

and analyzed by $^{1}$H-NMR spectroscopy. $D_2O$ was added stepwise and the sample measured again until the signals due to different enantiomers converged (cf. section 3.3.5, table 3.6).

### 6.4.7 Activation of ethane

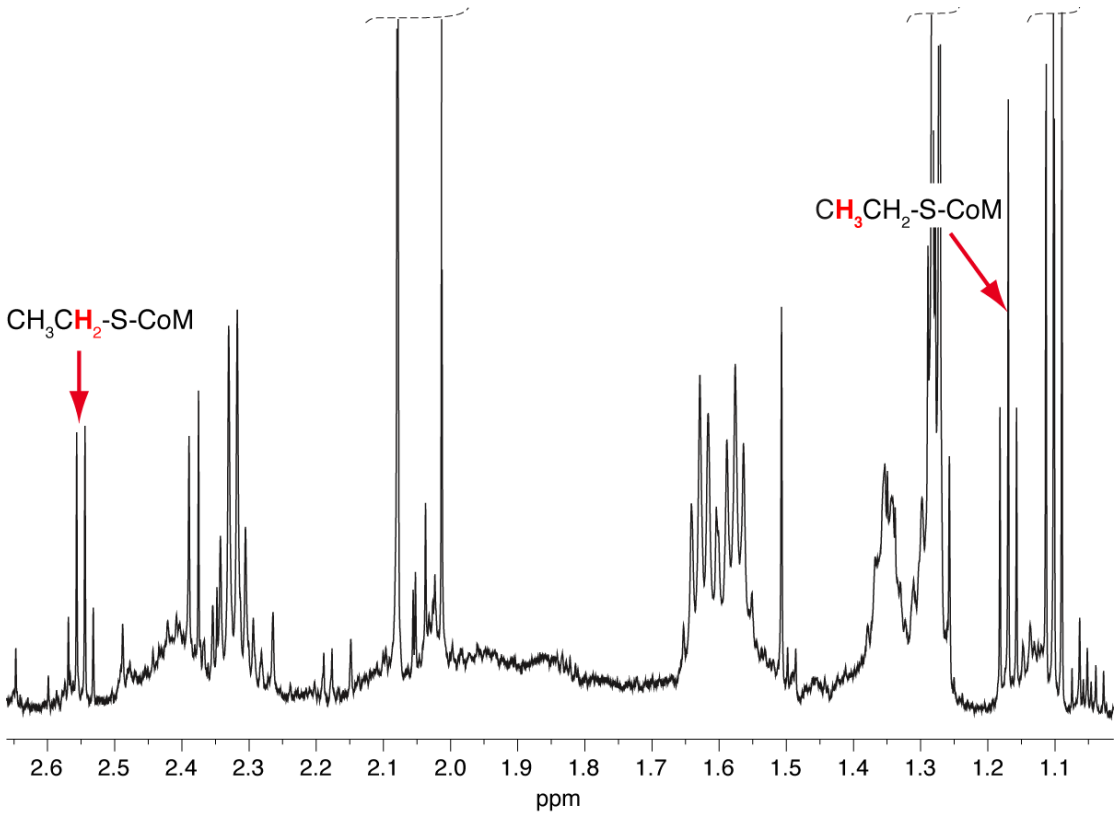


**Figure 6.12**: Formation of ethyl-coenzyme from ethane (1 bar) catalyzed by 40.6 mg enzyme. 600 MHz $^{1}$H-NMR spectrum after precipitation of the enzyme with $HClO_4$ and centrifugation.

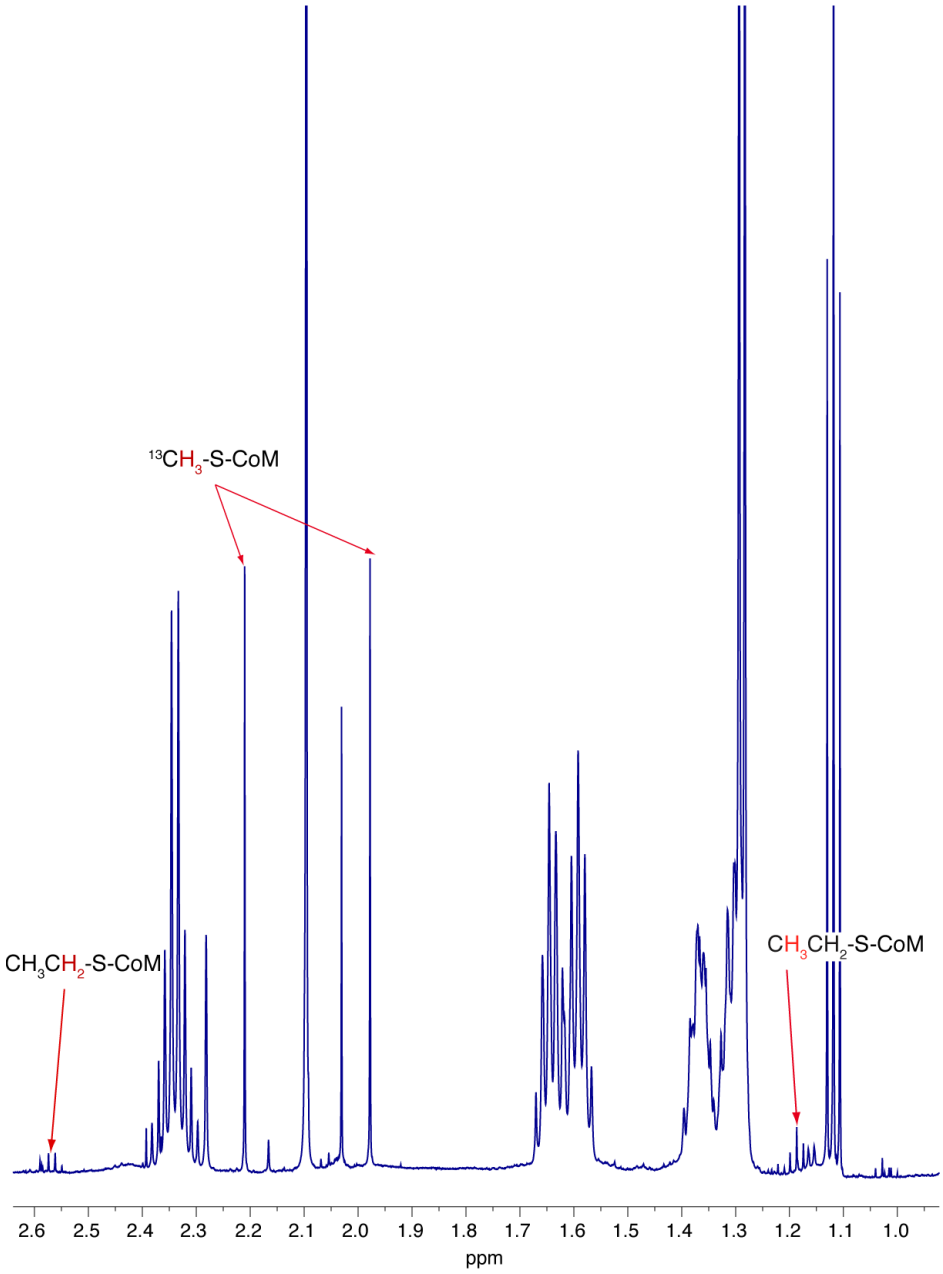


**Figure 6.13**: Formation of ethyl-S-CoM and $^{13}CH_3$-S-CoM from a mixture of ethane (0.5 bar) and $^{13}CH_4$ (0.5 bar) catalyzed by 4.06 mg enzyme. 600 MHz $^1$H-NMR spectrum after precipitation of the enzyme with $HClO_4$ and centrifugation.

### 6.4.8 UV-Vis spectra of incubation with ethyl-coenzyme M

10 mM Ethyl-coenzyme M and 2 mM coenzyme B were incubated in a 2.5 ml assay with 62 µl enzyme solution (0.75 mM, 46.5 nmol, 13.0 mg) at 30 °C in a UV-Vis cell. UV-Vis spectra were recorded immediately after the addition of the enzyme ("0 min"), followed by a measurement every min. Selected spectra are shown in **figure 6.14 A**. A difference spectrum is presented in **figure 6.14 B** (red) showing that during incubation only 5% of the red1 state is lost (according to UV-Vis).

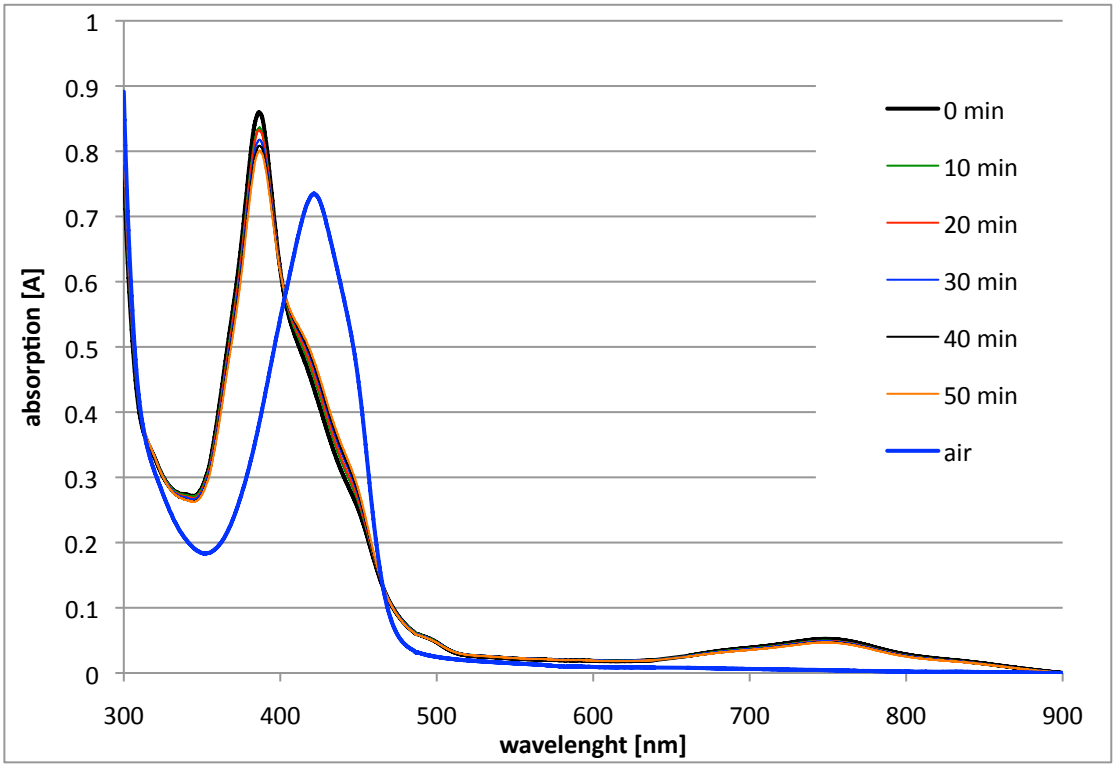


**Figure 6.14 A**: UV-Vis spectrum of and assay solution 10 mM ethyl-coenzyme M, 2 mM coenzyme B and 13 mg MCR. Calibrated to absorption = 0 at 900 nm.

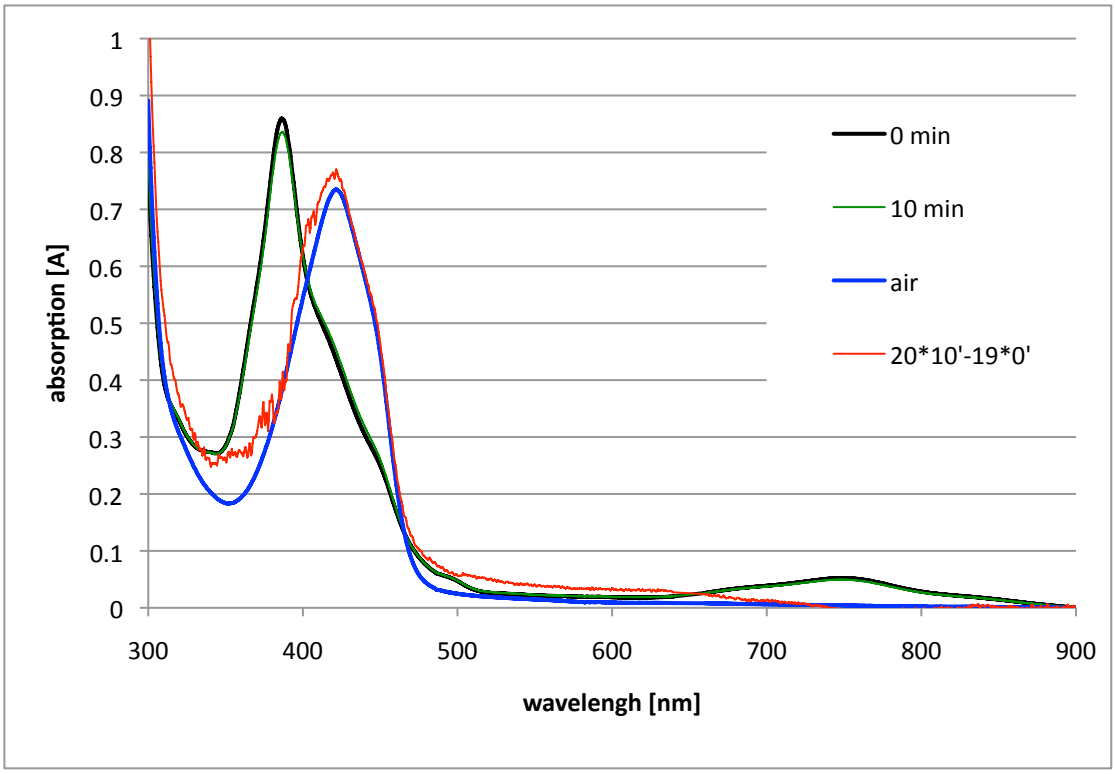


**Figure 6.14 B**: UV-Vis spectra from figure 6.14 A, including the difference spectrum 20 • ("0 min" – 0.95 • "10 min"), red curve.

### 6.4.9 Probing propyl- and allyl-coenzyme M for isotope exchange

Propyl-coenzyme M: 10 mM in an assay containing 30 mM Ti(III)-citrate. Incubation: 4 hours with 1.28 nmol enzyme.

Allyl-coenzyme M: 10 mM, including 2 mM CoB-SH, incubated for 32 min with 4.2 mg enzyme.

No significant incorporation of deuterium was found for either inhibitor.

### 6.4.10 Calculation of the specific rate of isotope exchange in ethyl-coenzyme M

From the fitted curve of $^{13}C$ label scrambling, $t_{1/2}$ = 3.63 min was obtained (cf. figure 3.9). The decay constant equals $\ln(2)/t_{1/2}$ = 0.19095 $min^{-1}$. With the initial substrate (16 µmol), the initial rate is 3.0552 µmol

$min^{-1}$. Taking the amount of enzyme (0.48 mg) into account, the specific activity is 7.274 μmol $min^{-1}$ $mg^{-1}$ (7.274 U $mg^{-1}$).

The substrate concentration used (10 mM) was below the $K_M$ value of ethyl-coenzyme M (20 mM[44]). Using the Michaelis Menten equation, the maximal rate (at saturation) can be calculated:

$v_0 = (v_{max} \bullet [S]) / (K_M + [S])$

$\Leftrightarrow v_{max} = v_0 \bullet (K_M + [S]) / [S]$

$\Leftrightarrow \mathbf{v_{max}} = 7.274\ U\ mg^{-1} \bullet (20\ mM + 10\ mM) / 10\ mM = \mathbf{21.82\ U\ mg^{-1}}$

### 6.4.11 Estimation of ee in chiral ethane neglecting isotope effects

Species according to figure 3.20:

$S^*_0$ = [²H, ³H]-ethyl-S-CoM at t = 0

S* = [²H, ³H]-ethyl-S-CoM

S = [³H]-ethyl-S-CoM

P* = [1-²H,1-³H]-ethane

P = [³H]-ethane

Time dependence of species:

$S^*(t) = S^*_0 \cdot \exp(-18 \cdot t)$

$P^*(t) = S^*_0 / 18 \cdot [1 - \exp(-18 \cdot t)]$

$S(t) = S^*_0 \cdot [\exp(-t) - \exp(-18 \cdot t)]$

$P(t) = 17/18 \cdot S^*_0 - S^*_0 \cdot [\exp(-t) - 1/18 \exp \cdot (-18 \cdot t)]$

$\mathbf{ee(t) = P^*(t) / [P^*(t) + P(t)] = [1 - \exp(-18 \cdot t)] / [18 - 18 \cdot \exp(-t)]}$

$conversion = P^*(t) + P(t) = S^*_0 \cdot [1 - \exp(-t)]$

$P^*(t) + P(t) = 0.05 \Leftrightarrow t = 0.05129$

$ee(0.05129) = 66.98\%$

$P^*(t) + P(t) = 0.1 \Leftrightarrow t = 0.10536$

$ee(0.10536) = 47.22\%$

$P^*(t) + P(t) = 0.28 \Leftrightarrow t = 0.3285$

$ee(0.3285) = 19.79\%$

## 6.5 Experimental Procedures and Raw Data for Chapter 4

### 6.5.1 $^{12}C/^{13}C$ KIE on methane formation

The competitive isotope effect on methane formation from $^{12}CH_3$-S-CoM/$^{13}CH_3$-S-CoM was determined by the method of high conversion in a Ti(III)-citrate assay (6.2.6). Because stopping the reaction in a Ti(III)-citrate medium with perchloric acid resulted in partial oxidation of the substrate to the corresponding sulfoxide (cf. 6.2.8), the sulfoxides formed had to be included in the calculation of the fraction of conversion. The ratio of remaining $^{13}CH_3$ /$^{12}CH_3$ substrate, however, was always calculated from the ratio of $^{12}CH_3$-S-CoM ("$^{12}CH_3$") and the right $^{13}C$ satellite of $^{13}CH_3$-S-CoM ("$^{13}CH_3$ (r)"). For the calculation of the conversion, the signals due to the methyl group of $CH_3$-(S=O)-CoM ("$^{12}CH_3$-(S=O)" and "$^{13}CH_3$-(S=O) (r)" = right $^{13}C$ satellite) were included in the calculation (**table 6.7**).

**Table 6.7 A**: Integral ratios of $^{12}CH_3$-S-CoM, $^{13}CH_3$-S-CoM and the corresponding sulfoxides.

| Integral ratios | | | | | | |
|---|---|---|---|---|---|---|
| t [min] | Disulfides | MeCoM | $^{12}CH_3$ | $^{13}CH_3$ (r) | $^{12}CH_3$-(S=O) | $^{13}CH_3$-(S=O) (r) |
| | | | A | B | C | D |
| 0 | 41.71 | 682.32 | 474.92 | 235.46 | 0 | 0 |
| 2 | 621.75 | 213.34 | 96.369 | 49.862 | 108.1 | 52.95 |
| 3 | 659.84 | 110.42 | 39.623 | 21.039 | 81.36 | 39.05 |
| 4 | 661.92 | 49.41 | 13.787 | 7.5464 | 43.5 | 23.31 |
| 5 | 628.58 | 24.37 | 4.335 | 2.4658 | 22.8 | 8.77 |
| 5.5 | 631.99 | little | 2.1893 | 1.2269 | 16.7 | 6.22 |
| 6 | 675.54 | little | 1.1242 | 0.631 | 13.7 | 4.297 |

**Table 6.7 B**: Calculation of the kinetic isotope effect $^{12}CH_3$-/$^{13}CH_3$-S-CoM of methane formation taking into account the oxidized substrate for the calculation of the fraction of conversion. Calculations based on table 6.7 A.

| t [min] | $^{12}CH_3$ (eff.) | $^{13}CH_3$ (r)(eff.) | R | 1-F | $R/R_0$ | KIE |
|---|---|---|---|---|---|---|
| | = A/B*(B+D) | = B+D | =2*B/A | =(E+2*F) /946 | = G /0.9916 | =ln(H)/ ln(H*I) |
| | E | F | G | H | I | |
| 0 | 474.92 | 235.46 | 0.9916 | 1.0000 | 1.0000 | |
| 2 | 198.71 | 102.81 | 1.0348 | 0.4277 | 1.0423 | 1.05130 |
| 3 | 113.17 | 60.09 | 1.0620 | 0.2471 | 1.0673 | 1.04885 |
| 4 | 56.37 | 30.86 | 1.0947 | 0.1248 | 1.1044 | 1.05009 |
| 5 | 19.75 | 11.24 | 1.1376 | 0.0446 | 1.1476 | 1.04635 |
| 5.5 | 13.29 | 7.45 | 1.1208 | 0.0298 | 1.1307 | 1.03623 |
| 6 | 8.78 | 4.93 | 1.1226 | 0.0197 | 1.1325 | 1.03271 |

### 6.5.2 Secondary KIE ($^{13}CH_3$-/$CD_3$-S-CoM) on methane formation

The ratio of $^{13}CH_3$-S-CoM to $CD_3$-S-CoM used as the substrate for the determination of the secondary kinetic isotope effect on methane formation was measured by $^1$H- and $^2$H-NMR spectroscopy (**table 6.8**).

**Table 6.8**: Integral ratios in $^1$H and $^2$H NMR spectra (relative to the internal standards acetonitrile-$d_0$ and -$d_3$ (1:1)) for the determination of the isotopologues $^{13}CH_3$-S-CoM and $CD_3$-S-CoM presenting the mixture of substrates.

| $^1$H-NMR: | | | | | |
|---|---|---|---|---|---|
| $^{13}CH_3$ (li) | $^{12}CH_3$ | ACN-$d_0$ | $^{13}CH_3$ (re) | $CL_3$/ACN | $CH_3$-S-CoM |
| 202.051 | 3.396 | 23.354 | 201.646 | 17.286 | 0.442 |

| $^2$H-NMR: | | | | | |
|---|---|---|---|---|---|
| | $^{12}CD_3$-CoM | ACN-$d_3$ | | | $CD_3$-S-CoM |
| | 579.205 | 26.566 | | 21.802 | 0.558 |

### 6.5.3 Methane activation with a mixture of $CH_4/CD_4$

A mixture of $CH_4$ and $CD_4$ was prepared in a 0.5 L gas cylinder as follows: The cylinder was evacuated and charged to 1.0 bar overpressure with $CD_4$ (Cambridge Isotope Laboratory). $CH_4$ was added until an overpressure of 3.0 bar was reached. All experiments to measure the intermolecular isotope effect of $CH_4/CD_4$ activation were done with this mixture (vials were filled with methane on the manifold inside the tent).

The relative amount of $CH_4$ and $CD_4$ was determined by $^1$H- and $^2$H-NMR measurements in $CDCl_3$ with a 1:1 mixture of acetonitrile-$d_0$ and acetonitrile-$d_3$ present as the internal standard (**table 6.9**).

**Table 6.9**: Determination of the ratio of $CH_4$ / $CD_4$ by $^1$H- and $^2$H-NMR spectroscopy using the same standard mixture of acetonitrile-$d_0$ and acetonitrile-$d_3$. The $^2$H-NMR measurement was carried out with pre-saturation of the $CDCl_3$ signal.

| | $CH_4$/ACN-$d_0$ ($^1$H-NMR) | $CD_4$/ACN-$d_3$ ($^2$H-NMR) |
|---|---|---|
| | 0.7885 | 0.63743 |
| | 0.72894 | 0.65692 |
| | 0.72274 | |
| average | 0.7467 | 0.6472 |
| % | 53.57 | 46.43 |

In order to establish the equilibrium conditions, $^{13}CH_3$-S-CoM was used which can be distinguished from the $CH_3$-S-CoM formed in the reaction via the $^{13}$C label. The amount of $^{12}CH_3$-S-CoM present due to incomplete labeling of the staring material (1.0%) was subtracted from the integral in order to obtain the amount of $^{12}CH_3$-S-CoM formed. The amount of $CH_4$ and $CD_4$ activated was determined by measuring the $CH_3$-S-CoM and $CD_3$-S-CoM via $^1$H- and $^2$H-NMR spectroscopy relative to the same

mixture of acetonitrile-$d_0$/ acetonitrile-$d_3$ used for the determination of the gas mixture.

### 6.5.4 Activation of $CH_2D_2$

Analysis of the methane isotopologue $CH_2D_2$ (Cambridge Isotope Laboratory) by $^1$H-NMR spectroscopy showed the presence of 3.70 mol% $CH_3D$ in addition to a small amount of $CHD_3$ (**table 4.10**).

**Table 6.10**: $^1$H-NMR analysis of the employed gas $CH_2D_2$ (Cambridge Isotope Laboratory).

| $CH_3D$ (integral) | $CH_2D_2$ (integral) | $CHD_3$ (integral) |
|---|---|---|
| 5.453 | 94.547 | small signal |

| "molar ratio" | "molar ratio" |
|---|---|
| 1.818 | 47.2735 |

Experiments performed with $CH_2D_2$ gas used as received from Cambridge Isotope Laboratory resulted in complete deactivation of the enzyme. Trace oxygen analysis revealed the presence of oxygen (>100 ppm). In order to remove the oxygen, the gas was filled into a previously evacuated 200 ml serum bottle which contained pellets of freshly activated copper catalyst (as used for the dry box). The methane activation experiments were performed with the treated $CH_2D_2$ by adding 5 ml gas with a syringe to the evacuated headspace of the assay vial in order to obtain 1 bar pressure. Experiments with 0.2 bar $CH_2D_2$ were performed by injection of 1.0 ml gas to the headspace without prior evacuation.

Establishment of the substrate/heterodisulfide equilibrium was obtained with $^{13}CH_3$-S-CoM as the initial substrate. In the $D_2O$ assays, formation of $^{12}CH_2D$-S-CoM from residual $^{12}CH_3$-S-CoM present in the initial substrate (1.0%) was subtracted to yield the amount of $^{12}CH_3$-S-CoM formed from $CH_2D_2$ (**table 6.11**).

**Table 6.11**: Integral ratios of substrate after activation of $CH_2D_2$. The numbers highlighted bold are taking into account the amount of $^{12}CH_2D$-S-CoM originated from incomplete labeling of the starting material $^{13}CH_3$-S-CoM (only required for the experiments in $D_2O$, obtained by subtraction 1.1% of the value of $^{13}CH_2D$-S-CoM). Values are not corrected for the 3.7% $CH_3D$ present in the gas mixture used.

| $H_2O$ | $^{13}CH_3$ li | $^{13}CH_2D$ li | $^{12}CH_3$ | $^{12}CH_2D$ | **$^{12}CH_2D$ formed** | $^{12}CHD_2$ | $^{13}CH_3$ re | $^{13}CH_2D$ re |
|---|---|---|---|---|---|---|---|---|
| Run1 | 43.062 | | 1.039 | 9.286 | **9.286** | 10.031 | 42.952 | |
| Run2 | 47.08 | | 1.02 | 8.22 | **8.22** | 9.18 | 47.14 | |
| $D_2O$ | | | | | | | | |
| Run1 | 54.96 | 7.40 | 1.22 | 9.29 | **9.13** | 9.30 | 55.34 | 7.38 |
| Run2 | 61.03 | 6.96 | 1.20 | 5.02 | **4.87** | 4.68 | 60.93 | 6.58 |
| Run3 | 55.39 | 8.83 | 1.15 | 3.98 | **3.79** | 3.96 | 54.92 | 8.29 |

### 6.5.5 Calculation of primary and secondary KIE of methane activation

Combining the intermolecular isotope effect of $CH_4/CD_4$ activation with the intramolecular isotope effect ($CH_2D_2$) allows determination of the primary and secondary isotope effect on methane activation. The $CH_4/CD_4$ isotope effect corresponds to the product of the primary isotope effect times the secondary isotope effect raised to the power 3 (as discussed in section 4.3.3). The isotope effect on $CH_2D_2$ activation corresponds to the ratio of primary to secondary isotope effects.

In this section, the calculation of the two isotope effects, including statistical error propagation according to the variances obtained from the experiments, is performed.

The measured isotope effects are denoted “a” and “b” here.
a and b = mean values
$s_a$ and $s_b$ the standard deviations of the measured values
$sm_a$ and $sm_b$ are the standard deviations of the mean values ($sm_a = s_a/\sqrt{3}$ , $sm_b = s_b/\sqrt{5}$, since 3 measurements of a and 5 measurements of b were performed)
$c_a$ and $c_b$ are the 95% confidence interval assuming a t-distribution.

Relative rate of $CH_4/CD_4$ activation = a
a = 3.85766
$s_a$ = 0.224438
$sm_a$ = 0.129579
$c_a$ = 0.55719

Relative rate of (C-H/C-D) activation in $CH_2D_2$ = b
b = 2.0888
$s_b$ = 0.118607
$sm_b$ = 0.053043
$c_b$ = 0.147459

The measured isotope effect a corresponds to $KIE_{prim} \bullet (KIE_{sec})^3$.
The measured isotope effect b corresponds to $KIE_{prim}$ / $KIE_{sec}$.

From these relations the two isotope effect can be calculated analytically:
**$KIE_{prim}$ (a, b)** = (a • b^3)^(1/4) = a^(1/4) • b^(3/4) **= 2.43503**
**$KIE_{sec}$ (a, b)** = (a / b)^(1/4) = a^(1/4) • b^(-1/4) **= 1.16575**

**Error propagation:**

$sm_{prim}$ = standard deviation of the mean value for $KIE_{prim}$

$sm_{sec}$ = standard deviation of the mean value for $KIE_{sec}$

$sm_{prim}$^2 = ($d$[$KIE_{\mathbf{prim}}$ (a, b)] / $d$a )^2 • $sm_a$^2 + ($d$[$KIE_{\mathbf{prim}}$ (a, b)] / $d$b )^2 • $sm_b$^2

$sm_{sec}$^2 = ($d$[$KIE_{\mathbf{sec}}$ (a, b)] / $d$a )^2 • $sm_a$^2 + ($d$[$KIE_{\mathbf{sec}}$ (a, b)] / $d$b )^2 • $sm_b$^2

with

$d$[$KIE_{\mathbf{prim}}$ (a, b)] / $d$a = 1/4 • b^(3/4) • a^(-3/4)

$d$[$KIE_{\mathbf{prim}}$ (a, b)] / $d$b = 3/4 • a^(1/4) • b^(-1/4)

$d$[$KIE_{\mathbf{sec}}$ (a, b)] / $d$a = 1/4 • b^(-1/4) • a^(-3/4)

$d$[$KIE_{\mathbf{sec}}$ (a, b)] / $d$b = -1/4 • a^(1/4) • b^(-5/4)

the following variances are obtained:

$sm_{prim}$^2 = 0.024902 • $sm_a$^2 + 0.764427 • $sm_b$^2 = 0.002569

$sm_{sec}$^2 = 0.005707 • $sm_a$^2 + 0.019467 • $sm_b$^2 = 0.000151

$sm_{prim}$ = 0.050684

$sm_{sec}$ = 0.012272

In order to assure the 95% confidence interval, the t-value for 3 measurements = 4.30 (2 degrees of freedom) is used although the value for b was obtained from 5 measurements.

Hence the 95% confidence interval equals 4.30 • 0.050684 = 0.217941 for the primary isotope effect and 4.30 • 0.012272 = 0.05277 for the secondary isotope effect.

**Rounded values:**

**$KIE_{prim}$ = 2.44 ± 0.22**

**$KIE_{sec}$ = 1.17 ± 0.05**

In order to verify the result, the primary and secondary isotope effects were calculated for the extreme values (outside the 95% confidence interval) of a ($a_{min}$ = 3.3005 and $a_{max}$ = 4.4149) and b ($b_{min}$ = 1.9413 and $b_{max}$ = 2.2363).

The results in **table 6.12** show that only a combination of $a_{max}/b_{min}$ or vice versa (together 2 • 2.5% • 2.5% = 0.125% probability) would result in a secondary isotope effect outside the interval calculated by error propagation (1.1130 to 1.2185). For all combinations, the primary isotope effect is in the calculated 95% confidence interval (2.217 to 2.653).

**Table 6.12**: Calculation of the primary KIE and secondary KIE at the borders of the confidence intervals of each measured initial values a and b.

| primary KIE | $b_{min}$ | $b_{max}$ |
|---|---|---|
| $a_{min}$ | 2.2168 | 2.4648 |
| $a_{max}$ | 2.3840 | 2.6508 |

| secondary KIE | $b_{min}$ | $b_{max}$ |
|---|---|---|
| $a_{min}$ | 1.14187 | 1.10221 |
| $a_{max}$ | 1.22801 | 1.18536 |

### 6.5.6 Isotope effect of label exchange in methyl-coenzyme M

**Table 6.13**: Molar fraction of different isotopologues present in the starting materials as measured by $^1$H-NMR spectroscopy.

| Molar fraction of isotopologues | | | |
|---|---|---|---|
| | $CH_3$-S-CoM | $CH_2D$-S-CoM | $CHD_2$-S-CoM |
| $CH_2D$-S-CoM | 0.006208 | 0.991977 | 0.001815 |
| $CHD_2$-S-CoM | 0.000337 | 0.001139 | 0.998524 |
| $CD_3$-S-CoM* | 0.000263 | 0.00005 | 0.01014 |

*: calibrated to the integral of $CD_3$-S-$CH_2$***$CH_2$**$SO_3^-$.

An overview of all methane isotopologues measured is given in **table 6.14**.

**Table 6.14**: Ratio of different isotopologues of methane measured in the 4 different experiments for isotope exchange in methyl-coenzyme M. Evaluation of the isotope effect is performed from the isotopologues highlighted bold after correction for the initial amount due to incomplete labeling (cf. table 6.12).

**A**) $CH_3$-S in $D_2O$: "$CH_3D$" formation

| $xCH_4$ | $xCH_3D$ | $xCH_2D_2$ |
|---|---|---|
| 0.021621 | **0.902859** | **0.075520** |

**B**) $CH_2D$-S in $H_2O$: "$CH_3D$" formation

| $xCH_4$ | $xCH_3D$ | $xCH_2D_2$ |
|---|---|---|
| **0.0159180** | **0.9829390** | 0.0011430 |

**C**) $CH_2D$-S in $D_2O$: "$CH_2D_2$" formation

| $CH_4$ | $CH_3D$ | $CH_2D_2$ | $CHD_3$ |
|---|---|---|---|
| 0.0008920 | 0.0314122 | **0.9244473** | **0.0432485** |

**D**) $CHD_2$-S in $H_2O$: "$CH_2D_2$" formation

| $CH_4$ | $CH_3D$ | $CH_2D_2$ | $CHD_3$ |
|---|---|---|---|
| 0.0011339 | **0.0186372** | **0.9709242** | 0.0093047 |

### 6.5.7 Isotope exchange in ethyl-coenzyme M

The observed isotope exchange was simulated with the program COPASI ("COmplex PAthway SImulator"[135])

A description is given in section 6.8.

### 6.5.8 Quantification of the residual protons in the $D_2O$ assays

The concentration of residual protons in the assays was determined by $^1$H-NMR spectroscopy. The signals for $H_2O$ and HDO in 700 µl DMSO-$d_6$ were integrated before and after addition of 10 µl assay solution relative to the internal standard (0.1 vol% acetonitrile). From the increase in the signals the H content in the assay solution was calculated.

For the experiments analyzing isotope exchange in ethyl-coenzyme M, a value of 1.6% was found (98.4% $D_2O$).

For experiments analyzing the apparent fractionation factor for methane formation and deuterium incorporation into the remaining substrate, a value of 2.71% was found (97.3% $D_2O$).

### 6.5.9 Proton inventory studies

Enzyme experiments were carried out analogous to the assay conditions described in section 6.2.4. The fraction of residual protons present in the "pure $D_2O$" assays was determined to be 2.7% (cf. previous section, 6.5.8). The $D_2O$ content of the other assay samples was extrapolated from this value by the appropriate $H_2O/D_2O$ mixing ratio. The amount of enzyme per assay was 1.07 nmol. Special care was taken to have a uniformly low delay between mixing the assay on ice and incubation at 60 °C because the ratio of the methane-forming rate and deuterium incorporation rate is strongly dependent on the temperature, hence a longer (small) enzyme activity between mixing on ice and incubation would lead to an artificially higher amount of deuterium incorporation into the substrate.

For each concentration of $D_2O$ in the solvent two independent stock solutions were mixed and distributed into the vials. In addition, from all assays one vial was incubated for 2 min and one for 4 min. Because no significant difference between the 2 min value and the 4 min value was observed, only the data from the 2 min values were evaluated in detail (presented in section 4.6.3).

Rearranging the equation for the apparent fractionation factor

$$\Phi_{app} = \frac{[CH_3D]}{[CH_4]} \bullet \frac{[H_2O]}{[D_2O]}$$

which depends on the molar fraction of $CH_3D$ formed and the amount of $D_2O$ in the solvent, one obtains:

$$[CH_3D] = \frac{\Phi \bullet [D_2O]}{[D_2O] \bullet (\Phi - 1) + 1}$$

With this formula, the value of Φ was fitted using least square residuals.

**Proton inventory study of deuterium incorporation into the substrate**

For the proton inventory study of deuterium incorporation into the substrate, the amount of $CH_2D$-S-CoM formed in hypothetical pure $D_2O$ is also unknown.

Denoting the maximal amount of $CH_2D$-S-CoM formed (unknown) = M, the following equation is obtained:

$$[CH_2D - S - CoM] = \frac{M \bullet \Phi \bullet [D_2O]}{[D_2O] \bullet (\Phi - 1) + 1}$$

Simultaneous least square fitting, varying both variables Φ and M, yielded the following values:

Φ = 0.382

M = 0.03547

## 6.6 NMR Measurements

### 6.6.1 Equipment

$^{1}$H-NMR spectra of the assay solution and of methane samples were recorded on a Bruker Avance II 600 MHz spectrometer with an inverse detection probe.
$^{2}$H-NMR spectroscopy and $^{13}$C-NMR spectroscopy was carried out on a Bruker Avance III 600 MHz spectrometer with a cryo detection probe.

NMR spectroscopy for the synthesis of substrates was carried out on Varian Gemini 300 MHz spectrometers if not stated otherwise.

### 6.6.2 Sample preparation from assay solution

620 µl enzyme solution was transferred to a 5 mm NMR tube (528-PP) without further treatment unless stated otherwise. 80 µl of a solution containing 0.025% v/v dioxane in $D_2O$ was added as the internal standard and the sample agitated. For samples in non-deuterated buffer, the added dioxane/$D_2O$ solution allowed us to lock on the $D_2O$ signal. For samples from which a $^{2}$H-NMR spectrum was also acquired, a standard solution of 0.025% v/v dioxane and 0.025% v/v dioxane-$d_8$ in $D_2O$ was added by default.
Deuterated internal standards (dioxane-$d_8$ and acetonitrile-$d_3$) were always mixed from a premixed stock solution of the deuterated standard and the un-deuterated standard 1:1 (v/v).

### 6.6.3 Sample preparation for methane measurements

2 ml of the headspace gas of interest was removed through the rubber stopper with a gas-tight syringe containing a small valve. The needle was replaced by a capillary and the methane bubbled through 700 µl $CDCl_3$ containing 0.01% dioxane (v/v) in an NMR tube. The tube was closed with a small septum and measured immediately.

### 6.6.4 Acquisition, processing and integration

The spectra were acquired at 298 K without spinning. For the samples in $H_2O$, the water signal was suppressed by CW-presaturation for 2 s. A 30 ° excitation pulse and 5 s acquisition time (repetition time 7 s) was used to ensure correct integration. Samples containing deuterated ethyl-coenzyme M were measured with broadband deuterium decoupling. For methane samples, an additional relaxation delay of 5 s was used (repetition time 10 s).

$^{13}$C-NMR spectra to be integrated were acquired with inverse gated simultaneous proton and deuterium decoupling, denoted as $^{13}$C-{$^{1}$H}{$^{2}$H}-NMR. A relaxation delay of 60 s was used in order to ensure correct integration. The influence of the relaxation delay was tested by measuring a mixture of $CH_3CH_2$-S-CoM (= $d_0$), $CH_3CD_2$-S-CoM (= $d_2$) and $CD_3CD_2$-S-CoM (= $d_5$) with different relaxation delays (**table 6.15**).

**Table 6.15**: $^{13}$C{$^{1}$H}{$^{2}$H}-NMR measurement of a mixture containing 0.3 M $CH_3CH_2$-S-CoM, 0.1 M $CH_3CD_2$-S-CoM and 0.2 M $CD_3CD_2$-S-CoM in $D_2O$ with different relaxation delays (d1). The integral of Et-S-$CH_2$***C*H$_2$**$SO_3^-$ was set to 100.

| | S-***C*H$_2$**$CH_3$ | | | S-$CH_2$***C*H$_3$** | | | $CH_2$ ($d_{0/2/5}$) | $CH_3$ ($d_{0/2/5}$) |
|---|---|---|---|---|---|---|---|---|
| d1 [s] | $d_0$ | $d_2$ | $d_5$ | $d_0$ | $d_2$ | $d_5$ | Sum | Sum |
| 15 | 53.66 | 15.909 | 27.393 | 66.128 | 21.503 | 27.566 | 96.962 | 115.197 |
| 30 | 48.277 | 15.679 | 31.926 | 54.775 | 20.98 | 32.785 | 95.882 | 108.54 |
| 60 | 48.864 | 17.273 | 35.2 | 49.684 | 18.636 | 33.163 | 101.337 | 101.483 |
| 120 | 49.073 | 17.86 | 33.986 | 51.886 | 18.211 | 35.104 | 100.919 | 105.201 |

Integration was performed with BRUKER Topspin 2.1 software. All integrals were calibrated relative to the internal standard dioxane. Chemical shifts were calibrated relative to the signal of dioxane (set to 3.70 ppm for $^{1}$H- and $^{2}$H-NMR spectra, 67.00 ppm for $^{13}$C-NMR spectra).

### 6.6.5 Fitting of NMR spectra

The molar fractions of individual isotopologues of ethyl-coenzyme M were determined by automatic iterative least square fitting of calculated spectra to the experimental spectra for each incubation time with the program iNMR. The spectrum of each isotopologue was calculated based on the isotope shifts, number of protons and coupling constants given in **table 6.16**, which were extracted from spectra at longer incubation times, where all isotopologues are present. The sum of the simulated spectra was then fitted to the experimental spectra with the relative populations of the isotopologues as the parameter to be optimized via least square procedure. For the quality of the fit, see figures 3.7, 6.8 and 6.11.

**Table 6.16**: Assignment of $^{1}$H-NMR signals for the isotopologues of Et-S-CoM.

| Nr | Species | Isotope shifts ($CL_3$)[1)] | m | Isotope shifts ($CL_2$) | m | $^{3}J_{HH}$ [Hz] | $\delta(CL_3)$ | $\delta(CL_2)$ |
|---|---|---|---|---|---|---|---|---|
| 1 | $CH_3CH_2SR$ | $\delta_{CH3}$ | t | $\delta_{CH2}$ | q | 7.4 | 1.17432 | 2.55407 |
| 2 | $CH_3CHDSR$ | $\delta_{CH3}+\Delta\beta_{CH3}$ | d | $\delta_{CH2}+\Delta\alpha_{CH2}$ | q | 7.4 | 1.16619 | 2.53627 |
| 3 | $CH_3CD_2SR$ | $\delta_{CH3}+2\bullet\Delta\beta_{CH3}$ | s | - | - | - | 1.15807 | - |
| 4 | $CH_2DCH_2SR$ | $\delta_{CH3}+\Delta\alpha_{CH3}$ | t | $\delta_{CH2}+\Delta\beta_{CH2}$ | t | 7.4 | 1.15734 | 2.5472 |
| 5 | $CH_2DCHDSR$ | $\delta_{CH3}+\Delta\alpha_{CH3}+\Delta\beta_{CH3}$ | d | $\delta_{CH2}+\Delta\alpha_{CH2}+\Delta\beta_{CH2}$ | t | 7.4 | 1.14924 | 2.5294 |
| 6 | $CH_2DCD_2SR$ | $\delta_{CH3}+\Delta\alpha_{CH3}+2\bullet\Delta\beta_{CH3}$ | s | - | - | - | 1.14118 | - |
| 7 | $CHD_2CH_2SR$ | $\delta_{CH3}+2\bullet\Delta\alpha_{CH3}$ | t | $\delta_{CH2}+2\bullet\Delta\beta_{CH2}$ | d | 7.4 | 1.14045 | 2.5403 |
| 8 | $CHD_2CHDSR$ | $\delta_{CH3}+2\bullet\Delta\alpha_{CH3}+\Delta\beta_{CH3}$ | d | $\delta_{CH2}+\Delta\alpha_{CH2}+2\bullet\Delta\beta_{CH2}$ | d | 7.4 | 1.13237 | 5.5225 |
| 9 | $CHD_2CD_2SR$ | $\delta_{CH3}+2\bullet\Delta\alpha_{CH3}+2\bullet\Delta\beta_{CH3}$ | s | - | - | - | 1.12433 | - |
| 10 | $CD_3CH_2SR$ | - | - | $\delta_{CH2}+3\bullet\Delta\beta_{CH2}$ | s | - | - | 2.5335 |
| 11 | $CD_3CHDSR$ | - | - | $\delta_{CH2}+\Delta\alpha_{CH2}+3\bullet\Delta\beta_{CH2}$ | s | - | - | 2.5157 |
| 12 | $CD_3CD_2SR$ | - | - | - | - | | - | - |

[1)] $\Delta\alpha_{CH3}$= -17.00 ppb; $\Delta\beta_{CH3}$ = -8.13 ppb; $\Delta\alpha_{CH2}$ = 17.80 ppb; $\Delta\beta_{CH2}$ = -6.87 ppb

## 6.7 Synthesis and Characterization of Substrates

### 6.7.1 General

All chemicals and solvents were purchased at the highest quality available and used as received if not stated otherwise.

Selected reagents:

| | |
|---|---|
| amberlite IR-120 | Fluka |
| amberlite XAD-2 | Fluka |
| dihydroquinine | Fluka |
| diisopropylethylamine | Sigma |
| 1,4-dithio-DL-threitol | Fluka |
| ethyl 7-bromo heptanoate | Aldrich |
| *O*-phospho-L-threonine | Sigma |
| sodium 2-mercaptoethanesulfonate | Fluka |
| sodium methoxide 0.5 M in methanol | Acros |

Deuterated solvents were obtained from ARMAR chemicals if not stated otherwise.
The origin of the labeled compounds for syntheses (usually Cambridge Isotope Laboratory) is stated in the description of the procedure.

Chemical shifts (δ) in ppm are relative to TMS as internal standard unless stated otherwise.

### 6.7.2 Coenzyme B and its derivatives

Coenzyme B disulfide was synthesized from 7-bromoheptanoic acid ethyl ester by a literature reaction sequence[147]. First, the corresponding *N*-succinimidyl-diester was synthesized and purified by recrystallization. This activated ester was then converted with *O*-phospho-L-threonine to coenzyme B disulfide, which was purified by adsorption on a XAD-2-column (see scheme below). CoB-SH was than obtained by reduction with DTT.

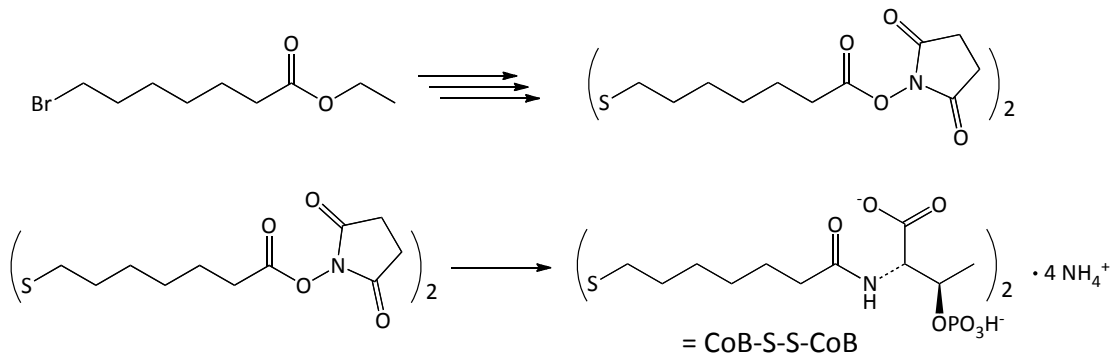


**7-Bromoheptanoic acid**

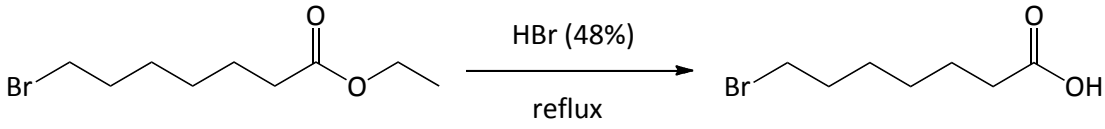


7-Bromoheptanoic acid ethyl ester (30.3 g, 127.8 mmol) was refluxed in 100 ml hydrobromic acid (48%, 890 mmol) for 14 h. The reflux condenser was exchanged by a vigroux column and a gentle stream of nitrogen was passed over the boiling mixture for 90 min in order to remove ethanol and bromoethane and to drive the reaction to completion. The reaction mixture was cooled with added ice and extracted twice with 300 ml $CH_2Cl_2$. The combined organic layers were washed with water and dried with $MgSO_4$. Evaporation of the solvent

and drying under high vacuum yielded 7-bromoheptanoic acid (26.0 g, 124.3 mmol, 97%).

$^1$H-NMR (300 MHz, $CD_3OD$): 3.44 (*t*, *J* = 6.8, 2 H, H-C(7)); 2.29 (*t*, *J* = 7.4, 2 H, H-C(2)); 1.85 (*quint*, *J* = 7.2, 2 H, H-C(6); 1.61 (*quint*, *J* = 7.7, 2 H, H-C(3)); 1.40-1.50 (*m*, 2 H, $CH_2$); 1.30-1.40 (*m*, 2 H, $CH_2$). $^{13}$C-NMR (75 MHz, $CD_3OD$): 177.39 (C(1)); 34.70 ($CH_2$); 34.23 ($CH_2$); 33.67 ($CH_2$); 29.18 ($CH_2$); 28.75 ($CH_2$); 25.74 ($CH_2$).

**7,7′-Dithioheptanoic acid**

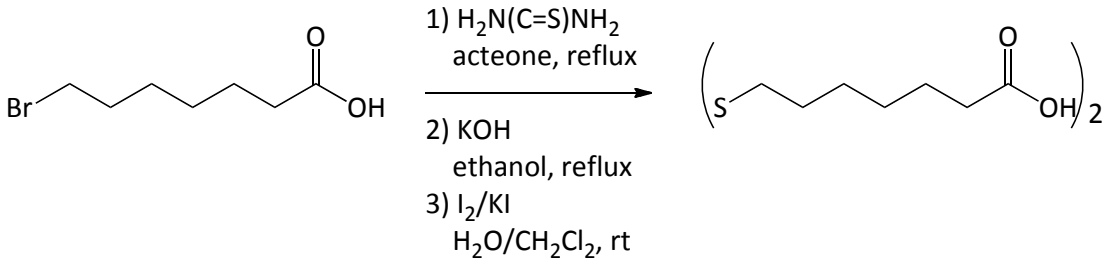


7-Bromoheptanoic acid (25.8 g, 123 mmol) was added to thiourea (47 g, 617 mmol) under nitrogen in 750 ml dry acetone. The mixture was refluxed for 16 h. After evaporation of the solvent and drying under high vacuum, the residue was dissolved under nitrogen in 1200 ml ethanol. Potassium hydroxide (56.1g, 1.0 mol) was added and refluxed for 2 h. The solvent was evaporated and the residue dried under high vacuum.

This solid was dissolved in approx. 900 ml HCl (1.0 M) to give a clear solution at pH = 1 that was extracted with $CH_2Cl_2$ (3 times 200 ml). The combined organic phases were washed with 200 ml of water, filtered and the solvent evaporated. Drying under high vacuum yielded the crude thiol (12.2 g, 76 mmol, 62%). The thiol was dissolved in 200 ml $CH_2Cl_2$. An aqueous solution of $I_2$/KI was added under vigorous stirring until the iodine color remained permanently in the organic layer. Sodium thiosulfate was added until all color disappeared. The aqueous phase was extracted with 250 ml $CH_2Cl_2$, the combined organic

phases dried with $MgSO_4$ and evaporated. The obtained solid was dissolved in $CH_2Cl_2$ and filtered through cotton in order to remove most of the elemental sulfur formed by the added thiosulfate. Drying under high vacuum over 3 days yielded 7,7′-dithioheptanoic acid (12.0 g, 37.2 mmol, 58% calculated from 7-bromoheptanoic acid).

$^1$H-NMR (300 MHz, $CDCl_3$): 2.69 (*t*, *J* = 7.5, 4 H, H-C(7/7′)); 2.37 (*t*, *J* = 7.2, 4 H, H-C(2/2′)); 1.62-1.75 (*m*, 8 H, H-C(3/3′, 6/6′)); 1.33-1.47 (*m*, 8 H, H-C(4/4′, 5/5′)). $^{13}$C-NMR (75 MHz, $CD_3OD$): 180.14 (C(1/1′)); 38.86 ($CH_2$); 22.96 ($CH_2$); 28.90 ($CH_2$); 28.56 ($CH_2$); 28.03 ($CH_2$); 24.44 ($CH_2$).

**7,7′-Dithioheptanoic acid di-*N*-succinimidyl ester**

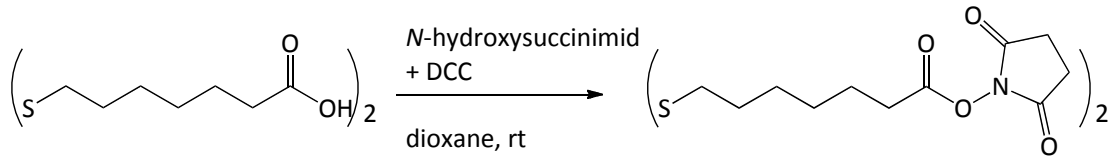


*N*-Hydroxysuccinimide (8.9 g, 77.3 mmol) was added under nitrogen to a solution of 7,7′-dithioheptanoic acid (12.0 g, 37.2 mmol) in dioxane (freshly distilled from $CaH_2$). Dicyclohexylcarbodiimide (15.9 g, 77.1 mmol) was dissolved anaerobically in dioxane (90 ml, freshly distilled from $CaH_2$) and added to the other components under stirring. The solution turned immediately cloudy and a slight warming could be observed. After stirring at rt for 19 h the suspension was filtered and the residue washed with dioxane (3 times 30 ml). The solid did not contain any product and was disposed. The filtrate was evaporated and dried under high vacuum to yield 25 g of a pinkish, wax-like solid. This crude product was dissolved under reflux in 250 ml isopropanol, cooled to room temperature, and filtrated. The mother liquor was evaporated and the residue again crystallized from 250 ml of boiling isopropanol. The resulting second mother liquor (7.6 g after drying) contained only about 60% product and was disposed. The two solid fractions were dissolved

in 500 ml boiling isopropanol and cooled to 4 °C within 24 h. Filtration, washing with isopropanol (2 times 40 ml), and drying under high vacuum for 4 days yielded pure 7,7′-dithioheptanoic acid di-*N*-succinimidyl ester as a colorless powder (11.0 g, 21.3 mmol, 57%).

$^{1}$H-NMR (300 MHz, $CDCl_3$): 2.84 (*s*, 8 H, H-C(succinimidyl)); 2.68 (*t*, *J* = 7.4, 4 H, H-C(7/7′)); 2.62 (*t*, *J* = 7.4, 4 H, H-C(2/2′)); 1.65-1.80 (*m*, 8 H, H-C(3/3′, 6/6′)); 1.40-1.48 (*m*, 8 H, H-C(4/4′, 5/5′)).

$^{13}$C-NMR (75 MHz, $CDCl_3$): 168.88 (C); 168.24 (C); 38.70 (C(7/7′)); 30.77 ($CH_2$); 28.78 ($CH_2$); 28.24 ($CH_2$); 27.84 ($CH_2$); 25.52 ($CH_2$); 24.37 ($CH_2$).

**Coenzyme B disulfide tetraammonium salt**

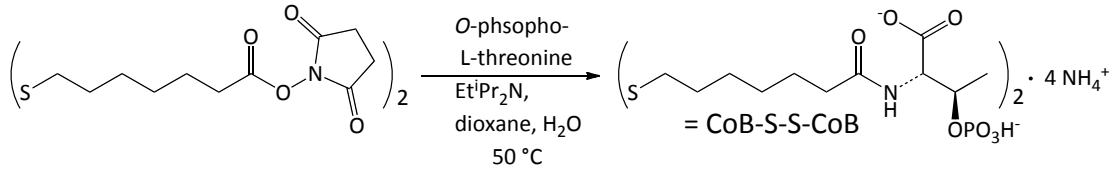


*O*-Phospho-L-threonine (6.970 g, 35.0 mmol) was suspended in dioxane (260 ml). *N*,*N*-Diisopropylethylamine (18.1 g, 140 mmol) and water (40 ml) was added which led to a clear solution within 30 min. The succinimidyl ester (6.20 g, 12.0 mmol) was added under stirring to give a dispersed emulsion. After 25 h at rt about 80% conversion of the activated ester was obtained. The reaction mixture was heated to 40 °C for 1.5 h (83% conversion) and then to 50 °C for additional 3 h (97% conversion, containing 25% of a side product). Evaporation of the solvents led to 27.5 g of a viscous mass.

The crude product was dissolved in water (100 ml) and $NH_3$ (aq., conc., 50 ml) to give an emulsion that was extracted with $CH_2Cl_2$ (200 ml) and ice (50g). Phase separation proved to be difficult because of a third emulsion phase in the middle. Pure organic and aqueous phases were removed and more $CH_2Cl_2$ and $H_2O/NH_3$ were added. This procedure was repeated 3 times and finally solid $NH_4Cl$ was added in order to

separate the middle phase completely. In total, 850 ml organic and 700 ml aqueous phase were obtained.
The aqueous phase was rotated at rt under reduced pressure (10 mbar) for 30 min in order to remove residual $CH_2Cl_2$ and some of the $NH_3$ to yield a clear solution which was kept at 4 °C overnight.

**Purification of Coenzyme B disulfide tetraammonium salt**
Coenzyme B and its derivatives can be adsorbed in the protonated (neutral) form on the hydrophobic XAD-2 material for purification if the material is carefully conditioned as described below.
XAD-2 material is extracted in portions in a Soxhlet extractor for 2 days with ethyl acetate followed by 2 days with methanol. A column (8 cm diameter) is packed with the conditioned XAD-2 material (height 17 cm) in degassed (rotary evaporator) methanol, topped with a filter paper and weighted with 10 cm of sand. After standing overnight under methanol the liquid is gradually replaced by water (first degassed methanol/water mixtures, then degassed water). The water is replaced by degassed 1 M HCl and the column allowed to equilibrate for 2 days.
The product-containing aqueous phase was acidified with HCl (aq., conc., 100 ml) to pH = 0 and charged onto the column. The column was washed with 5 L degassed 1 M HCl until no impurities could be detected in the flow-through by UV spectroscopy ($\lambda_{max}$ = 210-220 nm). The column was then washed with 3 L degassed water to reach pH = 4.5 of the eluent. The product was eluted with 33% methanol (1.5 L), 50% methanol (1.2 L), 66% methanol (1.8 L) and pure methanol (2 L). Fractions of 500 ml were collected and analyzed by UV spectroscopy (local $\lambda_{max}$ = 245-250 nm). Each fraction was made alkaline by addition of $NH_3$ (aq., conc., 1 ml) and concentrated under vacuum to approx. 5 ml. From each fraction a small amount was dried under high vacuum and analyzed by $^1$H-NMR spectroscopy (**table 6.17**).

**Table 6.17**: Determination of the amount of disulfide (UV spectroscopy) and purity according to coenzyme B moieties ($^1$H-NMR spectroscopy).

| fraction | $E_{245}$ (1 cm) | purity (CoB moieties) |
|---|---|---|
| 7 | 0.1 | 100% |
| 8 | 0.28 | 100% |
| 9 | 0.57 | 100% |
| 10 | 0.54 | 100% |
| 11 | 0.47 | 100% |
| 12 | 0.87 | 100% |
| 13 | 0.93 | 99% |
| 14 | 1.57 | 92% |
| 15 | 1.33 | 85% |
| 16 | 0.93 | 79% |
| 17 | 1.14 | 58% |
| 18 | 0.25 | 0% |

Fractions 7-13 were combined and evaporated to give 3.5 g of a solid. The small amount of remaining *N*,*N*-diisopropylethylamine could be removed by extracting a solution in $NH_3$ (aq., 5%, 50 ml) with $CH_2Cl_2$ (2 times 25 ml). The aqueous phase was filtered through cotton and evaporated to give 3.1 g of a colorless solid, which was dissolved in 60 ml water and lyophilized. Additional drying under high vacuum for 4 days yielded pure coenzyme B disulfide tetraammonium salt as a hygroscopic microcrystalline powder (2.782 g, 3.696 mmol, 31%). The product was assigned as the tetraammonium salt because this gave the best match to the elemental analysis and because a solution in water was slightly acidic.

$^1$H-NMR (600 MHz, $D_2O$, dioxane = 3.700 ppm): 4.60 (*dqd*, *J* = 7.44, 6.42, 3.78, 2 H, C***H***$OPO_3^{2-}$); 4.13 (*dd*, *J* = 3.78, 1.92, 2 H, C***H***NC=O); 2.71 (*t*, *J* = 7.26, 4 H, C***H***$_2$S); 2.33 (*dt*, *J* = 14.16, 7.68, 2 H, C***H***$_2$C=O); 2.28 (*dt*, *J* = 14.22, 7.32, 2 H, C***H***$_2$C=O); 1.64 (*quint*, *J* = 7.32, 4 H, $CH_2$); 1.58 (*quint*, *J* =

7.52, 4 H, $CH_2$); 1.37 (*quintetoid*, $J_{obs}$ = 7.5, 4 H, $CH_2$); 1.31 (*quartetoid*, $J_{obs}$ = 7.6, 4 H, $CH_2$); 1.25 (*d*, *J* = 6.36, 6 H, $CH_3$).
$^{13}$C-NMR (150 MHz, $D_2O$, dioxane = 67.00 ppm): 177.44 (C); 177.06 (C); 73.07 (CH, $^2J_{CP}$ = 5.40 Hz); 60.62 (CH, $^3J_{CP}$ = 7.50 Hz); 38.65 ($CH_2$); 36.14 ($CH_2$); 28.61 ($CH_2$); 28.33 ($CH_2$); 27.67 ($CH_2$); 25.61 ($CH_2$); 18.97 ($CH_3$).
elem. anal. calcd. for $C_{22}H_{54}N_6O_{14}P_2S_2$ (752.78): C 35.10, H 7.23, N 11.16, O 29.76, P 8.23, S 8.52; found: C 34.68, H 7.23, N 11.51, O 30.24, P 7.87, S 8.82.
HRMS (ESI-TOF, positive ion mode): (m/z) calcd. for $C_{22}H_{43}O_{14}N_2P_2S_2^+$: 685.16254; found: 685.1625.

Fractions 17 and 18 were combined, concentrated and filtered to remove colloid particles originating from the XAD-2 column. Drying under high vacuum yielded 1.26 g of a solid, which could be identified as the heterodisulfide of coenzyme B and 7-mercaptoheptanoic acid (2.27 mmol):

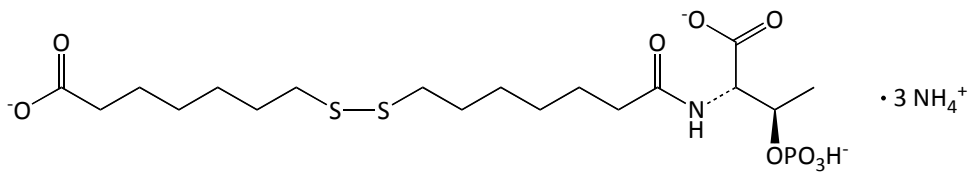


$^1$H-NMR was indistinguishable from an equimolar mixture of the corresponding homodisulfides.

Fractions 14-16 were concentrated under reduced pressure to give 3.9 g of a solid. Remaining Hünig's base was removed as described for the pure fractions. The resulting solid (ca. 3.6 g) was dissolved in 10 ml water. Ethanol (100 ml) was added under gentle stirring and the precipitate was allowed to settle. The liquid was decanted and the precipitate dried under high vacuum to give 2.5 g product with a purity of 92% according to CoB signals in the $^1$H-NMR spectrum (liquid: 70% purity). This procedure was repeated to give a product with about 98%

purity. The liquid fractions were evaporated and precipitated twice the same way. The two product-enriched fractions were dissolved in 50 ml water and lyophilized. Additional drying under high vacuum yielded 1.90 g of 95% pure coenzyme B disulfide tetraammonium salt (2.56 mmol disulfides, 97.5% purity according to CoB signals).
The mother liquors of the precipitations were lyophilized and dried under high vacuum to give 1.47 g of 60% pure coenzyme B disulfide tetraammonium salt (2.18 mmol disulfides, 80% purity according to CoB moieties).

Total yield of "CoB moieties" as disulfides: 3.696 mmol (100% pure) + 2.496 mmol (97.5% pure) + 1.744 mmol (80% pure) + 1.135 mmol (50% pure) = 9.071 mmol, 76%.

**Coenzyme B diammonium salt**

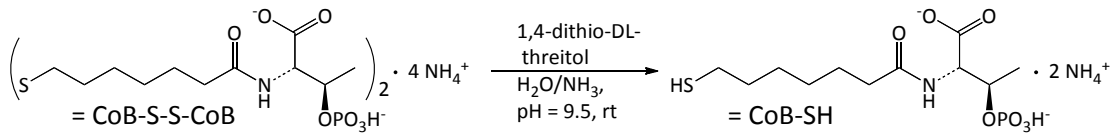


For the synthesis of CoB-SH the fractions containing the mixed disulfide with 7-mercaptoheptanoic acid were used since the latter could be removed by extraction after reducing the disulfide.
Coenzyme B disulfide tetraammonium salt (1.47 g, 80% purity according to CoB signals, 3.488 mmol CoB-component) was dissolved in 10 ml water. 1,4-Dithio-DL-threitol (617 mg, 4.0 mmol) was added and the pH was raised to 9.5 by addition of $NH_3$ (aq., conc., 0.40 ml). After stirring at rt for 2 h Amberlite IR120 (strongly acidic, 50 g) was added and allowed to stand for 30 min. The liquid was removed and the Amberlite washed with water (4 times 15 ml, until pH = 4). The combined aqueous phases were extracted with $CH_2Cl_2$ (50 ml, first phase separation overnight). This extraction with $CH_2Cl_2$ was repeated 3 times until no 7-mercaptoheptanoic acid could be detected in the

aqueous phase. The solution was made basic (pH > 10) by addition of $NH_3$ (aq., conc., 1 ml), evaporated and dried under high vacuum.
In order to get rid of 1,4-dithio-DL-threitol and its oxidized form, the residue was dissolved in 2 ml methanol and the product precipitated by addition of 15 ml diethyl ether. The precipitate was dried under high vacuum and precipitated twice again. The combined solutions were evaporated and again precipitated twice.
The solutions were evaporated and stored since they contain more CoB-SH. The combined precipitates were dissolved in 50 ml water and lyophilized to give coenzyme B diammonium salt as a microcrystalline, very hygroscopic powder (>99% pure, 410 mg, 1.09 mmol, 31%).
$^{1}$H-NMR (600 MHz, $D_2O$, dioxane = 3.700 ppm): 4.65 (*dqd*, *J* = 7.50, 6.48, 3.54, 1 H, C***H***$OPO_3^{2-}$); 4.21 (*dd*, *J* = 3.42, 1.92, 1 H, C***H***NC=O); 2.49 (*t*, *J* = 7.17, 2 H, C***H***$_2$S); 2.34 (*dt*, *J* = 14.16, 7.65, 1 H, C***H***$_2$C=O); 2.29 (*dt*, *J* = 14.16, 7.35, 1 H, C***H***$_2$C=O); 1.58 (*quint*, *J* = 7.47, 2 H, $CH_2$); 1.55 (*quint*, *J* = 7.38, 2 H, $CH_2$); 1.35 (*quintetoid*, $J_{obs}$ = 7.5, 2 H, $CH_2$); 1.29 (*quartetoid*, $J_{obs}$ = 7.0, 2 H, $CH_2$); 1.25 (*d*, *J* = 6.42, 3 H, C***H***$_3$).
$^{13}$C-NMR (150 MHz, $D_2O$, dioxane = 67.00 ppm): 177.69 (C); 176.44 (C); 73.08 (CH, $^{2}J_{CP}$ = 5.48 Hz); 60.01 (CH, $^{3}J_{CP}$ = 7.68 Hz); 36.04 ($CH_2$); 33.25 ($CH_2$); 28.11 ($CH_2$); 27.54 ($CH_2$); 25.62 ($CH_2$); 24.11 ($CH_2$); 18.86 ($CH_3$, $^{3}J_{CP}$ = 1.10 Hz).

The same procedure was applied for the starting material containing 97.5% CoB moieties in the following scale:
Coenzyme B disulfide tetraammonium salt: 1.70 g = 4.992 mmol CoB-moieties
1,4-dithio-DL-threitol: 790 mg = 5.1 mmol
water: 40 ml + $NH_3$ (conc., 0.60 ml) to give pH = 9.5
The resulting microcrystalline product was 99% pure according to CoB moieties but 2% had been oxidized to the homodisulfide. Yield: 1097.7 mg, 2.909 mmol, 59%.

**Heterodisulfide CoB-S-S-CoM**

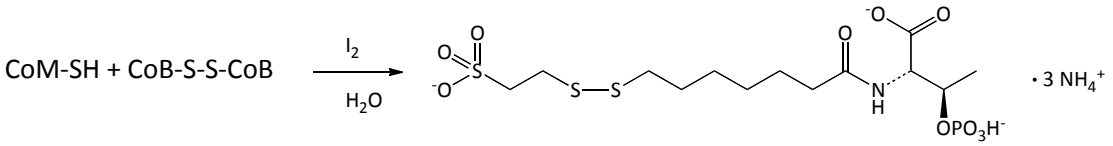


Coenzyme B disulfide tetraammonium salt (73 mg, 0.097 mmol) and coenzyme M sodium salt (330 mg, 2.0 mmol) were dissolved in water (5 ml) and $NH_3$ (aq., conc., 0.50 ml). After stirring for one hour $KI_3$ (0.5 M in water) was added dropwise until the brown color faded away very slowly. The solution was acidified with HCl (20%) to pH = 0 and loaded to an XAD-2 column conditioned as described for the purification of coenzyme B disulfide but equilibrated in 20% HCl overnight. The column was washed with HCl (aq., 1 M, 0.5 M, 0.2 M, 0.1 M and finally 0.025 M) until all coenzyme M homodisulfide had eluted (UV: $\lambda_{max}$ ca. 240 nm). The product was eluted with water, followed by methanol in water (10%, 25% and 50%). The product containing fractions (UV: $\lambda_{max}$ = 245 nm) were checked for purity ($^1$H-NMR), combined, and the pH adjuusted to 5 with $NH_3$ (aq., 100 mM). Lyophilization yielded the product as colorless beads (85 mg, 0.159 mmol, 82%).

$^1$H-NMR analysis displayed formation of 5% of each of the two homodisulfides and loss of 2% of the phosphate groups ($^1$H-NMR: 1.11 (*d*, *J* = 6.18, 3 H, C$H_3$) with a smaller line-width due to the absence of the coupling to $^{31}$P).

$^1$H-NMR (600 MHz, $D_2O$, dioxane = 3.700 ppm): 4.74 (overlapping with the solvent signal at 4.72 ppm, C***H***$OPO_3^{2-}$), 4.41 (*dd*, *J* = 2.67, 2.01, 1 H, C***H***NC=O); 3.23 (**AA'**BB', 2 H; C***H*****$_2$**$SO_3^-$), 2.98 (AA'**BB'**, 2 H; C***H*****$_2$**S), 2.73 (*t*, *J* = 7.29, 2 H, C***H*****$_2$**S); 2.35 (*dt*, *J* = 14.22, 7.53, 1 H, C***H*****$_2$**C=O); 2.31 (*dt*, *J* = 14.16, 7.32, 1 H, C***H*****$_2$**C=O); 1.65 (*quint*, *J* = 7.34, 2 H, $CH_2$); 1.59 (*quint*, *J* = 7.46, 2 H, $CH_2$); 1.38 (*quintetoid*, $J_{obs}$ = 7.3, 2 H, $CH_2$); 1.31 (*quartetoid*, $J_{obs}$ = 7.1, 2 H, $CH_2$); 1.26 (*d*, *J* = 6.42, 3 H, $CH_3$).

### 6.7.3 Isotopologues of methyl- and ethyl-coenzyme M

The different substrates were synthesized by alkylation of commercially available coenzyme M with the corresponding alkyl iodides. A slight excess of the alkylating agent was used since the corresponding sulfonium ions (formed by "overalkylation") can be detected and easily removed, whereas unreacted coenzyme M (which forms the corresponding disulfide during work up) could not always be removed. Thus some substrates contained up to 1% of coenzyme M homodisulfide.

Coenzyme M sodium salt (1.0 eq., Fluka) was dissolved anaerobically in a solution of sodium methoxide in methanol (0.5 M, 0.99 eq., Acros). Alkyl iodide (1.01 to 1.06 eq.) was added under vigorous stirring at room temperature and the reaction mixture was refluxed overnight. After evaporation of the solvent the crude product was dissolved three times in water, precipitated with acetone, and dried under high vacuum in order to remove iodide and all sulfonium ions. Crystallization from boiling ethanol/water and cooling down over several days to 4 °C gave the product as colorless plates.

**$CH_3SCH_2CH_2SO_3^-Na^+$**

Scale: $CH_3I$ (Acros): 36.7 g, 259 mmol. Yield: 21.0 g, 118 mmol, 46%.

$^1$H-NMR (600 MHz, $D_2O$, dioxane = 3.700 ppm): 3.12 (**AA'**BB', 2 H, C***H***$_2SO_3^-$); 2.80 (AA'**BB'**, 2 H, C***H***$_2SCH_3$); 2.10 ppm (*s*, 3 H; SC***H***$_3$).

$^{13}$C-NMR (150 MHz, $D_2O$, dioxane = 67.00 ppm): 51.03 (***C***$H_2SO_3^-$); 28.07 (***C***$H_2SCH_3$); 14.73 (S***C***$H_3$).

elem. anal. calcd. for $C_3H_7NaO_3S_2$ (178.21): C 20.22, H 3.96, O 26.93, Na 12.90, S 35.99; found: C 20.24, H 3.99, O 27.16, S 35.81.

**$^{12}CH_3SCH_2CH_2SO_3^-Na^+$**

$^{12}CH_3I$ was prepared from $^{12}CH_3OH$ (Cambridge Isotope Laboratories) by reaction with aqueous hydrogen iodide and purified by distillation.

Scale: $^{12}CH_3I$: 1.95 ml, 31 mmol. Yield: 2.138 g, 12.0 mmol, 40%.

$^{1}$H-NMR (600 MHz, $D_2O$, dioxane = 3.700 ppm): 3.12 (**AA'**BB', 2 H, C***H***$_2$$SO_3^-$); 2.80 (AA'**BB'**, 2 H, C***H***$_2$$SCH_3$); 2.10 (s, 3 H, C***H***$_3$). $^{13}$C-content of the $CH_3$ group according to integration of $^{1}$H-NMR spectrum: 0.00134% = 13.4 parts per million.
$^{13}$C-NMR (150 MHz, $D_2O$, dioxane = 67.00 ppm): 51.02 (***C***$H_2SO_3^-$); 28.04 (***C***$H_2SCH_3$); $CH_3$ group not detectable.
HRMS (ESI-TOF, negative ion mode): (m/z) calcd. for $C_3H_7O_3S_2$: 154.9842; found: 154.9837.

**$^{13}CH_3SCH_2CH_2SO_3^-Na^+$**
Scale: $^{13}CH_3I$ (Cambridge Isotope Laboratories): 4.45 g, 31.1 mmol. Yield: 3.3 g, 18.4 mmol, 61%.
$^{1}$H-NMR (300 MHz, $D_2O$, dioxane = 3.700 ppm): 3.12 (**AA'**BB', 2 H, C***H***$_2$$SO_3^-$); 2.81 (AA'**BB'**, 2 H, C***H***$_2$$S^{13}CH_3$); 2.10 (*d*, *J* = 139.1, 3 H, $S^{13}C$***H***$_3$).
$^{13}$C-NMR (75 MHz, $D_2O$, dioxane = 67.00 ppm): 51.09 (***C***$H_2SO_3^-$); 28.22 (***C***$H_2S^{13}CH_3$); 14.93 ($S^{13}$***C***$H_3$).

**$CH_2DSCH_2CH_2SO_3^-Na^+$**
$CH_2DI$ was prepared from $CH_2DOH$ (Cambridge Isotope Laboratories) by reaction with aqueous hydrogen iodide and purified by distillation.
Scale: $CH_2DI$: 3.219 g, 22.5 mmol. Yield: 2.915 g, 16.27 mmol, 74%.
$^{1}$H-NMR (300 MHz, $D_2O$, dioxane = 3.700 ppm): 3.12 (**AA'**BB', 2 H, C***H***$_2$$SO_3^-$); 2.80 (AA'**BB'**, 2 H, C***H***$_2$$SCH_2D$); 2.08 ($t_{111}$, *J* = 1.8, 2 H, SC***H***$_2$D).

**$CHD_2SCH_2CH_2SO_3^-Na^+$**
$CHD_2I$ was prepared from $CHD_2OH$ (Cambridge Isotope Laboratories) by reaction with aqueous hydrogen iodide and purified by distillation.
Scale: $CHD_2I$: 3.29 g, 22.9 mmol. Yield: 3.2 g, 17.8 mmol, 81%.
$^{1}$H-NMR (300 MHz, $D_2O$, dioxane = 3.700 ppm): 3.12 (**AA'**BB', 2 H, C***H***$_2$$SO_3^-$); 2.80 (AA'**BB'**, 2 H, C***H***$_2$$SCHD_2$); 2.07 ($quint_{12321}$, *J* = 1.9, 1 H, SC***H***$D_2$).

**$CD_3SCH_2CH_2SO_3^-Na^+$**

Scale: $CD_3I$ (Dr. Glaser AG): 1.5 g, 10.3 mmol. Yield: 1.272 g, 7.02 mmol, 70%.

$^1$H-NMR (300 MHz, $D_2O$, dioxane = 3.700 ppm): 3.12 (**AA'**BB', 2 H, C***H*****$_2$**$SO_3^-$); 2.80 (AA'**BB'**, 2 H; C***H*****$_2$**$SCD_3$).

$^{13}$C-NMR (150 MHz, $D_2O$, dioxane = 67.00 ppm): 51.07 (***C***$H_2SO_3^-$); 27.92 (***C***$H_2SCD_3$); 14.02 (*sept*$_{1367631}$, *J* = 21.3, S***C***$D_3$).

**$CH_3CH_2SCH_2CH_2SO_3^-Na^+$**

Scale: $CH_3CH_2I$ (Fluka): 4.02 g, 25.8 mmol. Yield: 3.68 g, 19.1 mmol, 76%.

$^1$H-NMR (600 MHz, $D_2O$, dioxane = 3.700 ppm): 3.10 (**AA'**BB', 2 H, C***H*****$_2$**$SO_3^-$); 2.84 (AA'**BB'**, 2 H, C***H*****$_2$**$SCH_2CH_3$), 2.57 (*q*, *J* = 7.4, 2 H, SC***H*****$_2$**$CH_3$); 1.19 (*t*, *J* = 7.4, 3 H, $CH_2C$***H*****$_3$**).

$^{13}$C-NMR (75 MHz, $D_2O$, dioxane = 67.00 ppm): 51.51 (***C***$H_2SO_3^-$); 25.74 (S***C***$H_2CH_3$); 25.52 (***C***$H_2SCH_2CH_3$); 14.39 ($CH_2SCH_2$***C***$H_3$).

elem. anal. calcd. for $C_4H_9O_3NaS_2$ (192.24): C 24.99, H 4.72, O 24.97, Na 11.96, S 33.36; found: C 24.40, H 4.77, O 25.67, S 33.01.

**$CH_3{}^{13}CH_2SCH_2CH_2SO_3^-Na^+$**

Scale: $CH_3{}^{13}CH_2I$ (Cambridge Isotope Laboratories): 2.008 g, 12.79 mmol. Yield: 1.576 g, 8.16 mmol, 67%.

$^1$H-NMR (600 MHz, $D_2O$, dioxane = 3.700 ppm): 3.10 (**AA'**BB', 2 H, C***H*****$_2$**$SO_3^-$); 2.84 (AA'**BB'**, $^3J_{CH}$ = 4.1, 2 H, C***H*****$_2$**$SCH_2CH_3$); 2.56 (*dq*, $^1J_{CH}$ = 139.8, $^3J_{HH}$ = 7.4, 2 H, S$^{13}$C***H*****$_2$**$CH_3$); 1.19 (*qd*, $^3J_{HH}$ = 7.4, $^2J_{CH}$ = 4.7, 3 H, S$^{13}CH_2C$***H*****$_3$**).

The $^{13}$C content of the S-*$^{13}$*$CH_2CH_3$ group was determined from the integration of the $^1$H-NMR spectrum: 99.0%.

$^{13}$C-NMR (75 MHz, $D_2O$, dioxane = 67.00 ppm): 51.45 (***C***$H_2SO_3^-$); 25.58 ($CH_2S$***$^{13}$C***$H_2CH_3$); 25.34 (***C***$H_2S^{13}CH_2CH_3$); 14.16 ($CH_2S^{13}CH_2$***C***$H_3$, $^1J_{CC}$ = 34.8 Hz).

**$^{13}CH_3{}^{13}CH_2SCH_2CH_2SO_3^-Na^+$**

Scale: $^{13}CH_3{}^{13}CH_2I$ (Cambridge Isotope Laboratories): 1.04 g, 6.6 mmol. Yield: 838 mg, 4.3 mmol, 72%.

$^1$H-NMR (300 MHz, $D_2O$, dioxane = 3.700 ppm): 3.11 (**AA'**BB', 2 H, C***H*****$_2$**$SO_3^-$); 2.84 (AA'**BB'**, 2 H; C***H*****$_2$**$S^{13}CH_2{}^{13}CH_3$); 2.57 (*dqd*, $^1J_{CH}$ = 139.2, $^3J_{HH}$ = 7.4, $^2J_{CH}$ = 3.8, 2 H, $S^{13}C$***H*****$_2{}^{13}CH_3$); 1.19 (*dtd*, $^1J_{CH}$ = 127.3, $^3J_{HH}$ = 7.4, $^2J_{CH}$ = 4.8, 3 H, $S^{13}CH_2{}^{13}C$***H*****$_3$**).

$^{13}$C-NMR (150 MHz, $D_2O$, dioxane = 67.00 ppm): 51.44 (***C***$H_2SO_3^-$); 25.57 (*d*, $^1J_{CC}$ = 35.1, $S^{13}$***C***$H_2{}^{13}CH_3$); 25.35 (*dd*, $^2J_{CC}$ = 2.0, $^3J_{CC}$ = 0.7, ***C***$H_2S^{13}CH_2{}^{13}CH_3$ ); 14.16 (*d*, $^1J_{CC}$ = 35.1, $S^{13}CH_2{}^{13}$***C***$H_3$).

**$CH_3CD_2SCH_2CH_2SO_3^-Na^+$**

Scale: $CH_3CD_2I$ (Cambridge Isotope Laboratories): 1.72 g, 10.89 mmol. Yield: 1.368 g, 7.04 mmol, 70%.

$^1$H-NMR (600 MHz, $D_2O$, dioxane = 3.700 ppm): 3.10 (**AA'**BB', 2 H , C***H*****$_2$**$SO_3^-$); 2.84 (AA'**BB'**, 2 H, C***H*****$_2$**$SCD_2CH_3$); 1.17 (*quint*$_{12321}$, *J* = 0.9, 3 H, $CD_2C$***H*****$_3$**).

$^{13}$C-NMR (150 MHz, $D_2O$, dioxane = 67.00 ppm): 51.46 (***C***$H_2SO_3^-$); 25.28 (***C***$H_2SCD_2CH_3$); 24.99 (*quint*$_{12321}$, *J* = 21.2, S***C***$D_2CH_3$); 13.93 ($SCD_2$***C***$H_3$).

**$CD_3CD_2SCH_2CH_2SO_3^-Na^+$**

Scale: $CD_3CD_2I$ (Cambridge Isotope Laboratories): 1.90 g, 11.5 mmol. Yield: 1.107 g, 5.6 mmol, 56%.

$^1$H-NMR (600 MHz, $D_2O$, dioxane = 3.700 ppm): 3.10 (**AA'**BB', 2 H, C***H*****$_2$**$SO_3^-$); 2.84 (AA'**BB'**, 2 H, C***H*****$_2$**$SCD_2CD_3$).

$^{13}$C-NMR (150 MHz, $D_2O$, dioxane = 67.00 ppm): 51.49 (***C***$H_2SO_3^-$); 25.34 (***C***$H_2SCD_2CD_3$); 24.79 (*quint*$_{12321}$, *J* = 21.6, S***C***$D_2CD_3$); 13.13 (*sept*$_{1367631}$, *J* = 21.6, $SCD_2CD_3$).

**$CH_3CH_2CH_2SCH_2CH_2SO_3^-Na^+$**

Scale: $CH_3CH_2CH_2I$ (Aldrich): 4.42 g, 26.0 mmol. Yield: 3.715 g, 18.0 mmol, 72%.

$^1$H-NMR (300 MHz, $D_2O$, dioxane = 3.700 ppm): 3.10 (**AA'**BB', 2 H, C***H*****$_2$**$SO_3^-$); 2.83 (AA'**BB'**, 2 H, C***H*****$_2$**$SCH_2CH_2CH_3$); 2.54 (*t*, *J* = 7.3, 2 H, $SC$***H*****$_2$**$CH_2CH_3$); 1.56 (*sext*, *J* = 7.4, 2 H, $SCH_2C$***H*****$_2$**$CH_3$); 0.91 (*t*, *J* = 7.3, 3 H, $SCH_2CH_2C$***H*****$_3$**).

$^{13}$C-NMR (75 MHz, $D_2O$, dioxane = 67.00 ppm): 51.54 (***C***$H_2SO_3^-$); 33.72 ($SC$***C***$H_2CH_2CH_3$); 25.83 (***C***$H_2SCH_2CH_2CH_3$); 22.64 ($SCH_2$***C***$H_2CH_3$); 13.17 ($SCH_2CH_2$***C***$H_3$).

**$CH_2$=CHCH$_2$SCH$_2$CH$_2$SO$_3^-$Na$^+$**

Scale: Allyl iodide (Fluka, freshly distilled at rt into a cold trap in $N_2$(l)): 4.39 g, 26 mmol. Yield: 3.03 g, 14.8 mmol, 59%.

$^1$H-NMR (300 MHz, $D_2O$, dioxane = 3.700 ppm): 5.79 (*ddt*, *J* = 16.9, 10.0, 7.2, 1 H, $SCH_2C$***H***$=CH_2$); 5.15 (*d"quartetoid"*, *J* = 17.1, 1.5, 1 H, $SCH_2CH=C$***H*****$_2$**(*trans*-coupling)); 5.12 (*d"quartetoid"*, *J* = 10.0, 0.9, 1 H, $SCH_2CH=C$***H*****$_2$**(*cis*-coupling)); 3.18 (*d"tripletoid"*, *J* = 7.2, 0.9, 2 H, $SC$***H*****$_2$**$CH=CH_2$); 3.09 (**AA'**BB', 2 H, C***H*****$_2$**$SO_3^-$); 2.78 (AA'**BB'**, 2 H, C***H*****$_2$**$SCH_2CH=CH_2$).

$^{13}$C-NMR (75 MHz, $D_2O$, dioxane = 67.00 ppm): 133.95 ($SCH_2$***C***$H=CH_2$); 118.26 ($SCH_2CH=$***C***$H_2$); 51.26 (***C***$H_2SO_3^-$); 34.21 ($SC$***C***$H_2CH=CH_2$); 25.52 (***C***$H_2SCH_2CH=CH_2$).

**Side product Dimethylsulfonium-CoM**

$^1$H-NMR (300 MHz, $D_2O$, dioxane = 3.700 ppm): 3.62 (*t*, *J* = 7.2 , 2 H, $CH_2$); 3.37 (*t*, *J* = 7.1, 2 H, $CH_2$); 2.93 (*s*, 6 H, $CH_3$).

### 6.7.4 Alkyl-coenzyme M sulfoxides and sulfones

The oxidized substrates were synthesized by non-optimized procedures via oxidation with hydrogen peroxide. A small excess of neutral hydrogen peroxide led to selective formation of the corresponding sulfoxides. Addition of excess hydrogen peroxide in combination with a strong acid or base yielded the corresponding sulfone.

**$CH_3(S{=}O)CH_2CH_2SO_3^-Na^+$**

Methyl-coenzyme M sodium salt (360 mg, 2.0 mmol) was added under ice cooling to a stirred solution of aqueous hydrogen peroxide (10%, 0.90 ml, 3.0 mmol). Potassium iodide (ca. 2 mg) was added after stirring for one h in order to remove some of the excess hydrogen peroxide. The product was precipitated by addition of ethanol under ice cooling, centrifuged, washed with ethanol, and centrifuged again. Drying under high vacuum yielded the product as a colorless powder (130 mg, 0.67 mmol, 33%).

$^1$H-NMR (600 MHz, $D_2O$, dioxane = 3.700 ppm): 3.23-3.30 (*m*, 3 H, $CH_2CH_2$); 3.11-3.19 (*m*, 1 H, $CH_2CH_2$); 2.71 (*s*, 3 H, $CH_3$).

HRMS (ESI-TOF, negative ion mode): (m/z) calcd. for $C_3H_7O_4S_2$: 170.9791; found: 170.9785.

**$CH_3CH_2(S{=}O)CH_2CH_2SO_3^-Na^+$**

Ethyl-coenzyme M sodium salt (385 mg, 2.0 mmol) was added under ice cooling to a stirred solution of aqueous hydrogen peroxide (10%, 0.90 ml, 3.0 mmol). Potassium iodide (ca. 2 mg) was added after stirring for 2 h in order to remove some of the excess hydrogen peroxide. The product was precipitated by addition of acetone under ice cooling, centrifuged, washed with acetone, and centrifuged again. All acetone solutions were diluted and immediately disposed. Drying the precipitate under high vacuum yielded the product as a colorless powder (270 mg, 1.3 mmol, 65%).

$^{1}$H-NMR (600 MHz, $D_2O$, dioxane = 3.700 ppm): 3.19-3.29 (*m*, 3 H, $CH_2CH_2$); 3.09-3.15 (*m*, 1 H, $CH_2CH_2$); 2.95 (*dq*, *J* = 13.6, 7.6, 1 H, $SC\boldsymbol{H_2}CH_3$); 2.85 (*dq*, *J* = 13.6, 7.4, 1 H, $SC\boldsymbol{H_2}CH_3$); 1.27 (*t*, *J* = 7.5, 3 H, $SCH_2C\boldsymbol{H_3}$).

HRMS (ESI-TOF, negative ion mode): (m/z) calcd. for $C_4H_9O_4S_2$: 184.9948; found: 184.9943.

**$CH_3CD_2(S{=}O)CH_2CH_2SO_3^-Na^+$**

[1′,1′-$d_2$]-Ethyl-coenzyme M sodium salt (194.2 mg, 1.0 mmol) was added under ice cooling to a stirred solution of aqueous hydrogen peroxide (10%, 0.45 ml, 1.5 mmol). Because NMR analysis revealed only 88% conversion, the solution was warmed to 45 °C for 5 min which lead to full conversion.

Sodium iodide (ca. 5 mg) was added in order to remove some of the excess hydrogen peroxide. Sodium hydroxide (3 drops 1.0 M) was added to remove the yellow color. After stirring for 3 hours the product was precipitated by addition of acetone under ice cooling, centrifuged, washed with acetone, and centrifuged again. All acetone solutions were diluted and immediately disposed. Drying the precipitate under high vacuum yielded the product as a colorless powder (130 mg, 0.62 mmol, 62%).

$^{1}$H-NMR (600 MHz, $D_2O$, dioxane = 3.700 ppm): 3.16-3.30 (*m*, 3 H, $CH_2CH_2$); 3.09-3.16 (*m*, 1 H, $CH_2CH_2$); 1.26 (*s* (br), $SCD_2C\boldsymbol{H_3}$).

$^{13}$C-NMR (150 MHz, $D_2O$, dioxane = 67.00 ppm): 45.31 ($CH_2$); 44.51 ($CH_2$); 44.37 ($quint_{12321}$, $^{1}J_{CD}$ = 21.2, $CD_2$); 6.18 ($CH_3$).

$^{2}$H-NMR (92 MHz, $H_2O$, dioxane-$d_8$ = 3.700 ppm): 2.97 (*s* (br), 1 D, $CD_2$); 2.87 (*s* (br), 1 D, $CD_2$).

**$CH_3(SO_2)CH_2CH_2SO_3^-Na^+$**

Methyl-coenzyme M sodium salt (360 mg, 2.0 mmol) was added under ice cooling to a stirred solution of aqueous hydrogen peroxide (30%, 1.0 ml, 10 mmol). NMR analysis revealed the selective formation of the sulfoxide. Additional hydrogen peroxide (30%, 1.0 ml, 10 mmol) and sodium hydroxide (one pellet, ca. 0.5 g) were added and dissolved in the ultrasonic bath. NMR analysis showed full conversion to the sulfone. The aqueous product was precipitated 3 times and washed with ethanol. Because it was still very basic, The solution was neutralized with acetic acid to pH = 5 and precipitated 4 times in the same way. Drying under high vacuum for 3 days yielded the product as a colorless powder (240 mg, 1.14 mmol, 57%).

$^1$H-NMR (600 MHz, $D_2O$, dioxane = 3.700 ppm): 3.59 (**AA'**BB', 2 H, $CH_2$); 3.31 (AA'**BB'**, 2 H, $CH_2$); 3.12 (*t*, *J* = 0.6, 3 H, $CH_3$).

**$CH_3CH_2(SO_2)CH_2CH_2SO_3^-Na^+$**

Ethyl-coenzyme M sulfoxide sodium salt (50 mg, 0.24 mmol) was added under ice cooling to a stirred solution of aqueous hydrogen peroxide (10%, 0.9 ml, 3 mmol). Trifluoroacetic acid (0.2 ml) was added and the solution stirred for 1 h. After removal of some of the excess hydrogen peroxide with potassium iodide (ca. 5 mg), the product was precipitated with acetone, centrifuged and dried under high vacuum. All acetone solutions were diluted and immediately disposed. The product (ca. 20 mg) still contained some sulfoxide as well as an unknown impurity ($^1$H-NMR: *s* at 3.2 ppm).

$^1$H-NMR (600 MHz, $D_2O$, dioxane = 3.700 ppm): 3.54 (**AA'**BB', 2 H, $CH_2$); 3.30 (AA'**BB'**, 2 H, $CH_2$); 3.25 (*q*, *J* = 7.5, 2 H, $SCH_2CH_3$); 1.32 (t, *J* = 7.5, 3 H, $CH_2CH_3$).

## 6.8 Simulation with the Program Copasi

### 6.8.1 Simulation of $^{13}C$ scambling and D incorporation kinetics of the MCR-catalyzed reaction of $CH_3{}^{13}CH_2$-S-CoM in $D_2O$

The experimental data consisted of the concentration versus time profiles of the 24 isotopologues as determined by $^{13}C$-NMR with simultaneous $^{1}H$ and $^{2}H$ decoupling.
Points for the time series 0, 2, 4, 8, 16 and 32 min were available. The conversion to ethane (all isotopologues) was determined by $^{1}H$-NMR through the $^{1}H$ integral of the ethyl-coenzyme M signals (both $CH_2$ group of the "CoM-moiety") relative to the disulfides formed.

Simulations were performed with COPASI version 4.6 (build 32)[135].
The kinetic model consisted of 4 steps connecting the "free enzyme plus substrates" (E+S1+S2) with the "free enzyme plus products" (E+P) states via two ternary complexes (**figure 6.15**).

Step 1. Binding of ethyl-coenzyme M
Step 2. Binding of Coenzyme B
Step 3. Isomerization of the ternary complex
Step 4. Product release (rate limiting, combined into a single step because no details about the order or randomness of product release are known)

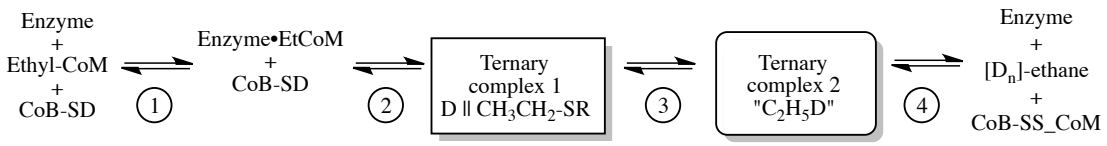


**Figure 6.15**: Reaction steps simulated for the formation of ethane and isotope exchange in ethyl-coenzyme M.

All four reactions were simulated as reversible. The thermodynamics of substrate binding was modeled using the best estimates for the $K_M$ values of ethyl-coenzyme M (20 mM) and coenzyme B (0.1 mM) as guesses for the ratio of on and off rate constants ($K_S$). For the "combined" product release a $K_M^{app}$ value of 20 mM was used because it is known that the reverse reaction (activation of ethane) is much slower than the forward reaction.

Free parameters in the kinetic model were the rates of substrate binding (1&2), the rate of isomerization (3) and the equilibrium constant between the ternary complexes, and the rate of product release (4). *Free* coenzyme B was assumed to be able to exchange the R-SH group with $D_2O$ to give R-SD at a high rate.

Exchange of protons/deuterons from solvent into the active site of ternary complexes was excluded because it is known that no deuterium is incorporated into substrates in the reverse reaction with methane (activation of methane by MCR in deuterated medium), which points to a shielded active site for the two ternary complexes.

Formally, a hydrogen (brought into the active site via the SH group of coenzyme B) replaces the sulfur of coenzyme M in the isomerization (step 3). In the reverse isomerization, sulfur replaces one of the hydrogens in the "ethane" moiety present in the second ternary complex. Whereas this hydrogen isotope is always D in the forward direction (the solvent is fully deuterated), the hydrogen isotope activated in the reverse direction can be D or H with a probability that depends on statistics and possible isotope effects and is different for different isotopologues. Because one of the carbons of the ethyl moiety is $^{13}C$-labeled, activation occurring at one or the other methyl group of the "ethane" moiety of the second ternary complex can be distinguished in both the experiment and the kinetic model.

The rate constants were modeled as a base rate multiplied by statistical factors and divided by the primary and secondary isotope effects, which were assumed to obey the product rule. Six isotope effects were

defined as free parameters: the 1°KIEs for the forward and the backward isomerization, the 2°αKIE and the 2°βKIE, each for the forward and the backward reaction. All isomerization rate constants were then calculated from the free parameters $k_H^{fwd}$ or $k_H^{bck}$ by dividing by the appropriate product of isotope effects.

e.g. $k_{D\alpha\beta3}^{bck} = k_H^{bck} / [1°KIE^{bck} \bullet 2°\alpha KIE^{bck} \bullet (2°\beta KIE^{bck})^3]$

No potential isotope effects on binding equilibria were considered and the two methyl ends of the "ethane" moiety in the second ternary complex were considered to react with equal probability in the backwards isomerization.

The two $CH_2$ hydrogens of the ethyl group in ethyl-S-CoM are enantiotopic. The model considered $CL_3CHD$-S-CoM species with (1'*R*) and (1'*S*) configuration separately but for the comparison with the NMR data their concentrations were added.

The experimentally observed slow decay of enzyme activity with time at 60 °C was simulated with an irreversible deactivation reaction of free enzyme: $E \rightarrow E_{dead}$.

As an example, the possible isomerization reactions for one of the dideuterated ternary complexes "$^{13}CH_2DCH_2D$" are shown in **figure 6.16**.

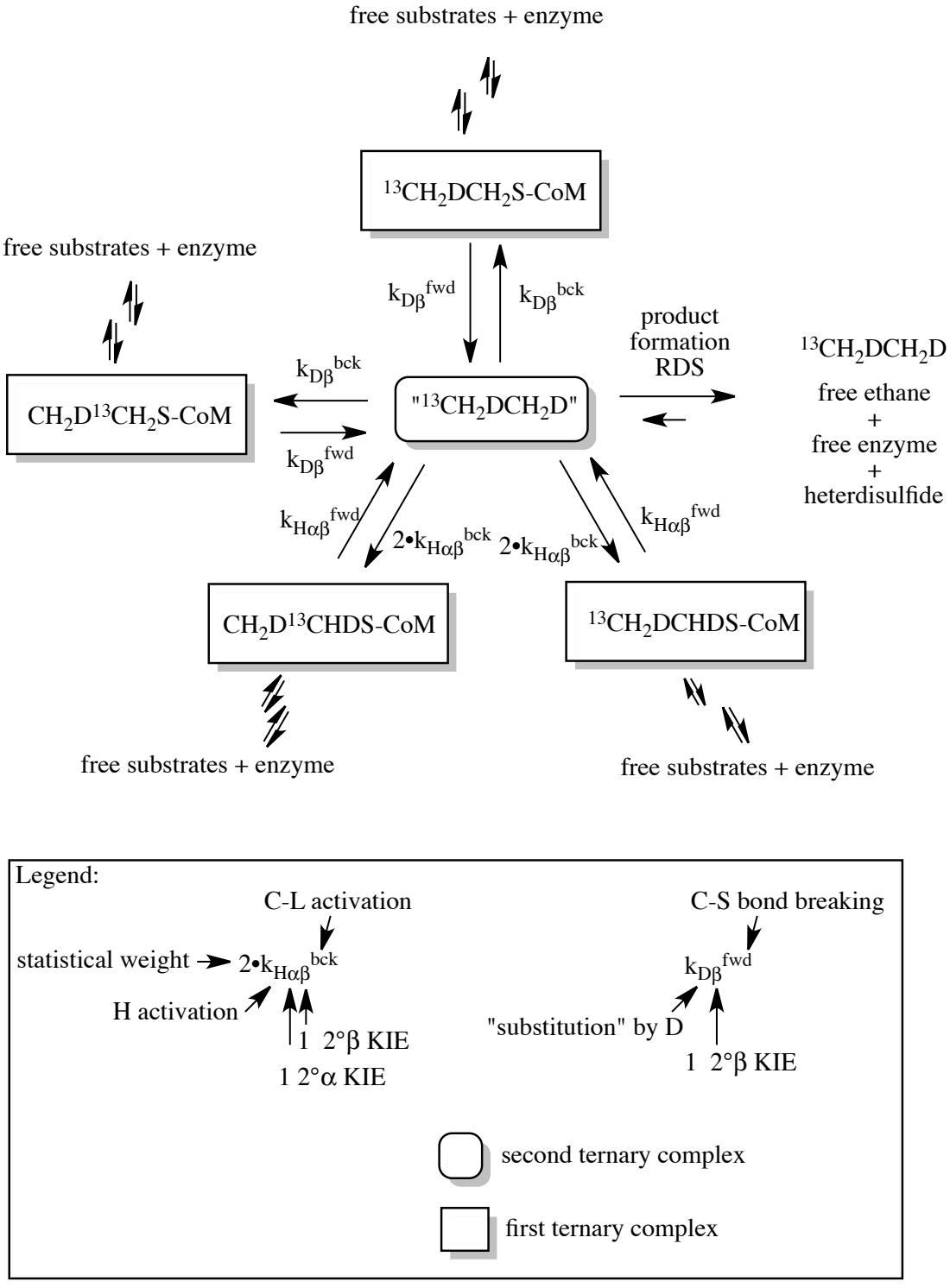


**Figure 6.16**: Isomerization reactions from the second ternary complex ("intermediate").

### 6.8.2 Results of the simulation without isotope effects

Substrate binding for both Et-S-CoM and CoB-SD was assumed to be very fast ($k_{on}$ = $1 \bullet 10^8$ $s^{-1}M^{-1}$ and $1 \bullet 10^7$ $s^{-1}M^{-1}$, respectively). The rate determining $k_{off}$ for products was adjusted to give the experimentally observed conversion of 5% after 32 min. The equilibrium constant for isomerization was set as $K_{iso}$ = 1 and the forward isomerization rate $k_H^{fwd}$ was adjusted to give the correct initial rate of formation of the monodeuterated substrates. In contrast to the experimental data, the simulated curves showed maxima not only for the monodeuterated but also for the dideuterated substrates. Therefore, the enzyme deactivation rate $k_{dead}$ was adjusted to reproduce the experimental curves at time ≥ 8 min (**figure 6.17 A and B**).

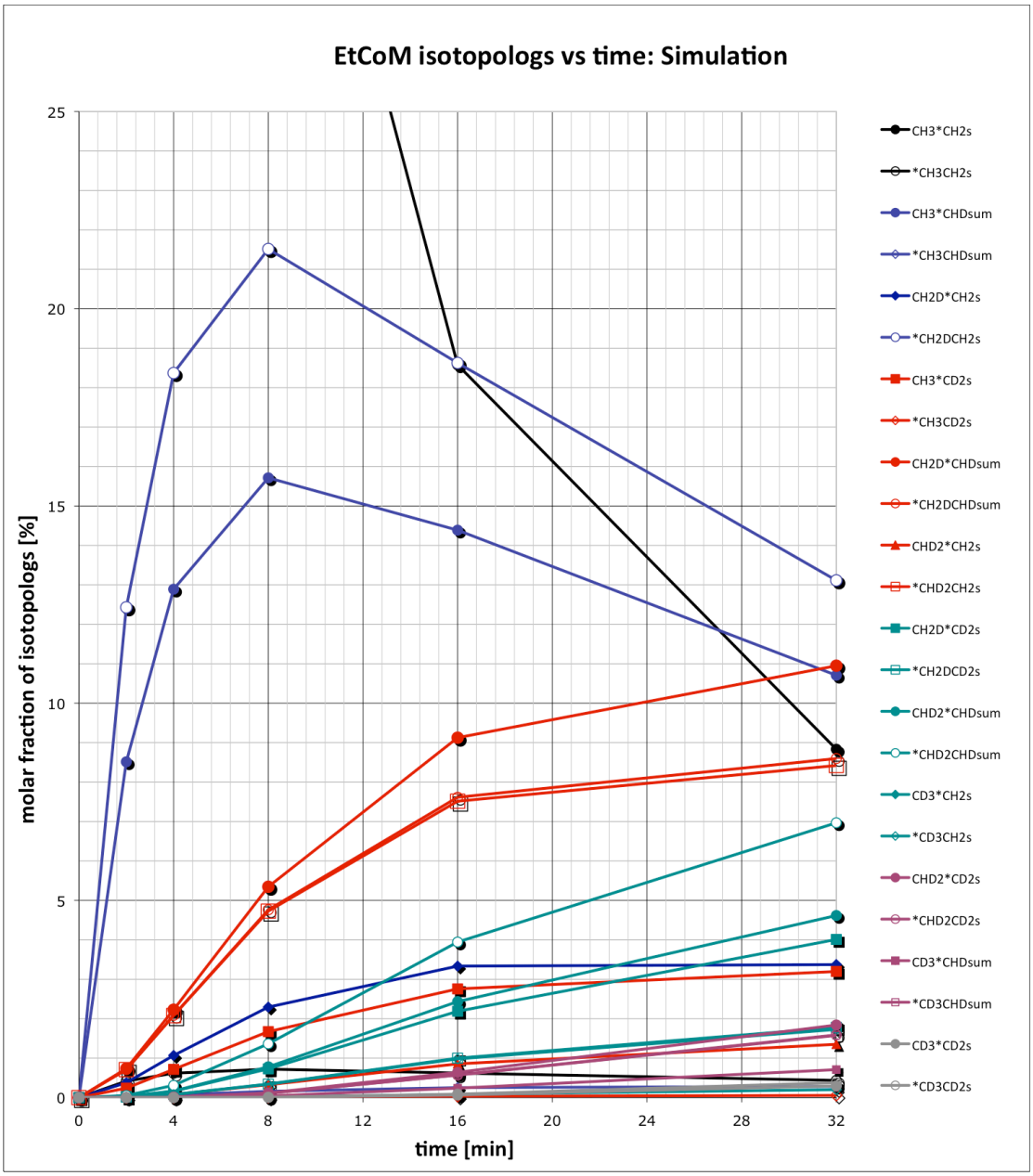


**Figure 6.17 A**: Simulation without isotope effects.

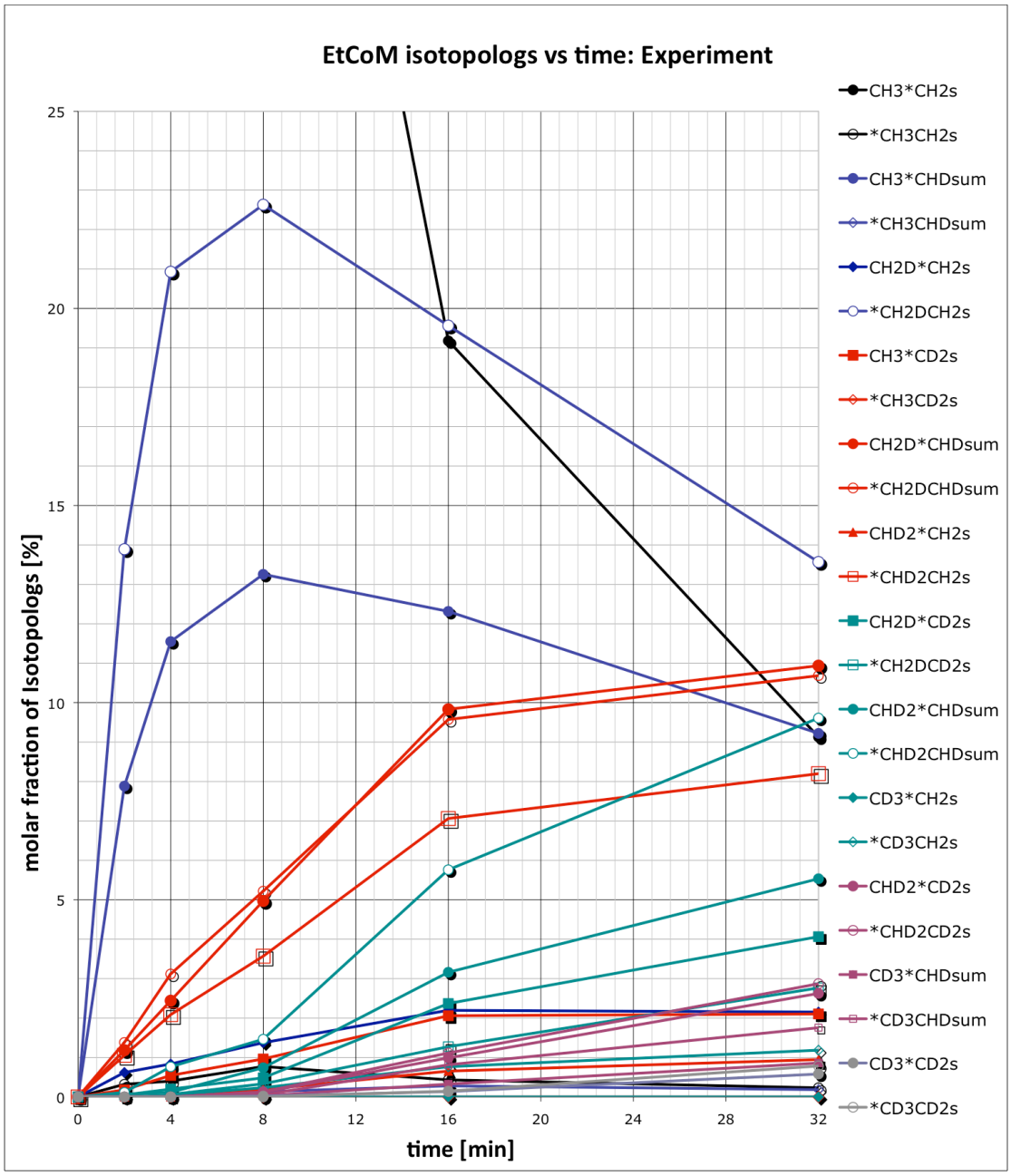


**Figure 6.17 B**: Experimental data (same figure as 4.8).

The most obvious discrepancies between simulation and experiment are the ratios among the three monodeuterated species, and among the five dideuterated species.

### 6.8.3 Results of simulations including isotope effects

Variation of the two primary isotope effects ($1°KIE^{fwd}$ and $1°KIE^{bck}$) and the two secondary α-isoptope effects ($2°\alpha KIE^{fwd}$ and $2°\alpha KIE^{bck}$) gave a reasonable reproduction of the experimental curves with the values $1°KIE^{fwd} = 1.1$, $1°KIE^{bck} = 2.5$, $2°\alpha KIE^{fwd} = 1.25$, $2°\alpha KIE^{bck} = 1.25$ (**figure 6.18 A and B**).

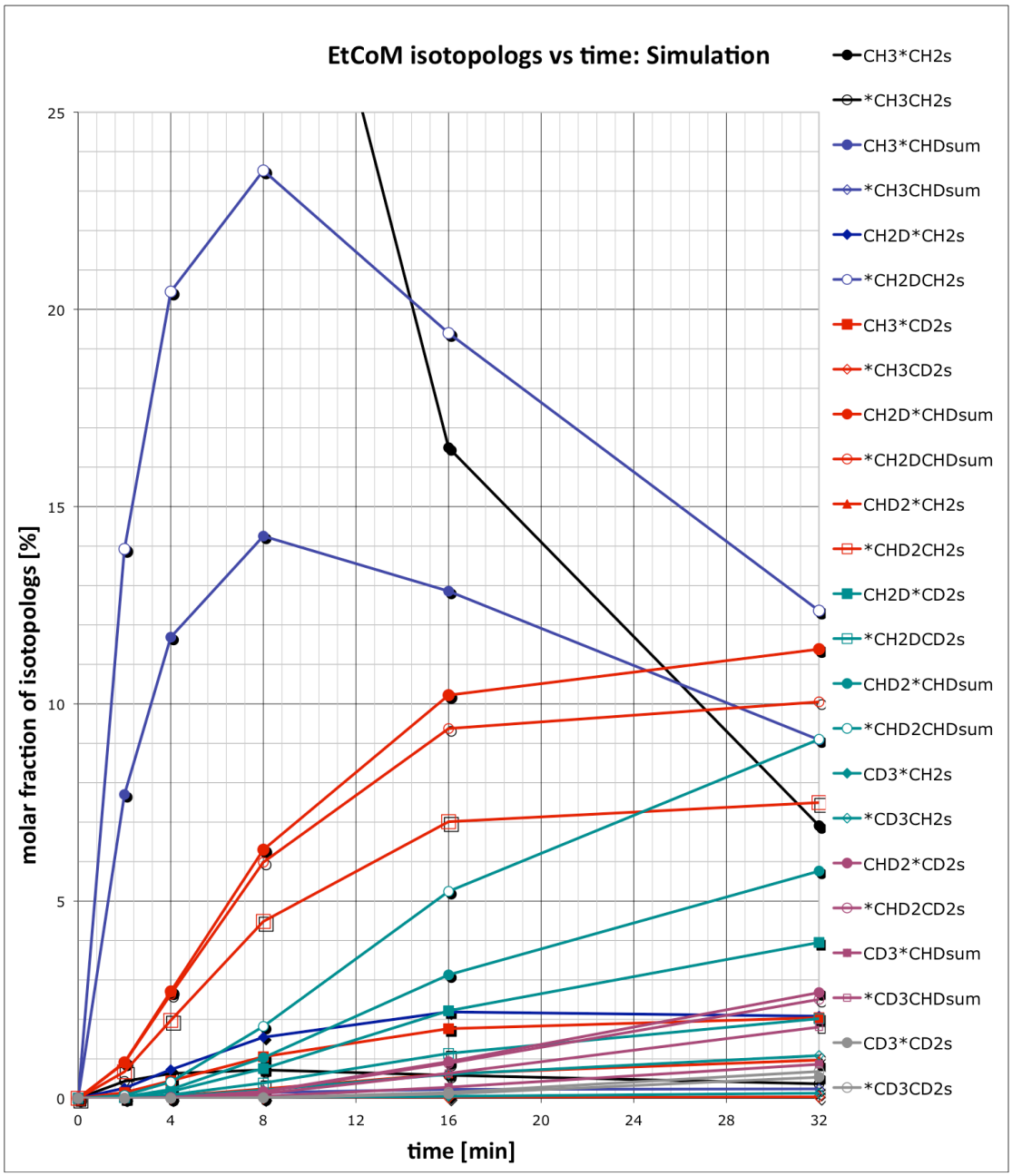


**Figure 6.18 A**: Simulation including isotope effects (same figure as 4.9).

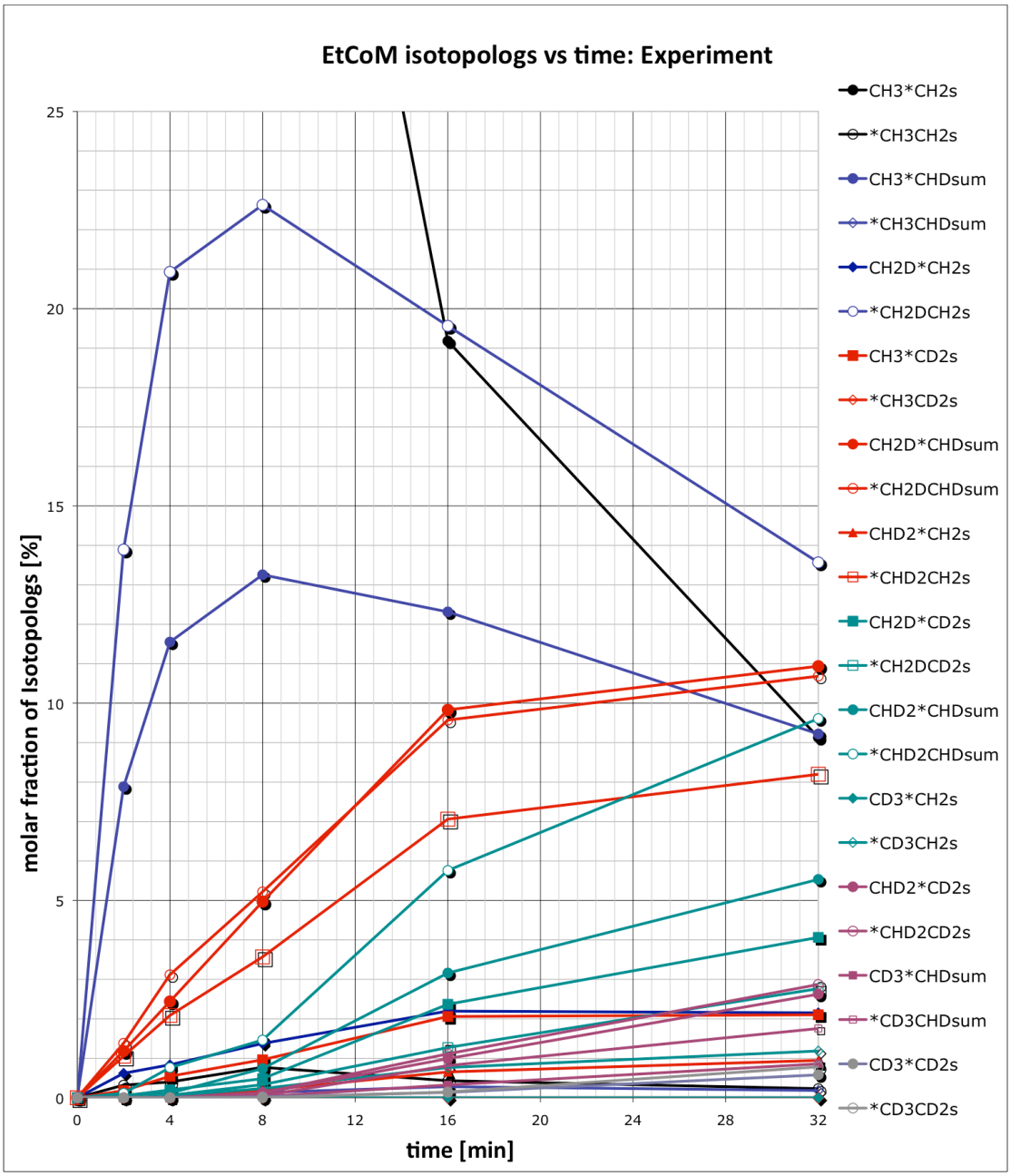


**Figure 6.18 B**: Experimental data (same figure as 4.8).

**Remaining discrepancies:**

Although the initial rates of formation of the two major monodeuterated species (blue) are correct, the maximal values at 8 min are slightly too high. The rates of formation of the two major doubly deuterated forms (red) are predicted to be slightly different in the simulation, whereas they are practically identical in the experiment. In the simulation the dideuterated species (red) show a small lag (2 min, 4 min values) whereas these curves are not sigmaoidal in the experiment. The rate of disappearance of the non-deuterated initial substrate (black) is slightly too high in the simulation.

### 6.8.4 Simulation of kinetics of the MCR-catalyzed reaction of $CH_3CDT$-S-CoM in $H_2O$

The model is chemical, no substrate binding and product release is considered.

Nomenclature used: $CH_3CDTs$ is the enantiomer of $CH_3CTDs$ and $CH_3CDTH$ is the enantiomer of $CH_3CTDH$.

The forward reaction corresponds to the "substitution" of sulfur in Et-S-CoM by "$H^-$" with basic rate constant $k_s$. Only H is considered, since the reaction was run in $H_2O$.

The backward reaction is the "substitution" of one hydrogen ($^1H$) in the intermediate by S to give back Et-S-CoM. The basic rate constant is $k_H$. Backward reactions abstracting a D or T are irreversible because only H is present in the forward reaction with the rate constants $k_D$ and $k_T$ for the activation of $^2H$ and $^3H$, respectively.

Both reactions, forward substitution of S by H and reverse activation ("substitution" of H/D/T by S), are assumed to occur with pure inversion of configuration.

Rate constants $k_H$ are statistically weighted by the number of H atoms that can be abstracted for a given intermediate.

The rate constants can be modified further by isotope effects. KIE is the primary H/D isotope effect for the activation ($k_H/k_D$). No primary IE is

considered for the forward substitution (always $^1H$). The tritium isotope effects are calculated from the deuterium IE according to Swain-Schaad with an exponent of 1.442. Secondary isotope effects are considered whenever a non-$^1H$ isotope is geminal to that activated or present in the $CH_3CH_2$-S group during forward substitution. For geminal D and T, the product rule is assumed to be valid for the secondary IEs.

The product (free ethane) is formed from each of the 5 isotopologs of the intermediate with rate constant $k_f$. The ratio of $k_f/k_b$ (commitment) is one of the free parameters of the system.

Initially, there are 4 species (2 mM total according to Floss). The two enantiomeric T-, D-labeled substrates are present according to the %ee estimated for the substrate by Floss (75% max.) and the dilution (1.4/28000) corresponding to the activity (1.6 mCi and 2.8 mCi) given by Floss. Most of the substrate is $CH_3CDH$-S-CoM and $CH_3CHD$-S-CoM (where H replaces the T), again in a ratio corresponding to the %ee of 75%.

The product $CH_3CTH_2$ is counted but achiral. In the F-value analysis of acetate, this material behaves as if it were racemic (F value near 50%).

The %ee of the ethane is therefore calculated as:

$|(CH_3CDHT - CH_3CHDT)|/(CH_3CDHT + CH_3CHDT + CH_3CTH_2)$.

The radiochemical yield (%act) is calculated as the sum of tritiated free ethane species divided by the sum of the initial concentrations of $CH_3CDT$-S-CoM and $CH_3CTD$-S-CoM.

**Choice of parameters:**

The commitment was set to 0.01, roughly corresponding to the results obtained with the enzyme.

The basic rate constant was set to give a total conversion of ca. 25% in 10 h (in Floss' experiments reaction with cell free extract overnight gave 28% conversion for the *R*-substrate and 10.3% for the *S*-substrate).

**Results without isotope effects:**

In the first simulation, a complete absence of isotope effects was assumed. This results in a loss of %ee from 75% (initial) down to ca. 38% and a conversion of 28% in 10 h. The calculated radiochemical yield is 5.8%. At 10% conversion, these values are %ee: 44% radiochemical yield 5% (**figure 6.19**).

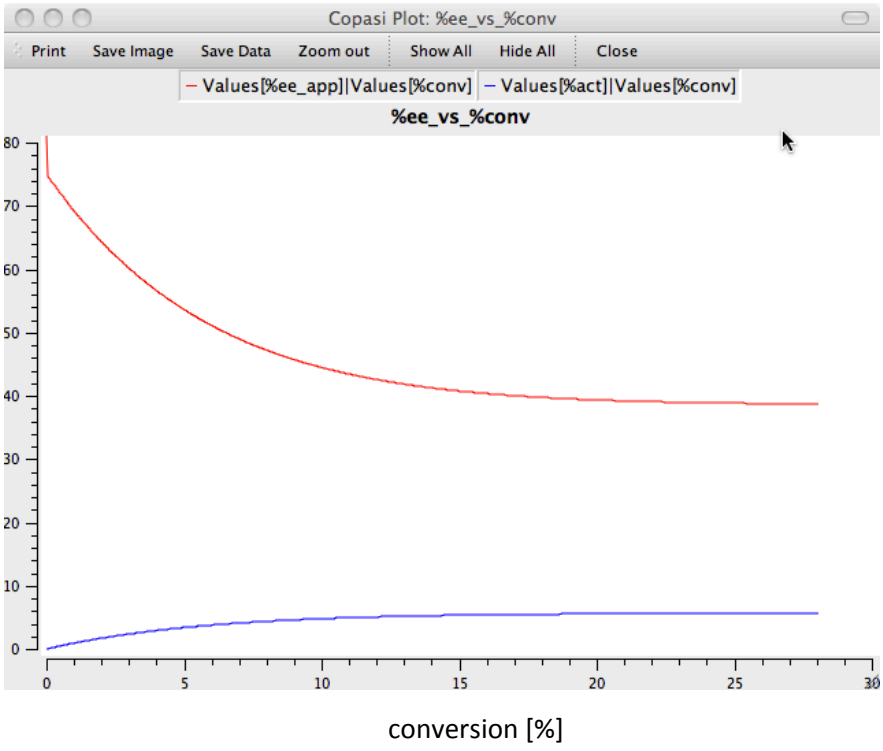


**Figure 6.19**: Simulation of the enantiomeric excess (red curve) and radiochemical yield (blue curve) that would be found in the absence of isotope effects relative to the conversion to ethane.

**Results with isotope effects as determined in our experiments:**

In the second simulation, the isotope effects found in our experiments were introduced: 1°KIE(H/D) = 2.5; 2°KIE(H/D) = 1.25 in both directions. Now, the loss of %ee is from 75% (initial) down to ca. 44.5% again with a conversion of 28% in 10 h. The calculated radiochemical yield after 10 h is 14.2%. At 10% conversion, these values are: 58%ee, radiochemical yield 7.7% (**figure 6.20**).

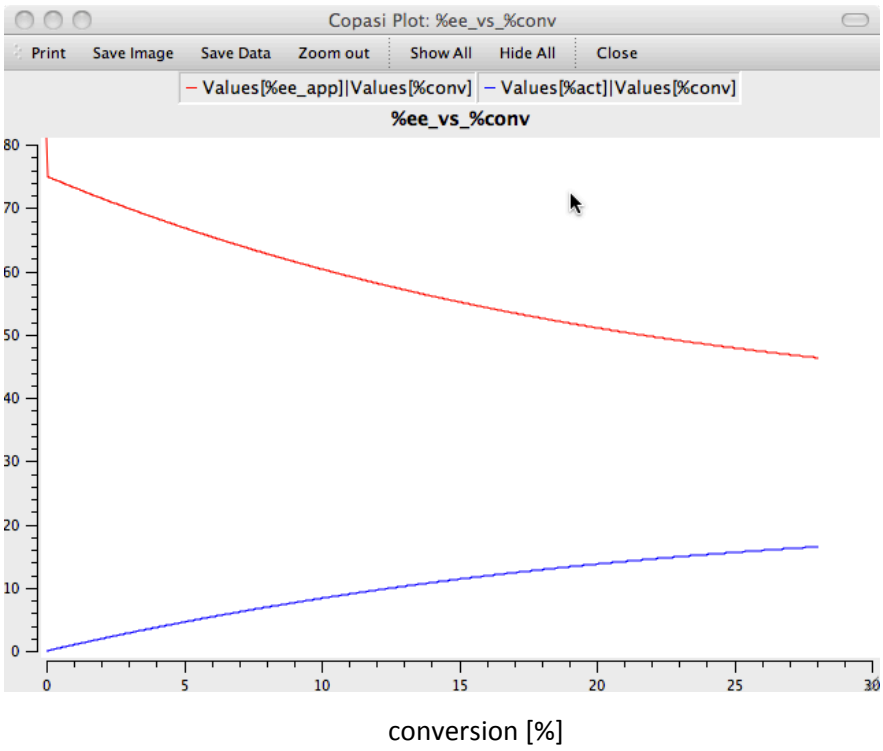


**Figure 6.20**: Simulation of the enantiomeric excess (red curve) and radiochemical yield (blue curve) relative to the conversion to ethane taking into account the isotope effects determined from our experiments.

## References


[1] K. Nauhaus, M. Albrecht, M. Elvert, A. Boetius, F. Widdel, "In vitro cell growth of marine archaeal-bacterial consortia during anaerobic oxidation of methane with sulfate" *Environ. Microbiol.* **2007**, *9*, 187.

[2] S. J. Hallam, N. Putnam, C. M. Preston, J. C. Detter, D. Rokhsar, P. M. Richardson, E. F. DeLong, "Reverse methanogenesis: Testing the hypothesis with environmental genomics" *Science* **2004**, *305*, 1457.

[3] T. M. Hoehler, M. J. Alperin, D. B. Albert, C. S. Martens, "Field and laboratory studies of methane oxidation in an anoxic marine sediment - evidence for a methanogen-sulfate reducer consortium" *Global Biogeochem. Cycles* **1994**, *8*, 451.

[4] B. Chappe, P. Albrecht, W. Michaelis, "Polar lipids of archaebacteria in sediments and petroleums" *Science* **1982**, *217*, 65.

[5] U. H. Wiechert, "Earth's early atmosphere" *Science* **2002**, *298*, 2341.

[6] C. R. Woese, L. J. Magrum, G. E. Fox, "Archaebacteria" *J. Mol. Evol.* **1978**, *11*, 245.

[7] K. F. Jarrell, A. D. Walters, C. Bochiwal, J. M. Borgia, T. Dickinson, J. P. J. Chong, "Major players on the microbial stage: why archaea are important" *Microbiology (Reading, U.K.)* **2011**, *157*, 919.

[8] R. Cavicchioli, "Archaea - timeline of the third domain" *Nature Reviews Microbiology* **2011**, *9*, 51.

[9] N. R. Pace, "Time for a change" *Nature* **2006**, *441*, 289.

[10] C. R. Woese, O. Kandler, M. L. Wheelis, "Towards a natural system of organisms - proposal for the domains Archaea, Bacteria, and Eucarya" *Proc. Natl. Acad. Sci. USA* **1990**, *87*, 4576.

[11] E. G. Nisbet, N. H. Sleep, "The habitat and nature of early life" *Nature* **2001**, *409*, 1083.

[12] D. C. Catling, M. W. Claire, "How Earth's atmosphere evolved to an oxic state: A status report" *Earth. Planet. Sci. Lett.* **2005**, *237*, 1.

[13] R. E. Kopp, J. L. Kirschvink, I. A. Hilburn, C. Z. Nash, "The paleoproterozoic snowball Earth: A climate disaster triggered by the evolution of oxygenic photosynthesis" *Proc. Natl. Acad. Sci. USA* **2005**, *102*, 11131.

[14] E. Blochl, R. Rachel, S. Burggraf, D. Hafenbradl, H. W. Jannasch, K. O. Stetter, "Pyrolobus fumarii, gen. and sp. nov., represents a novel group of archaea, extending the upper temperature limit for life to 113 degrees C" *Extremophiles* **1997**, *1*, 14.

[15] T. Ochsenreiter, F. Pfeifer, C. Schleper, "Diversity of Archaea in hypersaline environments characterized by molecular-phylogenetic and cultivation studies" *Extremophiles* **2002**, *6*, 267.

[16] C. Schleper, G. Puhler, B. Kuhlmorgen, W. Zillig, "Life at extremely low pH" *Nature* **1995**, *375*, 741.

[17] R. K. Thauer, "Functionalization of Methane in Anaerobic Microorganisms" *Angew. Chem. Int. Ed.* **2010**, *49*, 6712.

[18] B. S. Lollar, T. D. Westgate, J. A. Ward, G. F. Slater, G. Lacrampe-Couloume, "Abiogenic formation of alkanes in the Earth's crust as a minor source for global hydrocarbon reservoirs" *Nature* **2002**, *416*, 522.

[19] J. Lelieveld, P. J. Crutzen, F. J. Dentener, "Changing concentration, lifetime and climate forcing of atmospheric methane" *Tellus (B Chem. Phys. Meteorol.)* **1998**, *50*, 128.

[20] R. Conrad, "The global methane cycle: recent advances in understanding the microbial processes involved" *Environ. Microbiol. Rep.* **2009**, *1*, 285.

[21] G. L. Vaghjiani, A. R. Ravishankara, "New measurement of the rate coefficient for the reaction of OH with methane" *Nature* **1991**, *350*, 406.

[22] P. Regnier, A. W. Dale, S. Arndt, D. E. LaRowe, J. Mogollon, P. Van Cappellen, "Quantitative analysis of anaerobic oxidation of methane (AOM) in marine sediments: A modeling perspective" *Earth-Sci. Rev.* **2011**, *106*, 105.

[23] A. Boetius, K. Ravenschlag, C. J. Schubert, D. Rickert, F. Widdel, A. Gieseke, R. Amann, B. B. Jorgensen, U. Witte, O. Pfannkuche, "A marine microbial consortium apparently mediating anaerobic oxidation of methane" *Nature* **2000**, *407*, 623.

[24] S. J. Hallam, P. R. Girguis, C. M. Preston, P. M. Richardson, E. F. DeLong, "Identification of methyl coenzyme M reductase A (mcrA) genes associated with methane-oxidizing archaea" *Appl. Environ. Microbiol.* **2003**, *69*, 5483.

[25] S. J. Hallam, A. P. Page, L. Constan, Y. C. Song, A. D. Norbeck, H. Brewer, L. Pasa-Tolic, in *Methods in Enzymology: Methods in Methane Metabolism, Pt A, Vol. 494*, Elsevier Academic Press Inc, San Diego, **2011**, pp. 75.

[26] A. A. Raghoebarsing, A. Pol, K. T. van de Pas-Schoonen, A. J. P. Smolders, K. F. Ettwig, W. I. C. Rijpstra, S. Schouten, J. S. S. Damste, H. J. M. Op den Camp, M. S. M. Jetten, M. Strous, "A microbial consortium couples anaerobic methane oxidation to denitrification" *Nature* **2006**, *440*, 918.

[27] F. Keppler, J. T. G. Hamilton, M. Brass, T. Rockmann, "Methane emissions from terrestrial plants under aerobic conditions" *Nature* **2006**, *439*, 187.

[28] T. A. Dueck, R. de Visser, H. Poorter, S. Persijn, A. Gorissen, W. de Visser, A. Schapendonk, J. Verhagen, J. Snel, F. J. M. Harren, A. K. Y. Ngai, F. Verstappen, H. Bouwmeester, L. Voesenek, A. van der Werf, "No evidence for substantial aerobic methane emission by terrestrial plants: a C-13-labelling approach" *New Phytol.* **2007**, *175*, 29.

[29] R. K. Thauer, "Biochemistry of methanogenesis: a tribute to Marjory Stephenson. 1998 Marjory Stephenson Prize Lecture" *Microbiology* **1998**, *144*, 2377.

[30] P. A. Bertram, M. Karrasch, R. A. Schmitz, R. Bocher, S. P. J. Albracht, R. K. Thauer, "Formylmethanofuran dehydrogenases from methanogenic archaea - substrate-specificity, EPR properties and reversible inactivation by cyanide of the molybdenum or tungsten iron-sulfur proteins" *Eur. J. Biochem.* **1994**, *220*, 477.

[31] A. R. Klein, J. Breitung, D. Linder, K. O. Stetter, R. K. Thauer, "N5,N10-Methenyltetrahydromethanopterin cyclohydrolase from the extremely thermophilic sulfate reducing Archaeoglobus fulgidus: comparison of its properties with those of the cyclohydrolase from the extremely thermophilic Methanopyrus kandleri" *Arch. Microbiol.* **1993**, *159*, 213.

[32] B. Schwoerer, J. Breitung, A. R. Klein, K. O. Stetter, R. K. Thauer, "Formylmethanofuran:tetrahydromethanopterin formyltransferase and N5,N10-methylenetetrahydromethanopterin dehydrogenase from the sulfate-reducing Archaeoglobus fulgidus: similarities with the enzymes from methanogenic Archaea" *Arch. Microbiol.* **1993**, *159*, 225.

[33] M. Vaupel, R. K. Thauer, "Coenzyme F420-dependent N5,N10-methylenetetrahydromethanopterin reductase (Mer) from Methanobacterium thermoautotrophicum strain Marburg. Cloning, sequencing, transcriptional analysis, and functional expression in Escherichia coli of the mer gene" *Eur. J. Biochem.* **1995**, *231*, 773.

[34] E. Stupperich, R. Konle, "Corrinoid-dependent methyl transfer-reactions are involved in methanol and 3,4-dimethoxybenzoate metabolism by sporomusa-ovata" *Appl. Environ. Microbiol.* **1993**, *59*, 3110.

[35] L. G. Bonacker, S. Baudner, E. Moerschel, R. Boecher, R. K. Thauer, "Properties of the two isoenzymes of methyl-coenzyme M reductase in Methanobacterium thermoautotrophicum" *Eur. J. Biochem.* **1993**, *217*, 587.

[36] R. Hedderich, J. Koch, D. Linder, R. K. Thauer, "The heterodisulfide reductase from Methanobacterium thermoautotrophicum contains sequence motifs characteristic of pyridine-nucleotide-dependent thioredoxin reductases" *Eur. J. Biochem.* **1994**, *225*, 253.

[37] R. K. Thauer, A. K. Kaster, H. Seedorf, W. Buckel, R. Hedderich, "Methanogenic archaea: ecologically relevant differences in energy conservation" *Nat. Rev. Microbiol.* **2008**, *6*, 579.

[38] R. P. Gunsalus, R. S. Wolfe, "Stimulation of CO2 reduction to methane by methyl-coenzyme M in extracts of methanobacterium" *Biochem. Biophys. Res. Commun.* **1977**, *76*, 790.

[39] K. C. Costa, P. M. Wong, T. S. Wang, T. J. Lie, J. A. Dodsworth, I. Swanson, J. A. Burn, M. Hackett, J. A. Leigh, "Protein complexing in a methanogen suggests electron bifurcation and electron delivery from formate to heterodisulfide reductase" *Proc. Natl. Acad. Sci. USA* **2010**, *107*, 11050.

[40] G. Gottschalk, R. K. Thauer, "The Na+-translocating methyltransferase complex from methanogenic archaea" *Biochim. Biophys. Acta Bioenergetics* **2001**, *1505*, 28.

[41] M. Blaut, G. Gottschalk, "Coupling of ATP synthesis and methane formation from methanol and molecular-hydrogen in methanosarcina-barkeri" *Eur. J. Biochem.* **1984**, *141*, 217.

[42] M. Krüger, A. Meyerdierks, F. O. Glockner, R. Amann, F. Widdel, M. Kube, R. Reinhardt, J. Kahnt, R. Bocher, R. K. Thauer, S. Shima, "A conspicuous nickel protein in microbial mats that oxidize methane anaerobically" *Nature* **2003**, *426*, 878.

[43] R. P. Gunsalus, J. A. Romesser, R. S. Wolfe, "Preparation of coenzyme-M analogs and their activity in methyl coenzyme-M reductase system of methanobacterium-thermoautotrophicum" *Biochemistry* **1978**, *17*, 2374.

[44] M. Goenrich, F. Mahlert, E. C. Duin, C. Bauer, B. Jaun, R. K. Thauer, "Probing the reactivity of Ni in the active site of methyl-coenzyme M reductase with substrate analogues" *J. Biol. Inorg. Chem.* **2004**, *9*, 691.

[45] U. Ermler, W. Grabarse, S. Shima, M. Goubeaud, R. K. Thauer, "Crystal structure of methyl-coenzyme M reductase: the key enzyme of biological methane formation" *Science* **1997**, *278*, 1457.

[46] W. Grabarse, F. Mahlert, E. C. Duin, M. Goubeaud, S. Shima, R. K. Thauer, V. Lamzin, U. Ermler, "On the mechanism of biological methane formation: Structural evidence for conformational changes in methyl-coenzyme M reductase upon substrate binding" *J. Mol. Biol.* **2001**, *309*, 315.

[47] S. Ebner, B. Jaun, M. Goenrich, R. K. Thauer, J. Harmer, "Binding of Coenzyme B Induces a Major Conformational Change in the Active Site of Methyl-Coenzyme M Reductase" *J. Am. Chem. Soc.* **2010**, *132*, 567.

[48] W. L. Ellefson, W. B. Whitman, R. S. Wolfe, "Nickel-containing factor-F430 - chromophore of the methylreductase of methanobacterium" *Proc. Natl. Acad. Sci. USA* **1982**, *79*, 3707.

[49] G. Faerber, W. Keller, C. Kratky, B. Jaun, A. Pfaltz, C. Spinner, A. Kobelt, A. Eschenmoser, "Coenzyme F430 from methanogenic bacteria complete assignment of configuration based on an X-ray analysis of 12 13 diepi-F430 pentamethyl ester and on NMR spectroscopy" *Helv. Chim. Acta* **1991**, *74*, 697.

[50] D. A. Livingston, A. Pfaltz, J. Schreiber, A. Eschenmoser, D. Ankel-Fuchs, J. Moll, R. Jaenchen, R. K. Thauer, "Factor-F430 from Methanogenic Bacteria - Structure of the Protein-Free Factor" *Helv. Chim. Acta* **1984**, *67*, 334.

[51] A. Pfaltz, B. Jaun, A. Fassler, A. Eschenmoser, R. Jaenchen, H. H. Gilles, G. Diekert, R. K. Thauer, "Factor-F430 from methanogenic bacteria - structure of the porphinoid ligand system" *Helv. Chim. Acta* **1982**, *65*, 828.

[52] A. P. Johnson, P. Wehrli, R. Fletcher, A. Eschenmoser, "Corphin a corrinoid-porphinoid ligand system" *Angew. Chem. Int. Ed.* **1968**, *7*, 623.

[53] B. Jaun, A. Pfaltz, "Coenzyme-F430 from methanogenic bacteria - reversible one-electron reduction of F430 pentamethyl ester to the nickel(I) form" *J. Chem. Soc., Chem. Commun.* **1986**, 1327.

[54] B. Jaun, "Coenzyme-F430 from methanogenic bacteria - oxidation of F430 pentamethyl ester to the Ni(III) form" *Helv. Chim. Acta* **1990**, *73*, 2209.

[55] C. Spinner, PhD Thesis from Eidgenoessische Technische Hochschule (Zurich), **1993**.

[56] S. Mayr, C. Latkoczy, M. Kruger, D. Gunther, S. Shima, R. K. Thauer, F. Widdel, B. Jaun, "Structure of an F430 Variant from Archaea Associated with Anaerobic Oxidation of Methane" *J. Am. Chem. Soc.* **2008**, *130*, 10758.

[57] S. K. Lin, B. Jaun, "Coenzyme-F430 from methanogenic bacteria - mechanistic studies on the reductive cleavage of sulfonium ions catalyzed by F430 pentamethyl ester" *Helv. Chim. Acta* **1992**, *75*, 1478.

[58] S. Rospert, R. Bocher, S. P. J. Albracht, R. K. Thauer, "Methyl-coenzyme-M reductase preparations with high specific activity from H2-preincubated cells of methanobacterium-thermoautotrophicum" *FEBS Lett.* **1991**, *291*, 371.

[59] F. Mahlert, W. Grabarse, J. Kahnt, R. K. Thauer, E. C. Duin, "The nickel enzyme methyl-coenzyme M reductase from methanogenic archaea: in vitro interconversions among the EPR detectable MCR-red1 and MCR-red2 states" *J. Biol. Inorg. Chem.* **2002**, *7*, 101.

[60] E. C. Duin, D. Prakash, C. Brungess, in *Methods in Enzymology: Methods in Methane Metabolism, Pt A, Vol. 494*, Elsevier Academic Press Inc, San Diego, **2011**, pp. 159.

[61] A. Wasserfallen, J. Nolling, P. Pfister, J. Reeve, E. C. de Macario, "Phylogenetic analysis of 18 thermophilic Methanobacterium isolates supports the proposals to create a new genus, Methanothermobacter gen. nov., and to reclassify several isolates in three species, Methanothermobacter thermautotrophicus comb. nov., methanothermobacter wolfeii comb. nov., and Methanothermobacter marburgensis sp nov" *Int. J. Syst. Evol. Microbiol.* **2000**, *50*, 43.

[62] M. Goenrich, E. C. Duin, F. Mahlert, R. K. Thauer, "Temperature dependence of methyl-coenzyme M reductase activity and of the formation of the methyl-coenzyme M reductase red2 state induced by coenzyme B" *J. Biol. Inorg. Chem.* **2005**, *10*, 333.

[63] L. P. Wackett, J. F. Honek, T. P. Begley, V. Wallace, W. H. Ormejohnson, C. T. Walsh, "Substrate-analogs as mechanistic probes of methyl-S-coenzyme-M reductase" *Biochemistry* **1987**, *26*, 6012.

[64] E. C. Duin, L. Signor, R. Piskorski, F. Mahlert, M. D. Clay, M. Goenrich, R. K. Thauer, B. Jaun, M. K. Johnson, "Spectroscopic investigation of the nickel-containing porphinoid cofactor F-430. Comparison of the free cofactor in the +1, +2 and +3 oxidation states with the cofactor bound to methyl-coenzyme M reductase in the silent, red and ox forms" *J. Biol. Inorg. Chem.* **2004**, *9*, 563.

[65] D. Hinderberger, S. Ebner, S. Mayr, B. Jaun, M. Reiher, M. Goenrich, R. K. Thauer, J. Harmer, "Coordination and binding geometry of methyl-coenzyme M in the red1m state of methyl-coenzyme M reductase" *J. Biol. Inorg. Chem.* **2008**, *13*, 1275.

[66] J. Harmer, C. Finazzo, R. Piskorski, S. Ebner, E. C. Duin, M. Goenrich, R. K. Thauer, M. Reiher, A. Schweiger, D. Hinderberger, B. Jaun, "A nickel hydride complex in the active site of methyl-coenzyme M reductase: Implications for the catalytic cycle" *J. Am. Chem. Soc.* **2008**, *130*, 10907.

[67] C. Finazzo, J. Harmer, C. Bauer, B. Jaun, E. C. Duin, F. Mahlert, M. Goenrich, R. K. Thauer, S. Van Doorslaer, A. Schweiger, "Coenzyme B induced coordination of coenzyme M via its thiol group to Ni(I) of F-430 in active methyl-coenzyme M reductase" *J. Am. Chem. Soc.* **2003**, *125*, 4988.

[68] D. Hinderberger, R. R. Piskorski, M. Goenrich, R. K. Thauer, A. Schweiger, J. Harmer, B. Jaun, "A nickel-alkyl bond in an inactivated state of the enzyme catalyzing methane formation" *Angew. Chem. Int. Ed.* **2006**, *45*, 3602.

[69] N. Yang, M. Reiher, M. Wang, J. Harmer, E. C. Duin, "Formation of a nickel-methyl species in methyl-coenzyme M reductase, an enzyme catalyzing methane formation" *J. Am. Chem. Soc.* **2007**, *129*, 11028.

[70] R. Sarangi, M. Dey, S. W. Ragsdale, "Geometric and Electronic Structures of the Ni-I and Methyl-Ni-III Intermediates of Methyl-Coenzyme M Reductase" *Biochemistry* **2009**, *48*, 3146.

[71] J. Harmer, C. Finazzo, R. Piskorski, C. Bauer, B. Jaun, E. C. Duin, M. Goenrich, R. K. Thauer, S. Van Doorslaer, A. Schweiger, "Spin density and coenzyme M coordination geometry of the ox1 form of methyl-coenzyme M reductase: A pulse EPR study" *J. Am. Chem. Soc.* **2005**, *127*, 17744.

[72] S. Ebner, PhD Thesis from Eidgenoessische Technische Hochschule (Zurich), **2010**.

[73] V. Pelmenschikov, M. R. A. Blomberg, P. E. M. Siegbahn, R. H. Crabtree, "A mechanism from quantum chemical studies for methane formation in methanogenesis" *J. Am. Chem. Soc.* **2002**, *124*, 4039.

[74] V. Pelmenschikov, P. E. M. Siegbahn, "Catalysis by methyl-coenzyme M reductase: a theoretical study for heterodisulfide product formation" *J. Biol. Inorg. Chem.* **2003**, *8*, 653.

[75] E. C. Duin, M. L. McKee, "A new mechanism for methane production from methyl-coenzyme M reductase as derived from density functional calculations" *J. Phys. Chem. B* **2008**, *112*, 2466.

[76] X. H. Li, J. Telser, R. C. Kunz, B. M. Hoffman, G. Gerfen, S. W. Ragsdale, "Observation of Organometallic and Radical Intermediates Formed during the Reaction of Methyl-Coenzyme M Reductase with Bromoethanesulfonate" *Biochemistry* **2010**, *49*, 6866.

[77] Y. H. Ahn, J. A. Krzycki, H. G. Floss, "Steric course of the reduction of ethyl coenzyme M to ethane catalyzed by methyl coenzyme M reductase from methanosarcina-barkeri" *J. Am. Chem. Soc.* **1991**, *113*, 4700.

[78] R. H. Crabtree, "Aspects of methane chemistry" *Chem. Rev.* **1995**, *95*, 987.

[79] M. Brookhart, M. L. H. Green, G. Parkin, "Agostic interactions in transition metal compounds" *Proc. Natl. Acad. Sci. USA* **2007**, *104*, 6908.

[80] G. E. Ball, C. M. Brookes, A. J. Cowan, T. A. Darwish, M. W. George, H. K. Kawanami, P. Portius, J. P. Rourke, "A delicate balance of complexation vs. activation of alkanes interacting with Re(Cp)(CO)(PF3) studied with NMR and time-resolved IR spectroscopy" *Proc. Natl. Acad. Sci. USA* **2007**, *104*, 6927.

[81] A. J. Cowan, M. W. George, "Formation and reactivity of organometallic alkane complexes" *Coord. Chem. Rev.* **2008**, *252*, 2504.

[82] A. Bagno, G. Saielli, "Relativistic DFT calculations of the NMR properties and reactivity of transition metal methane sigma-complexes: insights on C-H bond activation" *Phys. Chem. Chem. Phys.* **2011**, *13*, 4285.

[83] S. Geftakis, G. E. Ball, "Direct observation of a transition metal alkane complex, CpRe(CO)(2)(cyclopentane), using NMR spectroscopy" *J. Am. Chem. Soc.* **1998**, *120*, 9953.

[84] D. J. Lawes, S. Geftakis, G. E. Ball, "Insight into binding of alkanes to transition metals from NMR spectroscopy of isomeric pentane and isotopically labeled alkane complexes" *J. Am. Chem. Soc.* **2005**, *127*, 4134.

[85] D. J. Lawes, T. A. Darwish, T. Clark, J. B. Harper, G. E. Ball, "A rhenium-cyclohexane complex with preferential binding of axial C-H bonds: A probe into the relative ability of C-H, C-D, and C-C bonds as hyperconjugative electron donors?" *Angew. Chem. Int. Ed.* **2006**, *45*, 4486.

[86] W. H. Bernskoetter, C. K. Schauer, K. I. Goldberg, M. Brookhart, "Characterization of a Rhodium(I) sigma-Methane Complex in Solution" *Science* **2009**, *326*, 553.

[87] J. A. Calladine, O. Torres, M. Anstey, G. E. Ball, R. G. Bergman, J. Curley, S. B. Duckett, M. W. George, A. I. Gilson, D. J. Lawes, R. N. Perutz, X. Z. Sun, K. P. C. Vollhardt, "Photoinduced N-2 loss as a route to long-lived organometallic alkane complexes: A time-resolved IR and NMR study" *Chem. Sci.* **2010**, *1*, 622.

[88] J. A. Calladine, S. B. Duckett, M. W. George, S. L. Matthews, R. N. Perutz, O. Torres, Q. V. Khuong, "Manganese Alkane Complexes: An IR and NMR Spectroscopic Investigation" *J. Am. Chem. Soc.* **2011**, *133*, 2303.

[89] D. R. Evans, T. Drovetskaya, R. Bau, C. A. Reed, P. D. W. Boyd, "Heptane coordination to an iron(II) porphyrin" *J. Am. Chem. Soc.* **1997**, *119*, 3633.

[90] I. Castro-Rodriguez, H. Nakai, P. Gantzel, L. N. Zakharov, A. L. Rheingold, K. Meyer, "Evidence for alkane coordination to an electron-rich uranium center" *J. Am. Chem. Soc.* **2003**, *125*, 15734.

[91] S. S. Stahl, J. A. Labinger, J. E. Bercaw, "Homogeneous oxidation of alkanes by electrophilic late transition metals" *Angew. Chem. Int. Ed.* **1998**, *37*, 2181.

[92] A. E. Shilov, G. B. Shul'pin, "Activation of C-H bonds by metal complexes" *Chem. Rev.* **1997**, *97*, 2879.

[93] N. F. Gol'dshleger, M. B. Tyabin, A. E. Shilov, A. A. Shteinman, "Activation of saturated hydrocarbons - deuterium-hydrogen exchange in solutions of transition metal complexes" *Russ. J. Phys. Chem.* **1969**, *43*, 1222.

[94] N. F. Gol'dshleger, V. V. Es'kova, A. E. Shilov, A. A. Shteinman, "Alkane reactions in solutions of chloride complexes of platinum" *Zh. Fiz. Khim.* **1972**, *46*, 1353.

[95] M. Lersch, M. Tilset, "Mechanistic Aspects of C-H Activation by Pt Complexes" *Chem. Rev.* **2005**, *105*, 2471.

[96] F. Basolo, H. B. Gray, R. G. Pearson, "Mechanism of substitution reactions of complex ions. 17. Rates of reaction of some platinum(II) and palladium(II) complexes with pyridine" *J. Am. Chem. Soc.* **1960**, *82*, 4200.

[97] J. Halpern, "Oxidative-addition reactions of transition metal complexes" *Acc. Chem. Res.* **1970**, *3*, 386.

[98] J. Chatt, J. M. Davidson, "Ein neuer Typ von Aromaten-Komplexen" *Angew. Chem. Int. Ed.* **1963**, *75*, 1026.

[99] J. Chatt, J. M. Davidson, "Tautomerism of arene and ditertiary phosphine complexes of ruthenium(0) and preparation of new types of hydridocomplexes of ruthenium(2)" *J. Chem. Soc.* **1965**, 843.

[100] A. H. Janowicz, R. G. Bergman, "C-H activation in completely saturated-hydrocarbons - direct observation of M + R-H- M(R)(H)" *J. Am. Chem. Soc.* **1982**, *104*, 352.

[101] J. K. Hoyano, W. A. G. Graham, "Oxidative addition of the carbon hydrogen-bonds of neopentane and cyclohexane to a photochemically generated iridium(I) complex" *J. Am. Chem. Soc.* **1982**, *104*, 3723.

[102] A. Chernega, J. Cook, M. L. H. Green, L. Labella, S. J. Simpson, J. Souter, A. H. H. Stephens, "New ansa-2,2-bis(eta-cyclopentadienyl)propane molybdenum and tungsten compounds and intramolecular hydrogen-deuterium exchange in methyl-hydride and ethyl-hydride derivatives" *J. Chem. Soc., Dalton Trans.* **1997**, 3225.

[103] H. Simon, D. Palm, "Isotope effects in organic chemistry and biochemistry" *Angew. Chem. Int. Ed.* **1966**, *5*, 920.

[104] W. D. Jones, "Isotope effects in C-H bond activation reactions by transition metals" *Acc. Chem. Res.* **2003**, *36*, 140.

[105] T. O. Northcutt, D. D. Wick, A. J. Vetter, W. D. Jones, "Investigation of the mechanism of alkane reductive elimination and skeletal isomerization in Tp'Rh(CNneopentyl)(R)H complexes: The role of alkane complexes" *J. Am. Chem. Soc.* **2001**, *123*, 7257.

[106] P. L. Watson, "Methane exchange-reactions of lanthanide and early-transition-metal methyl complexes" *J. Am. Chem. Soc.* **1983**, *105*, 6491.

[107] A. L. Reznichenko, K. C. Hultzsch, in *Molecular Catalysis of Rare-Earth Elements, Vol. 137*, Springer-Verlag Berlin, Berlin, **2010**, pp. 1.

[108] E. C. Sherer, C. J. Cramer, "Quantum chemical characterization of methane metathesis in L2MCH3 (L = H, Cl, Cp, Cp*; M = Sc, Y, Lu)" *Organometallics* **2003**, *22*, 1682.

[109] P. L. Watson, G. W. Parshall, "Organolanthanides in catalysis" *Acc. Chem. Res.* **1985**, *18*, 51.

[110] A. D. Sadow, T. D. Tilley, "Homogeneous catalysis with methane. A strategy for the hydromethylation of olefins based on the nondegenerate exchange of alkyl groups and sigma-bond metathesis at scandium" *J. Am. Chem. Soc.* **2003**, *125*, 7971.

[111] T. B. Rubtsova, N. V. Kirjakov, G. L. Soloveichik, A. E. Shilov, "Reaction of methane with nickel hydride complexes yielding methyl-derivatives" *Mendeleev Commun.* **1993**, 89.

[112] M. Schlangen, D. Schroder, H. Schwarz, "Pronounced ligand effects and the role of formal oxidation states in the nickel-mediated thermal activation of methane" *Angew. Chem. Int. Ed.* **2007**, *46*, 1641.

[113] S. Mayr, PhD Thesis from Eidgenoessische Technische Hochschule (Zurich), **2009**.

[114] M. J. Pine, H. A. Barker, "Studies on the methane fermentation. 12. The pathway of hydrogen in the acetate fermentation" *J. Bacteriol.* **1956**, *71*, 644.

[115] M. J. Pine, W. Vishniac, "The methane fermentations of acetate and methanol" *J. Bacteriol.* **1957**, *73*, 736.

[116] R. Walther, K. Fahlbusch, R. Sievert, G. Gottschalk, "Formation of trideuteromethane from deuterated trimethylamine or methylamine by methanosarcina-barkeri" *J. Bacteriol.* **1981**, *148*, 371.

[117] K. Knittel, A. Boetius, "Anaerobic oxidation of methane: progress with an unknown process" *Annu. Rev. Microbiol.* **2009**, *63*, 311.

[118] W. S. Reeburgh, "Oceanic methane biogeochemistry" *Chem. Rev.* **2007**, *107*, 486.

[119] C. S. Martens, R. A. Berner, "Methane production in interstitial waters of sulfate-depleted marine sediments" *Science* **1974**, *185*, 1167.

[120] A. J. B. Zehnder, T. D. Brock, "Methane formation and methane oxidation by methanogenic bacteria" *J. Bacteriol.* **1979**, *137*, 420.

[121] W. Michaelis, R. Seifert, K. Nauhaus, T. Treude, V. Thiel, M. Blumenberg, K. Knittel, A. Gieseke, K. Peterknecht, T. Pape, A. Boetius, R. Amann, B. B. Jergensen, F. Widdel, J. Peckmann, N. Pimenov, M. B. Gulin, "Microbial reefs in the Black Sea fueled by anaerobic oxidation of methane" *Science* **2002**, *297*, 1013.

[122] J. M. Levsky, R. H. Singer, "Fluorescence in situ hybridization: past, present and future" *J. Cell Sci.* **2003**, *116*, 2833.

[123] K. Nauhaus, T. Treude, A. Boetius, M. Krueger, "Environmental regulation of the anaerobic oxidation of methane: A comparison of ANME-I and ANME-II communities" *Environ. Microbiol.* **2005**, *7*, 98.

[124] M. Basen, M. Kruger, J. Milucka, J. Kuever, J. Kahnt, O. Grundmann, A. Meyerdierks, F. Widdel, S. Shima, "Bacterial enzymes for dissimilatory sulfate reduction in a marine microbial mat (Black Sea) mediating anaerobic oxidation of methane" *Environ. Microbiol.* **2011**, *13*, 1370.

[125] K. Nauhaus, A. Boetius, M. Kruger, F. Widdel, "In vitro demonstration of anaerobic oxidation of methane coupled to sulphate reduction in sediment from a marine gas hydrate area" *Environ. Microbiol.* **2002**, *4*, 296.

[126] Z. H. Duan, S. D. Mao, "A thermodynamic model for calculating methane solubility, density and gas phase composition of methane-bearing aqueous fluids from 273 to 523 K and from 1 to 2000 bar" *Geochim. Cosmochim. Acta* **2006**, *70*, 3369.

[127] J. W. Cornfort, J. W. Redmond, H. Eggerer, W. Buckel, C. Gutschow, "Synthesis and configurational assay of asymmetric methyl groups" *Eur. J. Biochem.* **1970**, *14*, 1.

[128] J. Luthy, J. Retey, D. Arigoni, "Preparation and detection of chiral methyl groups" *Nature* **1969**, *221*, 1213.

[129] R. A. Periana, R. G. Bergman, "Isomerization of the hydridoalkylrhodium complexes formed on oxidative addition of rhodium to alkane C-H bonds - evidence for the intermediacy of eta-2-alkane complexes" *J. Am. Chem. Soc.* **1986**, *108*, 7332.

[130] P. A. Small, "The equilibrium between hydrogen sulphide and heavy water" *Trans. Faraday Soc.* **1937**, *33*, 0820.

[131] K. B. Schowen, R. L. Schowen, "Solvent isotope effects on enzyme-systems" *Methods Enzymol.* **1982**, *87*, 551.

[132] D. A. Singleton, A. A. Thomas, "High-precision simultaneous determination of multiple small kinetic isotope effects at natural-abundance" *J. Am. Chem. Soc.* **1995**, *117*, 9357.

[133] L. S. Melander, W. H., Jr. , (Ed.: Wiley), New York, **1980**, pp. 95.

[134] Student, "The probable error of a mean" *Biometrika* **1908**, *6*, 1.

[135] S. Hoops, S. Sahle, R. Gauges, C. Lee, J. Pahle, N. Simus, M. Singhal, L. Xu, P. Mendes, U. Kummer, "COPASI- A COmplex PAthway SImulator" *Bioinformatics* **2006**, *22*, 3067.

[136] C. G. Swain, E. C. Stivers, J. F. Reuwer, L. J. Schaad, "Use of hydrogen isotope effects to identify the attacking nucleophile in the enolization of ketones catalyzed by acetic acid" *J. Am. Chem. Soc.* **1958**, *80*, 5885.

[137] K. S. Venkatasubban, R. L. Schowen, "The proton inventory technique" *Crit. Rev. Biochem.* **1984**, *17*, 1.

[138] K. R. Lynn, P. E. Yankwich, "High concentration-ratio experiments - isotope fractionation at methyl carbon in reaction of cyanide ion and methyl iodide - isotope effect under conditions of equal reagent concentrations" *J. Am. Chem. Soc.* **1961**, *83*, 790.

[139] G. Saueressig, P. Bergamaschi, J. N. Crowley, H. Fischer, G. W. Harris, "Carbon kinetic isotope effect in the reaction of CH4 with Cl atoms" *Geophys. Res. Lett.* **1995**, *22*, 1225.

[140] E. A. Halevi, "Secondary Isotope Effects" *Prog. Phys. Org. Chem.* **1963**, *1*, 109.

[141] V. Pelmenschikov, PhD Thesis from Stockholm University (Stockholm), **2005**.

[142] W. A. Pryor, K. G. Kneipp, E. H. Morkved, J. P. Stanley, "Kinetic isotope-effects in reactions of thiols with radicals formed by radiolysis" *Radiat. Res.* **1973**, *53*, 181.

[143] J. J. Grabowski, L. J. Zhang, "Dimethyl disulfide - anion molecule reactions in the gas-phase at 300 K" *J. Am. Chem. Soc.* **1989**, *111*, 1193.

[144] P. E. Cedervall, M. Dey, A. R. Pearson, S. W. Ragsdale, C. M. Wilmot, "Structural Insight into Methyl-Coenzyme M Reductase Chemistry Using Coenzyme B Analogues" *Biochemistry* **2010**, *49*, 7683.

[145] M. Dey, X. H. Li, R. C. Kunz, S. W. Ragsdale, "Detection of Organometallic and Radical Intermediates in the Catalytic Mechanism of Methyl-Coenzyme M Reductase Using the Natural Substrate Methyl-Coenzyme M and a Coenzyme B Substrate Analogue" *Biochemistry* **2010**, *49*, 10902.

[146] F. Mahlert, C. Bauer, B. Jaun, R. K. Thauer, E. C. Duin, "The nickel enzyme methyl-coenzyme M reductase from methanogenic archaea: In vitro induction of the nickel-based MCR-ox EPR signals from MCR-red2" *J. Biol. Inorg. Chem.* **2002**, *7*, 500.

[147] K. M. Noll, M. I. Donnelly, R. S. Wolfe, "Synthesis of 7-mercaptoheptanoylthreonine phosphate and its activity in the methylcoenzyme-M methylreductase system" *J. Biol. Chem.* **1987**, *262*, 513.